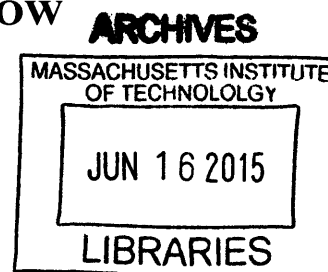


**CONTINUOUS SEPARATION AND RECYCLE OF
HOMOGENEOUS CATALYSTS IN SMALL SCALE FLOW
SYSTEMS**

by

Everett John O'Neal

Bachelor of Science, Chemical Engineering, Vanderbilt University, 2009
Master of Science, Chemical Engineering Practice, Massachusetts Institute of Technology, 2011



SUBMITTED TO THE DEPARTMENT OF CHEMICAL ENGINEERING
IN PARTIAL FULFILLMENT OF THE REQUIREMENTS FOR THE DEGREE OF

DOCTOR OF PHILOSOPHY IN CHEMICAL ENGINEERING
AT THE
MASSACHUSETTS INSTITUTE OF TECHNOLOGY

OCTOBER 2014 [February 2015]

© 2014 Massachusetts Institute of Technology. All rights reserved.

Signature redacted

Author _____

Everett J. O'Neal

Department of Chemical Engineering

October 9, 2014

Signature redacted

Certified by _____

Klavs F. Jensen

Warren K. Lewis Professor of Chemical Engineering

Professor of Materials Science and Engineering

Thesis Supervisor

Signature redacted

Accepted by _____

Patrick S. Doyle

Professor of Chemical Engineering

Chairman, Committee for Graduate Students



77 Massachusetts Avenue
Cambridge, MA 02139
<http://libraries.mit.edu/ask>

DISCLAIMER NOTICE

Due to the condition of the original material, there are unavoidable flaws in this reproduction. We have made every effort possible to provide you with the best copy available.

Thank you.

The images contained in this document are of the best quality available.

Appendix C (pages 193-237) contains light colored text.

Contents

1	Background, Motivation and Objectives.....	17
1.1	Organometallic Catalyst Separation and Recycle in Flow	17
1.1.1	Homogeneous Systems	17
1.1.2	Heterogeneous Catalytic Systems.....	21
1.2	Fundamentals of Chemical Synthesis in Small Scale Flow Systems.....	25
1.2.1	Reactive Small Scale Flow Systems	25
1.2.2	Dispersion	27
1.2.3	Mixing in Flow Systems	29
1.2.4	Liquid-Liquid Systems.....	32
1.2.5	Gas-Liquid Systems.....	35
1.2.6	Automation and optimization	36
1.3	Thesis Goals	40
1.4	Thesis Outline.....	41
2	Chapter 2. Thermomorphic Solvent Systems in Flow	44
2.1	Introduction	44
2.2	Experimental	48
2.2.1	Solvent Screening Experiments in Flow	48
2.2.2	Catalyst preparation for Alkenol Isomerization	49
2.2.3	Catalyst Characterization	49
2.2.4	Thermomorphic Isomerization.....	50
2.3	Results and Discussion	50
2.3.1	Theoretical Exploration of New Solvent Systems	50
2.3.2	Experimental Exploration of New Solvent Systems	55
2.3.3	Alkenol Isomerization.....	58
2.4	Conclusion.....	61
3	Separation and Recycle of a Metathesis Catalyst in a Small Scale Flow System	63

3.1	Introduction	63
3.2	Process Design	65
3.2.2	Second Generation Microfluidic Nanofiltration Chuck	71
3.2.3	Teflon-AF Reactor.....	72
3.2.4	Holding Tank with Liquid Level Control	75
3.2.5	Continuous Flow System Equipment Specifications	76
3.3	Experimental.....	77
3.3.1	Metathesis Reactant Synthesis	77
3.3.2	Metathesis Reactions	78
3.3.3	Testing of membrane rejections: UV-Vis and AAS.....	78
3.3.4	Continuous Recycle System Operation	80
3.4	Results and Discussion	81
3.5	Conclusion	91
4	Separation and Recycle of a Hydrogenation Catalyst in a Small Scale Flow System	93
4.1	Introduction	93
4.2	Process Design	94
4.2.1	Packed Bed Reactor Design.....	94
4.2.2	Hybrid Nanofiltration Module with Holding Tank	97
4.2.3	Pumping and Sampling System	101
4.3	Experimental.....	102
4.3.1	Batch Hydrogenation Experiments	102
4.3.2	High-Pressure Batch Catalyst Recycle Tests.....	103
4.3.3	Kinetic Screening in Flow	104
4.3.4	Nanofiltration Tests.....	108
4.3.5	Continuous Recycle System Operation	108
4.3.6	Analytical Methods	111
4.4	Results and Discussion	112
4.4.1	Batch Recycle Tests	112
4.4.2	Design Space Exploration in Flow	115

4.4.3	Continuous Recycle Performance	119
4.5	Economic Analysis.....	126
4.6	Conclusion.....	133
5	Separation and Recycle of a Buchwald-Hartwig Amination Catalyst in a Small Scale Flow System	135
5.1	Introduction	135
5.2	Process Design	139
5.2.1	Nanofiltration Cell	139
5.2.2	Holding Tank Design.....	139
5.2.3	Backpressure Regulator Parallelization.....	141
5.2.4	Pumping and Sampling System	142
5.3	Experimental.....	143
5.3.1	Batch Reactions	143
5.3.2	Batch Recycle Tests	143
5.3.3	Packed Bed Reactions	144
5.3.4	Nanofiltration Tests.....	144
5.3.5	Continuous Recycle System Operation	145
5.4	Results and Discussion	148
5.4.1	Batch Recycle Experiments	148
5.4.2	Packed Bed Reactor Tests	151
5.4.3	Continuous Recycle System	152
5.5	Conclusions	160
6	Dynamic Process Modeling	162
6.1	Introduction	162
6.2	Model Assumptions	163
6.3	Model Equations	164
6.3.1	Reactor	164
6.3.2	Nanofiltration Module	165
6.3.3	Splitter	167

6.3.4	Mixer	167
6.3.5	Overall Balance.....	168
6.3.6	Start-Up.....	168
6.4	Parameter Fitting.....	169
6.5	Model Applications	170
6.5.1	Metathesis Catalyst Recycle.....	170
6.5.2	Hydrogenation Catalyst Recycle.....	171
6.6	Conclusions	173
7	Conclusion	175
7.1	Summary of Thesis Contributions.....	175
7.2	Future Work and Recommendations.....	179
8	References.....	183
	Appendix A	190
	Appendix B	192
	Appendix C	193
	Appendix D	196
	Appendix E.....	197
	Appendix F.....	211
	Appendix G	213
	Appendix H.....	215
	Appendix I.....	222
	Appendix J	235
	Appendix K	236

List of Figures

Figure 1. Generic process scheme employing OATS, image taken from Pollet et al. ^[25]	18
Figure 2. Examples of microreactors for studying heterogeneous reactions. a) Gas-liquid packed bed reactor ^[55] , b) structured bed of silicon posts for catalysts immobilization ^[55] , c) cross flow packed bed ^[56] , d) parallel packed bed with integrated temperature sensors ^[57] , e) Packed bed and SEM detail (f) of weir for retaining solid catalyst particles. ^[58]	21
Figure 3. Enantioselective copper catalyzed cyclopropanation supported on siliceous mesocellular foam (MCF) microparticles. Recirculating flow reactor must be run in a batchwise fashion. ^[63]	24
Figure 4. Representation of a plug-flow reactor vs. a dynamic batch experiment from Moore and Jensen. ^[69]	26
Figure 5. Fluid velocity profile in plug flow vs. that in laminar flow (Left). Residence time distribution of a microreactor (Right). ^[71]	27
Figure 6. Given a certain channel width (for square channels) or tube diameter (for tubes) and the residence time, deviations from plug flow can be predicted. Figures from Nagy et. al. ^[72]	29
Figure 7. Mixing of homogeneous acid-base system in a microfluidic junction. The yellow and orange streams mix via diffusion only. ^[77]	30
Figure 8. Plot of Da as a function of tube diameter and residence time (for 95% conversion), assuming a T or Y-junction is used for mixing the streams. For $Da < 1$, the diffusion rates exceed the reaction rate and so no additional mixing scheme is necessary.	31
Figure 9. Illustration of micromixing via stream lamination and recombination. a.) The blue stream and red streams are first split into small-diameter channels before being contacted. ^[78] b.) Acid and base being mixed via a similar stream lamination approach. ^[80]	32
Figure 10. Different flow regimes for liquid-liquid flow in microchannels. ^[82] The continuous phase is defined as the phase wetting the walls of the channel.	33
Figure 11. Mixing via segmented flow from Song et al. ^[83]	33

Figure 12. Coupling reaction using <i>n</i> -Bu ₄ Br as a phase transfer catalyst (optimized to 1 mol%). Segmented flow results vs. two-phase flow through an inert packed bed. ^[85]	35
Figure 13. Gas-Liquid flow regime diagram for microreactors. ^[82] Picture of common gas-liquid flow conditions (left to right: bubbly, slug, annular). ^[86]	35
Figure 14. Automated screening system from Griffiths-Jones et al. ^[94]	37
Figure 15. Optimization of a sonogashira coupling reaction. ^[95]	37
Figure 16. Four automatically varied parameters produced yields, as determined by inline HPLC, which were fed to an optimization algorithm. In this way, the system was able to continually update planned experiments using recent experiments.	38
Figure 17. Continuous recycle system applied to a metathesis catalyst.	41
Figure 18. Continuous catalyst recycle system applied to a hydrogenation catalyst.	42
Figure 19. Buchwald-Hartwig amination catalyst recycle system.	43
Figure 20. Diagram of a thermomorphic catalyst separation process. ^[97]	44
Figure 21. Experimental layout for thermomorphic solvent system screening in flow.	49
Figure 22. Explanation of two important criteria in judging ternary thermomorphic solvent systems.	51
Figure 23: Left: UNIQUAC/UNIFAC simulation of PC-NMP-Dodecane. Right: Data from Behr et. al. ^[20]	53
Figure 24. Data from Behr et al. ^[20] demonstrating the change in ternary phase behavior with the addition of morpholine.	53
Figure 25. Experimental data (black points in diagram) demonstrating the effect of changing cyclohexane to cyclohexene.	54
Figure 26. Paths traced on a ternary diagram during microflow solvent screening. Lines between the data points are interpretations of the data.	56
Figure 27. Kinetic data comparing thermomorphic to biphasic reaction performance. All experiments: 80°C, 0.65M 1-Octen-3-ol in nonaqueous phase. 6 mM Catalyst. Thermomorphic: Volume Ratios Ethyl Acetate/Ethanol/Water: 32%/25%/43%. Biphasic: Volume Ratios: Heptane/Water: 43%/57%.	58
Figure 28. Mass transfer regression from the biphasic batch data from Figure 27.	60
Figure 29. Effect of partition coefficient on multiple mass transfer steps in series.	60
Figure 30. Hoveyda-Grubbs metathesis mechanism for our substrate. The mechanism follows an initiation-propagation scheme.	65

Figure 31. SolidWorks rendering of the permeate half (left) and retentate half (right) of the membrane chuck. Two o-rings are used for the retentate half of the module, and a 3/4" steel frit fits tightly into the permeate cavity.	66
Figure 32. Block diagram depicting the equipment setup and connections for nanofiltration rejection tests.	67
Figure 33. Time-dependent data for the generation of calibration curves and rejection values using in-line UV data, and the setup shown in Figure 32.	68
Figure 34. Second Generation microfluidic nanofiltration module using epoxy and an o-ring to seal the membrane.	72
Figure 35. Teflon AF reactor, previously developed by Sahoo et al. ^[147]	72
Figure 36. Design calculations predicting adequate removal of ethylene for a 600 second residence time.	74
Figure 37. Kinetic results for 1 mol% 4 and 0.05M 1 at r.t. using either a batch or pervaporation flow reactor.	75
Figure 38. Cartoon of small-scale holding tank with level control.	76
Figure 39. Continuous separation/recycle system for a metathesis catalyst.	76
Figure 40. Absorption of catalyst and RuCl ₃ in HCl are equivalent. Thus, catalyst 4 need not be worked-up before applying GF-AAS method.	79
Figure 41. Loading catalyst into the recycle system and using the catalyst until it is spent gives a declining product curve in our permeate. This justifies the use of a catalyst co-feed in subsequent experiments.	83
Figure 42. Approximate flow rate decline due to concentration polarization and fouling of the membrane.	84
Figure 43. Percent product in permeate, retentate, and reactor outlet samples for a 50 hour run.	85
Figure 44. Product and substrate concentrations in the permeate stream as a function of experimental time.	86
Figure 45. Rejections changed significantly upon accumulation of materials in the recycle loop.	87
Figure 46. Permeate ruthenium content remained below 0.5 ppm during the continuous run.	88

Figure 47. TON of a function of experimental time. Decline in rate of growth of TON with time represents a reduction in throughput rather than catalyst decomposition. Connected dots represent autosampler results using the approximate permeation rate from Figure 42. Stars represent TONs measured after the experiment.	89
Figure 48. Raw data for residence time distribution of our multiphase packed bed.	95
Figure 49. Deconvolution of bypass RTD from the total system RTD to obtain the reactor RTD (blue).....	96
Figure 50. Result of step changes and concentration and linear ramping changes on transient packed bed output.	97
Figure 51. First generation of Nanofiltration module designed to provide a high-pressure holding tank with built-in stir bar visualization.	99
Figure 52. Image of first-generation Nanofiltration module assembled for operation.	99
Figure 53. Holding tank/nanofiltration module hybrid used in our continuous flow system. The retentate side behaves as an ideal stirred tank.	100
Figure 54. Our second-generation hybrid nanofiltration/high-pressure holding tank with volume minimization, gas/liquid separation, and recirculation-induced mixing.....	101
Figure 55. Flow system used to screen kinetics efficiently using a transient upflow packed bed reactor.	103
Figure 56. Process diagram for our small-scale continuous recycle system.	109
Figure 57. Batch system for re-using catalyst without reducing hydrogen pressure below 200 psi in between catalyst uses.	114
Figure 58. Batch catalyst re-use results the setup shown in Figure 57. Data represents three separate re-uses of the catalyst, showing that some catalyst activity is maintained between cycles. Time waited in between cycles not included. See Supporting Information for details.	114
Figure 59. Base and TPP concentrations have little effect on kinetics near our operating point, giving us robust kinetic behavior near our operating conditions.....	116
Figure 60. TON obtained as a function of inlet substrate concentration. Substrate concentration has no effect on reaction rate.....	117
Figure 61. Yield as a function of residence time obtained during a kinetic ramping experiment.....	118

Figure 62. Conversion as a function of catalyst concentration obtained during a kinetic ramping experiment. Steady-state data were obtained afterwards to verify the accuracy of the more efficient ramping approach.118

Figure 63. Fraction product in the retentate of our system as a function of experimental time. No catalyst is co-fed during this run.121

Figure 64. Conversion as a function of time during a system run which includes a catalyst co-feed.....123

Figure 65. Rejection of product by the membrane as a function of experimental time for our run with a catalyst cofeed.124

Figure 66. Dynamic Jacobian® model calculations match our experimental product concentrations at two points in our system.125

Figure 67. Suzuki Reaction scheme with polymer-anchored catalyst packed in a microchannel.^[207]137

Figure 68. Custom holding tank with organic-phase mixing and liquid-liquid separation.140

Figure 69. Scheme showing LabVIEW information flow to and from the holding tank.....140

Figure 70. Parallelization of backpressure regulators to add to system robustness. This setup automatically uses a pressure measurement to decide when to switch between the parallelized backpressure regulators.142

Figure 71. Degassing piecewise system without a holding tank before a start-up.....145

Figure 72. Catalyst loading into the system during start-up. Catalyst was kept separate from the reactor during this time.147

Figure 73. System after start-up was completed, and all control systems/automation was activated.148

Figure 74. Fraction product in permeate stream for an initial charge of catalyst in our recycle system.....153

Figure 75. Reduced product fractions shown for reduced (60%) catalyst loading.153

Figure 76. Permeate and retentate product fractions throughout our continuous-coupling catalyst recycle experiment.154

Figure 77. Organic pump flow rate into system as a function experimental time.155

Figure 78. DMO content in recycle system (Volume%) as a function of experimental time.156

Figure 79. Rejection of palladium as a function of experimental time (AAS).	157
Figure 80. Rejection of product as a function of experimental time.	157
Figure 81. Concentrations of product in the retentate and permeate streams as a function of experimental time.	158
Figure 82. Holding tank liquid level as a function of time throughout the continuous recycle run.....	159
Figure 83. Abstraction of our catalyst recycle process which is simulated using our dynamic model.....	164
Figure 84. Nanofiltration module abstraction.....	166
Figure 85. Fit of dynamic model of metathesis catalyst recycle system to continuous data. Abbreviations for legend: [Sub] = Substrate Concentration, [Prod] = Product Concentration, RO = Reactor Outlet, Ret = Retentate Stream, Perm = Permeate Stream.....	171
Figure 86. Dynamic model prediction of our continuous hydrogenation run. Full conversion is assumed in the model; only product concentrations are considered.....	172
Figure 87. Engineering drawing of our microfluidic nanofiltration module.	196

List of Tables

Table 1. Results of microfluidic solvent screening at 80°C. Only the most useful results are shown here.	56
Table 2. Comparison of TOF from de Bellefon et al. to this work.	59
Table 3. Different rejection values achieved as a function of O-ring material. Only the best values achieved are shown.	69
Table 4. Different rejection values obtained using a Kalrez o-ring with different, unmeasured degrees of tightness.	70
Table 5. Comparisons of performances of batch reactor with nitrogen bubbling, closed tubes, and Teflon AF tubing as a reactor for various metathesis substrates. Formation of gas slugs in closed tubing makes some substrate residence times difficult to interpret, and so values are not reported.	75
Table 6. The temperature-time recipe used to create these calibration curves in the GF-AAS.	79
Table 7. Comparison of our results with highlights from the batch recycle literature.	90
Table 8. Summary of order-of-magnitude economic evaluations of six different process configurations.	130
Table 9. Batch recycle experiments using p-chloroanisole as the substrate.	149
Table 10. Batch recycle experiments using m-chloroanisole as the substrate.	150
Table 11. Batch recycle data using a 4:1, 2:1, and 1:1 mixtures of Toluene:DMO as the solvent to aid in system throughput. The substrates are aniline and m-chloroanisole.	151
Table 12. Conversions as a function of flow rates for our packed bed.	152

List of Schemes

Scheme 1. Ruthenium-catalyzed hydrogen transfer reaction. ^[62]	23
Scheme 2. Hydrogenation of MAA using an immobilized rhodium catalyst at a few bar of pressure. ^[66]	24
Scheme 3. Example of palladium-catalyzed C-N cross coupling reaction run in two phase (toluene-water) flow.	34
Scheme 4. Paal-Knorr reaction considered by Moore and Jensen. ^[69]	39
Scheme 5. Unmodified triphenylphosphine ligand (a) and its trisulfonated form (b).	47
Scheme 6. Allylic alcohol isomerization.....	47
Scheme 7. Ring-Closing metathesis chemistry and 2 nd Generation Hoveyda-Grubbs catalyst.	65
Scheme 8. Ring-closing metathesis of N-Tosyl-diallylamine with the 2 nd generation Hoveyda-Grubbs catalyst.	82
Scheme 9. Asymmetric hydrogenation of α -tetralone using molecular hydrogen, a ruthenium catalyst, and a strong base co-catalyst.	94
Scheme 10. Asymmetric hydrogenation of α -tetralone using a diphosphine/diamine catalyst. An ee of 97% is obtained for this substrate.	113
Scheme 11. Simple Suzuki coupling reaction over PdEnCat. ^[202]	136
Scheme 12. Buchwald-Hartwig Amination of an m-chloroanisole using the N-Methylated 3 rd Generation BrettPhos catalyst.	138

Abstract

The development of organometallic catalysts with high activity and selectivity has transformed the way both bulk and fine chemicals are produced. When such catalysts are applied in fine chemicals production, the presence of toxic heavy metals in these catalysts (Pd, Pt, Ru, Rh, etc.) can pose significant separation challenges. Regulatory bodies (such as the FDA and EMA) require that many popular catalytic heavy metals stay below 10 ppm in pharmaceutical drugs. Organic solvent nanofiltration (OSN) membranes are an upcoming technology with the potential to solve this problem by allowing heavy metal-containing catalysts to be molecularly separated from smaller product molecules. This size-based molecular separation makes the technique general, but challenges still exist in further broadening the chemical compatibility of nanofiltration membranes. Recent efforts have succeeded in creating membranes which are compatible with strong bases, and these membranes are applied in this thesis.

The work in this thesis developed continuous catalyst recycle systems for a metathesis catalyst, a hydrogenation catalyst, and a palladium Buchwald-Hartwig amination catalyst. During the initial stages of designing such small scale catalyst recycle systems, significant technology gaps were identified. These included microfluidic OSN modules, microfluidic holding tanks with level sensing, milli-scale OSN modules with integrated high-pressure holding tanks and liquid level sensing, and a milli-scale holding tank with two-phase level sensing. These small scale process blocks were designed, built, and implemented in this work.

Our metathesis catalyst recycle system included a reactor, holding tank, and nanofiltration module with a total internal volume of less than 3 ml. The system was used to automatically recycle the catalyst, obtaining a catalyst turnover number (TON) of 935, and reducing the ruthenium contamination in the product stream by a factor of 100. For our hydrogenation catalyst recycle system, we built a high-pressure small-scale catalyst recycle flow process (less than 50 ml). The system improved catalyst TONs from 500 to 4750, and reduced catalyst contamination in the product stream by a factor of 200. Finally, our palladium catalyst recycle system was able to perform a liquid-liquid separation before a nanofiltration step, and improved the TON of our reaction from 125 to 550 while decreasing the palladium contamination in the product stream by almost an order of magnitude.

We also discovered significant disadvantages in operating these continuous systems, including reduced throughput due to membrane fouling, reduced catalyst activity due to product inhibition, reduced substrate concentrations in the recycle loop (leading to reduced reaction rates), enantioselectivity decline, and increased process complexity. This thesis contributes to understanding the advantages/disadvantages of OSN-containing catalyst recycle systems, provides new tools for future work in many areas involving small scale process design, and generates recommendations regarding the next generation of small-scale OSN pilot processes.

Thesis Supervisor: Klavs F. Jensen
Title: Department Head, Chemical Engineering
Warren K. Lewis Professor of Chemical Engineering
Professor of Materials Science and Engineering

Acknowledgements

I would like to thank Klavs Jensen for his technical guidance throughout my projects and for being a fair and understanding thesis advisor. I would also like to thank my committee members, Steve Buchwald and Allan Myerson, for their valuable feedback during committee meetings.

I would like to thank the Jensen Group as a whole for providing an interesting and comfortable work environment. I have to thank Baris for helping me through many experimental/design obstacles in the lab, especially during my first three years of thesis work. I would doubtlessly still be toiling in the lab if not for him. I would like to thank Kevin Nagy for helping me get started in the lab and even suggesting this thesis topic to me. I would like to thank Patrick for always taking the time to teach me something new, Steve and Stephen for their chemical expertise and willingness to share it, Saurabh for helping with the coupling catalyst project, and Brandon for his statistics know-how. I would like to thank Andrea for his liquid/liquid separators, gas/liquid separators, backpressure regulators, and his indispensable pump heads. I would like to thank Klavs and the rest of the group, along with my family, for helping me deal with the more difficult times of my doctoral thesis experience.

I would like to thank Ludmila Peeva, Andrew Livingston, and the rest of the Livingston Group for providing our projects with nanofiltration membranes and their custom membrane module. Their advice and expertise with respect to membrane applications were extremely helpful. Spencer Schaber was very helpful by providing a C++ code to help me integrate MATLAB with the Jacobian software.

I would also like to thank the MIT central machine shop. Specifically, Andy Ryan and Andrew Gallant - both were very helpful and took the time to help improve my mechanical designs and provide mechanical engineering advice on short notice. Finally, I would like to thank Novartis and the Novartis-MIT Center for Continuous Manufacturing for providing funding and useful feedback regarding the work in this thesis.

1 Background, Motivation and Objectives

1.1 Organometallic Catalyst Separation and Recycle in Flow

1.1.1 Homogeneous Systems

Homogeneous organometallic catalysts allow for the precise tunability of activity and selectivity via the alteration of the ligand structure and metal choice.^[1] The exploitation of these properties have allowed for the 2001 and 2005 Nobel Prizes to be awarded on this topic. The continual improvement of homogeneous catalyst activity makes their implementation in industry increasingly viable. Cornilis et al.^[2] point out that in 50 years homogeneous hydroformylation catalysts have increased in activity by a factor of 10,000. The unambiguous spectroscopic characterization of homogeneous catalysts allows for efficient improvement in the stability and activity of homogeneous catalysts.^[2] The immobilization of homogeneous metals onto catalyst supports is one path to conquering the separation problem, however catalyst stability and deactivation are more difficult to study in this case and this has been cited as the reason why more industrial applications do not exist.^[2, 3] Heterogenization of organometallic catalysts is reviewed in the next section.

In fine chemicals production, homogeneous organometallic catalysts have become important tools, though challenges still exist.^{[4],[5, 6]} The toxicity profile of these catalysts in pharmaceutical applications renders their efficient separation of paramount importance.^[7, 8] The expensive transition metal centers and/or ligands provide motivation for the re-use of these catalysts. The development of continuous flow processes in the pharmaceutical industry gives further incentive for the development of methods for catalyst recycling.^[9-11] A microflow catalyst separation-recycle system allows for the safe investigation of catalyst recycling strategies under continuous flow conditions while simultaneously minimizing waste. This thesis will explore phase-change and nanofiltration-based methods to separate and recycle the homogeneous catalysts without the use of immobilization techniques.

1.1.1.1 Separations using Phase Behavior

Liquid/Liquid biphasic systems^[1] are popular approaches to homogeneous catalyst separation/recycle, and has been applied industrially in the hydroformylation of 1-butene^[12]

and oligomerization of ethylene.^[13] Liquid/liquid systems have been made by combining aqueous^[12], organic, fluoruous^[14, 15], ionic liquid^[16, 17], and/or supercritical^[18, 19] solvents. The limitations of this approach are the loss of activity after catalyst modification, mass transfer limitations, catalyst stability in multiple solvents, and the narrowness of the application due to substrate/product solubility requirements.

Thermomorphic solvent systems have been used to reduce the mass transfer limitations associated with many of the previously described liquid/liquid biphasic systems.^[20-22] This is achieved by using solvents which are miscible at the reaction temperature, but separate in the post-reaction mixture to separate the catalyst. The removal of mass transfer limitations should also help with scalability. This approach exacerbates catalyst stability concerns, increases catalyst leaching compared to the biphasic approach, and has an even more narrow application than liquid/liquid biphasic approaches. This approach is applied in Chapter 2 of this thesis. Switchable solvents use pH as an alternative to using temperature to regulate phase behavior. Reversible ionic liquids, which switch between being nonionic and ionic liquids, can change polarity upon acidification with carbon dioxide.^[23] Reversing this process requires the removal of the CO₂ via temperature increase or introducing N₂. High pressures of a gas can also be used to regulate phase behavior to the same end. Organic-aqueous tunable solvent (OATS) systems use 20-60 bar of CO₂ to separate otherwise miscible water-organic solvents such as water/THF.^[24] Recent articles outlining and applying these processes such as Pollet et al.^[25] have envisioned a continuous recycling scheme such as that in Figure 1.

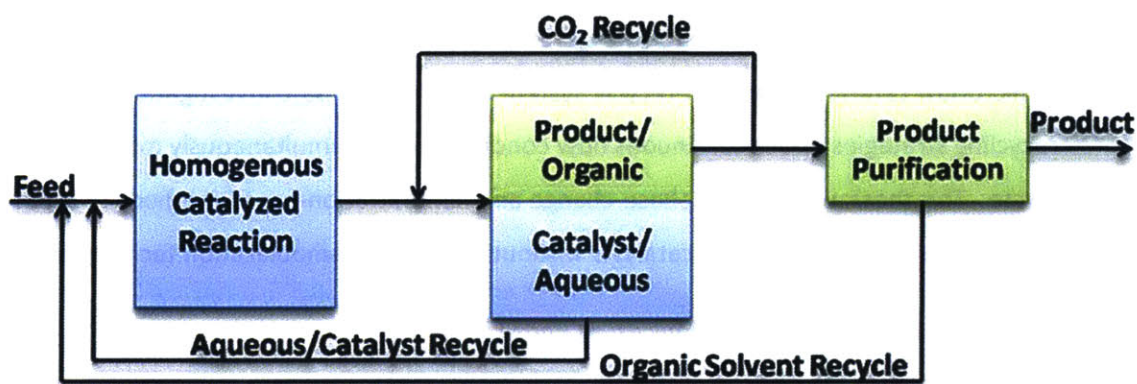


Figure 1. Generic process scheme employing OATS, image taken from Pollet et al.^[25]

When a homogeneous solution of THF and water are exposed to high pressures of CO₂, the high solubility of CO₂ in THF causes CO₂ to “salt out” the water phase so that a THF/ CO₂ phase and a water-containing phase results, along with a gaseous CO₂ phase, since CO₂ is not supercritical until near 73 bar.^[26] Under these pressures (20-60 bar), the water phase is removed and recycled. The product phase is then depressurized and a gas/liquid separation to remove the CO₂ takes place. Propane has been shown to reduce the pressure required in these OATS separations to about 10 bar.^[25, 27, 28] All of these phase-change based separation techniques share the property of having homogeneous reaction conditions combined with a way to cause a phase change after the reaction to enact catalyst separation. These approaches are likely to be rare in pharmaceutical application due to the narrow range of possible solvents to employ.

Solid/liquid biphasic systems often make use of a polymeric modification of a homogeneous catalyst, with separation being performed via filtration, centrifugation, and/or decanting to remove the solid catalyst after the reaction.^[29, 30] Nanoparticles have also been used to anchor catalysts.^[31] Systems have been devised to solubilize a modified catalyst during the reaction and precipitate it afterwards using temperature^[32, 33], pH change^[34], and anti-solvent addition.^[35] The major limitation of this approach is the reduced reactivity upon modifying the catalyst with large polymers. There are also solids-handling challenges which arise when applying these techniques in flow. Contrary to thermomorphic, OATS, and switchable solvent systems, solid/liquid biphasic approaches could be broad in application if the previously mentioned problems are solved.

1.1.1.2 *Separation using Nanofiltration Membranes*

Organic solvent resistant nanofiltration (OSN) membranes are central to the work in this thesis. OSN membranes can be compatible with polar protic, nonpolar, and/or polar aprotic solvents. Their small pores allow them to separate larger dissolved molecules (200-1000 Da) from smaller dissolved molecules at relatively low pressures (10-40 bar). OSN membranes are normally made out of a cellulose acetate, polyamide, polyimide, or polymethylsiloxane material.^[36] The pore sizes of these membranes are measured in terms of the molecular weights of a polymer (such as polystyrene) able to pass through a particular membrane. A

given membrane has a specified molecular weight cutoff (MWCO) when 90% of the polymers of a greater molecular weight are retained by the membrane. Rejection is defined as:

$$Rejection (\%) = \left(1 - \frac{C_P}{C_R}\right) \times 100 \quad (1)$$

Where C_P is the concentration of species in the permeate and C_R is the concentration of species in the retentate. Evonik's Duramem[®] and Puramem[®] membranes will be tested and applied in this work. These membranes are similar to the polyimide Starmem[®] membranes, since the original Starmem[®] brand was acquired by Evonik.^[37] The rejections of species in different membranes were shown to vary with pressure and solvent by Livingston et al.,^[38] and by Bhanushali et al.^[39] Further variations in species rejection values were observed in cross-flow membrane experiments with higher solute content (>5 wt%) due to concentration polarization^[40]. These factors make rejections of a catalyst difficult to predict.

For polyimide membranes used in this work, both the solution-diffusion model and the pore-flow model are generally fit to experimental data to determine which is appropriate for a particular case.^[36] For example, Silva et al.^[41] found that both the solution-diffusion and pore-flow models gave reasonable agreement with the solution-diffusion being the best fit for predicting fluxes of mixtures from pure component data. On the other hand, Iwama et al.^[42] were able to fit a pore-flow model to their data. Modeling effort is still required for these polyimide membranes. PDMS membranes, on the other hand, have been studied much more extensively.^[36] Solute transport through PDMS nanofiltration membranes have been found to be modeled by a pore-flow model or a solution-diffusion model depending on the swelling of the membrane (choice of solvent) and size of the solute.^[43, 44] Nanofiltration membranes have been used to separate organometallic, enzymatic, metallic, and organic catalysts from smaller product molecules, mostly in batch or semi-batch systems.^[45-47] In organometallic catalyst applications, recycling experiments have been performed in metathesis^[48, 49], hydroformylation^[50], coupling^[51], epoxidation^[52], and hydrogenation^[53] reactions.^{144, 145} Chapters 3, 4, 5, and 6 of this thesis expand upon what can be accomplished with nanofiltration membranes in small scale flow systems. This is achieved through a combination of novel process block design, flow system automation, process block characterization, and dynamic modeling of the full flow system.

1.1.2 Heterogeneous Catalytic Systems

This thesis focuses on the investigation of homogeneous catalyst recycling. Since the heterogenization of organometallic catalysts is a promising alternative approach, the advantages and disadvantages of this approach are discussed here. Furthermore, a complete flow system for a heterogenized catalyst is relatively easy to realize, and so more work has been done studying organometallic catalyst re-use in these systems.

The most common reactor design for solid-supported organometallic catalysts is a packed bed, where the reaction solution passes over the retained catalyst particles (Figure 2). Solid-liquid catalytic systems hold potential advantages over homogeneous liquid phase and liquid-liquid biphasic systems. High catalyst loadings per unit volume may be achieved, which results in reduced residence times. Downstream purification steps to remove catalyst from the product are eliminated, and the production process is simplified. A recent detailed review by Frost and Mutton provides an overview of chemical transformations using supported catalysts.^[54]

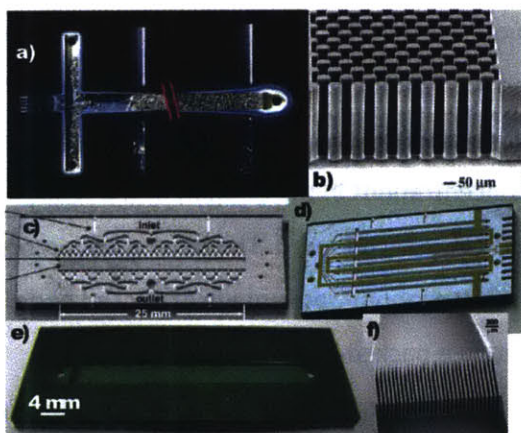


Figure 2. Examples of microreactors for studying heterogeneous reactions. a) Gas-liquid packed bed reactor^[55], b) structured bed of silicon posts for catalysts immobilization^[55], c) cross flow packed bed^[56], d) parallel packed bed with integrated temperature sensors^[57], e) Packed bed and SEM detail (f) of weir for retaining solid catalyst particles.^[58]

The mass transfer rate between two fluid phases is typically enhanced by flowing over an inert packed bed. The overall mass transfer coefficient between a solid catalyst and a fluid flowing through a packed-bed microreactor is typically on the order of $1\text{-}15\text{ s}^{-1}$.^[55, 57, 59]

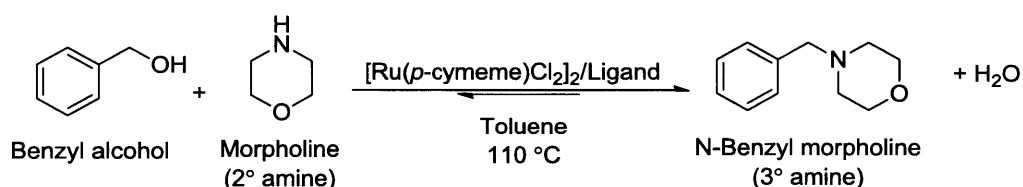
Losey et al.^[59, 60] have found that these mass transfer coefficients are about two orders of magnitude greater than larger scale trick-bed reactors. Furthermore, Losey et al. found that the increased mass transfer in these packed beds did not come at the cost of efficiency on a power-per-reactor-volume basis. With respect to safety, working with micro packed beds on a small scale for catalytic processes is also advantageous. For example, palladium-mediated hydrogen peroxide synthesis from an explosive mixture of hydrogen/oxygen was performed at 20-30 bar.^[57]

Packed bed microreactors are the smallest-scale method of testing immobilized organometallic materials in a flow system, and so naturally they have found application in a number of catalytic processes including Heck coupling, Sonogashira coupling, Suzuki coupling, Kumada coupling, olefin metathesis, hydrogenation, hydroformylation, epoxidation, cyclopropanation, and benzannulation.^[54] These immobilization tests have contributed towards solving the industrial problem of downstream catalyst separation and recycling of the corresponding homogeneous catalyst. Some representative examples from this field are discussed in this section.

The reduced activity of a catalyst upon immobilization is an issue in this field. Since one of the purposes of these immobilization techniques is to obtain a higher turnover number (TON), and since a reduction in activity may require higher catalyst loadings (and therefore lower TON), maintaining an active catalyst is of paramount importance. The other purpose of the immobilization is to keep heavy metal concentrations in the effluent of the reactor low – typically less than 10 ppm for pharmaceutical applications.^[7] The latter goal is more frequently accomplished than the former. Another economic advantage of packed beds is process intensification. Under typical conditions in a packed-bed microreactor, a large amount of catalyst is present compared to the amount of substrate in the reactor. The high catalyst loadings relative to the substrate holdup in a packed bed reduces residence times, which implies smaller reactor volumes to meet a required throughput.

Functionalized polymers have been loaded into monoliths to carry out a number of other transformations, including catalytic transfer hydrogenation, heck reactions, and dynamic kinetic resolutions of epoxides.^[61] One example of a solid supported ruthenium catalysts, Lamb et al. successfully coupled amines and alcohols via a metal-catalyzed hydrogen transfer reaction utilizing ruthenium complexed to an immobilized, polymer-bound phosphine ligand (Scheme 1).^[62] Initially running at 150 °C in toluene at 5 bar

backpressure, they observed a decrease in yield in conjunction with the reactor outlet's product stream turning from clear to dark red. This was attributed to ruthenium leaching. Running the reactor at 150 °C at 0.1 ml/min under atmospheric pressure with the higher boiling *p*-xylene led to high conversions (98%) and reduced ruthenium leaching. In order to test catalyst stability, the reactor was run continuously at these conditions, using a feed solution of 16 vol% reactants in *p*-xylene for 72 h, processing nearly 500 mL of feed. The calculated TON was 438, which compared favorably to typical homogeneous systems operating at 1 mol% of catalyst (TON = 100). Immobilized catalyst systems often have a more narrow range of possible solvents to prevent catalyst leaching.



Scheme 1. Ruthenium-catalyzed hydrogen transfer reaction.^[62]

Lim et al.^[63] attached a copper-based cyclopropanation catalyst to siliceous mesocellular foam (MCF) microparticles and capped leftover silanol groups with hexamethyldisilazane (HMDS). The authors found the nitrogen byproduct to be detrimental to their conversions and enantioselectivity, so a recirculating flow setup was built to continuously remove the nitrogen from the system (Figure 3). The effluent was then fed back into the reactor until full conversion was obtained. They found their catalyst to retain its enantioselectivity, and good catalyst activity was obtained as well (75 min total recirculation time per run). Furthermore, only 8% of their copper leached from the bed after 20 reuses of the catalyst, giving a total TON of about 3500. These results were the product of in-depth optimization of the catalyst support system. The linker length and rigidity, ligand loading on the MCF, and pre/post silanol capping procedures were optimized to give good catalyst stability, activity and enantioselectivity.^[63] Lim et al.^[64] also applied their recirculation flow reactor to a metathesis catalyst supported on MCF, this time to remove the ethylene byproduct with a TON of over 700 achieved (with high conversions). It should be noted that these recirculating flow reactors need to be run batchwise.

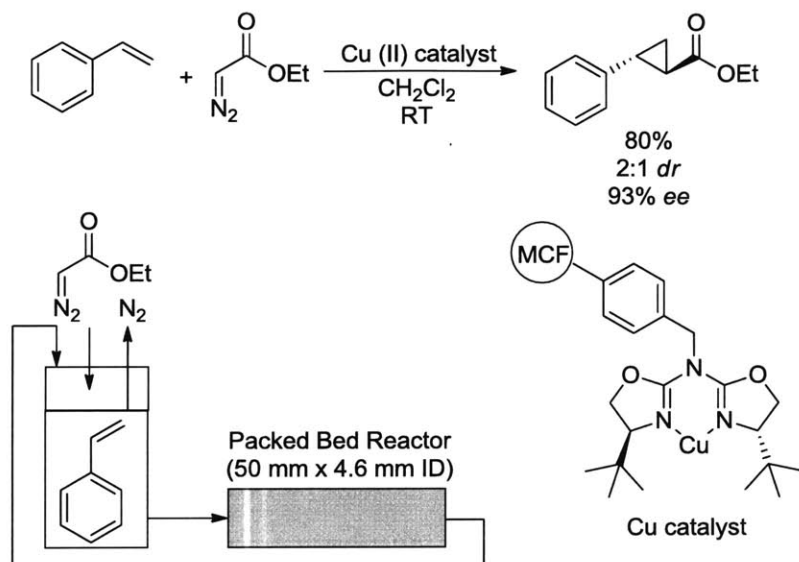
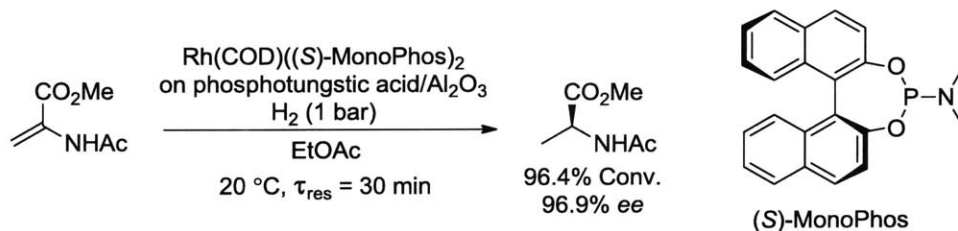


Figure 3. Enantioselective copper catalyzed cyclopropanation supported on siliceous mesocellular foam (MCF) microparticles. Recirculating flow reactor must be run in a batchwise fashion.^[63]

Following explorations by Simons et al.^[65], Madarász et al. heterogenized a cationic rhodium complex electrostatically to phosphotungstic acid/alumina and tested it in an H-Cube reactor.^[66] The asymmetric hydrogenation of the common test substrate methyl-2-acetamidoacrylate (MAA) with the immobilized $\text{Rh}(\text{COD})((S)\text{-MonoPhos})_2$ (Scheme 2) was optimized over temperature, concentration, pressure, and residence time. After optimization, a packed bed was subjected to a continuous substrate feed for 700 minutes before conversions and ee's dropped significantly. We estimate their TON to be at least 1400 with an average TOF of about 120 h^{-1} for residence times on the order of one second. This compares favorably to one-pass homogeneous tests for this substrate giving a TOF near 1200 h^{-1} at 5 bar.^[67] Leaching was low ppm or less based upon batch tests. One limitation of this technique is that polar protic solvents increase leaching substantially due to the non-covalent nature of the immobilization, which narrows which solvents can be used.



Scheme 2. Hydrogenation of MAA using an immobilized rhodium catalyst at a few bar of pressure.^[66]

1.2 Fundamentals of Chemical Synthesis in Small Scale Flow Systems

1.2.1 Reactive Small Scale Flow Systems

The work in this thesis applies a number of fundamental reaction engineering principles to small-scale flow systems. The relevant fundamentals, as they pertain to small scale flow systems, are briefly reviewed in this section. A transient, laminar flow reactor with an n^{th} order reaction (without volume change) can generally be described with the conservation equation:^[68]

$$\frac{\partial C_A}{\partial t} + v_x \frac{\partial C_A}{\partial x} = D \left(\frac{\partial^2 C_A}{\partial x^2} + \frac{\partial^2 C_A}{\partial y^2} \right) - k C_A^n \quad (2)$$

In this background section, various simplifications of this equation will be explored as they apply to small scale flow systems. Consider the simplest case of a plug-flow reactor which is at steady-state. In this case, there is no axial diffusion in the reactor and concentration is uniform across the channel width. Moreover, the velocity in the reactor is the same for every fluid element in the reactor. At steady-state, every point in a plug flow reactor should have an unchanging concentration. Batch reactors and steady-state plug-flow reactors obey the same equation with the difference being that experimental time in a batch reactor corresponds to residence time in a plug flow reactor. Consider the kinetic equation for a batch reactor:

$$\frac{dC_A}{dt} = -k C_A^n \quad (3)$$

Where C_A is the concentration of reactant, k is the rate constant, and t is experimental time. At steady-state in a plug-flow reactor, it is also true that:

$$\frac{dC_A}{d\tau} = -k C_A^n, \text{ where } \tau = \frac{V}{\dot{v}} \quad (4)$$

Where V is the reactor volume and \dot{v} is the flow rate. τ is the residence time in the reactor rather than the experimental time, t . Figure 4 from Moore and Jensen^[69] visually

represents the relationship between residence time in a plug flow reactor and experimental time in a batch reaction.

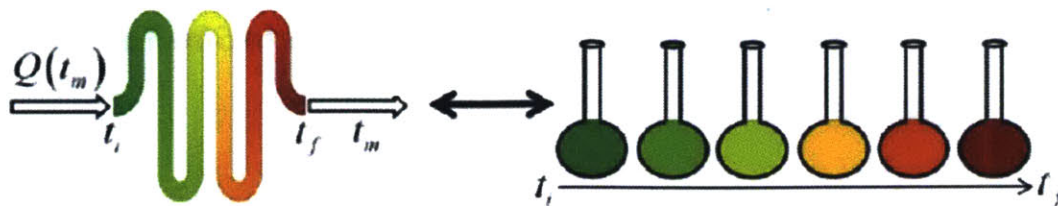


Figure 4. Representation of a plug-flow reactor vs. a dynamic batch experiment from Moore and Jensen.^[69]

In order to vary residence time in a plug-flow reactor, flow rates are normally changed and the system approaches steady state after three or more residence times. This behavior is time consuming for long residence times. In an effort to alleviate this experimental inefficiency, techniques have been developed to screen residence times and concentrations under transient operation, allowing conditions to be screened more efficiently. The equation governing this process is a transient plug-flow reactor:

$$\frac{\partial C_A}{\partial t} + \frac{\partial C_A}{\partial \tau} = -kC_A^n \quad (5)$$

Note that both experimental time, t , and reactor residence time, τ , are present in the differential equation. This equation, when solved with the correct boundary conditions, can describe a transient flow-ramping experiment using a plug-flow microreactor. Moore and Jensen^[69] showed that, when pump flow rates were continuously ramped during microreactor operation, a predictable residence time is experienced by outlet fluid exiting at any given experimental time. Sampling the reactor outlet at different experimental times thus allowed for the effective sampling of different residence times, as related by Equation 5. More importantly, these samples, representing different reactor residence times, were consistent with those obtained by waiting for a reactor to reach steady state at a fixed flow rate before sampling. This recent advance in taking advantage of the plug-flow characteristics of microreactors can be used to efficiently screen kinetics under conditions which are impractical or inaccurate to probe with batch experiments. We make use of a modified version of this technique to screen hydrogenation kinetics in Chapter 4 of this thesis.

1.2.2 Dispersion

Treating a microreactor as a plug flow reactor is a useful concept, but as flow rates increase and the width of the channel becomes larger, this assumption eventually fails. In laminar flow, which governs many small scale flow systems, the fluid in the center of the tube is moving twice as fast as the average fluid velocity, resulting in axial dispersion. Axial dispersion is also affected by diffusion. The presence of dispersion in a reactor means there is a distribution of residence times rather than a single residence time. Figure 5 shows the residence time distribution (RTD) for a microreactor. When a tracer is pulsed into the reactor, the effluent concentration can be measured in terms of absorbance. Although the average residence time is 1,143 seconds (Figure 5), the tracer also exits the reactor at substantially earlier and later residence times. This behavior, called Taylor Dispersion, is predicted by the equation:^[70]

$$\frac{\partial C_A}{\partial \tau} = D \frac{\partial^2 C_A}{\partial x^2} - k C_A^n \quad (6)$$

Where D is the dispersion number, which will be discussed in greater detail later in this section. Many fluid elements spend substantially more or substantially less time in the reactor than the average residence time set by the flow rate and reactor volume in Equation 4. This in itself can affect yield and/or selectivity. Furthermore, there can be significant interaction between fluid packets of different residence times in the reactor, which can adversely affect selectivity. It should be noted that the average residence time does not change as dispersion increases.

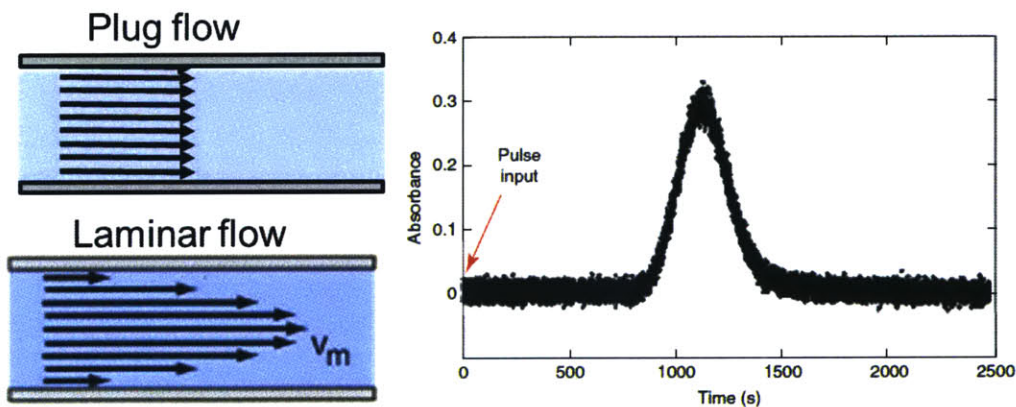


Figure 5. Fluid velocity profile in plug flow vs. that in laminar flow (Left). Residence time distribution of a microreactor (Right).^[71]

A continuously stirred tank reactor (CSTR) represents the extreme form of total dispersion, where fluid packets of all residence times are mixed together. As a flow reactor approaches the behavior of a CSTR via increasing dispersion, yield and selectivity will suffer in most systems, as can be predicted using textbook approaches.^[70] Thus, it is important to design microfluidic systems to avoid dispersion, and to know when dispersion exists so as to interpret data appropriately. The magnitude of the Bodenstein number indicates whether large deviations from plug flow exist. The Bodenstein number is defined as:

$$Bo = \frac{uL}{D} \quad (7)$$

Where u is the velocity of the fluid, L is the length of the reactor, and D is the dispersion number. The dispersion number represents the “effective diffusivity” of a species along the length of a microreactor when including the hydrodynamic effects from laminar flow. It can be predicted depending on the flow conditions.^[70] For $10,000 > Bo > 10$, the Taylor-Aris dispersion model applies:

$$D = D + \frac{u^2 d_t^2}{4\beta D} \quad (8)$$

Where D is the molecular diffusion coefficient, d_t is the tube diameter or channel width, and the parameter β is 48 for tubes and 30 for square channels. Nagy et al.^[72] derived plots (**Figure 6**) that give the Bodenstein number (Bo) as a function of channel width and the residence time for conditions frequently encountered in small scale flow systems. For $Bo > 1000$, plug flow is a good assumption. For $100 < Bo < 1000$, small deviations from plug flow occur and for $10 < Bo < 100$, larger deviations occur. These cases can be modeled using the classical Taylor-Aris approach to dispersion (Equation 4).^[70] When $Bo < 10$, alternative models are needed for accurately predicting reactor performance.^[70]

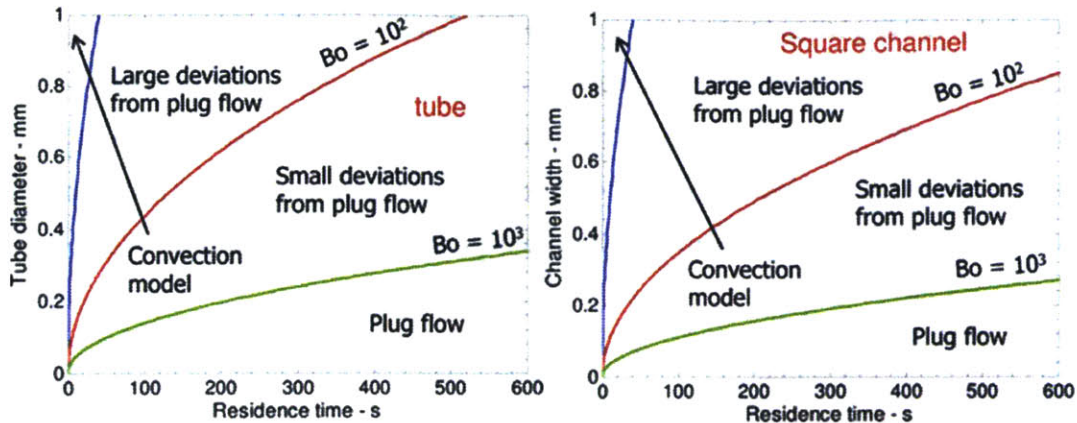


Figure 6. Given a certain channel width (for square channels) or tube diameter (for tubes) and the residence time, deviations from plug flow can be predicted. Figures from Nagy et. al.^[72]

The relative terms 'small' and 'large' in Figure 6 can be understood with an example. Consider a reaction which reaches 95% conversion at a 300 second residence time in a 400 μm diameter tubing. According to Figure 6, there will be small deviations from plug flow, which implies a <1% decrease in conversion for first and second order reactions. When large deviations from plug flow are present, <3% decrease in conversion will generally result at 95% conversion. Effects will generally be larger for substantially lower conversions. For example, a <5% decrease in conversion is expected in the 'Large Deviations' regime when running a reaction at 50% conversion. Reaction engineering textbooks^[70] were used to derive these numbers, and should be consulted for details on how to calculate dispersion numbers and their effects for conditions not considered here (larger tubes, higher flow rates, operation at different conversions). As mentioned in the introduction to this section, systems with high dispersion approach the behavior of a CSTR in the limit of infinite dispersion. Reduced dispersion is one reason why small-scale reactive flow systems can often outperform larger scale flow systems. Special considerations have to be included with extending the above discussion for homogeneous laminar flow to reactors loaded with static mixers or solid spheres.^[70]

1.2.3 Mixing in Flow Systems

Each of the flow systems discussed in this work utilize at least one passive, diffusion-based mixer. The rate at which two fluids are mixed can have a large effect on selectivity

and yield for fast reactions.^[73-75] This section will provide a basis for understanding these effects and predicting when improved mixing techniques are expected to be beneficial. This concept has recently been discussed by Nagy et. al.^[72] specifically for small scale flow systems, and so this section will follow their analytical approach. When two miscible laminar streams are mixed in a T-junction, mixing occurs via diffusion only between the two streams (unless very high flow rates are used^[76]), and a homogeneous mixture will result after some mixing time, τ_{Diff} .

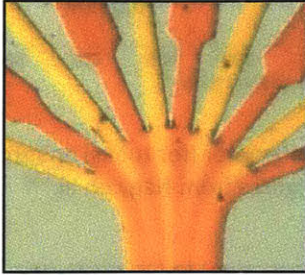


Figure 7. Mixing of homogeneous acid-base system in a microfluidic junction. The yellow and orange streams mix via diffusion only.^[77]

The timescale for mixing is approximated to be the diffusion timescale:

$$\tau_{Diff} = \frac{d_t^2}{4D} \quad (9)$$

Where d_t is the diameter or channel width and D is the diffusion coefficient. For a reactive process, comparing the reactive timescale with the diffusion timescale allows us to estimate whether a reaction rate is limited by diffusive mixing. If a selectivity profile determined by a reaction's intrinsic kinetics is desired for a fast reaction, then such diffusive limitations will hurt selectivity. The Damköler number, Da , represents the ratio of reaction to diffusive mixing rates:

$$Da = \frac{\text{Rate of Reactoin}}{\text{Rate of Diffusive Mixing}} = \frac{\tau_{Diff}}{\tau_{Rxn}} = \frac{kC_0^{n-1}d_t^2}{4D} \quad (10)$$

Here, C_0 is the initial concentration of reacting species, and k is the reaction rate constant. For $Da < 1$, we expect improved mixing to have a negligible impact whereas for $Da > 1$ improved mixing techniques are recommended for optimal yield and selectivity. The Damköler number can be easily estimated if the rate constant is known. For a first order reaction, the relationship between the rate constant and conversion follows the form:

$$k = -\frac{\ln(1 - X)}{\tau} \quad (11)$$

Where X is the conversion after some residence time, τ . A single experiment is thus sufficient to obtain an order-of-magnitude estimate the rate constant for use in our calculation of Da . For reactions of higher order and various initial concentrations, Nagy et al.^[72] provide convenient tables and charts for estimating whether mixing is important for reactions. A plot of various Damköler numbers for our example of a first order reaction is shown in **Figure 8**.

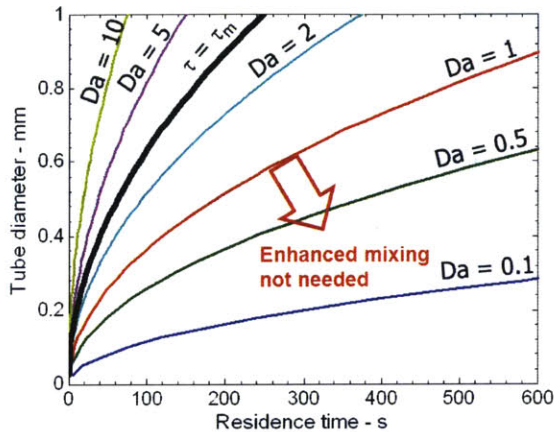


Figure 8. Plot of Da as a function of tube diameter and residence time (for 95% conversion), assuming a T or Y-junction is used for mixing the streams. For $Da < 1$, the diffusion rates exceed the reaction rate and so no additional mixing scheme is necessary.

For cases where $Da > 1$, improvements in performance can be obtained using passive micromixers in which the inlet streams are laminated into smaller streams and then mixed by diffusion over smaller length scales,^[74, 78] but these mixers are especially prone to clogging. Another effective method is introducing an inert second phase into the channel, causing segmented flow and internal mixing.^[79] If the reaction does not proceed at low temperatures, a cooled mixing zone can be included in the system, to ensure that the reaction begins only after mixing is complete. The diffusive timescale (Equation 9) can be used to estimate the required mixing time for this approach.

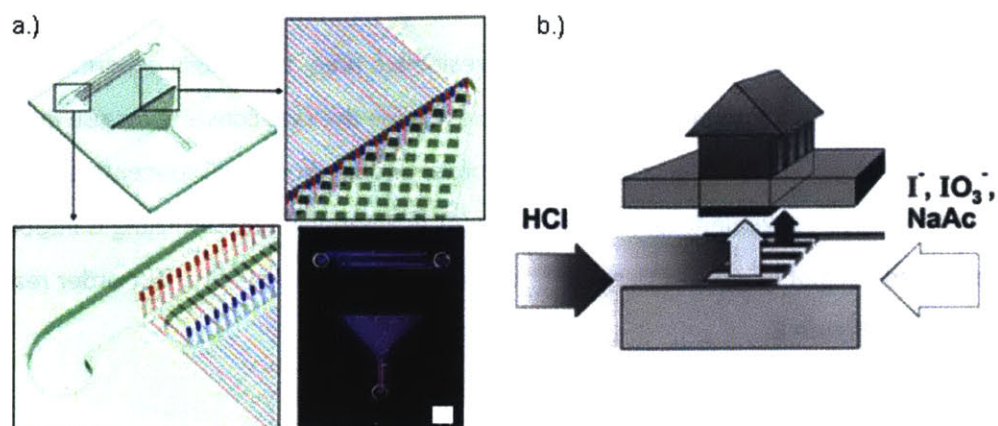


Figure 9. Illustration of micromixing via stream lamination and recombination. a.) The blue stream and red streams are first split into small-diameter channels before being contacted.^[78] b.) Acid and base being mixed via a similar stream lamination approach.^[80]

1.2.4 Liquid-Liquid Systems

The application of biphasic liquid-liquid reactions to microfluidic systems is particularly interesting because of the opportunities to manipulate flow patterns between the two immiscible phases. High rates of mass transfer between the two phases can be achieved, often leading to significant enhancements in reaction rates and selectivity. The flow of two immiscible liquids in a microreactor displays different hydrodynamics depending on both the absolute and relative velocities of the two liquids involved (Figure 10).^[81, 82] Segmented flow is the most common liquid-liquid flow regime used for chemical synthesis in microfluidic devices. During segmented flow, the individual packets of fluid undergo internal recirculation, so-called Taylor flow, which improves mass transfer between the two phases.

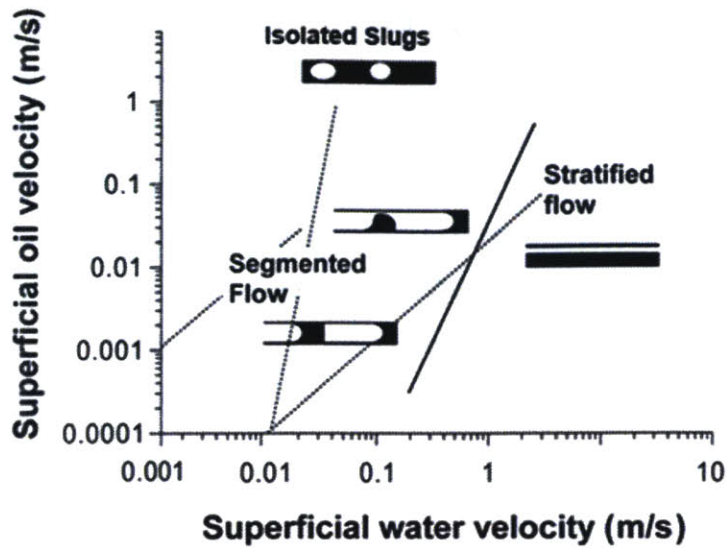


Figure 10. Different flow regimes for liquid-liquid flow in microchannels.^[82] The continuous phase is defined as the phase wetting the walls of the channel.

As one might expect, mixing two miscible liquids along with an inert immiscible liquid to form segmented flow will provide enhanced mixing exceeding that from just diffusion between the miscible liquids (see Figure 11).^[83] Mixing times between 100 ms and 10 seconds can be obtained in 400 μm channels depending on the flow conditions^[82], with mixing times less than 100 ms having been obtained for smaller channels.^[83] This represents a significant improvement compared to mixing two miscible fluids without an added inert phase, which takes on the order of a minute for a 400 μm channel.

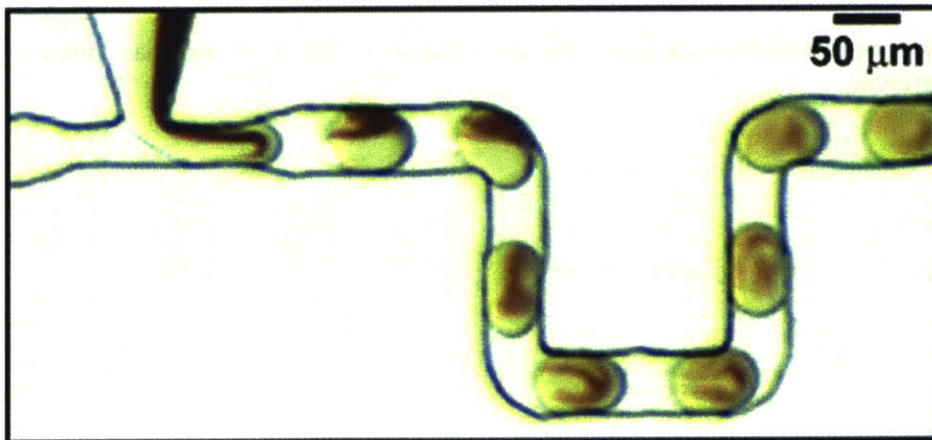
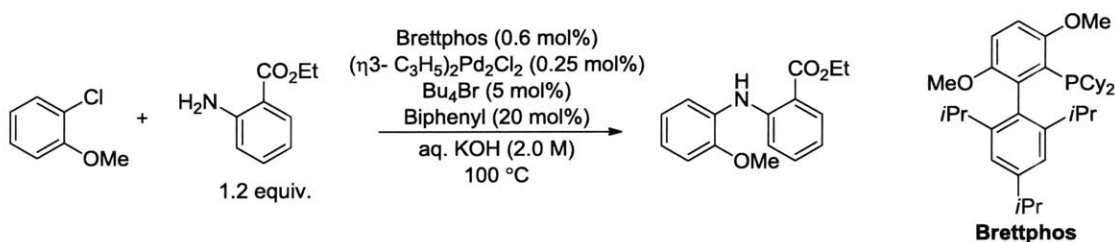


Figure 11. Mixing via segmented flow from Song et al.^[83]

The improved rates of mass transfer in segmented liquid-liquid flow are not always sufficient to provide high conversions at low enough residence times. This situation arises if the reaction is very fast or if the reactants of interest are both highly insoluble in the phase containing the other reactant. Further improvements in mixing can be achieved by using a packed bed of inert beads. For example, Bogdon et al.^[84] demonstrated that segmented flow into a packed bed created fine emulsions, significantly enhancing mass transfer between the two phases in alcohol oxidation experiments. Naber and Buchwald^[85] examined a palladium-catalyzed C-N cross coupling reaction in water-toluene (Scheme 3). This two-phase approach was taken to avoid precipitation of salt byproducts in the microchannel, but introduced a mass transfer limitation to the reaction rate. At 80°C in batch with a fast stir rate (~900 rpm), 94% yield was obtained 6 hours. Using a small diameter PFA tube with segmented flow under similar conditions produced a yield of ~20% obtained in 10 minutes (Figure 12). When inert stainless steel beads were packed into the tube, the mass transfer was greatly enhanced, and full yield was obtained in 6 minutes under equivalent conditions. The high catalyst loadings used in these examples motivated Chapter 5 of this thesis, which considers the recycle of this palladium catalyst in flow.



Scheme 3. Example of palladium-catalyzed C-N cross coupling reaction run in two phase (toluene-water) flow.

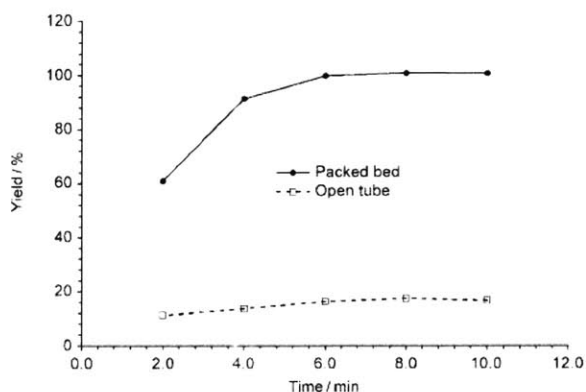


Figure 12. Coupling reaction using $n\text{-Bu}_4\text{Br}$ as a phase transfer catalyst (optimized to 1 mol%). Segmented flow results vs. two-phase flow through an inert packed bed.^[85]

1.2.5 Gas-Liquid Systems

Analogous to the liquid-liquid flows in the previous section, gas-liquid flows in microreactors have different flow regimes depending on the flow velocities of the different phases (Figure 13). For a fixed liquid flow rate, adding gas first creates a bubbly flow, which at higher gas flow rates transitions to slug flow.^[86] Slug flow is the analogue of segmented flow for the liquid-liquid flows. Further increases in gas flow leads to annular flow in which a thin liquid flow wets the wall and the central core is mostly gas. The different regimes have different mass transport and residence time distribution properties.^[82]

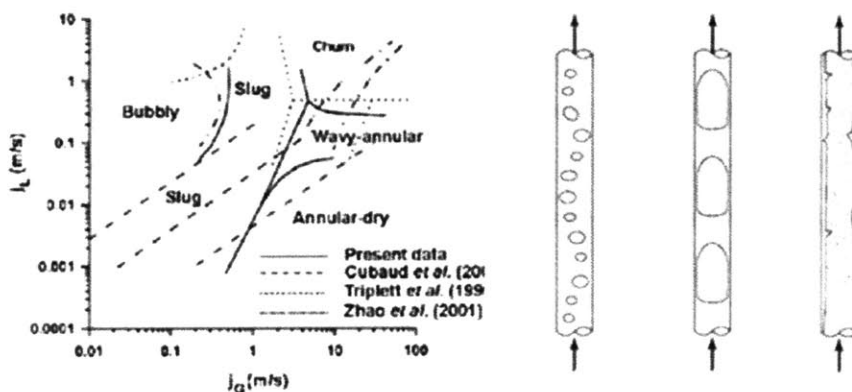


Figure 13. Gas-Liquid flow regime diagram for microreactors.^[82] Picture of common gas-liquid flow conditions (left to right: bubbly, slug, annular).^[86]

Similar to liquid-liquid segmented flows, slug flow (Taylor flow) for gas-liquid flows occurs with strong internal recirculation which provides fast mass transfer. The rate of mass transfer has been shown to depend upon a number of variables including the length of the slugs/bubbles, channel diameter, and flow rates of the respective phases. These dependencies have been examined experimentally, as well as with computational fluid dynamic models.^[87, 88] Volumetric mass transfer coefficients quantifying the rate of mass transfer from the gas to the liquid on the order of $0.01\text{-}0.1\text{ s}^{-1}$ are typical for gas-liquid Taylor flow.^[89] If mass transfer from the liquid to the wall of the tube is of interest, coefficients of a similar order of magnitude have been observed,^[89] and have been calculated for variations in parameters such as slug length, gas holdup, and tube

diameter.^[88] If these mass transfer coefficients are insufficient, either an inert solid phase can be introduced, or operation in the annular flow regime can be considered (Figure 13). This latter regime is particularly useful for highly exothermic reactions with low gas solubility such as the direct fluorination.^[90]

Synthetic chemical transformations using toxic and/or corrosive gases are challenging to perform due to their hazardous and strongly reactive nature. Examples of gas-liquid reactions that have been successfully adapted to flow include hydrogenation^[55], aminocarbonylation^[91], fluorination^[90], and ozonolysis.^[92] Gas-liquid separators can also be integrated to separate the gaseous phase after completion of the reaction.^[79] The use of high pressures allows higher concentrations of gas phase species in the liquid phase than is the case conventionally, leading to the common observation of faster reaction rates. Moreover, given the comparatively small amounts of gas used in these systems, many of the special precautions normally required for handling dangerous gases are significantly reduced. This work utilizes this aspect of small scale flow systems in Chapter 4, where the recycle of a hydrogenation catalyst is considered.

1.2.6 Automation and optimization

Significant improvements in microsystem technology in the past decade has allowed many automation aspects to be routine, and were taken advantage of in this thesis. Autosamplers, valves, pumps, and fraction collectors can be controlled via a computer to run reactions in microreactors in an automated fashion. Such automated systems can be used for screening various reagents for a target synthetic step, profiling the design space of a known reaction, or optimizing a known reaction.^[93] Griffiths-Jones et al. were able to screen 48 combinations of sulfonamides (common medicinal functionalities) using the system outlined in Figure 14.^[94] Boc-protected sulfamides were screened, with immobilized sulfuric acid moieties to deprotect the sulfamide after alkylation. In many cases the products were pure enough for direct biological application without further purification. Purity was determined by offline UPLC.

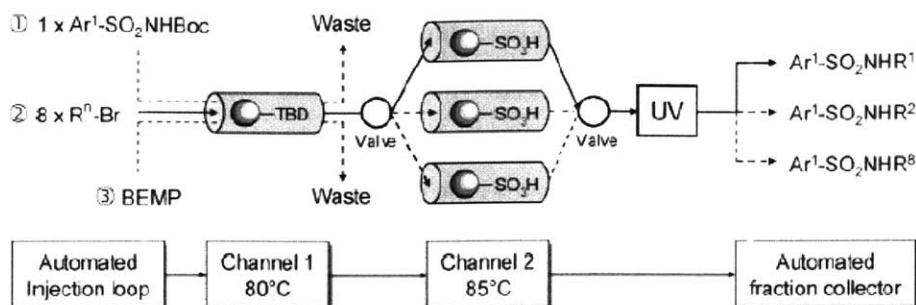


Figure 14. Automated screening system from Griffiths-Jones et al.^[94]

A related application of automated microreactor systems is systematically probing the design space of reactions of known interest. Sugimoto et al. recently built a system which automatically screened residence time and temperature. After intermediate offline HPLC analysis, new conditions were implemented using the information gained on an intuitive basis.

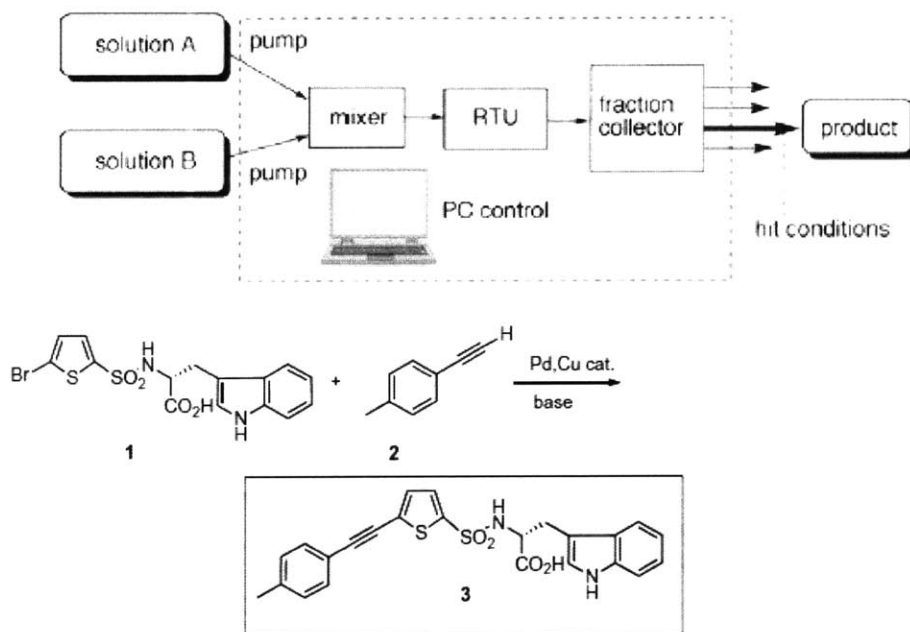
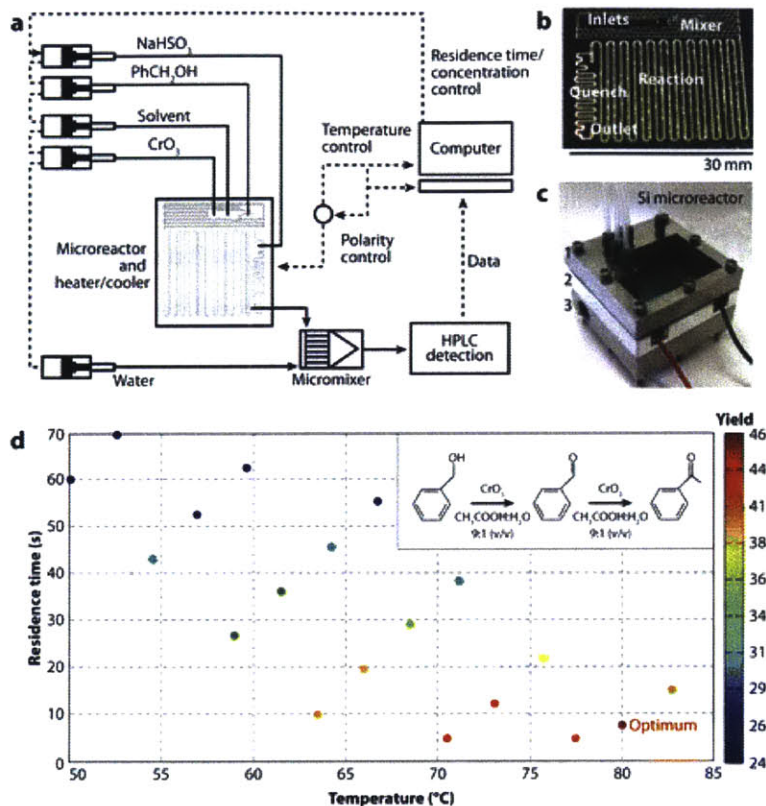


Figure 15. Optimization of a sonogashira coupling reaction.^[95]

The process of probing the design-space was improved upon considerably by using a true optimization approach which continually updated the planned experiments using new data. The automated optimization of the oxidation of an alcohol to an aldehyde using CrO_3

was explored by varying temperature, residence time, two pump flow rates. McMullen and Jensen ref were able to use online HPLC detection to have these results feed back to the computer and automatically update planned experiments using an optimization algorithm. The technology demonstrated to this point has the clear potential to expand upon standard batch optimization approaches.

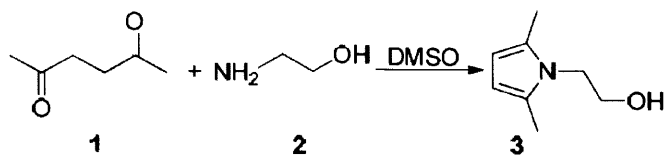


McMullen JP, Jensen KF. 2010. *Annu. Rev. Anal. Chem.* 3:19–42

Figure 16. Four automatically varied parameters produced yields, as determined by inline HPLC, which were fed to an optimization algorithm. In this way, the system was able to continually update planned experiments using recent experiments.

The optimization of a Paal-Knorr reaction over temperature and residence time using an in-line IR measurement device was recently carried out using a similar setup. Moore and Jensen^[96] considered different optimization algorithms and found substantial differences in the number of required experiments to obtain an optimal value of productivity. The use of an in-line IR allowed for a negligible work-up time in between experiments, streamlining the optimization process. Many of the practical aspects of microreactor automation are taken

advantage of and expanded upon in this thesis. Specifically, Chapters 3-5 include automated sample valve switching and flushing, new liquid level measurement systems for use in control schemes, and LabVIEW-controlled HPLC and syringe pumps.



Scheme 4. Paal-Knorr reaction considered by Moore and Jensen.^[69]

1.3 Thesis Goals

The general objectives of this thesis are:

- To investigate the potential of microfluidic and small-scale flow systems to rigorously investigate organometallic catalyst recycling.
- To evaluate the challenges, benefits, and disadvantages of incorporating a nanofiltration membrane into a continuous flow system to recycle the catalyst. Of particular interest are applications involving metathesis catalysts, hydrogenation catalysts, and palladium coupling catalysts.
- To design and improve small-scale process blocks as necessary to aid in the pursuit of objectives (1) and (2) above.
- To develop an understanding of the individual process blocks and their relationships in order to identify opportunities for future work.

1.4 Thesis Outline

Chapter 2 presents the work done in designing thermomorphic solvent systems for catalyst recycle using a microreactor-based screening platform. A water-containing thermomorphic solvent system was developed for an allylic alcohol isomerization catalyst, and successfully applied to enhance the reaction rate by removing mass transfer limitations while preserving catalyst separation. However, the constraints introduced using this catalyst separation approach were deemed too significant for frequent practical application. Since organometallic catalyst recycling systems are already very rare in industry, we decided to investigate the potential the more general approach of nanofiltration.

In Chapter 3 we built a continuous separation and recycle system for a metathesis catalyst. Our continuous recycle system is shown below, and incorporates a new microfluidic membrane module, a microfluidic holding tank with level control, and the application of Teflon AF[®] to a metathesis reaction in flow.

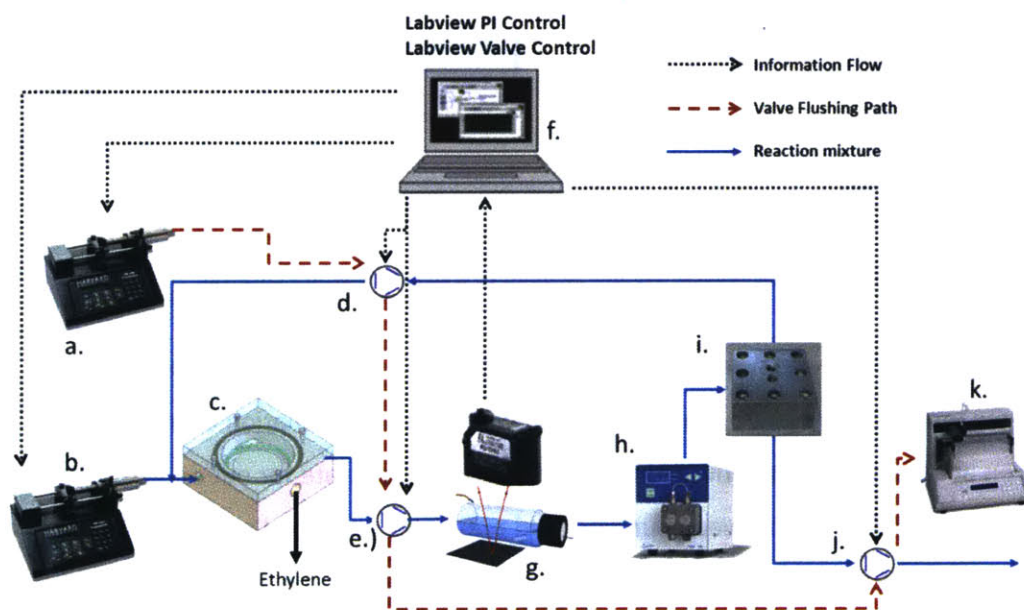


Figure 17. Continuous recycle system applied to a metathesis catalyst.

Chapter 4 applies what was learned from the metathesis catalyst recycle system to design a high-pressure catalyst recycle system for a hydrogenation catalyst. In this case, we employ a catalyst which has not yet been recycled in the literature. For this reason,

significant batch and flow design space exploration experiments were necessary before building the full system. This recycle system was built on a larger scale (less than 50 mL) due to the difficulty in working with microfluidic systems for such a complex application. Our completed recycle system is showing schematically below.

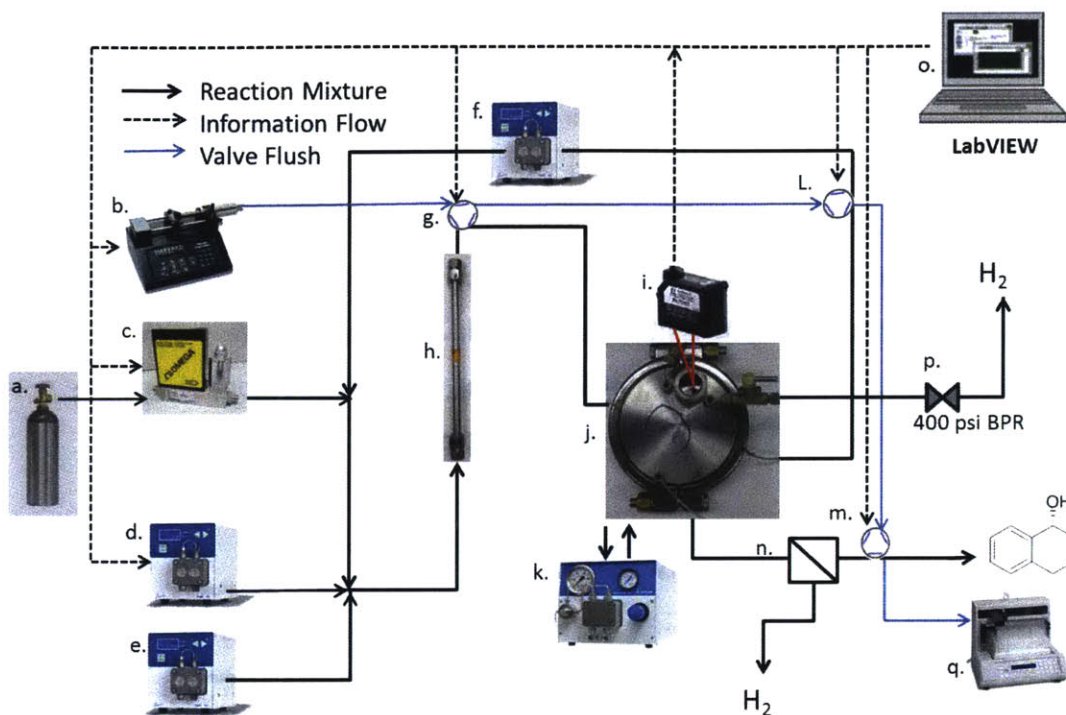


Figure 18. Continuous catalyst recycle system applied to a hydrogenation catalyst.

In Chapter 5, a recycle system on the same scale as the previously described hydrogenation recycle system is built for a Buchwald–Hartwig amination chemistry. We focus on amination and a relatively difficult aryl chloride substrate for our application. This is a significant difference between our work and previously published work. One of the challenges of this application is a liquid/liquid separation before the nanofiltration separation block. A novel small-scale holding tank with a WebCam-based two-phase level control is designed to enact the first liquid/liquid separation. The complete catalyst recycle system is shown below.

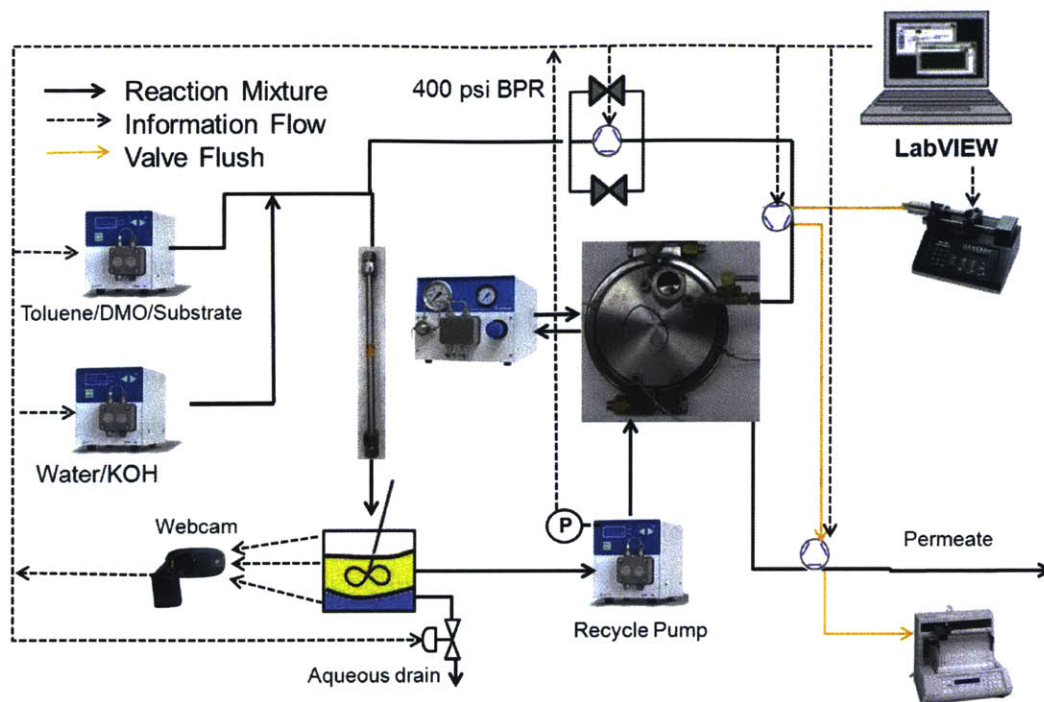


Figure 19. Buchwald-Hartwig amination catalyst recycle system.

In Chapter 6, a dynamic process model is written in Jacobian[®] and the model assumptions/equations are explained. This dynamic process model is applied to the experimental hydrogenation catalyst recycle system in Chapter 4. The model is shown to accurately predict the dynamic mass balances when given sufficient empirical data. The necessary modifications are also made such that the model can approximate the metathesis catalyst recycle system. Both of these applications demonstrate the integrity of the model equations and assumptions.

2 Chapter 2. Thermomorphic Solvent Systems in Flow

2.1 Introduction

Thermomorphic solvent systems consist of a mixture of solvents which form one homogeneous phase or two immiscible liquid phases depending on the temperature of the liquid mixture. This phase behavior is useful in homogeneous catalyst separation. The solvents can be chosen to keep the reagents and catalyst in a homogeneous solution at the reaction temperature to enable fast reaction rates, while at the separation temperature the catalyst remains mostly in one of the two immiscible liquid phases with the product residing mostly in the other liquid phase. This process is shown schematically in Figure 20, below.

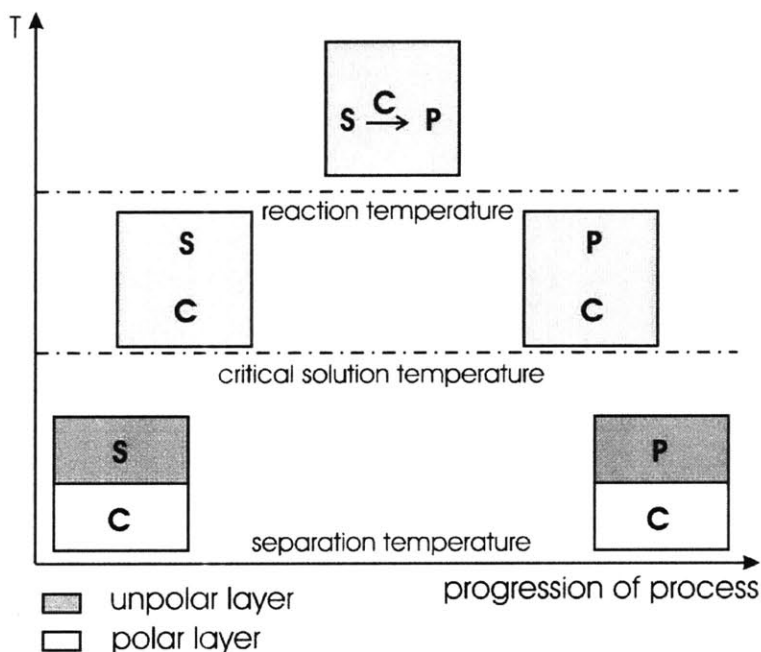


Figure 20. Diagram of a thermomorphic catalyst separation process.^[97]

Thermomorphic phase behavior depends upon a mixture exhibiting an upper critical solution temperature (UCST) or lower critical solution temperature (LCST). Binary UCSTs and LCSTs have been reported for common solvents^[98] and simulated using UNIQUAC/UNIFAC.^[99] A third solvent, however, is often necessary to keep the UCST sufficiently low to permit homogeneous catalyst applications. One motivation for these separation schemes is the temperature sensitivity of many organometallic catalysts (usually

decomposing below 150°C)^[4] which often precludes distillation as a method of separating heavy products prior to catalyst recycling. Thus, UCSTs of interest must be significantly lower than this value. Note the distinction between thermomorphic solvent processes and thermoregulated phase transfer catalysis, in which the catalyst itself is tagged such that it switches between two phases in the event of a temperature change. Common approaches in thermoregulated catalysis are the use of polyethers (such as PEG) tails to tag expensive catalysts^[100], the use PNIPAM and PNOPAM phase tags^[32, 33, 101], or the use of fluororous phase tags.^[102, 103]

A thermomorphic separation system is applied in the literature in cases where biphasic reaction schemes proceed too slowly due to the poor solubility of a reagent in the catalyst phase. One such example is the hydroformylation of higher olefins,^[104] where propylene carbonate, dodecane, and N-methyl-2-pyrrolidone were applied as a thermomorphic solvent system. The importance of this work was the demonstration that good separations could be achieved via the thermomorphic phase splitting if the solvents were chosen carefully. Behr et al. claimed ligand leaching as low as 0.5% into the product phase. DMF/heptane and acetonitrile/heptane thermomorphic systems have been recently applied in hydroamination chemistry with 4% catalyst leaching.^[105] The technique has also been applied to hydrosilylation^[106] and hydroaminomethylation^[21] by the same group. The hydrosilylation example used the solvent composition of cyclohexane/toluene/propylene carbonate at 90°C. Catalyst leaching is typically higher in binary thermomorphic systems than for well-designed ternary systems. Behr et al., for this reason, distinguish between a “Type I” and “Type II” thermomorphic systems based upon the shape of the ternary diagrams (and therefore the separation quality achieved).^[21, 105] A comprehensive set of binary thermomorphic solvent systems which have been verified experimentally are given in Appendix A.

In addition to the use of common organic solvents, thermomorphic solvent systems containing ionic liquids have been explored.^[107, 108] Such systems can make use of the fast reaction rates afforded by thermomorphic systems and combine them with some of the advantages of ionic liquids. Thermomorphic fluororous systems have also been discovered and applied to catalyst recycling.^[109, 110] These systems avoid potential issues associated with using water as the catalyst phase (such as side reactions and catalyst deactivation).

Hansen solubility parameters have been used to qualitatively infer new solvents to try to obtain a better separation for thermomorphic systems,^[104] however the method is not very systematic or reliable for a wide range of solvent types. Hansen solubility parameters are empirical parameters representing how dispersion, hydrogen-bonding, and dipolar forces contribute to molecules' thermodynamic driving force for dissolution.^[111] They have found application in the calculation of mixture critical solution temperatures.^[112] The general definitions and notation for the three types of Hansen solubility parameters are given below.

δ_A^V = Energy required to vaporize A due to dispersion (Van der Waals) interactions

δ_A^D = Energy required to vaporize A due to dipole-dipole interactions

δ_A^H = Energy required to vaporize A due to intermolecular hydrogen bonding interactions

If the three Hansen solubility parameters of two solvents are similar enough, we expect those solvents to dissolve. Some cutoff magnitude r is generally defined such that below some threshold value, R , the solvents are likely to dissolve in one another.^[111]

$$r = \sqrt{(\delta_A^H - \delta_B^H)^2 + (\delta_A^D - \delta_B^D)^2 + 4(\delta_A^V - \delta_B^V)^2} \quad (12)$$

if $r \leq R$, then A and B are miscible

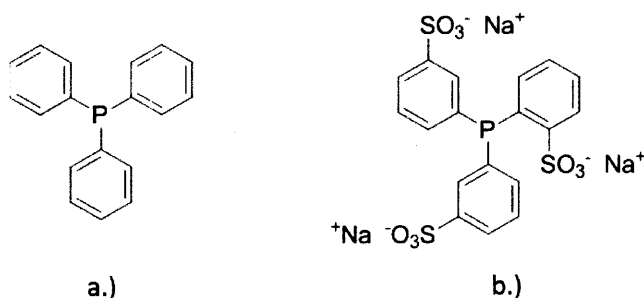
if $r > R$, then A and B are immiscible

Microreactors can be used to efficiently study and implement these solvent systems due to the accurate and precise temperature control when compared to batch experiments.^[113] Furthermore, varying degrees of backpressure are easily employed in such systems, allowing for convenient and efficient exploration of solvent systems with critical temperatures above their pure solvent boiling points. This allows for the exploration of low-boiling solvents in particular, which are expected to be easier to separate downstream via distillation or flashing methods. Silicon microreactors also afford the experimentalist a convenient way to visualize all the residence times within a reactor at once. This is a significant point when studying thermomorphic systems, because as the residence time changes, so does the reactant and product concentrations. These concentrations can in turn affect whether one or two liquid phases are present. In thermomorphic applications it is important that, during

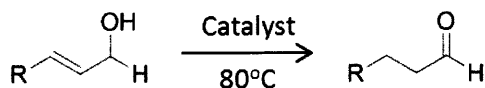
the reaction, the system remains homogeneous. This information is used to ensure easy scalability of the reaction. Microreactors make it easier to reproducibly ensure this is the case with both precise temperature control and easy residence time visualization.

There are few successful applications of water-containing thermomorphic solvents for the purpose of catalyst recycling. Such water-containing thermomorphic solvents could take advantage of simple salt-functionalized ligands such as 3,3',3''-trisulfonated triphenylphosphine (TPPTS). This ligand is generally nonpolar (Scheme 5a), but upon sulfonation (Scheme 5b) becomes very hydrophilic, exhibiting partition coefficients over 1000 between water and nonpolar solvents.^[25] The ligand has been used in industrial-scale hydroformylation.^[114] Herein it is applied in a model isomerization chemistry

Scheme 6).^[115]



Scheme 5. Unmodified triphenylphosphine ligand (a) and its trisulfonated form (b).



Scheme 6. Allylic alcohol isomerization.

This was originally applied as a biphasic chemistry, where longer chained reactants were causing mass-transfer limitations and slow turn-over frequencies.^[115] A long-chain reactant (1-octen-3-ol) was selected for this demonstration. The catalyst salt was designed to be hydrophilic, and the reaction was demonstrated to be quickest in water^[115], so a water-

containing thermomorphic solvent system would be ideal. It is known that water forms lower critical solution temperature mixtures with butanol, THF, MEK, and others,^[98] but these would not be as useful under our reaction conditions. Thus, water-containing thermomorphic solvent systems with relatively low UCSTs needed to be developed. Use of water as a solvent is expected to meet a number of ecological goals in the pharmaceutical industry,^[116] and fits the theme of this work: to minimize heavy metal waste via catalyst recycling.

2.2 Experimental

2.2.1 Solvent Screening Experiments in Flow

Multiple syringe pumps were used when screening binary or ternary solvent systems in flow, each connected to a separate inlet of a four-port microreactor. In this system, the four-port silicon/glass microreactors have three inlets such that the three solvents entered and mixed in a cold zone, then entered the heated portion of the microreactor and were cooled again before exiting. A 240 μ l microreactor was used for this purpose, along with 2-3 Harvard Apparatus Syringe pumps. A 10 ml plastic syringe (Henk Sass Wolf) of pure solvent was loaded into each syringe pump. Anhydrous solvents were used if the solvent was hygroscopic (such as ethanol). The syringe pumps were run until the plastic syringes were primed, at which point the syringes were connected to the microreactors. This would ultimately make it easier to achieve synchronous flow (i.e., avoid backflow from one syringe to another via the microreactor's inlet ports). These syringes were each connected to the microreactor via 0.03" inner diameter 1/16" PFA tubing. When the pumps were started, backflow often occurred, and some pumps needed to be stopped while others were allowed to catch up in applied pressure. The microreactor was heated with an in-house heating chuck to the desired temperature and controlled with an Omega temperature controller with its thermocouple inserted between the graphite sheet of the microreactor heating chuck and the microreactor. For temperatures above the boiling points of the solvents, a 75 psi backpressure regulator from Upchurch Scientific was added to the outlet tubing from the microreactor.

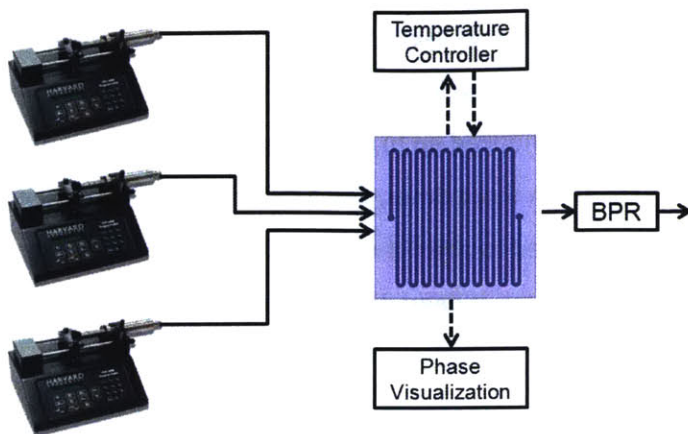


Figure 21. Experimental layout for thermomorphic solvent system screening in flow.

2.2.2 Catalyst preparation for Alkenol Isomerization

A typical $\text{Rh}(\text{TPPTS})_3\text{Cl}$ catalyst batch was prepared with the following method. Using an accurate (± 0.01 mg) analytical balance, 15.78 mg rhodium was massed and added to a 10 ml vial with a screw-on septum. A Teflon stir bar was added. The vial was hooked up to a Schlenk line and purged with argon 4 times. The vial was then put into a glovebox. Inside the glovebox, 136.4 mg TPPTS was massed and added to the vial. The vial was then removed from the glove box and hooked back up to the Schlenk line. Deionized water, degassed via argon bubbling for an hour, was then introduced (4 ml) via Schlenk line. The vial was then mixed and immersed partially in an 80°C silicone oil bath on a stir plate (1000 rpm). When fully heated, the pH of the mixture was tested (always with purged needed). After finding the mixture acidic, about 0.1 ml of degassed 1 M NaOH was added dropwise (slowly, testing the pH frequently) until a pH of 10 was achieved. The mixture continued to be heated and stirred for 20 minutes after a pH of 10 was achieved. The mixture was then cooled, and its pH adjusted back to pH 7 with about 0.1 ml of degassed 1M perchloric acid. Catalyst was added to the reaction in liquid form.

2.2.3 Catalyst Characterization

The rhodium catalyst was characterized via proton and inverse-gate decoupled phosphorous NMR on a 400 MHz NMR instrument. Filling a normal NMR tube with argon, quickly adding sample, and then capping the sample was inadequate in keeping the sample oxygen-free, and oxidation of the catalyst with time was clearly observed in subsequent

NMRs. Instead, an NMR tube with a septum was used. In this way the tube could be connected to the Schlenk line, evacuated, and cycled with argon 4 times before sample addition. The sample of catalyst was also hooked up to a Schlenk line, the needle used to sample the catalyst was purged with argon three times, and a 0.6 ml sample was added to the NMR tube. A similar approach was used to add 0.1 ml of D₂O to the NMR tube. Subsequent NMRs found no substantial catalyst degradation over two days (See Appendix B).

2.2.4 Thermomorphic Isomerization

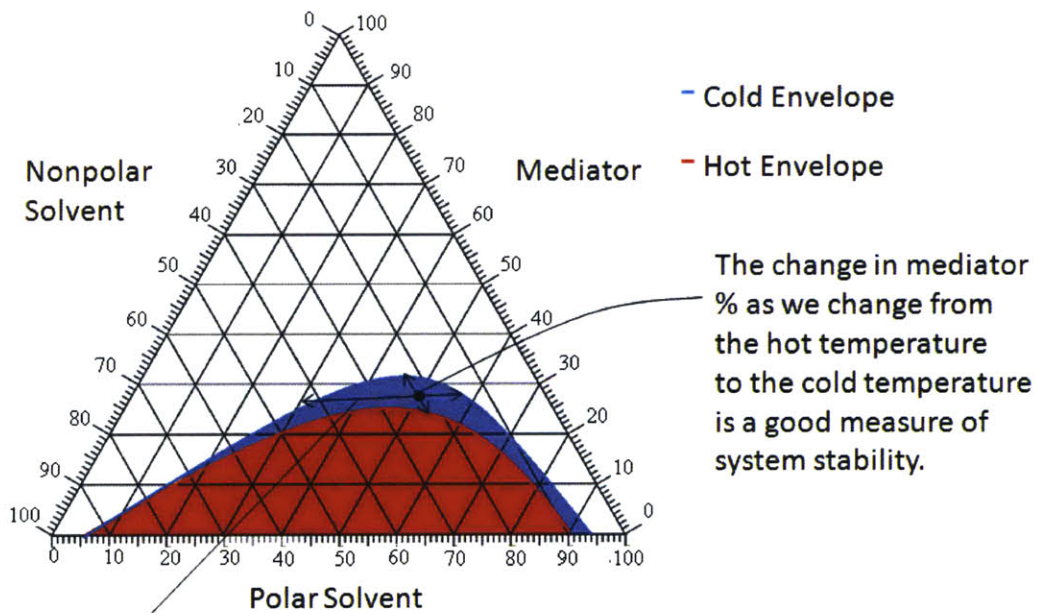
Three Harvard Apparatus syringe pumps were loaded with the catalyst solution, degassed anhydrous ethanol, and degassed ethyl acetate, respectively. The ethyl acetate solution contained 0.65M substrate (1-octene-3-ol) with a hexanol internal standard for GC analysis. The start-up of the three syringe pumps feeds into a 240 µl reactor followed the technique described in the solvent screening experimental section. A flow rate of 2.25 µl/min ethyl acetate solution, 1.75 µl/min ethanol, and 3 ul/min water (with catalyst) was chosen. The microreactor was set to 80°C, and a 75 psi backpressure regulator was connected downstream from the reactor. Samples were taken at 4 and 5 residence times. Samples were collected for 5 minutes and then diluted to a homogeneous solution using ethanol. This was then sampled, run through a Celite column to remove the catalyst, and run on the GC. This ligand has been used in catalysts involved in industrial-scale hydroformylation^[114] it will be applied here in a model isomerization chemistry^[115, 117]: Separate experiments verified that the Celite column had no effect on the result.

2.3 Results and Discussion

2.3.1 Theoretical Exploration of New Solvent Systems

Our theoretical investigation of the behavior of thermomorphic solvent systems was approached with the goal of predicting thermomorphic solvent system behavior using thermodynamic calculations in ASPEN. To this end, two relevant variables were identified during the search for new ternary thermomorphic solvent systems. The first is the polarity difference between the two phases at the separation temperature. Also important is the degree of dependence of mixture solubility with temperature.

The first variable is important when considering the high cost of the catalyst. The second variable is important from a process design standpoint. If the solvents, when mixed in the desired proportion, can be made miscible with smaller changes in temperature, then this ultimately confers more control and flexibility over the eventual process. High temperature dependence will allow a wider range of temperatures (particularly lower temperatures) to be explored when optimizing the reactor. Furthermore, the operating point is more likely to be robust with respect to small disturbances in flow rates at steady state. That is, small changes flow rates (and therefore concentrations) are less likely to force a phase change, resulting in unstable reactor operation. Figure 22 below illustrates these two properties of a thermomorphic solvent system using a ternary diagram. The width of the cold envelop (tie line through the operating point) corresponds to an extent of the separation at low temperature. The change in envelop height with temperature about the operating point corresponds to the temperature dependence of mixture solubility.



The width of the envelope at a tie line drawn through the operating point is a good indication of polarity difference between the two liquid phases.

Figure 22. Explanation of two important criteria in judging ternary thermomorphic solvent systems.

Although UNIQUAC/UNIFAC calculations were ultimately not accurate enough to be useful in predicting ternary solvent systems for practical applications, such simulations did give valuable insight into many relevant trends in phase envelope behavior, and are detailed here. Increasing the nonpolar solvent chain length (hexane → decane → dodecane) increases the polarity difference between the two phases at room temperature. However, longer chain lengths also reduce the temperature dependence of the solvent system miscibility. For example, consider the variation of the nonpolar solvent while holding the polar (water) and mediator (ethanol) fixed. The results of this variation show that decane is an apparent optimum in terms of temperature dependence (vs. hexane, dodecane). As the nonpolar chain length is increased, the separation at low temperature is better (i.e., less expected catalyst leaching), however the temperature dependence eventually suffers when the nonpolar chain length is too long (i.e., dodecane vs. decane). Thus, there is a tradeoff between catalyst separation efficiency and the flexibility of operating temperatures for a thermomorphic reactor.

Differences in mediators (i.e., cosolvents) also play a major role. Their polarities and structures result in differences in the shape of the phase envelopes as well as the temperature dependence of the envelopes. UNIFAC and UNIQUAC were found to be unable to accurately predict which ternary thermomorphic systems were most promising. For example, one of the most successful systems developed by Behr et al., using PC/NMP/dodecane, was found to be inaccurately predicted using UNIQUAC/UNIFAC. The ternary diagrams in Figure 23 demonstrate the deviation from Behr et al.'s data.

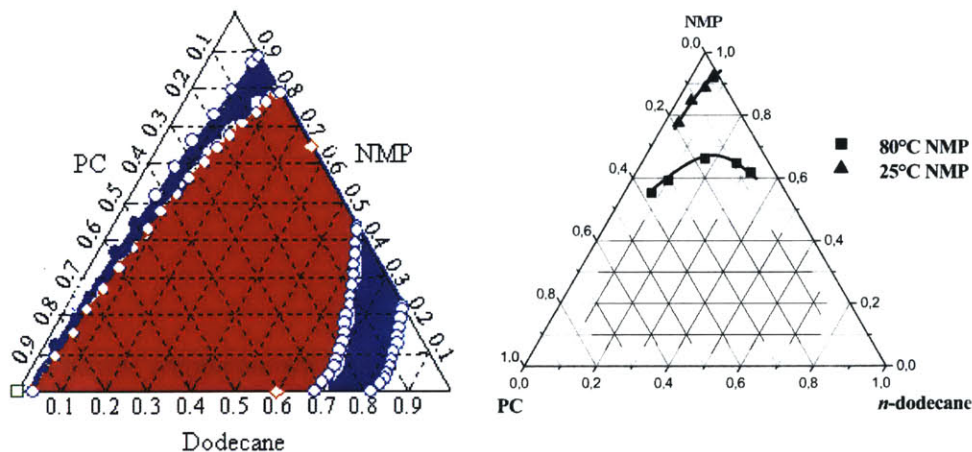


Figure 23: Left: UNIQUAC/UNIFAC simulation of PC-NMP-Dodecane. Right: Data from Behr et. al.^[20]

The difference between the UNIQUAC/UNIFAC predictions and the data have a large impact upon the predicted size of the design space. The UNIFAC/UNIQUAC in this case is underestimating the temperature dependence of the phase envelope. One interesting aspect of this solvent system is the large amount of mediator necessary. This generally occurs when the mediator is very similar to one of the other solvents; if the mediator is too similar, then excess mediator will likely be necessary to achieve a homogeneous phase. This is a good approach to take if the mediator under consideration is an ideal reaction solvent.

Finally, the existence of reactants, products and catalyst in the real reaction solution will tend to have an effect on the miscibility of mixtures and therefore their UCSTs. Consider Figure 24 below, where the addition of an 'educt', morpholine, changes the phase envelope.

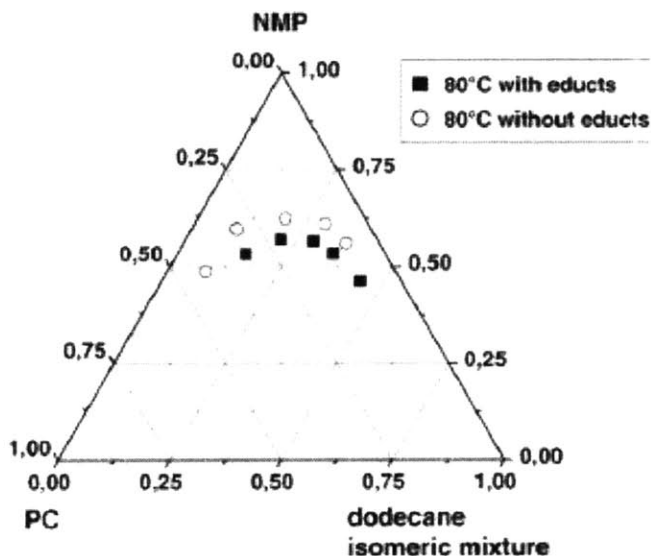


Figure 24. Data from Behr et al.^[20] demonstrating the change in ternary phase behavior with the addition of morpholine.

A simple rule can be used to predict whether the UCST is expected to be increased or decreased under these influences. If an additive is preferentially soluble in one of the two solvents present, the UCST will be raised (and, also the LCST will be lowered). On the other hand, if the additive has similar solubility in both the liquids, the UCST is decreased (and any

LCST is increased). Intuitively, this means that the additive essentially behaves as a cosolvent. Note that for water-containing mixtures these rules may be violated by “water structure enhancers” such as urea and thiourea, as they are often preferentially soluble in water yet have the effect of lowering the UCST of binary mixtures.^[118]

A final conceptual point to be made from the exploration of ternary solvent systems is the sensitivity of the phase envelope to small changes in the structure of solvents. A comparison of the water/cyclohexane/ethanol ternary diagram with that of water/cyclohexene/ethanol demonstrates the sensitivity of design space to small changes in solvent structure. The double bond in cyclohexene allows it to be slightly more polarizable and therefore easier to be miscible with water-ethanol mixtures. Figure 25 below shows our data from solvent screening using a microreactor.

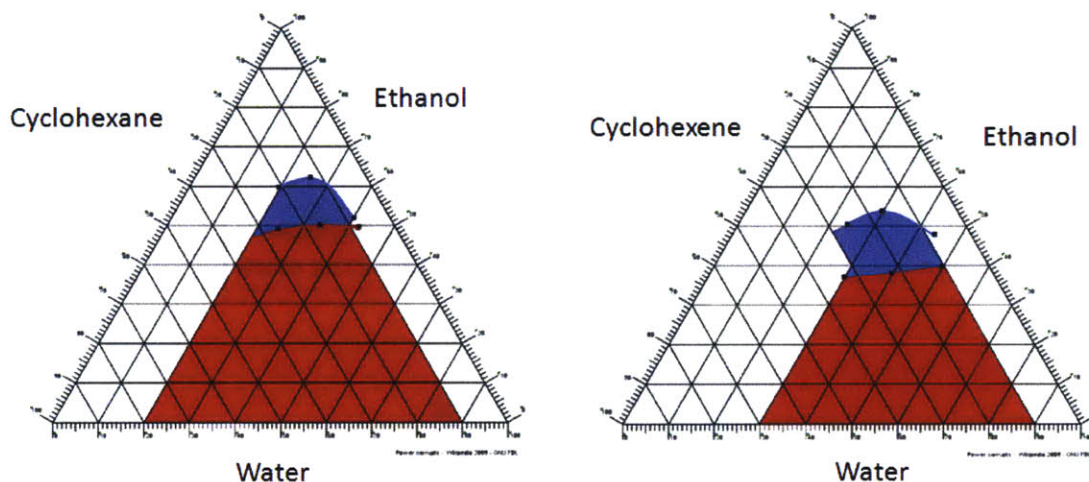


Figure 25. Experimental data (black points in diagram) demonstrating the effect of changing cyclohexane to cyclohexene.

As discussed, UNIFAC/UNIQUAC simulations had a level of accuracy which was useful in predicting whether a mixture of solvents was thermomorphic. However, the inaccuracies of thermomorphic predictions for solvents mixtures have been shown to be too large to be useful in experimental design, especially when considering the significant effects of reagents on thermomorphic behavior. It should be noted this contrasts with the conclusions of Nagy^[71] and Behr et. al.^[104] Substantial thermodynamic modeling work would be necessary to improve this situation, which would ultimately hinge on experimental data collection. Therefore, an experimental approach was chosen to proceed with solvent system discovery.

2.3.2 Experimental Exploration of New Solvent Systems

The reliability of using a microreactor to visualize and determine critical solution temperatures for solvent mixtures was tested with a methylethylketone(MEK)/water/ethanol thermomorphic mixture. For a 2:3 ratio of MEK:water, it was found in batch mixing experiments that between 3.8 and 5.3 vol% ethanol caused the mixture to switch from one to two phases. For a 2:3 ratio of MEK:water, it was found that in flow that between 3.8 and 6.4 vol% ethanol was necessary. Similarly, for 1:1 MEK:water, both flow and batch techniques predicted between 4.8 and 7.4 vol%. These inaccuracies could be reduced by using syringes made of glass or steel instead of plastic. Although the start-up of a plastic syringe pump network was unreliable, the steady-state values were shown to be reliable.

The isomerization of alkenols via a rhodium catalyst with (TPPTS) ligands required a water-containing thermomorphic solvent system to be developed. Our solvent screening technique involved holding the microreactor at the desired reaction temperature (80°C gave high reaction rates^[117]) while flowing solvents with three separate syringe pumps (Figure 21). The flow rate of the syringe pump which contained the mediator was changed every 5 residence times, and miscibility of the solvent system at 80°C and room temperature (reactor outlet) was recorded. This type of experiment gave data which is represented in a ternary diagram in Figure 26.

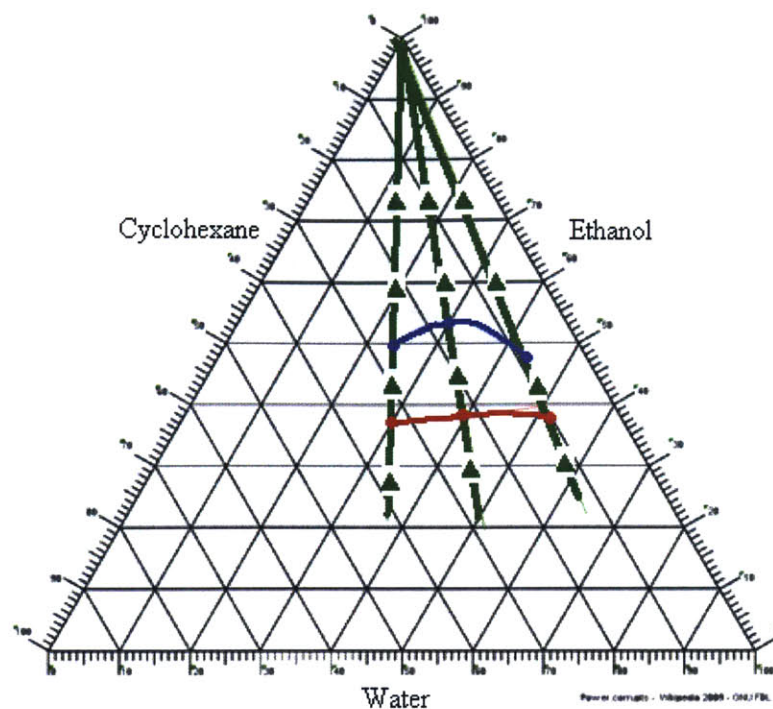


Figure 26. Paths traced on a ternary diagram during microflow solvent screening. Lines between the data points are interpretations of the data.

The green arrows represent the compositions probed in the experiment when the flow rate of the mediator (ethanol in this case) was continually increased. In this way the high temperature phase envelope (red) and low temperature phase envelope (blue) is traced. When following a green line in Figure 26, the percent change in ethanol volume fraction between the red and blue phase envelopes gives us the temperature dependence of the phase envelope. Also of interest is the volume fraction of water in these systems, since high water content is necessary to keep salts dissolved. The results of these experiments yielded a number of potentially useful water-containing thermomorphic solvent systems, shown in the Table 1.

Table 1. Results of microfluidic solvent screening at 80°C. Only the most useful results are shown here.

Polar Solv	Nonpolar Solv	Mediator	Phase Envelope T-dependence*	Water content (vol%)
Water	Ethyl Acetate	Ethanol	45%	30%
Water	Cyclohexene	Ethanol	20%	11%

water	Cyclohexane	ethanol	14%	10%
Water	Heptane	Ethanol	10%	9%
Water	Ethyl Acetate	DMF	40%	33%
Water	Ethyl Acetate	Dioxane	<15%	30%
Water	Ethyl Acetate	Propanol	50%	29%
Water	Cyclohexene	Dioxane	38%	10%
Water	Hexanol	Ethanol	<28%	22%
Water	Butanal	Hexadione	21%	25%
Water	Ethyl Acetate	50:50v Acetone&Ethanol	21%	27%

*Temperature dependence of solvent system measured in terms of the percent change in mediator volume fraction between hot and cold phase envelopes (see Figure 26).

The experimental search for water-containing thermomorphic solvent systems was coupled with a MATLAB Hansen Solubility Parameter (HSP) program which would be used to read from a database of over 700 solvent HSPs. The HSP program found use in the solvent-screening process by having the program return solvents with similar solubility properties to target solvents. Thus, when good combinations of solvents were found experimentally, the HSP program was used to find other solvents with similar solubility characteristics. This method was responsible for discovering the ethyl acetate/ethanol/water system which was ultimately applied to our alkenol isomerization, and the MATLAB code is provided in Appendix C. This search was implemented based upon user input (i.e., distances in HSP-space which worked best in the past) in an attempt to find a useful relationship which could be used to find similar solvents. Differences between HSPs were defined as follows:

$$\Delta\delta_{NP} = \sqrt{(\delta_N^H - \delta_P^H)^2 + (\delta_N^D - \delta_P^D)^2 + 4(\delta_N^V - \delta_P^V)^2} \quad (13)$$

Here, $\Delta\delta_{NP}$ represents the difference between nonpolar and polar solvent solubility parameters in Hansen parameter space. Similar definitions exist for differences between the mediator and nonpolar solvents ($\Delta\delta_{MN}$) as well as differences between the mediator and polar solvents ($\Delta\delta_{MP}$). The solubility parameters have meanings as defined in Equation 12. With water always being the polar solvent, different mediators and nonpolar solvents were experimentally screened. Attempts to correlate the results in Table 1 with various HSP differences ultimately failed. The exact nature of the solvents in each system (functional group interactions, sizes and shapes of molecules), which are not represented in HSP, play too large a role in phase behavior. This runs contrary to the claims of Behr et al.,^[104] who

proposed that HSPs were a useful and generally applicable method of selecting thermomorphic solvent systems.

2.3.3 Alkenol Isomerization

Water-ethanol-ethyl acetate was found to work well as a solvent system for alkenol isomerization. The thermomorphic mixture (~40% v/v water) was polar enough to keep the catalyst salts dissolved (1-6 mol%) at reaction temperature. Furthermore, ethyl acetate and ethanol are both low-boiling, cheap, and relatively benign solvents. However, acidic or basic conditions will likely cause hydrolysis of ethyl acetate to occur, and alcohol reagents could undergo transesterification. This limits the range of application of this solvent system. A catalyst concentration of 6 mM was used with this solvent system (similar to the value used by de Bellefon et al.) to produce the thermomorphic and biphasic isomerization results are shown in Figure 27.

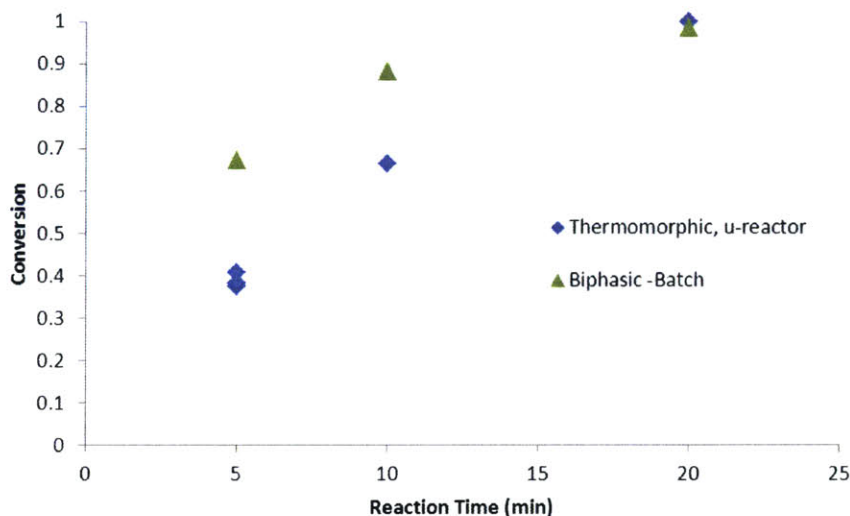


Figure 27. Kinetic data comparing thermomorphic to biphasic reaction performance. All experiments: 80°C, 0.65M 1-Octen-3-ol in nonaqueous phase. 6 mM Catalyst. Thermomorphic: Volume Ratios Ethyl Acetate/Ethanol/Water: 32%/25%/43%. Biphasic: Volume Ratios: Heptane/Water: 43%/57%.

The thermomorphic reaction in the microreactor was not as fast as the biphasic (water/ethyl acetate) when mass transfer is not limiting. The TOF (time \rightarrow 0) of the catalyst in the thermomorphic environment was 450 h⁻¹ compared to rates in water with 4-carbon

chain reactants as high as 2500 h^{-1} from de Bellefon et al. This was probably due to the decreased polarity of the homogeneous thermomorphic system compared that of pure water. The proposed mechanisms of similar ruthenium-based catalysts include a final step of a desorption of an enol, followed by tautomerization to the aldehyde/ketone product.^[119] Since this tautomerization is known to be quickest in water^[120] it has been suggested^[115] that this explains the decrease in reaction rate associated with running in less polar solvents. This can be seen in row 4 of Table 2, where the homogeneous reaction in THF proceeds at a TOF of only 60 h^{-1} .

Table 2. Comparison of TOF from de Bellefon et al. to this work.

Substrate	Method	TOF (h^{-1} , $t \rightarrow 0$)	Source
1-buten-3-ol	Batch, 80°C	2520	de Bellefon et. al
1-hexen-3-ol	Batch-Biphasic, 80°C	490	de Bellefon et. al
1-octene-3-ol	Batch-Biphasic, 80°C	30	de Bellefon et. al
1-octene-3-ol	Batch-Homogeneous, THF, 70°C	60	de Bellefon et. al
1-octene-3ol	Microreactor/thermomorphic/homogeneous, 80°C	450	This work

Despite our results in small scale batch equipment, our scalable thermomorphic system has the advantage of substantially outperforming larger-scale batch equipment. Our 450 h^{-1} TOF for 1-octene-3-ol isomerization is over an order of magnitude faster than 30 h^{-1} for a larger-scale batch reaction. The faster biphasic data can be fit to a simple mass transfer model in order to extract an effective ‘overall’ mass transfer coefficient. Figure 28 below shows the fit, and that a very small overall mass transfer coefficient is obtained: 0.2 min^{-1} , or 0.003 s^{-1} . This small overall mass transfer coefficient reflects the small partition coefficient of 1-octen-3-ol in water.

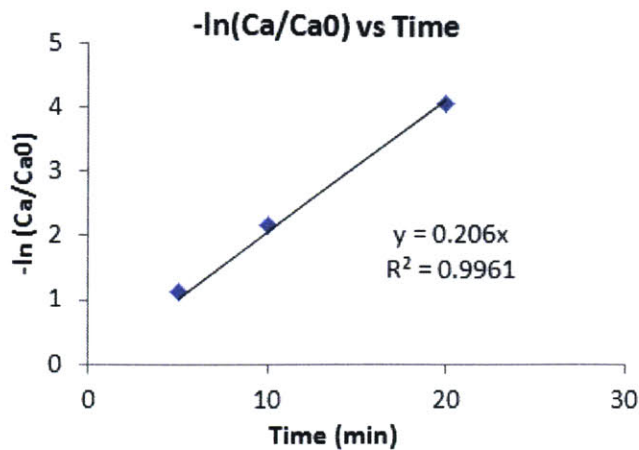


Figure 28. Mass transfer regression from the biphasic batch data from Figure 27.

Figure 29 illustrates how the partition coefficient (m) reduces the magnitude of the overall mass transfer coefficient. In Figure 29, species A (in this case, 1-octen-3-ol) transported from Phase I to Phase II, where it reacts. The mass transfer coefficient calculated from Figure 28, then, represents the overall mass transfer coefficient. Systems with small values of m are the best targets of the thermomorphic approach since even state-of-the-art reactor designs (i.e., optimal k_{La}) may fail to provide reasonable residence times. Assuming the mass transfer in the organic phase is not limiting, we can estimate the mass transfer coefficient in the aqueous phase using solubility data, and we obtain a mass transfer coefficient approaching 2 s^{-1} , which is a very high mass transfer coefficient obtained in our small batch reactor. This explains why the results of larger scale batch equipment from de Bellefon et al. have significantly lower TOFs, and why our kinetically-limited thermomorphic system outperforms the large batch equipment.

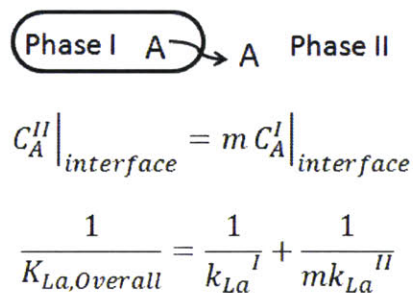


Figure 29. Effect of partition coefficient on multiple mass transfer steps in series.

Since the thermomorphic system is kinetically limited, one can push the catalyst concentration higher (from 1 mol% to 5 mol%) and observe an increase in reaction rate whereas this is not observed for the biphasic, mass-transfer limited case. At these higher catalyst loadings, a 6.6 min reaction biphasic in a microreactor yielded 70% conversion while the corresponding thermomorphic reaction (with the same batch of catalyst) was fully converted at this residence time in the microreactor. The challenge with this higher catalyst concentration is that the catalyst synthesis causes a few equivalents of salt per mole of catalyst. It is expected that, as the catalyst concentration is pushed higher, precipitation will occur, clogging the microreactor. Our ethyl acetate/ethanol/water thermomorphic solvent system cannot dissolve sodium chloride concentrations over 0.5M upon heating (past the UCST, salts precipitate and the solvents become miscible). Higher temperatures could also be used to increase the reaction rate of our kinetically-limited thermomorphic system.

Despite some progress with this thermomorphic system, it was terminated due to a number of impractical aspects with the approach. The major contributing factors were (i) presence of three solvents creating non-optimal kinetic behavior, (ii) reduction of throughput from lower concentrations of reactant (necessary to keep everything dissolved at temperature), and (iii) the requirement of significant catalyst modification. Rather than continuing to try to find a niche application of thermomorphic solvent systems, a transition was made to a more general approach to catalyst separation: organic solvent nanofiltration.

2.4 Conclusion

Thermomorphic solvent system design was approached both theoretically and experimentally. For ternary thermomorphic systems, the lower temperature separation efficiency and the phase envelope temperature dependence were identified as important properties. It was found that UNIQUAC/UNIFAC models were not sufficient to predict the relative utility of different thermomorphic solvent systems. For this reason, an experimental approach was taken. It should be noted that many useful conceptual relationships between solvent structure and phase-behavior of mixtures were uncovered in these theoretical analyses, and the intuition gained from this were useful experimentally. Hansen Solubility Parameters (HSPs) were used to generate similar solvents (with a MATLAB script) and such

systems could be experimentally screened using microreactors. The experimental screening process allowed for the discovery of a number of potentially useful water-containing thermomorphic solvent systems. A thermomorphic water/ethanol/ethyl acetate system was used for an alkenol isomerization. These solvents are relatively benign, cheap, and dissolved the catalyst salts at both room temperature and at the reaction temperature. The kinetic-limitation of the reaction in this thermomorphic solvent system is then leveraged to create a faster reaction than a similar biphasic reaction. This was done by increasing catalyst loading, although increasing temperature is also possible. This is a significant advantage of a thermomorphic solvent system compared with a mass-transfer limited biphasic system. The scalability of such a system is expected to be much better, with a TOF of 450 h^{-1} vs. larger scale batch data at only 30 h^{-1} due to mass transfer limitations. Despite this success, the constraints identified during the process of applying thermomorphic solvent systems casted considerable doubt on the generality of the technique. Specifically, the chemical and solubility constraints imposed by using a narrow range of three-solvent mixtures make future applications limited. For this reason, thermomorphic solvent system applications are expected to be rare in homogeneous catalysis. In particular, they may be applicable when biphasic approaches result in a very slow reaction rate (due to insoluble substrates), and this slow rate is a significant cost-driver. The rest of this thesis focuses on nanofiltration as a catalyst separation technique, as it has the potential to be a much more general approach to organometallic catalyst separation challenges.

3 Separation and Recycle of a Metathesis Catalyst in a Small Scale Flow System

3.1 Introduction

Research efforts have succeeded in the development of stable ring-closing metathesis catalysts with good functional group tolerance.^[121-123] The use of ring-closing metathesis by the pharmaceutical industry could require efficient catalyst separation, as ruthenium content in drugs needs to be < 5 ppm for oral dosage and < 0.5 ppm for parenteral dosage.^[7] The relatively high costs of these metathesis catalysts provide an economic motivation for recycling the separated catalyst. In order for catalyst recycling to be successful, deactivation needs to be minimized. The ethylene byproduct is an important preventable source of catalyst deactivation in ring-closing metathesis reactions,^[124] as well as oxygen-mediated mechanisms.^[125] In most batch metathesis reactions, nitrogen is bubbled through the reactor and vented to remove ethylene. Recently, efforts have been made to adopt this process to small scale flow systems. Lim *et al.* designed a system where reagents flowed through a heterogenized metathesis catalyst bed followed by a degassing block and complete recycle back to the bed.^[126] This process removed ethylene in a flowing system, but needed to be run as a batch process. We use (ethylene-permeable) Teflon® AF-2400 tubing as an effective flow-reactor for a metathesis reaction. This material has been used previously by Zaborenko *et al.*^[78] to remove gas byproducts, and in a number of other applications as a way to introduce or remove gas-phase reagents to or from a liquid phase in the tube-in-tube reactor.^[127-129] Recently, Teflon AF-2400 has been shown to increase the yield of a variety of metathesis reactions due to the efficient ethylene removal across the membrane.^[129]

One approach to the problem of metathesis catalyst separation and recycle is the immobilization of the catalyst to a second liquid or solid phase. Recent efforts at modifying the Hoveyda-Grubbs catalyst with poly(ethylene glycol)^[130], light fluoros chains^[131], fluoros polymers^[132], silica^[133, 134], and nanoparticles^[135] have been reported. Metathesis catalysts are often modified and employed homogeneously as well. Recycling a homogeneous version of a metathesis catalyst via ionic modification^[136], fluoros-tagging^[71], switchable phase tagging^[137], and nanofiltration^[48, 49, 138] have been explored in

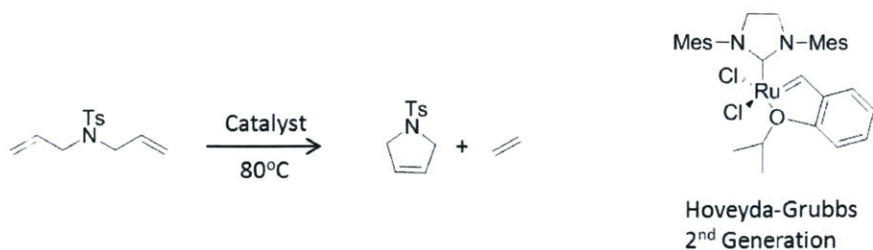
the recent literature. The recycle of a metathesis catalyst in a flow system has also been published recently.^[139]

A recent attempt to recycle a metathesis catalyst in flow using nanofiltration occurred on a 100 ml scale.^[139] Kajetanowicz et al. obtained good catalyst rejections using a molecular weight enhanced metathesis catalyst, but resulted in low turnover numbers (~144) for their continuous system. Further, level control and sampling were performed manually. In this work, we make improvements in all of these areas.

Recent attempts to make small-scale membrane modules with polyamide membrane materials have been successful,^[140, 141] while those for polyimide membranes have been problematic.^[48, 142] We demonstrate here an alternative way to seal these polyimide membranes while maintaining high catalyst rejections. There are few examples of microflow systems designed for the separation and recycle of homogeneous catalysts. Two examples are the fluorous-aqueous biphasic separation and recycle of a fluorous coupling catalyst,^[143] and the ionic liquid-organic biphasic separation and recycle of a palladium coupling catalyst.^[144] We present the design of a small scale (2.9 ml total system volume) continuous-flow nanofiltration-mediated catalyst-recycle system (Figure 39).

The system includes the first fully functional microfluidic OSN module using polyimide membranes, a stirred holding tank with a liquid level control system to respond to membrane flux decline, a membrane reactor using Teflon® AF, and automated sampling at three points in the system. Our system performs small-scale continuous-flow tests of catalyst recyclability without the need of building larger scale, more expensive pilots. For example, our system can test whether, after days of continuous recycling, the catalyst breaks down into smaller species which pass through the nanofiltration membrane. We can also learn whether a closed recycle loop leads to further process development challenges for a particular chemistry.

Our model chemistry, the ring-closing metathesis of N-tosyl diallylamine with a 2nd generation Hoveyda-Grubbs catalyst, is shown in Scheme 7. The initiation-propagation mechanism for this transformation, drawn with our substrate, is provided in Figure 30 for reference.^[145]



Scheme 7. Ring-Closing metathesis chemistry and 2nd Generation Hoveyda-Grubbs catalyst.

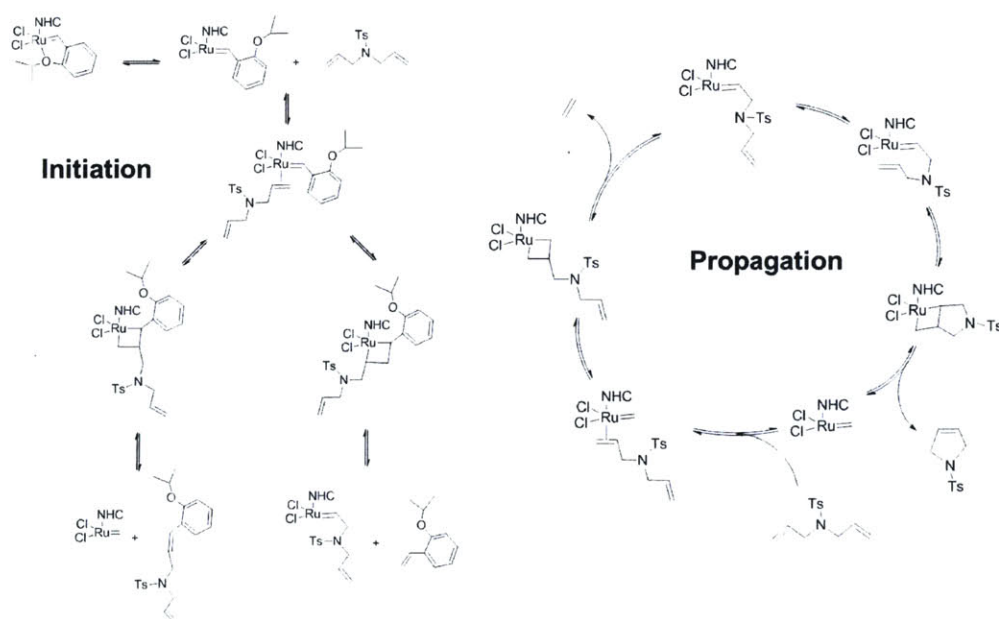


Figure 30. Hoveyda-Grubbs metathesis mechanism for our substrate. The mechanism follows an initiation-propagation scheme.

3.2 Process Design

3.2.1.1 First Generation Microfluidic Nanofiltration Chuck

The first attempt to implement the Puramem membranes in a microfluidic system made use of the pre-existing membrane chucks from the group. These chucks were previously applied at low pressures for liquid-liquid or gas-liquid separations over a Teflon membrane.^[146] Upon pressurization, the membrane was found to deform into the permeate channel, ruining any membrane selectivity of bulky Fluorescein molecules (used

as a visual test). A further issue was the steel directly impinging on the delicate active polyimide later of the membrane. Using the pre-existing chuck, implementation of a Viton gasket to remove this steel contact resulted in some selectivity finally being achieved – however much less than expected for a functional Puramem membrane. The lack of a membrane support was likely the cause. It was further recognized that for an application in catalyst recycling, a larger membrane area was necessary to remove at least half of the feed solvent. For these reasons, a new membrane chuck with O-ring grooves, a built-in membrane support, and a larger membrane area was designed. SolidWorks images of the top and bottom chuck halves are shown below (Figure 31), and Appendix D contains engineering drawings of the membrane chuck design (Figure 87).

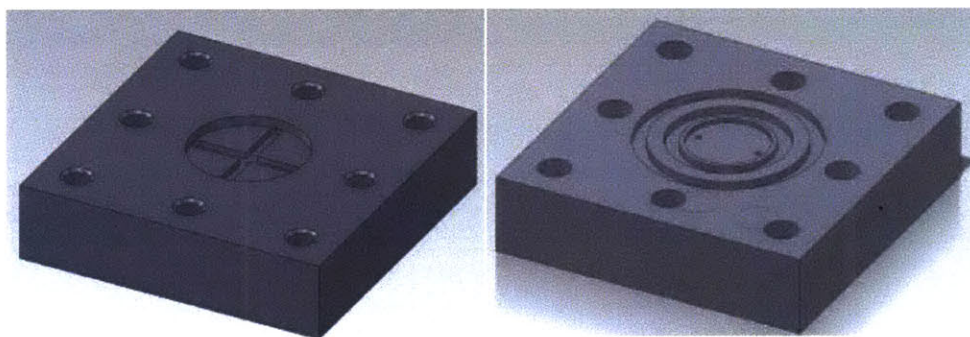


Figure 31. SolidWorks rendering of the permeate half (left) and retentate half (right) of the membrane chuck. Two o-rings are used for the retentate half of the module, and a $\frac{3}{4}$ " steel frit fits tightly into the permeate cavity.

The membrane chuck is used by first inserting a $\frac{3}{4}$ " steel frit (~40 micron pores) into the permeate half of the chuck. Two O-rings (sizes 016 and 021) are then inserted into the retentate half of the chuck, and these two parts are then used to sandwich the membrane such that the glossy yellow active layer faces the O-rings.

3.2.1.2 Validation of Chuck Design

In order to validate the new membrane chuck, we developed a platform which could pump ~100 ul/min at a high pressure (~30 bar) into the membrane, continuously monitor the permeate or retentate catalyst composition, and be capable of continuously feeding for up to several days without halting the process. The flow diagram below depicts the

experimental setup which was used for this purpose. The details of this system are covered in the experimental section. In this section, only results which were relevant to further our membrane chuck design are included.

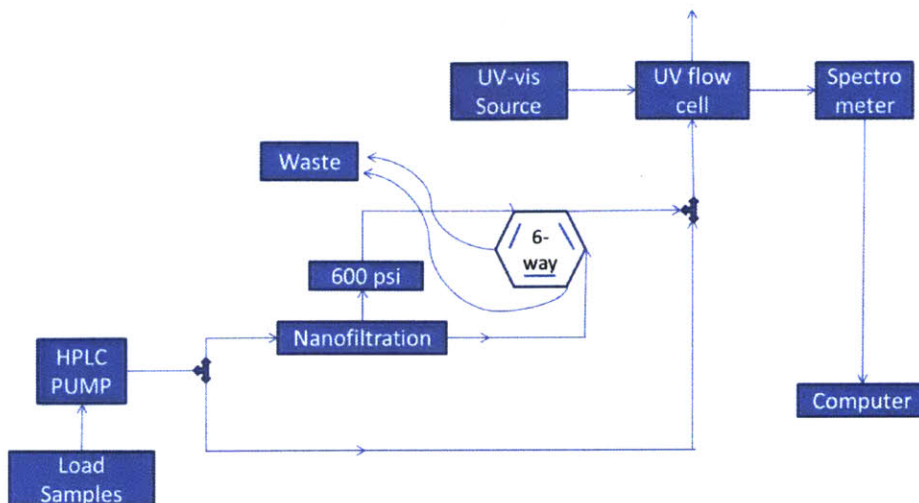


Figure 32. Block diagram depicting the equipment setup and connections for nanofiltration rejection tests.

The first successful run used Buna-N O-rings which eventually failed as they were incompatible with the solvent. Figure 33 below shows the real-time UV signal as a function of time. For the metathesis ring-closing reaction, detection of the 2nd Generation Grubbs catalyst can be achieved in the 300-500 nm range, and so the UV-vis signal represents integrated values from 350 to 425 nm. The first few peaks are calibration peaks obtained by flowing known solution concentrations and bypassing the membrane (see Figure 32). Afterwards, a known feed is loaded and the retentate and permeate are measured sequentially. Finally, pure toluene is loaded to ensure that only an insignificant baseline shift has occurred during the entire process.

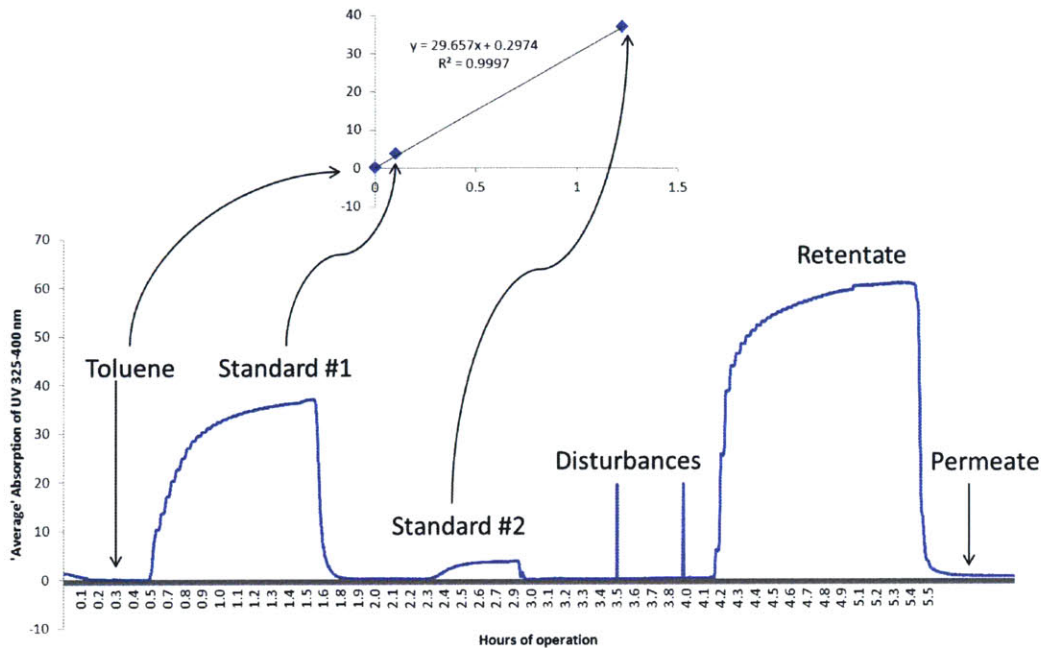


Figure 33. Time-dependent data for the generation of calibration curves and rejection values using in-line UV data, and the setup shown in Figure 32.

The calibration curve obtained using the two standards can then be used to interpret the subsequent membrane test. In this case, the permeate was barely detectable, so a >97% rejection was measured. Since the membrane required at least a day of high pressure compaction before use, it ultimately takes two days to test a membrane rejection in this way.

Due to the swelling of the N-Buna O-ring in the toluene, a Kalrez (perfluoroelastomer) O-ring was used. After two days of membrane compaction, the chuck was again used to filter a toluene solution of 3.4g/ml catalyst. Despite a good calibration and steady, reproducible results (measuring over longer periods of time), only a 95% rejection was obtained. This was a concern since a higher rejection had been achieved using the Buna-N O-ring. Subsequent variations in O-ring material showed that there may be a dependence of the results on the O-ring material, although it is clearly not the whole story. Soft 'Shore A' O-rings seemed to be a prerequisite for high rejections with this module. Note that some attempts to assemble the chuck resulted in a large amount of damage to the membrane and/or a misplaced membrane caused the membrane to be unable to sustain a reasonable steady state pressure (>20 bar). These experimental results were discarded.

Table 3. Different rejection values achieved as a function of O-ring material. Only the best values achieved are shown.

Rejection, 40 bar (nominal)	O-ring
>97%, 40 bar	Buna-N
95%, 40 bar	Kalrez
66%, 40 bar	Teflon
66%, 25 bar	Viton

It was not clear whether the O-ring material impinging on the fragile active layer of the membrane was responsible for this result. Every time a new run is performed, a new piece of membrane is cut (variation in membrane active layer defects) to the desired size (variation in size of membrane piece ultimately causes differences in how tight the chuck can be assembled), sandwiched by two chuck halves (variations in how membrane moves during compression), and finally tightened (differing degrees of tightness could cause differing degrees of leaking vs. membrane tearing, and the uniformity of bolt tightening could also affect the shear experienced by the membrane). Furthermore, the shape of the O-ring groove could be non-optimal in terms of preventing these issues. All of these issues affect either reproducibility or optimal system performance. However, multiple 95% rejections were able to be achieved using the Kalrez O-ring, although about half of the time the assembly would produce a rejection <70%. Therefore, variations in membrane chuck design were undertaken.

3.2.1.3 Variation of First Generation Design

A number of slight modifications to the first generation chuck design were made in an attempt to optimize membrane rejection. The inner O-ring groove of the retentate chuck was made to be wider such that the O-ring had more room to expand. This required only a slight modification of an old chuck, but this modification turned out to hurt rejection substantially. Due to the easier movement of the O-ring during the make-up of the chuck, a reproducible chuck make-up where the sintered steel was fully covered by the O-ring was not possible to achieve.

Next, a new chuck half was designed such that the inner O-ring groove was shaped differently. In this design, the inner diameter of the O-ring was made to be flush with the O-ring groove (rather than the outer diameter of the O-ring made to be flush with the groove). This applied the idea that an outward-expanding O-ring might shear the membrane in a more favorable manner than the original design. This was not the case, however, and much more leaking occurred than the original design.

Another chuck was made with the O-ring being designed as a “liquid type” application rather than a “gas type” application, which ultimately requires the broadening of the O-ring groove. This again only decreased the performance of the membrane chuck.

A series of gasket materials were applied to the original chuck. Aramid gaskets, PTFE gaskets, corrosion-resistant Viton gaskets, and expanded-PTFE gaskets were all considered and applied. Although some success was achieved in terms of obtaining leak-free operation, ultimately a low rejection (<70%) was measured during their applications. The original retentate half of the chuck was also replaced with a flat chuck with no imprints for channels/space and this was used to seal the gasket instead. This system failed as well, with rejections only in the range of 60-70% achieved in three separate runs with a 1/32” Viton gasket.

As the original design with a Kalrez o-ring was superior to the previously described design iterations, a study was undertaken to reproduce this result, and then repeat the experiment after tightening the chuck even further to see how this affected the rejection. The table below presents these results.

Table 4. Different rejection values obtained using a Kalrez o-ring with different, unmeasured degrees of tightness.

Trial	Average Rejection	Volume balance	Days of Compression	Flow rate
Trial #1 6/6/11	94.6%	--	2	100 ul/min
Trial #2 7/15/11	95.8%	95%	1	200 ul/min
Trial #3 7/17/11	98.0%	100% (max compression)	3	200 ul/min

The first trial from Table 4 was conducted using an inner and outer Kalrez O-ring and two days of compression. The small differences in rejection values between trial 1 and trial

2 are on the same order as the variability between repeated trials with the same membrane chuck (variability of 1% rejection is not uncommon).

After varying the sealing technique (o-rings, gaskets), o-ring groove dimensions, o-ring material, and tightness/module-makeup procedures, reproducible high rejections were still not obtained with this membrane module design. The next generation module added more complexity to achieve reproducible, high rejections of catalyst.

3.2.2 Second Generation Microfluidic Nanofiltration Chuck

Although our first-generation membrane module could be used to do approximate small-scale pilot work, we set out to design a nanofiltration cell which accurately reproduces the high rejection (>99%) of our catalyst at larger scales. For this reason, we developed a nanofiltration module with a retentate-side volume of 550 μl that tightly seals Evonik's Puramem[®] 280 membrane (Evonik, Germany) (Figure 34). We were able to avoid damage to the membrane during the sealing process by epoxying (Epic Resins, S7136) a non-permeable polyimide film (0.001" thick Kapton[®] from McMaster-Carr) to the Puramem[®] 280 membrane and then compressing this polyimide film with an O-ring (Figure 34). We were able to reliably obtain catalyst rejections between 99.0-99.8% at 45 bar, which is comparable to larger scale batch filtration results with this catalyst.^[36] Rejection measurements using UV-vis and atomic absorption spectroscopy (AAS) were consistent, indicating that the permeating metal also retained its ligand structure. The membrane area was only (approximately) 1.27 cm^2 , with a post-compaction permeation of pure toluene of about 45 $\mu\text{l}/\text{min}$, giving a flux of 21.3 $\text{L}/\text{m}^2\text{h}$. Membranes were broken in using toluene for an hour to remove any preservative from the membrane. Membranes were compacted at pressure for two days before use.

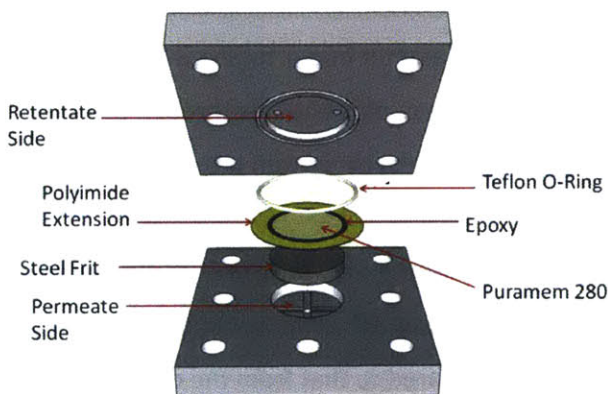


Figure 34. Second Generation microfluidic nanofiltration module using epoxy and an o-ring to seal the membrane.

3.2.3 Teflon-AF Reactor

In our investigation of the ring-closing metathesis of N-tosyl diallylamine in toluene (Scheme 7), we employed 1.3 m of 0.04" OD and 0.032" ID Teflon® AF-2400 tubing (Biogeneral, San Diego, CA) in a previously developed in-house Teflon® AF reactor^[147] (Figure 35).

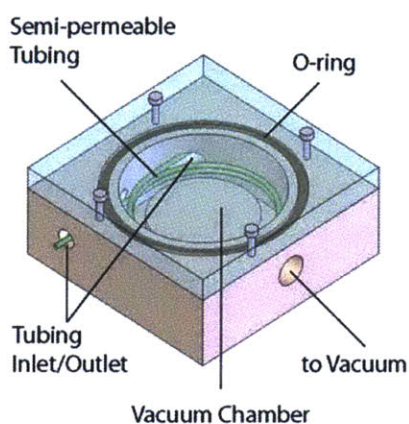


Figure 35. Teflon AF reactor, previously developed by Sahoo et al.^[147]

The reactor removed dissolved ethylene from the toluene solution as it was formed (via pervaporation^[128]), and has the additional advantage of continually removing any dissolved oxygen from the system. Calculations (shown in this section) using empirical data^[148] support this efficient removal of ethylene, and further calculations ensured that mass-transfer was unlikely to be rate-limiting on the liquid side of the membrane due to the small internal diameter of the tube. Thus, reducing the diameter of our tubing will not increase the efficiency of ethylene removal (i.e., will not increase ethylene flux through the membrane). The relatively high TONs achieved in our recycle system provide further evidence for the efficient removal of ethylene.

We calculated ethylene permeability from data where high pressures of ethylene was being added to toluene^[148], and used this to predict how ethylene would be removed in the pervaporation reactor. This data was different compared to that from the original Teflon®

AF patent using dry ethylene gas^[149] because swelling of the Teflon® AF from toluene should increase permeability substantially. We assumed conservatively that ethylene solubility in toluene was not reduced by the presence of substrate, product or catalyst. We operate at a slightly higher temperature (35°C vs. r.t.), however permeability of Teflon® AF is only weakly dependent on temperature. It is clear that some extra residence time would in principle be useful for ethylene removal, but the high cost of Teflon® AF deterred this approach. A simple plug-flow reaction model with homogeneous loss of ethylene was used:

$$\frac{dC_e}{d\tau} = k_1 C_r - k_p C_e, \quad C_e(0) = 0 \quad (14)$$

$$\frac{dC_r}{d\tau} = -k_1 C_r, \quad C_r(0) = 0.05 \text{ M} \quad (15)$$

Where τ is the residence time, C_e is the concentration of ethylene in the reactor, C_r is the concentration of reactant in the reactor, k_1 is the (approximate) reaction rate constant from our kinetic data, and k_p is a modified permeability coefficient (to obtain the correct units). Radial gradients in concentration are ignored in this model (no mass transfer limitations within the tube). This was checked by simply comparing the value of the membrane mass transfer coefficient k'_p (units: cm/s) to the liquid-side, laminar flow-based mass-transfer coefficient. The latter was estimated using the D/R where D is the diffusion coefficient of ethylene in toluene, and R is the channel radius. A factor of 3 was used to conservatively allow for the effect of laminar flow increasing the mass-transfer coefficient (same mechanism as in a Graetz problem)^[68]. We obtain:

$$\frac{3 \frac{D}{R}}{k'_p} \sim 10.5 \quad (16)$$

Since the liquid-side mass transfer coefficient of ethylene is a factor of 10 larger than the mass transfer coefficient in the Teflon® AF wall, we ignore the liquid-side mass transfer resistance as a first-order approximation, since the transport rate through the wall should be proportional to:^[68]

$$\left(\frac{k'_p 3 \frac{D}{R}}{k'_p + 3 \frac{D}{R}} \right) \quad (17)$$

Decreased solubility of ethylene in our solution due to the dissolved substrate/product/catalyst will also increase the effective overall mass transfer coefficient,

but this is not considered. The predicted variation in ethylene concentration with residence time is shown in Figure 36.

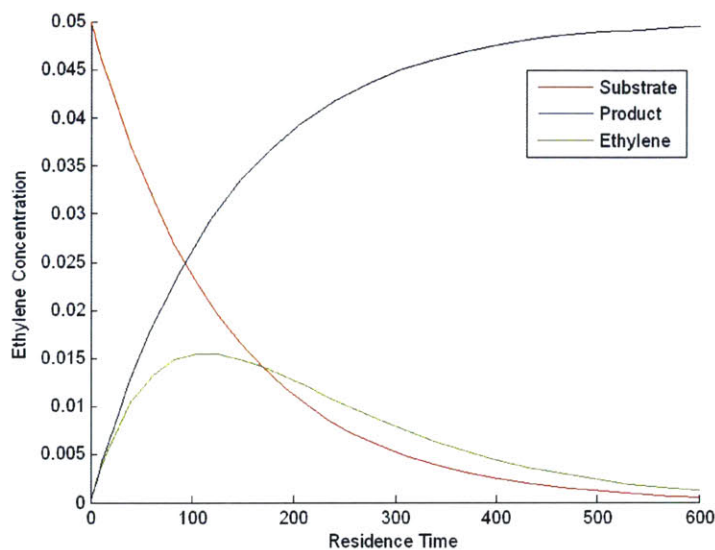


Figure 36. Design calculations predicting adequate removal of ethylene for a 600 second residence time.

The kinetics of the ring closing metathesis reaction in batch glassware compared to the pervaporation reactor in flow are shown in Figure 37 below to be equivalent. This is expected due to the near irreversibility of the ring-closing metathesis reaction for this particular thermodynamically stable product. Further work demonstrated that, for substrates with thermodynamically less stable products, the pervaporation reactor gave higher yields than the reaction in in closed tubing. These results demonstrate the efficiency of ethylene removal of Teflon AF compared to what can be obtained in batch with vigorous nitrogen bubbling. Table 5 summarizes the results for three different substrates. The effect is most clear when considering a large metathesis substrate, which is run sufficiently dilute so as to prevent ethylene slug formation. For such a case, Teflon AF is clearly superior to close tubing with equal residence time, due to efficient ethylene removal. Batch is superior to Teflon AF due to the ability to sparge at very high rates on a small scale. This contrasts with the results of Skowerski et al.,^[129] who report Teflon AF being superior to small scale reactors with active sparging. This could be due to differences in the

(unmeasured) nitrogen/argon sparging/mixing rates employed in batch.

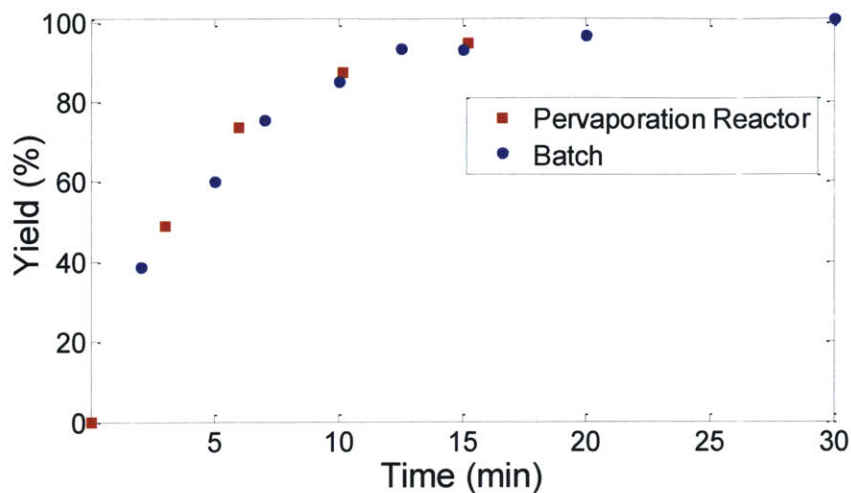
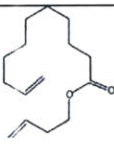

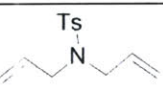


Figure 37. Kinetic results for 1 mol% **4** and 0.05M **1** at r.t. using either a batch or pervaporation flow reactor.

Table 5. Comparisons of performances of batch reactor with nitrogen bubbling, closed tubes, and Teflon AF tubing as a reactor for various metathesis substrates. Formation of gas slugs in closed tubing makes some substrate residence times difficult to interpret, and so values are not reported.

Substrate	Batch Conv. (Yield)	Tube Conv. (Yield)	Teflon AF Conv. (Yield)
	99 (90%)	73 (66%)	90% (85%)
	87% (66%)	--	83% (78%)
	93% (93%)	--	93% (93%)

3.2.4 Holding Tank with Liquid Level Control

A holding tank (Figure 38) with a target holdup of 800 μl was made by shortening an unmarked HPLC vial. A triangulating laser (Keyence, IL-065) was used to measure the liquid

level. A gently heated ($< 30^{\circ}\text{C}$) stream of air was continuously blown onto the top of the vial to prevent fogging during operation. The signal from the laser was fed to a National Instruments FieldPoint board and interpreted via Labview to serve as the signal for a PI control system (with the substrate/catalyst inlet flow to the system serving as the control variable).

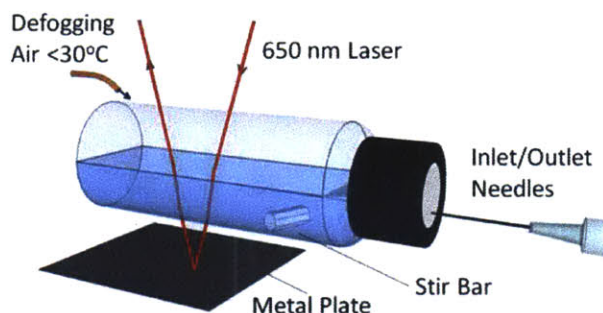


Figure 38. Cartoon of small-scale holding tank with level control.

3.2.5 Continuous Flow System Equipment Specifications

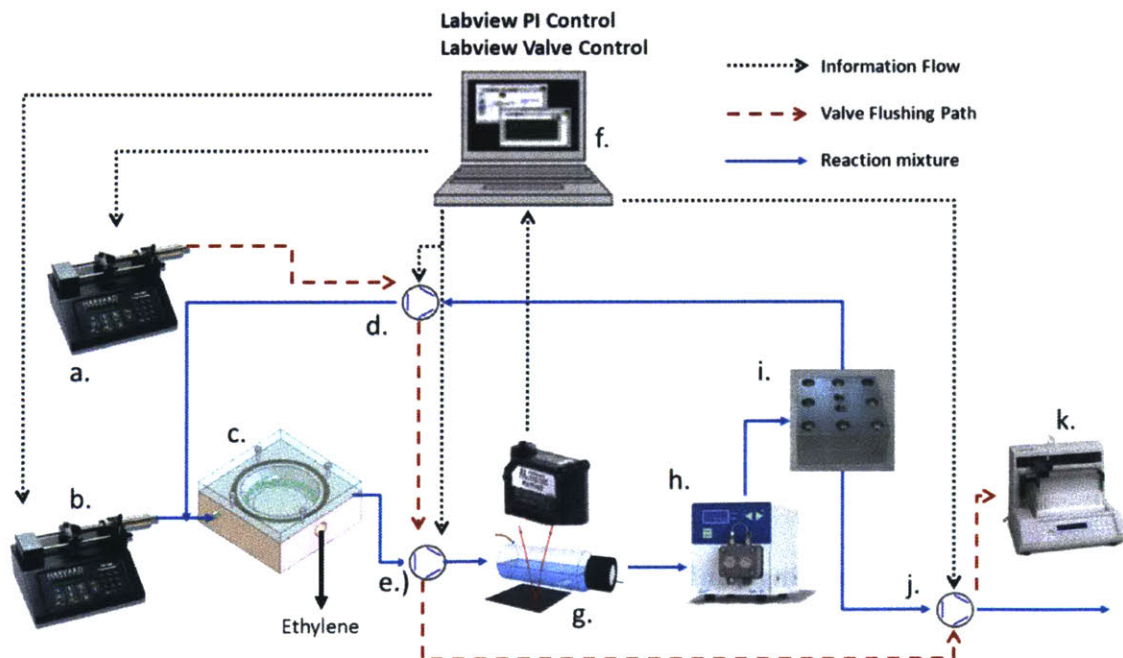


Figure 39. Continuous separation/recycle system for a metathesis catalyst.

The system was built inside a fume hood, and is shown schematically in Figure 39. The main pieces of equipment labelled in are: a.) Harvard PHD 2000 Programmable Syringe Pump. Flow rates varied according to control scheme. b.) Harvard PHD Programmable 2000 Syringe Pump set to 100 μl /min during 5-min flushing events c.) 1.3 m Teflon[®] AF-2400 from BioGeneral, with 0.04" OD and 0.032" ID was used as the reactor. The vacuum module was submerged in water kept at 35°C with an Omega temperature controller. d.) Rheodyne automatic 2-position, 6-way valve with a 10.1 μl sample loop installed. e.) Rheodyne automatic 2-position, 6-way valve with a 20 μl sample loop installed. f.) Computer to control pumps and valves g.) Keyence IL-065 laser sensor with modified HPLC vial h.) Knauer Smartline HPLC pump (10 ml/min max) set to 70 μl /min during the whole experiment, fixing the residence time of the system regardless of inlet flow rate changes. i.) Custom nanofiltration module made from aluminium. No Stir bar present (was not found to help). A Puramem[®] 280 from Evonik was cut and epoxied to a 0.001 " thick Polyimide film (Kapton from McMaster-Carr) using Epic Resins epoxy S7136A. Membrane is compacted for two days at 45 bar (under toluene) before use. j.) Rheodyne automatic 2-position, 6-way valve with a 58.8 μl sample loop. k.) Gilson FC 204 Fraction Collector. All tubing was 0.01" ID, 1/16" OD PEEK, stainless steel, or PFA tubing from Upchurch Scientific. A backpressure regulator (500 psi nominal, 640 psi actual) from Upchurch Scientific, provided the backpressure on the retentate side of the membrane, and was followed by an additional check valve from Upchurch Scientific to prevent backflow during start-up. Temperature recorded in fume hood was near 21°C during experiments.

3.3 Experimental

3.3.1 Metathesis Reactant Synthesis

It is necessary to synthesize tosylated diallyl amine from diallyl amine. First, 2.5 ml of diallyl amine was added to 50 ml of dichloromethane. Next, 4g of TsCl was dissolved in 20 ml dichloromethane and added slowly using a syringe pump over 20 minutes. The solution was continuously stirred at room temperature in an Erlenmeyer flask overnight. The solution was then rigorously contacted with 50ml of a 1 M KH_2PO_4 solution, and the aqueous phase discarded. This was performed twice. Next, two washes of 1 M NaHCO_3

were performed. Finally, two washes of H₂O were performed, again discarding the aqueous phase. Magnesium chloride was added to dry the solution, and the solution was then dried via a rotary evaporator. The remaining yellow liquid was dissolved in ethyl acetate and washed through a silica column with ethyl acetate. The collected solution was dried again via rotary evaporation until only the product remained. Addition of hexane with rotary evaporation repeats were necessary until the NMR showed no ethyl acetate.

3.3.2 Metathesis Reactions

A Harvard PhD Ultra syringe pump with two 8ml stainless steel syringes were used to deliver the substrate and catalyst respectively to the reactor. PFA tubing 1/16" OD with 0.03" ID was used for a "closed tubing" reactor. The previously described Teflon AF reactor was also employed. Concentrations of solutions in the stainless steel syringes were chosen such that, for equal flowrates, the correct concentrations resulted in the reactor. For the catalyst stock, 10 mg of catalyst was weighed and dissolved in 10 ML of toluene. To create the substrate stock, 1ml of substrate was measured and dissolved in 10 ML of toluene. The stock solutions were loaded into a stainless steel syringe under a Schlink line. Upon beginning the experiment by starting the pump, four residence times were waited before sampling. Batch experiments were performed by creating the same stock solutions by directly mixing 2ml of each stock solution under a Schlenk line, and stirring while bubbling nitrogen at 35°C.

3.3.3 Testing of membrane rejections: UV-Vis and AAS

An Agilent 200 Series graphite furnace atomic absorption spectrometer (GF-AAS) was used to measure rejections in all cases presented here. UV-vis measurements (measuring the catalyst ligand rather than the metal center) gave rejection values consistent with GF-AAS (within the reduced accuracy level of the UV-vis flow-cell). A UV-vis flowcell was incorporated downstream from the membrane with a manual 2-position, 6-way valve used to switch between measuring the permeate or retentate with the UV-vis flow cell. The setup is shown in Figure 32. The UV-flow cell was made by Kevin Nagy^[71] and the UV source was an Ocean Optics DH-2000-Cal, and the spectrometer was a USB4000-UV-VIS from Ocean Optics.

The integrated 325-425 nm UV absorbance (a function of concentration of NHC ligand on 4) was measured for two known concentrations of 4 to construct a calibration curve, and then the permeate and retentate were measured. The ratio between the permeate and retentate concentrations implied >98% rejection (higher accuracy not possible with this setup). GF-AAS measurements provided information about the rejection of the metal center to complement the UV measurements of the ligand. Calibration work (Figure 40) showed that running a GF-AAS routine on unmodified 2nd Generation Hoveyda-Grubbs catalyst in toluene gave the same calibration curve as a 1g/L RuCl₃ standard in 1 M HCl (AAS Standard from Sigma Aldrich). Thus, no intermediate work-up was deemed necessary when running GF-AAS on permeate and retentate samples, other than dilution to the 50 ppb level before measurement. Glassware or polypropylene containers gave equivalent results. All dilutions were performed with toluene, but ruthenium concentration calculations were done on a water-basis (i.e., assuming 1 kg/L density of solution mixture rather than using an actual reaction mixture density).

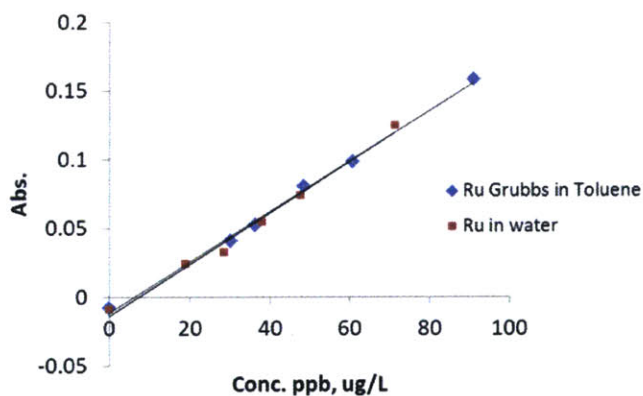


Figure 40. Absorption of catalyst and RuCl₃ in HCl are equivalent. Thus, catalyst 4 need not be worked-up before applying GF-AAS method.

Table 6. The temperature-time recipe used to create these calibration curves in the GF-AAS.

Table S1. Temperature-time recipe for GF-AAS analysis.	
Temperature (°C)	Time (s)

85	5
95	40
120	10
1000	7
2600	4.8

3.3.4 Continuous Recycle System Operation

A system integrating the three above techniques was built to separate and recycle the catalyst **4** in a continuous flow system (Figure 39). A PHD 2000 syringe pump (Harvard Apparatus, Holliston, MA) with two glass syringes (SGE, Austin, TX) (0.049 M substrate **1** and 0.075 mM catalyst **4**) were fed into the evacuated Teflon[®]-AF reactor. The outlet fed into the liquid-level controlled holding tank (under 0.2 psi nitrogen pressure), from which a Smartline 10 ml HPLC pump (Knauer, Germany) withdrew and delivered the solution to the nanofiltration module at 45 bar and 70 $\mu\text{l}/\text{min}$. The retentate passed through a 45 bar backpressure regulator (IDEX, Oak Harbor, WA) and was recycled back to the reactor inlet. The permeate was always collected. Figure 39 shows the locations of three sample loops (automatic 2-position, 6-way valves) (IDEX, Oak Harbor, WA). These loops were flushed (according to a Labview program) with degassed toluene and deposited into a FC 204 fraction collector (Gilson, Middleton, WI) for GC and AAS analysis. Di(ethylene glycol) vinyl ether (100 μl) was present in each collection vial to quench the reaction.^[150] Quenching integrity was checked in previous runs with partial conversions. The sampling valves at the reactor outlet and retentate also served as the effective purge stream for this system, putting a limit on the amount of deactivated catalyst products and dimer byproducts that could accumulate in the system.

3.3.4.1 Continuous Recycle with Co-feed Experiment

The 50 hour continuous run start-up was performed by first filling the system with a catalyst solution (0.18 mM) under oxygen-free conditions (after purging the system with 5 volumes of degassed toluene). Next, two glass SGE 25 ml syringes filled with substrate (0.098 M) and a catalyst co-feed (0.075 mM), respectively, were primed with the syringe pump and set to flow at 40 $\mu\text{l}/\text{min}$ (20 $\mu\text{l}/\text{min}$ per syringe). A 50 ml glass Hamilton syringe of pure toluene was loaded onto an identical pump for use in flushing the 6-way valves

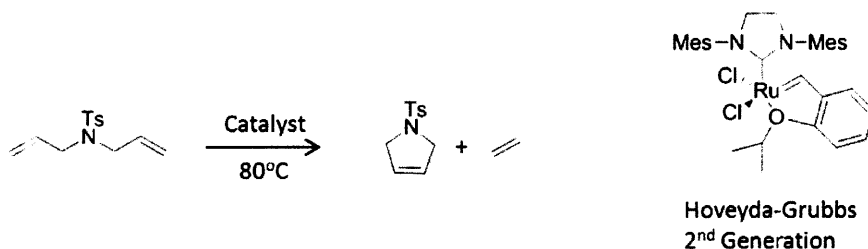
according to the automated scheduled procedure. Vacuum was pulled on the Teflon® AF. The PI level control algorithm, autosampler, and automatic valve procedures were then started up. At this point, everything was handled automatically by the system and did not require an operator except to make sure equipment was not breaking down. Deposited samples reacted immediately with the 100 µl of di(ethylene glycol) vinyl ether deposited beforehand into every sample vial. Samples were analyzed by first adding 10 µl of a 0.16 M biphenyl solution (in toluene) to each sample. This allowed for adjustments due to evaporative loss of toluene from sample tubes during the 50 hour run. Sample conversions were analyzed offline using gas chromatography, and rejections were handled with GF-AAS.

3.3.4.2 Continuous Recycle No Co-feed

This 10 hour experiment used the same startup procedure described in the previous section, with the following differences. A catalyst load conc. (0.125 mM) and substrate concentration (0.097M) was used with no co-feed (a higher concentration of substrate due to a lack of dilution by catalyst co-feed). The automatic sampler at the retentate was not used during this run.

3.4 Results and Discussion

The reaction in Scheme 8 was investigated as a model chemistry to demonstrate our catalyst recycle system. The reaction was first conducted in batch glassware and the results were compared to steady-state flow results at similar residence times using the pervaporation reactor. The irreversibility and speed of this reaction caused ethylene removal to be irrelevant to the kinetics of a one-pass reaction. However, the removal of ethylene and oxygen via pervaporation in our flow reactor could be very useful for extending catalyst lifetime in our flow system.



Scheme 8. Ring-closing metathesis of N-Tosyl-diallylamine with the 2nd generation Hoveyda-Grubbs catalyst.

The reaction-separation-recycle setup (Figure 39) was first used to recycle the catalyst **4** with no co-feed of catalyst (only substrate and solvent were fed). Running the system with an initial charge of catalyst made it possible to determine the order of magnitude of TON that was achievable with **4** in this flow system. A 0.125 mM catalyst solution was loaded into the system and then used until it was no longer active. Figure 41 shows the decline in product fraction through the system with time. The cumulative TON is calculated and plotted on the same figure. At the end of the 10 hour experiment, when including the leftover product in the 2.9 ml system hold-up, a TON of 1300 was obtained, albeit with low yields.

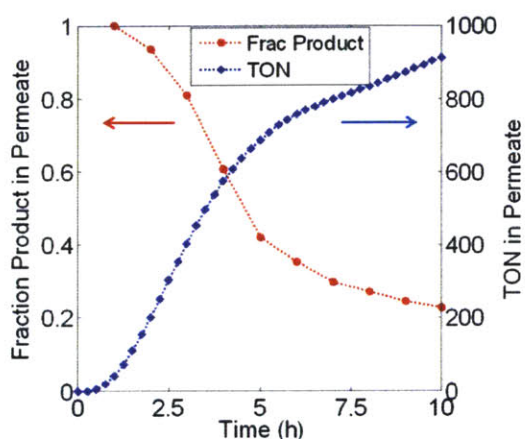


Figure 41. Loading catalyst into the recycle system and using the catalyst until it is spent gives a declining product curve in our permeate. This justifies the use of a catalyst co-feed in subsequent experiments.

In a continuous system with a catalyst co-feed, the yield can be kept high at steady state by co-feeding an amount of catalyst close to the rate of deactivation. Thus, in designing our subsequent experiment with a co-feed of catalyst, we chose 1300 as the feed ratio of **1** to **4**. It should be noted that after 10 hours, the membrane clogged completely due to large amounts of deactivated catalyst and precipitated product. Slightly lower concentrations were chosen for the experiment involving a catalyst co-feed.

The reaction-separation-recycle system with catalyst co-feed was used to recycle the catalyst **4** over a 50 hour period with no shutdowns or manual interventions. During the run, accumulations in the liquid level of the tank meant that solvent flux in the membrane was being

reduced due to concentration polarization and/or fouling, and the proportional-integral control system properly reduced the feed flow rate to account for the reduced solvent flux.

Accumulation of product or deactivated catalyst in the system likely caused substantial concentration polarization and/or fouling, with the flow rate being reduced from an initial 41 $\mu\text{l}/\text{min}$ to 8 $\mu\text{l}/\text{min}$ (Figure 42), reflecting a drop in permeation rate. Peeva et al. have studied concentration polarization with similar nanofiltration membranes, observing flux declines of a similar magnitude.^[40] Nanofiltration applications with > 5 wt% substrate concentrations (our steady-state value is near 6 wt%) are rare in the literature due to such challenges.^[151] The accumulation of product (and possibly catalyst deactivation products) the recycle loop may have exacerbated the flux decline.

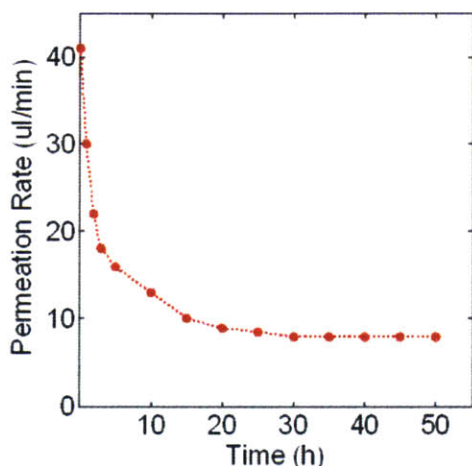


Figure 42. Approximate flow rate decline due to concentration polarization and fouling of the membrane.

Despite this decline in throughput, the amount of product relative to substrate at the reactor outlet, retentate, and permeate sample loops was consistently high (always above 97.5% for the permeate), seeing only a slight decline over the course of the experiment (Figure 43). This decline could be caused by the accumulation of product in the recycle loop, which would tie up some of the catalyst through reversible interactions. It could also be the result of

a reduction in active catalyst concentration due to catalyst deactivation and removal being slightly faster than the fresh catalyst feed. It should be noted that catalyst permeation and purging were less than 15% of the fresh catalyst fed and thus not the dominant mechanism of active catalyst removal from the system.

The actual permeate concentrations collected over time were also measured over the 50 hours (Figure 44). A steady product concentration is approached after about 15 hours of experimental time. This timescale is much longer than the time expected for product to reach a steady state in the recycle loop, and is instead representative of the timescale of membrane flux decline. The concentration in the permeate is reduced to 0.04 M (from a substrate feed of 0.049 M) due to the system purge necessitated by sampling, and some incomplete conversion. This system purge represented an average flow rate of 0.36 ul/min during the experiment and was needed to cap byproduct accumulation. The purge rate, along with reaction temperature, loop flow rate, and reactor volume, could be optimized to maximize catalyst TON. For this model chemistry, we were not concerned with system optimization.

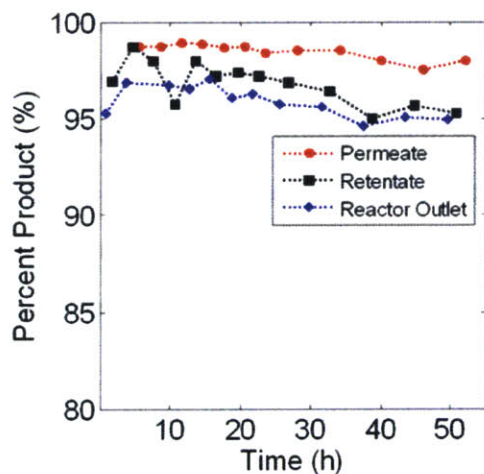


Figure 43. Percent product in permeate, retentate, and reactor outlet samples for a 50 hour run.

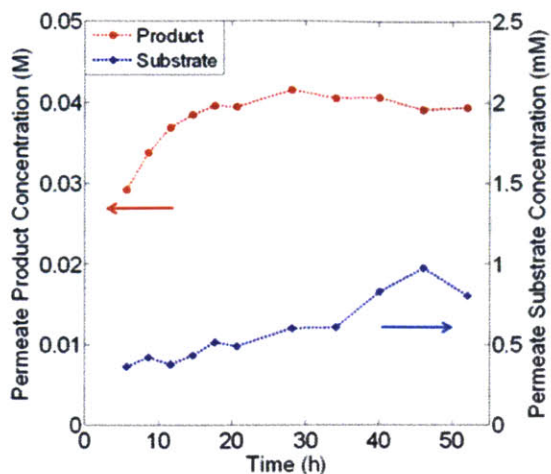


Figure 44. Product and substrate concentrations in the permeate stream as a function of experimental time.

Data from the reactor outlet and retentate concentration also indicated that steady concentrations of product and reactant were approached (see Supporting Information). Running the system at increased substrate concentration was not possible due to the accumulation of product causing precipitation and complete pore blockage of the membrane after about 10 hours. The closed recycle loop therefore imposes throughput limitations in the form of a reduced substrate loading (affecting the throughput of product from the reactor). Thus, our system can help one understand the increases in reactor size and membrane size that are required for a desired throughput when closing a recycle loop on a reaction-nanofiltration process.

A small number of nanofiltration-based recycles in batch mode would likely miss much of the behavior easily unmasked with our continuous flow system. We note that during the 50 hour run, our system performed the equivalent of about 70 such batch tests in series. Obtaining such efficiency requires the minimization of free volume outside of the reactor itself. Thus, the small scale of the holding tank and nanofiltration modules are important aspects of the system. Near the end of the experiment, large amounts of product (~0.22 M) are being

recycled back to the reactor with 0.04 M permeating. This implies a product rejection of 80%, which was much higher than the 32% obtained in initial rejection tests, indicating that the rejection of the membrane changed throughout the experiment.

The presence of automatic sampling valves allowed probing of the dynamic performance of the membrane via the retentate and permeates sample loops throughout this process. The rejections of substrate and product increased very rapidly early on in the experiment (Figure 45). The rejection of catalyst 4 also increased from 99% to 99.5% due to this fouling process. Flowing toluene through the membrane after the experiment only partially recovered the initial flux of the membrane, and the used membrane had a thin, deposited layer of brown material even after this flushing. This brown layer indicated that catalyst decomposition products were fouling the membrane surface, and ruthenium was detected in the layer. As the molecular weight of the substrate and product were 250 and 220 Da respectively, the observed rejections for a 280 MWCO membrane became very high. These results indicate that during the practical application of nanofiltration to catalyst separation, significantly less than expected throughput may be realized as a result of the adverse effects of a closed recycle loop on membrane performance.

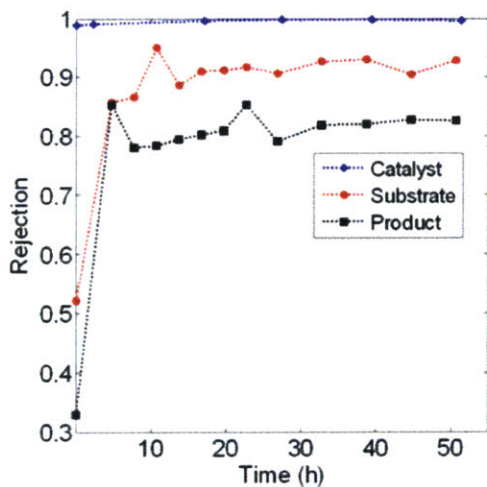


Figure 45. Rejections changed significantly upon accumulation of materials in the recycle loop.

The metal contamination in permeate and retentate product was also monitored throughout the run (Figure 46). A low catalyst contamination in the product (permeate) stream (< 0.5 ppm) is achieved. Comparing with the retentate concentrations, a reduction of over two orders of magnitude in catalyst concentration was realized in the product.

Two turn over numbers (TONs) were calculated for this system. One is the TON calculated based upon the measured permeated product, i.e, the total product collected divided by the total catalyst used in the experiment. This TON was 677. The other TON includes the product in the hold-up in the system after the experiment is stopped, along with product present in samples. This TON was 935, corresponding to 1.83 mmol product produced. If the system were run until failure, 935 would be the minimum TON that would have been obtained (conservatively assuming that all of the active catalyst in the system immediately deactivated after 50 hours). Thus, the latter TON is the appropriate comparisons to other examples of batch-wise recycle of catalyst **4** in the literature.

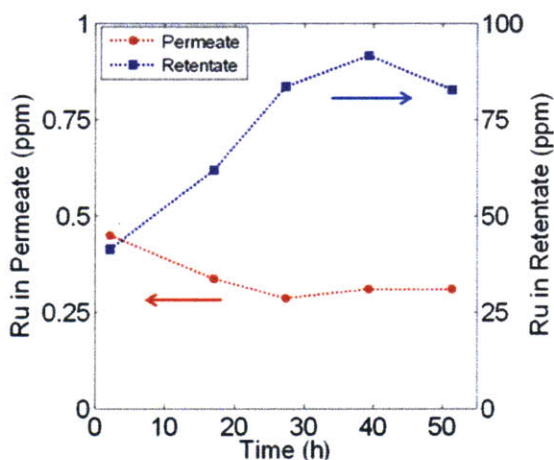


Figure 46. Permeate ruthenium content remained below 0.5 ppm during the continuous run.

In the present case the system was stopped when the syringes ran empty. Thus, these results do not reflect the optimal TON. During the experiment, the TON grew as the initial catalyst loading used to start-up the system became smaller relative to the substrate fed to the system (Figure 47). The decline in slope over time reflects the reduced membrane flux causing a

decrease in throughput (and therefore reduction in rate of usage of held-up catalyst). The upper bound for the TON for this system is set by the catalyst feed relative to the substrate, which is 1300 for this case. It should be noted that Figure 47 does not imply a steady state was not reached. Instead, the failure of the curve to plateau implies that the amount of catalyst **4** used to start-up the system is still a significant amount of catalyst relative to the amount co-fed during the entire run.

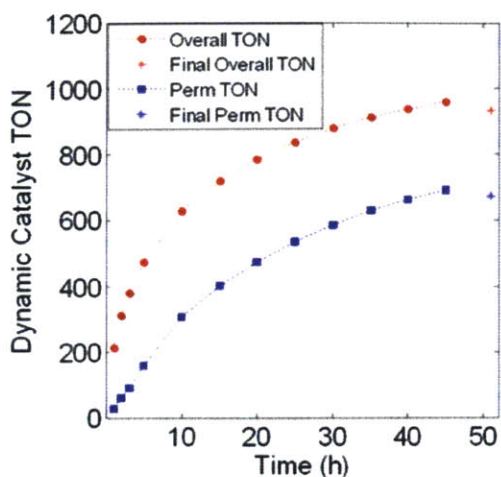


Figure 47. TON of a function of experimental time. Decline in rate of growth of TON with time represents a reduction in throughput rather than catalyst decomposition. Connected dots represent autosampler results using the approximate permeation rate from Figure 42. Stars represent TONs measured after the experiment.

The residence time of the entire system is approximately 40 minutes. To conceptualize (and greatly simplify) this experiment in terms of batch cycles, this 50 hour experiment corresponds to about 70 catalyst reactions, separations and recycles, combined with systematic partial purging combined with catalyst and substrate make-up during each recycle. As product and deactivated catalyst accumulates in the system over many recycles, membrane flux decline causes a decline in substrate feed and, thus, a drop in the TON-per-pass in the reactor. These adverse effects of a closed recycle loop during nanofiltration could be mitigated by using a membrane with a higher molecular weight cut-off of 400 (still retaining the 627 MW **4**), but at

the time of this work was not available commercially. Molecular weight enlargement of the catalyst is another solution, and would allow applying such a system to larger, more pharmaceutically relevant, metathesis substrates. The TON of a ring-closing metathesis reaction could be optimized further by minimizing the unreacted material leaving the reactor. This would help to prevent ethylene from being generated in downstream process blocks and minimize catalyst decomposition due to inefficient ethylene removal outside of the reactor.

Table 7. Comparison of our results with highlights from the batch recycle literature.

Method	Total TON	TOF (h ⁻¹)	Residence Time (min)	T (°C)	Notes
Our System	935	260	10.5	35	Fully automated continuous flow system.
Electrostatic immobilization to Fe nanoparticle ^[135]	735	74	120	r.t.	Batch Recycle. Ru Permeate: 40-200 ppm
Silica/zirconia supported ^[152]	714	38	225	30	Batch Recycle. 78% Avg. Yield
Ionic-liquid tagged ^[136]	1600	<60	>60	45	Batch Recycle. Complicated work-up: (untimed rotovap, 3x LLE, vacuum drying) and recycle.
Mesoporous silica support ^[64]	698	87	480	50	Batch Recirculating Flow Reactor. 2-8 ppm Ru.
Fluorous/DCM biphasic ^[132]	2500	<80	75	50	Batch recycle. Complicated work-up (rotovap, solvent switch, perfluoro-extractions), all untimed.

3.5 Conclusion

The continuous separation and recycle of a metathesis catalyst has been studied using a microflow system. Two microfluidic process blocks were designed for the process: an organic solvent nanofiltration (OSN) module and a holding tank with liquid level sensing. Also of interest is the application of Teflon® AF-2400 tubing as a membrane reactor for the ring-closing metathesis of **1**. The use of this polymer in the efficient removal of ethylene under flow conditions resulted in good TONs for this catalyst.

Our continuous-flow system had an active control loop to respond to membrane flux decline, with automated sampling at three points in the system. The small scale of this system (<3 ml total internal volume) meant that a 50 hour run required less than 2 mg of the catalyst **4**. Since the nanofiltration step allowed the catalysts to react in a homogeneous manner, TOFs as high as 750 h^{-1} were obtained in the reactor at the start of the experiment. These conditions allowed for a 10 minute residence time in the reactor, sufficient to obtain greater than 94% product at the reactor outlet. In addition, work-up procedures in the continuous flow system were automated and seamlessly excluded from oxygen.

A total TON of 935 was obtained using this system. Ruthenium contamination in the product was always less than 1 ppm. The microfluidic continuous flow recycle system has the potential to accurately investigate the continuous-flow separation and recycle of homogeneous catalysts using small amounts of materials. Although seamless exclusion of oxygen and efficient, automated recycling encourages further work in this area, the small scale (<3 ml total internal system volume) created a number of practical constraints (clogging, process block design constraints) which are best avoided by designing a small-scale flow system one order of magnitude larger. In subsequent chapters of this thesis, larger flow systems are built to avoid these issues.

4 Separation and Recycle of a Hydrogenation Catalyst in a Small Scale Flow System

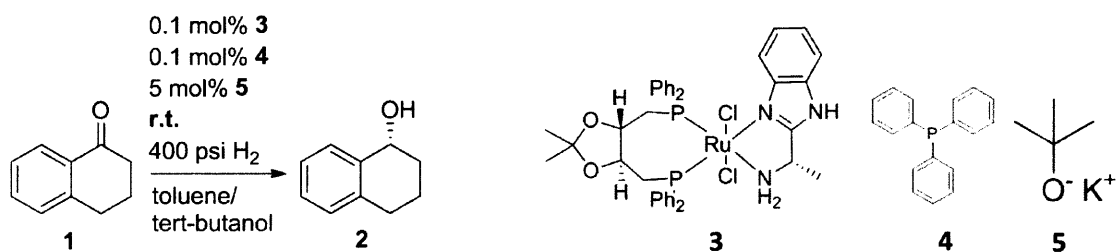
4.1 Introduction

Asymmetric hydrogenation of ketones is an important transformation in organic drug synthesis.^[153] For aryl ketones lacking an additional coordinating group, this transformation can use molecular hydrogen, an alcohol, or borane as the reductant.^[154] The latter approach often uses CBS oxazaborolidine catalysts^[155], which have been recycled in the literature using nanofiltration membranes.^[156-158] These applications generally increased TONs substantially while exhibiting some enantioselectivity decline. These catalysts have the disadvantage of requiring stoichiometric borane, as opposed to using alcohols or hydrogen gas as the reductant. Efficient ruthenium-containing organometallic catalysts have been developed to perform asymmetric ketone hydrogenation using both of these hydrogen sources.^[154] Flow systems have been used to investigate the recyclability of asymmetric transfer hydrogenation catalysts.^[159-161]

Here, we focus on a catalyst which uses molecular hydrogen as the reductant. The separation and recycle of diphosphine/diamine catalysts has been performed mostly in batch recycle experiments in the literature. Some examples include the modification of the catalyst using dendrimers^[162], magnetic nanoparticles^[163], mesoporous silica^[164], zirconium phosphonates^[165], and polystyrene.^[166] These approaches have the disadvantage of requiring significant catalyst modification, which often causes large reductions in turnover frequencies (at least one order of magnitude compared to the native catalyst species for all the cases cited). Here, we apply organic solvent nanofiltration (OSN) to separate an unmodified diphosphine/diamine catalyst which has not been recycled to date in the literature.^[167] This approach has the advantage of eliminating the catalyst modification step of process development and allows us to operate at TOFs of the original homogeneous catalyst. Since this

catalyst is 832 MW (Scheme 9), many drug products and intermediates could be used in our system without any catalyst modification.

We have designed and built a continuous-flow system to recycle a catalyst for the asymmetric hydrogenation of α -tetralone, as shown in Scheme 9. This substrate has received attention in industry, and has been run at a 200 L pilot scale with a transfer hydrogenation catalyst by Avecia.^[168] Our system has a high-pressure surge tank with PI control to respond to membrane flux decline, a base-compatible 800 MWCO PEEK nanofiltration membrane, automatic sampling, and a total internal volume of only 50 ml.



Scheme 9. Asymmetric hydrogenation of α -tetralone using molecular hydrogen, a ruthenium catalyst, and a strong base co-catalyst.

4.2 Process Design

4.2.1 Packed Bed Reactor Design

A 0.5" outer diameter, 10 mm inner diameter, 11" long stainless steel tube (McMaster-Carr) was used as a reactor. Glass beads (710-1180 μ m) (Sigma Aldrich, G1152) were packed into the reactor by continuously loading while tapping on the side of the reactor. Once loaded, the beads were emptied, weighed, and loaded back into the reactor. This process was repeated to ensure consistency of packing density. As long as the glass beads were loaded slowly, while tapping continuously on the side of the reactor, the packing was found to consistently have a void volume of 0.36. Valco fittings (Valco, ECEF8110.0) were used in conjunction with 0.5"

diameter, 10 μm frits to hold the glass beads in the reactor. These Valco fittings provided female 10-32 inlet and outlet ports to the reactor. In all cases, flow into the reactor entered the bottom of the reactor and exited the top of the reactor, with the reactor being clamped vertically.

We first needed to verify plug flow in our upflow packed bed reactor using a residence time distribution experiment. This residence time distribution experiment was performed using an in-house UV flow cell^[71] with an Ocean Optic's UV-vis. light source (DH-2000), fiber-optic cables, and spectrometer (USB4000-UV-VIS). Since the flow is gas-liquid, the RTD data is quite scattered, as shown in Figure 48.

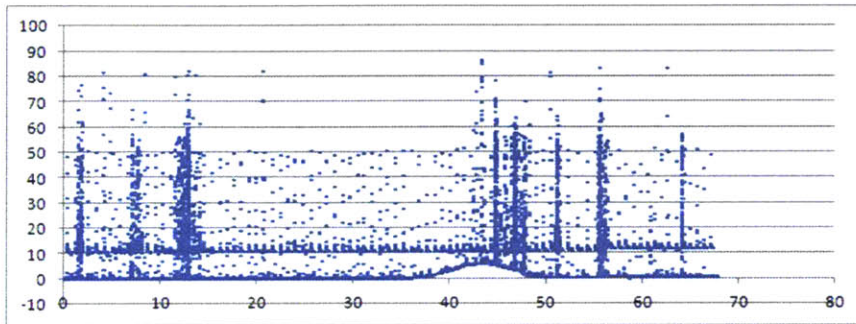


Figure 48. Raw data for residence time distribution of our multiphase packed bed.

In order to easily interpret this data, the curve was fit to a Taylor Dispersion model.^[70] A larger scale packed-bed of this type would typically use a PDE model, but here we observe no significant tailing.^[169]

$$E(t) = \frac{M_0}{\sqrt{4\pi} \frac{D}{uL}} \exp\left(-\frac{\left(1 - \frac{t}{\tau}\right)^2}{4 \frac{D}{uL}}\right) \quad (18)$$

The average residence time, τ , the nondimensional dispersion, $\frac{D}{uL}$, and the tracer amount, M_0 , were all fit by eye until our curve was approximately represented by the model function. Creating a script to perform this action would ultimately be rooted in this same intuitive

process, and so we did not automate the curve fitting procedure. This RTD represented our total system RTD, including the reactor, tracer injection valve, and flow cell. We needed to remove the effects of the tracer injection valve and flow cell from this total system RTD to obtain our actual reactor RTD. A bypass RTD experiment was performed and fit to a similar model function. Finally, the reactor RTD is obtained by deconvoluting the bypass RTD from the total system RTD. This is shown in Figure 49. This can be done using model functions and fast Fourier transforms:

$$RTD_{Deconv} = FFT^{-1} \left(\frac{FFT(RTD_2)}{FFT(RTD_1)} \right) \quad (19)$$

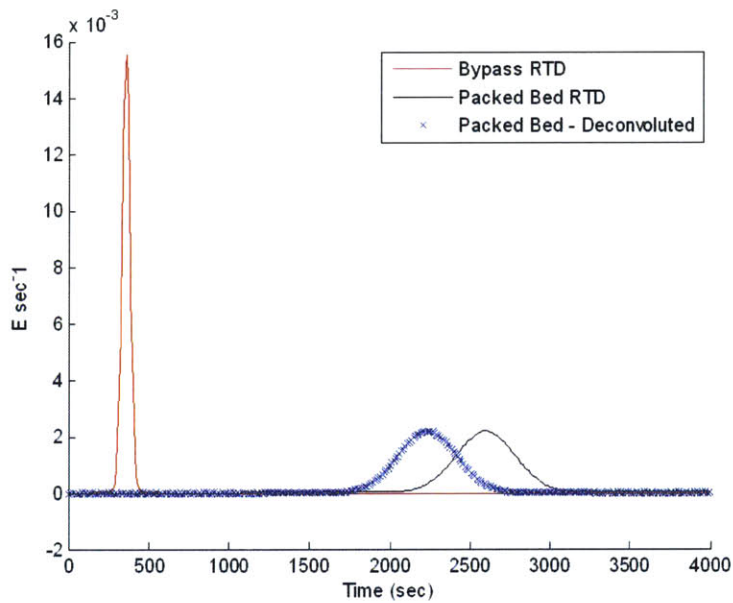


Figure 49. Deconvolution of bypass RTD from the total system RTD to obtain the reactor RTD (blue).

The resulting RTD can be fit to the model function to obtain dispersion characteristics. A nondimensional dispersion $\left(\frac{D}{uL}\right)$ of 0.0025 and a residence time of 40 minutes was obtained. Using this residence time distribution, dynamic simulations were performed to show the result

of step changes in concentration and linear ramping changes in concentration on the reactor outlet concentration curves. The results of the simulation are shown in Figure 50. It can be seen that, although large steps to screen differences in concentrations resulted significant nonidealities, linear ramps create linear reactor concentration outlets, making data interpretation much more straightforward. This is how we designed our concentration ramping experiments. It should be noted that, for our scale of reactor, a trickle bed approach gave plug flow at lower residence times. Since the enhanced mass transfer associated with a trickle bed orientation was shown not to be necessary (see catalyst ramping experiments in the Results and Discussion section), we used an upflow configuration for convenience.

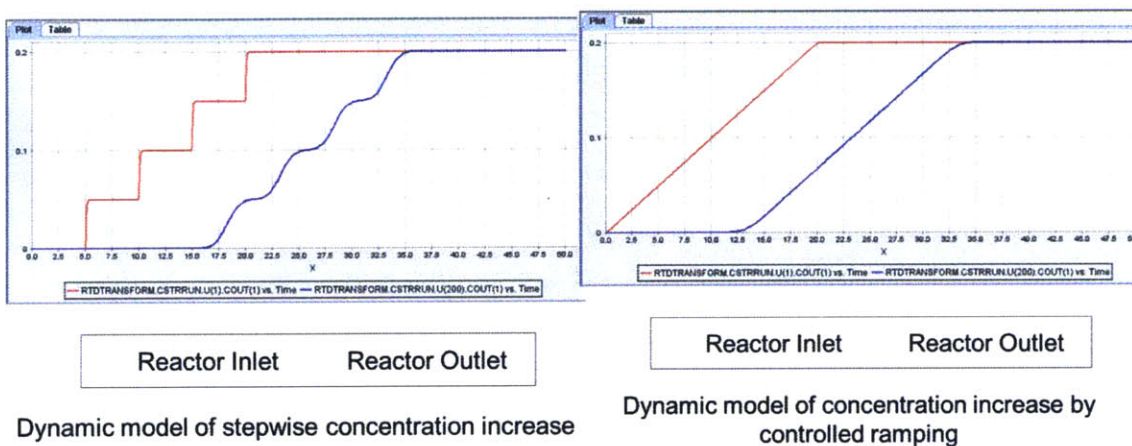


Figure 50. Result of step changes and concentration and linear ramping changes on transient packed bed output.

4.2.2 Hybrid Nanofiltration Module with Holding Tank

4.2.2.1 First Generation Design

The first generation of our nanofiltration membrane module was designed through significant modification of a published module.^[170] The use of this nanofiltration module from the Livingston Group in our flow system created a number of challenges. First, a large volume (>90 ml) cell resulted in a sub-optimal recycle system, given the membrane area and low

permeation rate of PEEK membranes. Second, the use of this cell would have required a second dedicated high-pressure holding tank with gas/liquid separation at 400 psi. This added even more volume to the system. For our first generation design, we minimized the volume of the cell, added low dead-volume ports for 1/16" tubing, and incorporated a holding tank into the membrane module.

The module retentate volume was reduced substantially, from a 20 mm depth to a 3 mm depth. It should be noted that incomplete O-ring compression adds a few more millimeters of depth to the fully assembled cell. A high-pressure sight glass is added to the retentate side of the membrane module which serves as a gas-liquid separation tank as well as a window for measuring the liquid level with a laser. This aspect of the device performed well, and is described in more detail for the 2nd generation membrane module.

The first generation membrane module made use of a stir plate/stir bar to enact mixing in the cell. Due to the confinement within the cell (required for volume minimization: ~25 ml), and the fact that a sightglass was positioned over the membrane area, mixing this way would have to make use of a stir bar on top of the membrane itself. The design shown in Figure 51 demonstrates this approach. The module is fitted with a 1 inch diameter stainless steel removable plug (with an o-ring seal). This plug is further outfitted with a welded glass sight to allow visualization of both the membrane and the stir bar. The sight glass is inverted to minimize dead volume in the cell. This plug is shown in Figure 51. This plug can be used to reposition the stir bar and thoroughly inspect the membrane integrity in between runs without fully disassembling the cell. In order to prevent the stir bar from shearing the membrane active layer, thin supports were used for the stir bar. A variety of materials were used to this effect including stainless steel meshes, aluminum meshes, and porous polyester sheets. All of these thin materials eventually rotated with the stir bar and damaged the membranes. Gaskets could not hold these materials in place during the stirring. Ultimately, a reliable way to enact stirring on the membrane without damaging the membrane itself over days of use was not found. The swelling of the membrane during operation, resulting in wrinkles which trap and perturb the

stir bar, are another reason for the failure of this design. This membrane module is still very useful when stirring through the retentate side of the membrane, forgoing the use of the built-in high-pressure holding tank (which can be replaced with a solid plug). For our application, this would not suffice.

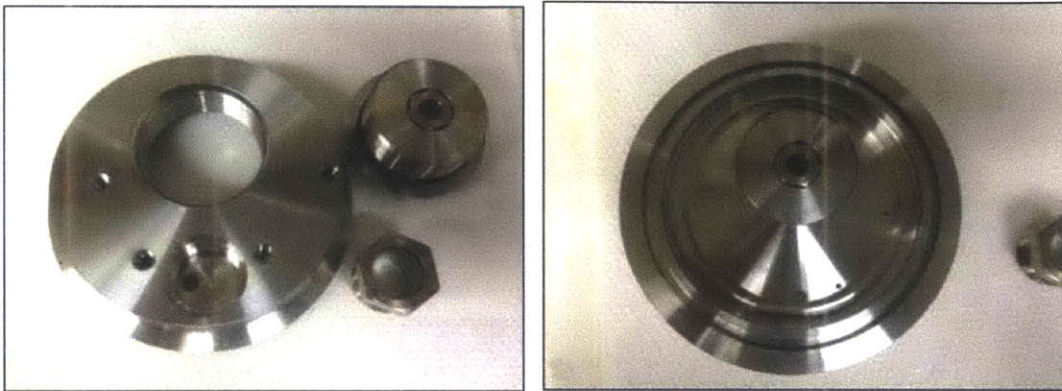


Figure 51. First generation of Nanofiltration module designed to provide a high-pressure holding tank with built-in stir bar visualization.



Figure 52. Image of first-generation Nanofiltration module assembled for operation.

4.2.2.2 *Second Generation Design*

In the second generation design, a further reduction in volume was combined with a high-flow pump recirculation mixing mechanism to replace the stir bar-driven mixing scheme. The residence time distribution in Figure 53 shows that the performance of the module approaches that of an ideal stirred tank, and validates our mixing scheme. A more confined geometry with flow-driven convection (rather than a stir bar) imitates the mixing mechanism of larger-scale spiral wound modules.^[171]

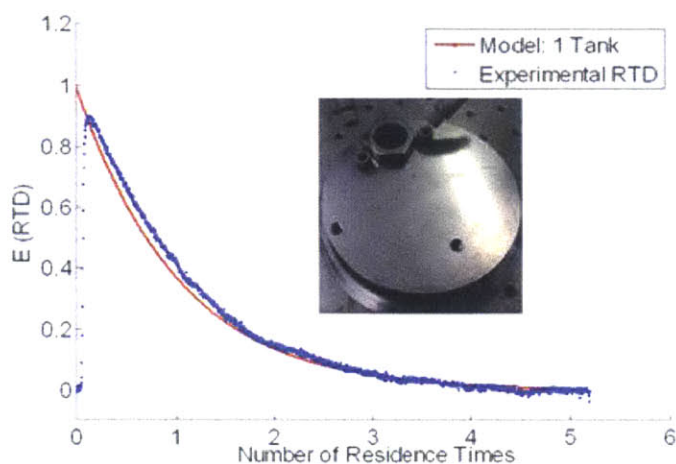


Figure 53. Holding tank/nanofiltration module hybrid used in our continuous flow system. The retentate side behaves as an ideal stirred tank.

Similar to the first generation membrane module, this module was made to incorporate a high-pressure sightglass to serve as a built-in surge tank. As shown in Figure 54, a laser was used to measure the liquid level in this sight glass. This sightglass would also serve as our high-pressure gas-liquid separation tank, with hydrogen being vented through a backpressure regulator.

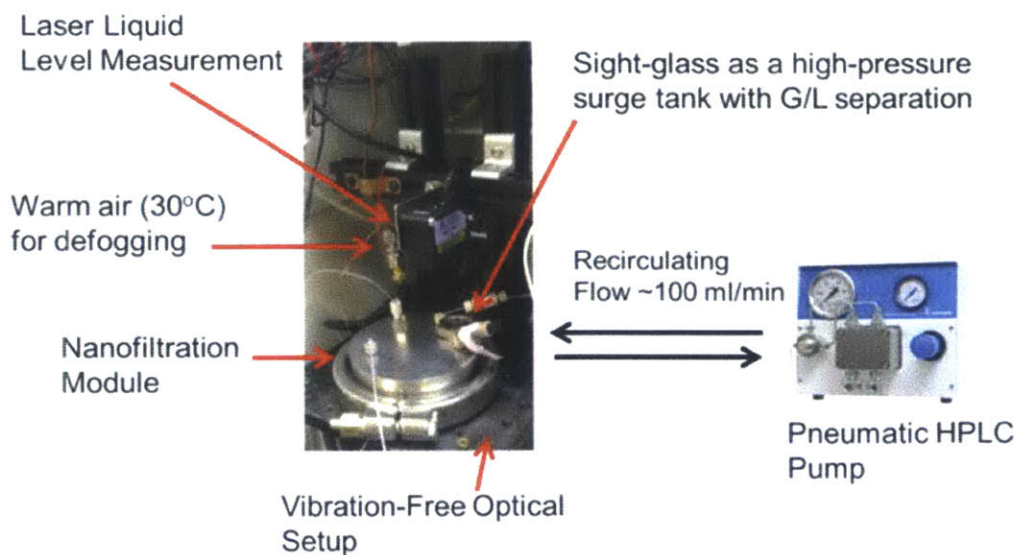


Figure 54. Our second-generation hybrid nanofiltration/high-pressure holding tank with volume minimization, gas/liquid separation, and recirculation-induced mixing.

4.2.3 Pumping and Sampling System

Knauer Smartline 100 pumps were used for the feed pumps and for the recycle pump in the final system. A Knauer pneumatic pump (250 ml head) was used to recirculate the membrane module at high flow rates to enact mixing. These HPLC pumps have a number of limitations, and are not recommended for future work without significant modification. In particular, Viton® gaskets are insufficient for long runs using toluene, and the check valves are not robust enough for long runs, possibly due to catalyst plating, pieces of gaskets which enter the check valve, or other non-ideal aspects of our recycle mixture. A Harvard PhD Ultra syringe pump was used to compress a toluene-filled 25 ml stainless steel syringe to periodically flush out the automatic 3-way valves during the runs.

A nearly identical sampling system to that described in Chapter 3 of this thesis was employed with this chemistry. The one exception was that a different brand of automatic 6-way

valves was employed, since the degraded catalyst created clogs in the smaller Rheodyne 6-way sample valves. For this reason, Gilson (Valvamate II Valve Actuator) with Vici 6-way valves (13S-0388H) were used, which had a 0.02" minimum channel dimension and resisted clogging.

4.3 Experimental

4.3.1 Batch Hydrogenation Experiments

Batch experiment reagents were all handled using a Schlenk line. In open air, 5.5 mg of Dichloro[(4S,5S)-(+)-4,5-bis(diphenylphosphinomethyl)-2,2-dimethyl-1,3-dioxolane][(S)-(-)-2-(alpha-methylmethanamine)-1H-benzimidazole]ruthenium(II) (Strem Chemicals, 44-0955) and 1.2 mg of triphenylphosphine (Sigma Aldrich, 93092) was weighed, added to a Schlenk vial, and cycled with argon (Airgas, grade 5.0) five times. Using purged needles, 0.25 ml of substrate was added to the catalyst vial. The contents of this vial were diluted with 4.25 ml of a 9:1 toluene (Sigma Aldrich, 244511):tert-butanol (Sigma Aldrich, 471712) solution. In a separate vial, 46.9 mg of potassium tert-butoxide (Sigma Aldrich, 659878) was weighed, cycled, and diluted with 1 ml of tert-butanol. Sonication was necessary to efficiently dissolve the base. Argon was flowed continuously into the empty in-house batch reactor to remove trace oxygen. After 10 minutes of argon purging, the base was added to the catalyst solution, and this mixture was then be added to the batch reaction chamber. With a purged needle, 0.175 ml of this base mixture was added to the catalyst vial. This solution was quickly added to the batch reaction chamber with the cap taken off. The batch chamber was drilled shut with an O-ring seal. Hydrogen pressure was adjusted to 400 psi in the batch reaction chamber, and the stir plate was turned on. The hydrogen was slowly vented down to 5 bar. This hydrogen pressure cycling procedure was repeated three times to remove trace oxygen, and the reaction is then run for 40 minutes under 400 psi of hydrogen. Adequate stirring was verified via a sight-glass in the batch reactor, where the reactor was centered such that a vortex was obtained. The solution appeared as a transparent light yellow. A darker color indicated that oxygen had likely poisoned some of the

catalyst during the start-up procedure, and more rigorous oxygen exclusion was therefore warranted.

4.3.2 High-Pressure Batch Catalyst Recycle Tests

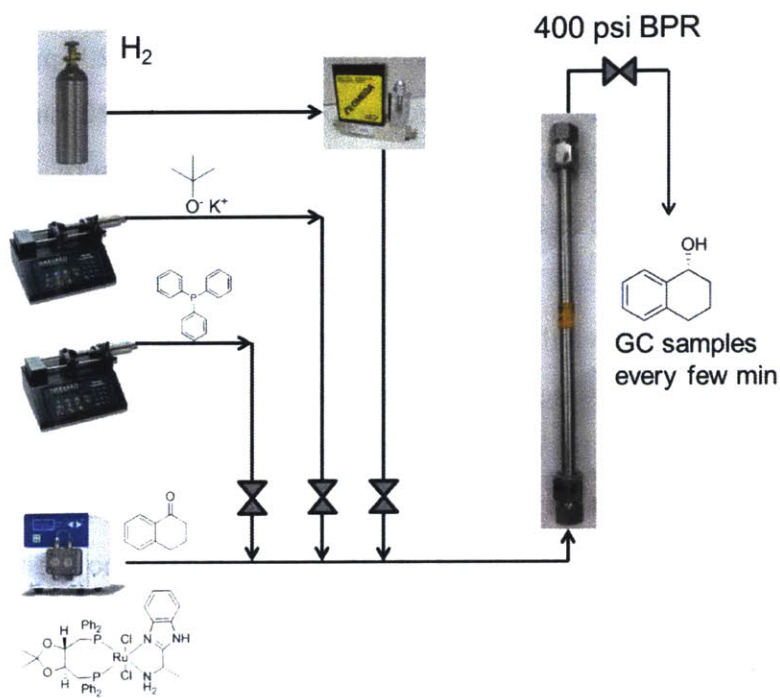


Figure 55. Flow system used to screen kinetics efficiently using a transient upflow packed bed reactor.

The set up shown in Figure 55 was used to perform high-pressure batch recycling experiments. During these catalyst recycling experiments, the hydrogen pressure never dipped below 200 psi in between catalyst uses. First, the normal batch hydrogenation procedure was followed, with the exception that all of the lines in Figure 57 were purged with argon prior to use. Once the batch reaction mixture was put into the chamber, the chamber was drilled shut and the argon source (hooked up to what becomes the vent valve) was closed. The valve positions were set such that hydrogen could be used to pressurize the reaction chamber. The

stir plate was activated and stirring was visually verified via the sight glass. The reaction was allowed to proceed for the 40 minutes. Afterwards, a sample was carefully extracted from the series of two way valves. This was done by starting with both valves closed, opening the valve closest to the reaction chamber, and then closing it again after a few seconds. The second valve was then opened to let the sample expand out into the GC vial. Normally, this was done three times to reduce cross-contamination from previous samples. After the reaction, the hydrogen regulator pressure was reduced to 200 psi, the chamber was vented until it was at 200 psi, and the reaction mixture was allowed to stir under this reduced hydrogen pressure for 20 minutes. The 6-way valve was switched such that the loop was not exposed to the high-pressure hydrogen line. The sample loop (0.25 ml) was then filled with pure substrate **1** from the Schlenk line. The hydrogen cylinder's (Airgas, Grade 5.0) regulator was set back to 400 psi, and the 6-way valve was manually actuated. This caused the substrate in the sample loop to be pushed into the reaction chamber by the high-pressure stream of hydrogen. The reactor pressure continued to rise until its pressure matched the hydrogen cylinder's regulator pressure. The reaction began again, and after 40 minutes another sample was taken as described earlier. This catalyst recycle procedure was repeated two more times. It should be noted that no additional solvent or base was added during these cycles. These experiments only provided a coarse test of catalyst recyclability without reducing hydrogen pressure to guide process design.

4.3.3 Kinetic Screening in Flow

The experimental layout is shown in . Unlike the batch experiments, all the reagents were handled in a glovebox (VAC, 101965) prior to being loaded into the continuous system. Toluene (anhydrous) and tert-butoxide (anhydrous) were purchased from Sigma Aldrich and degassed in the glovebox by stirring prior to use. The Schlenk line was used afterwards to load syringes when necessary. The reactor was connected to the three pumps using a four-way cross from Upchurch Scientific. The lines leading up to the syringe pumps were fitted with closed Upchurch Scientific two-way valves to prevent flow during system start-up. An HPLC pump (Knauer or Lab Alliance, see below) was used to deliver the solvent mixture to the reactor. A 500 psi Upchurch

Scientific back pressure regulator was tuned with an Allen key until the system reached a steady state pressure of 400 psi. During this iteration, the lines that were plugged leading from the cross at the reactor inlet were purged by opening the two-way valves while the system was under pressure and degassed. Five reactor volumes of liquid were put through the system at this pressure to degas the system thoroughly and to reach a hydrodynamic steady-state. Next the solvent mixture was switched out for the catalyst/substrate mixture from the glove box. Flow was paused intermittently during this switch to prevent argon from entering the HPLC pump. Next, the base and TPP stainless steel syringes were loaded with their respective solutions (from the glove box) using the Schlenk line. In order to do this, the solution was connected to the Schlenk line using a needle. Next, the stainless steel syringe was fitted with a needle using 1/4–28 male to female Luer Upchurch Scientific fitting. The stainless steel syringe was purged four times and then filled with the TPP or base solution under a Schlenk line. The two-way valves in the figure remained closed while the two stainless steel syringes were connected to their respective lines in the system. The stainless steel syringes were run until a few drops of solution exited the line, thoroughly purging the lines from the stainless steel syringes. Finally, the lines from the stainless steel syringes were connected to the two-way valves and the syringe pumps were run until they stalled. The two-way valves were then opened and the pumps were started again at the correct flowrates. The pumps were made to flow two reactor volumes, at which point the LabVIEW script was started and the experiment began. Samples for GC were manually collected from the reactor outlet every few minutes.

4.3.3.1 TPP Ramping Experiment

This experiment required two syringe pumps and one Lab Alliance Series 1500 HPLC pump. The two syringe pumps are Harvard PHD Ultra syringe pumps using 8 ml stainless steel syringes. Three stock solutions were necessary for this experiment: one triphenylphosphine stock solution, one potassium tert-butoxide stock solution, and one catalyst/substrate stock solution. The TPP stock solution was made up in the glovebox by weighing 100 mg of TPP and dissolving it in 14 ml of toluene. For the base stock solution, 230 mg of potassium tert-butoxide was

weighed out and dissolved in 6 ml tert-butanol and 3.6 ml of toluene. Finally, 18.5 mg of catalyst and 2.2 ml of substrate were dissolved in 32 ml toluene and 2 ml of tert-butanol. A hydrogen flow of 10 SCCM at 400 psi was used. The HPLC pump was used from this catalyst/substrate mixture at 600 $\mu\text{l}/\text{min}$, and the two syringe pumps were used to pump the TPP (48 $\mu\text{l}/\text{min}$) and base stock (40 $\mu\text{l}/\text{min}$) solutions. After two residence times, only the TPP solution was ramped during the experiment over a 15 minute period decreasing from 48 $\mu\text{l}/\text{min}$ at a rate of 3 $\mu\text{l}/\text{min}$ per minute. The concentration of this stock solution was high enough so that varying the flowrate changed the residence time less than 10%.

4.3.3.2 *Base Ramping Experiment*

This experiment required two syringe pumps and one Lab Alliance Series 1500 HPLC pump. The two syringe pumps were Harvard PHD Ultra syringe pumps using 8 ml stainless steel syringes. Three stock solutions were necessary for this experiment: one triphenylphosphine stock solution, one potassium tert-butoxide stock solution, and one catalyst/substrate stock solution. The TPP stock solution was made up in the glovebox by weighing 20.4 mg of TPP and dissolving it in 7 ml of toluene. For the base stock solution, 230 mg of potassium tert-butoxide was weighed out and dissolved in 6 ml tert-butanol and 3.6 ml of toluene. Finally, 18.8 mg of catalyst and 2.2 ml of substrate were dissolved in 32 ml toluene and 2 ml of tert-butanol. A hydrogen flow of 10 SCCM at 400 psi was used. The Lab Alliance HPLC pump was used to pump the catalyst/substrate mixture at 500 $\mu\text{l}/\text{min}$, and the two syringe pumps were used to pump the TPP (48 $\mu\text{l}/\text{min}$) and base stock (4 $\mu\text{l}/\text{min}$) solutions. After two residence times, only the base solution was ramped linearly during the experiment over a 15 minute period, increasing to 60 $\mu\text{l}/\text{min}$. The concentration of this stock solution was high enough so that varying the flowrate changed the residence time less than 10%.

4.3.3.3 *Residence Time Ramping Experiment*

This experiment required two Knauer Smartline HPLC pumps with 10ml heads. Two stock solutions were necessary for this experiment: a catalyst/substrate stock solution and a

potassium tert-butoxide stock solution. The catalyst stock solution was made up in the glovebox by weighing 3.3 mg of catalyst, adding 3 ml of substrate, and diluting to 40 ml with a 9:1 toluene:tert-butanol solution. The base stock solution was prepared with 134 mg potassium tert-butoxide, 8 mg TPP, and diluting to 40 ml with a 9:1 toluene:tert-butanol solution. A hydrogen flow of 10 SCCM at 400 psi was used. Flow rates of the two stock solutions were 400 $\mu\text{l}/\text{min}$, and were first run for two residence times to reach a steady state. Both of the Knauer HPLC pumps were then ramped from 400 $\mu\text{l}/\text{min}$ to 100 $\mu\text{l}/\text{min}$. Samples for GC were taken every 5 minutes after ramping began.

4.3.3.4 *Substrate Ramp*

This experiment required three Knauer Smartline HPLC pumps with 10ml heads. Three stock solutions were necessary for this experiment: a catalyst stock solution, a substrate stock solution, and a potassium tert-butoxide stock solution. The catalyst stock solution was made up in the glovebox by weighing 3 mg of TPP, 8 mg of catalyst, and diluting to 20 ml with a 9:1 toluene:tert-butanol solution. The substrate stock solution was prepared with 4 ml of substrate and 15 ml of toluene. For the base stock solution, 220 mg of potassium tert-butoxide was weighed out, and diluted to 125 ml of 9:1 toluene:tert-butanol solution. A hydrogen flow of 10 SCCM at 400 psi was used. Flow rates of the catalyst, substrate, and base were 55, 20, and 725 $\mu\text{l}/\text{min}$, respectively, and were first run for two residence times to reach a steady state. The Knauer HPLC pumps ramped the substrate solution from 20 $\mu\text{l}/\text{min}$ to 120 $\mu\text{l}/\text{min}$ while the base solution was ramped from 725 $\mu\text{l}/\text{min}$ to 625 $\mu\text{l}/\text{min}$ over a 25 minute period. This allowed us to continuously change substrate concentration without significantly affecting base concentration. Residence time was held constant in this way.

4.3.3.5 *Catalyst Ramp*

This experiment required two Knauer Smartline HPLC pumps with 10ml heads. Two stock solutions were necessary for this experiment: one catalyst stock solution and one potassium tert-butoxide stock solution. The catalyst stock solution was made up in the glovebox by

weighing 10 mg of TPP, 30 mg of catalyst, and diluting to 20 ml with a 9:1 toluene:tert-butanol solution. For the base stock solution, 210 mg of potassium tert-butoxide was weighed out, added to 3.8 ml of substrate, and diluted to 125 ml of toluene:tert-butanol solution. A hydrogen flow of 18 SCCM at 400 psi was used. Flow rates of the catalyst and base stocks were 60 and 1515 $\mu\text{l}/\text{min}$ and were first run for three residence times to reach a steady state. The Knauer HPLC pump ramped the catalyst/TPP solution from 60 to 190 $\mu\text{l}/\text{min}$ while the base solution was ramped from 1515 $\mu\text{l}/\text{min}$ to 1385 $\mu\text{l}/\text{min}$ over a 10 minute period to continuously change catalyst concentration without significantly affecting base concentration. Residence time was held constant in this way.

4.3.4 Nanofiltration Tests

Rejection of the precatalyst was tested by pressurizing the membrane module with degassed toluene, and allowing five system volumes to permeate. Next the HPLC pump feed was loaded with degassed precatalyst solution, and three system volumes were allowed to permeate. Finally, the permeate and retentate samples were measured by AAS to detect ruthenium rejection. Separate AAS tests were used to show that ruthenium precatalyst and AAS ruthenium standards produced identical calibration curves.

4.3.5 Continuous Recycle System Operation

4.3.5.1 Continuous System Purging (Pre-run)

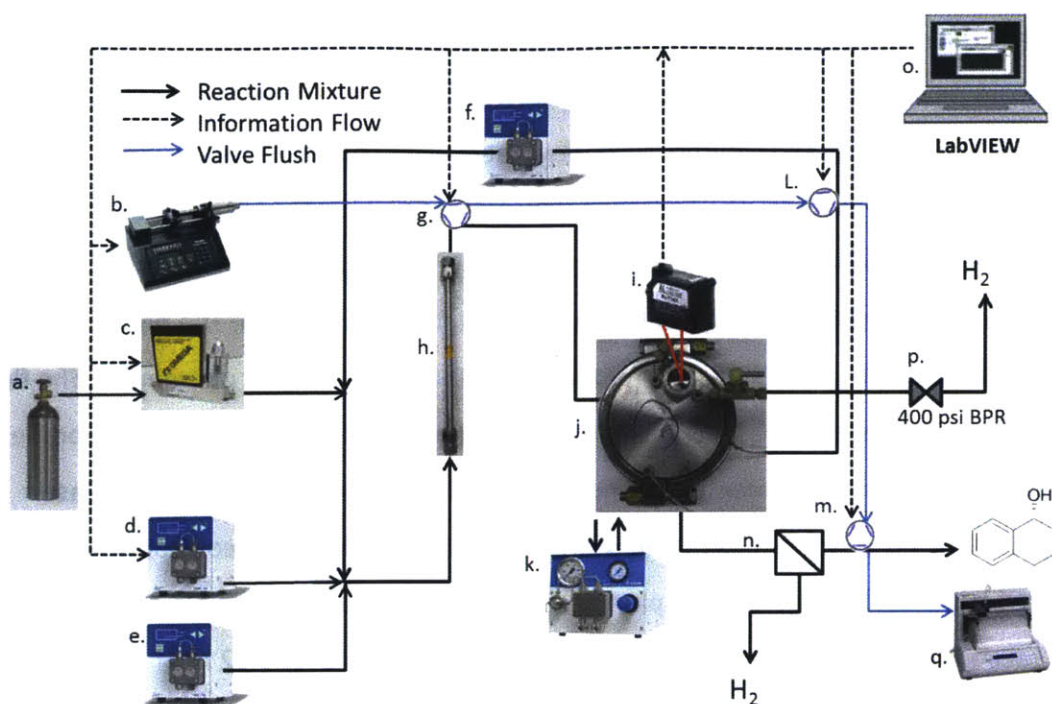


Figure 56. Process diagram for our small-scale continuous recycle system.

With reference to Figure 56, the major pieces of the system include the following: a.) Hydrogen cylinder with regulator b.) Syringe pump for valve-flushing c.) Mass flow controller d.) Inlet pump for catalyst/substrate e.) Inlet pump for base/TPP f.) Recycle HPLC pump g.) Reactor outlet sample valve h.) Packed bed reactor i.) Laser for liquid level measurement j.) Nanofiltration flow cell with built in high-pressure holding tank k.) Recirculation pump for nanofiltration cell L.) Retentate sampling valve m.) Permeate sample valve n.) In-house gas/liquid separator for permeate stream o.) Computer running LabVIEW p.) Series of that pressure regulators adding up to 400 psi q.) Fraction collector. Total internal volume of system is less than 50 ml.

It should be noted that all of the HPLC pump back seals were flushed with degassed, anhydrous isopropanol, and this flush solution was used during the entire system run (including degassing steps) to prevent oxygen from entering our reaction mixtures through the back seals

of the pumps. The entire system was first filled with a 9:1 toluene:tert-butanol mixture. Next, a similar solvent mixture taken from the glove box in a 500 mL Erlenmeyer flask with a septum is hooked up to the two inlet HPLC pump. Next, flow rates were chosen to balance the permeation rate of the module. The hydrogen flow was started (20 SCCM) by actuating the mass flow controller (Omega, FMA5504) using Fieldpoint (National Instruments, cFP-2020). The recycle pump was still switched off such that no solvent recycle occurred. The pneumatic pump (Knauer, Pneumatic Pump 1950) was set to operate at 250 piston strokes per minute. The flow rate of liquid into the system was manually controlled during this time while the membrane module built up pressure. The membrane module was allowed to reach 400 psi. The laser (Keyence, IL-065) was carefully positioned 6 cm above the sightglass. The control system was then started (LabVIEW script). Control parameters of 3300 Kc and 6 τ_i were chosen. The solvent mixture, taken from the glove box, was used to degas the system over a 12 hour period.

The volume of the recycle loop/recycle pump was then purged. First, the retentate 6-way valve sample loop was replaced with 10–32 plugs. Since the system was under high-pressure, the retentate 6-way valve was first switched to isolate the sample loop from the high pressure system. Once the valve's sample loop positions were plugged, the retentate side of the membrane was purged independently from the hydrogen feed. This was done by switching the 6-way valve such that the membrane retentate was isolated from the recycle pump inlet. The recycle pump was purged carefully via the recycle HPLC pump's purge valve. Next, the 6-way valve was switched, and the sample loop was added back onto to the 6-way valve. The 6-way valve was then switched such that the sample loop was contacting the high pressure system and the recycle pump purge valve was quickly opened and closed. Pressure was allowed to build up again and this procedure was repeated two more times.

4.3.5.2 *System Start-Up*

In a glove box, 60 mg of potassium tert-butoxide was weighed out and added to a 40 ml vial. Next, 40 ml of solvent mixture 9:1 toluene:tert-butanol was added. While the control system for the system was running, the base solution was loaded into the HPLC feed pumps.

The recycle pump was set to 1.05 ml/min. This solution was loaded into the system at a rate equal to the permeation rate. In a glove box, 14 mg of catalyst and 5 mg of triphenylphosphine was weighed and added to a 40 ml vial. 40 ml of the same solvent mixture was added to this catalyst. When the base was fully loaded into the system, the catalyst solution was then loaded onto the HPLC pump.. Loading the catalyst required roughly 1.5 hours. This was the amount of time required to permeate almost 40 ml under these conditions. To prepare a base cofeed, 100 mg of base was added to 500 mL of solvent mixture. To prepare a substrate/catalyst cofeed, 17.2 mg of catalyst, 26 ml of substrate, and 30.5 mg of triphenylphosphine were mixed in a 40 ml vial. These materials were diluted by the 9:1 solvent mixture to 40 ml. When only a few ml of the catalyst start-up solution was left over, the catalyst cofeed and base cofeed was loaded onto the two inlet HPLC pumps. The catalyst/substrate cofeed has a fixed 32 μ l/min flowrate. The base cofeed was loaded onto the HPLC pump that was hooked up to the control system. At this point, the fraction collector was started and the associated LabVIEW script was run. This program controlled the flushing pump and automatic 6-way valves so that samples could be automatically obtained.

4.3.6 Analytical Methods

4.3.6.1 GC

Isobutylbenzene was added to each sample in the fraction collector manually as an external standard before running GC (Agilent, HP 6890). This way, absolute concentrations of species at the permeate and retentate sample valves could be inferred using the known volumes of the sample loops.

4.3.6.2 Chiral HPLC

Chiral HPLC was performed with a Chiracel OJ column, 95:5 hexane:isopropanol, flow rate 0.5 ml/min, $\lambda = 215$ nm. Racemic product and the (S) isomer were purchased from Sigma Aldrich for calibration and discovering peak location.

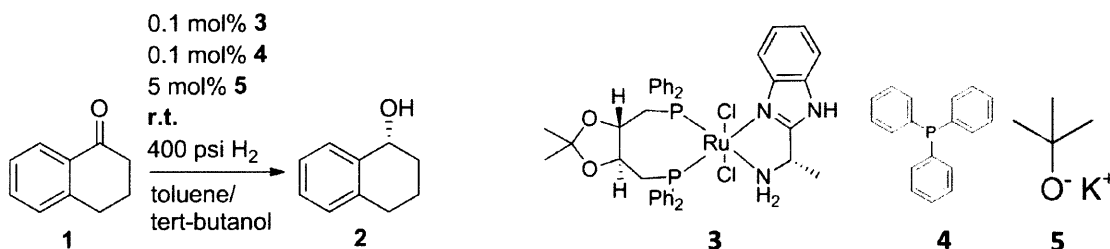
4.3.6.3 Atomic Absorption Spectroscopy (AAS)

Calibration work showed that running a GF-AAS (Agilent, GTA 120, 200 Series AA) routine on unmodified catalyst in 9:1 toluene/tert-butanol gave the same calibration curve as a 1g/L RuCl₂ standard in 1 M HCl (AAS Standard from Sigma Aldrich). No intermediate work-up was necessary when running GF-AAS on permeate and retentate samples, other than dilution to the 50 ppb level before measurement. Glassware or polypropylene containers gave equivalent results. All dilutions were performed with toluene, but ruthenium concentration calculations were performed on a water-basis (i.e., assuming 1 kg/L density of solution mixture rather than using an actual reaction mixture density).

4.4 Results and Discussion

4.4.1 Batch Recycle Tests

For this work, we consider the asymmetric hydrogenation of α -tetralone using a recently improved diphosphine/diamine catalyst shown in Scheme 10 (our batch operating conditions are shown).^[167] As shown in the scheme, a large (832 MW) catalyst was used with two base cocatalysts: triphenylphosphine (TPP) and potassium tert-butoxide. The large non-labile ligands of this catalyst make nanofiltration a good choice for the catalyst separation process block. After being activated by the strong base, this catalyst is rapidly oxidized by air, so it would be important for our continuous recycle system to rigorously exclude oxygen.



Scheme 10. Asymmetric hydrogenation of α -tetralone using a diphosphine/diamine catalyst. An ee of 97% is obtained for this substrate.

We first reproduced Li et al.'s results for a 5 hour batch experiment with substrate **1**. Upon increasing the pressure to 400 psi and increasing the catalyst loading, we were able to reduce the residence time in batch to 40 minutes. These shorter residence times allowed us to test catalyst recyclability more efficiently. Batch catalyst recycling experiments were first employed to test catalyst stability after a reaction since this particular catalyst system had not yet been recycled in the literature,. In order to do this, a high-pressure hydrogenation reaction was first performed. After the reaction, the cell was depressurized and allowed to stir under argon bubbling for an additional 40 minutes. Next, more substrate was added to the reaction mixture and the cell was re-pressurized. It was found that this procedure resulted in a fully deactivated catalyst. When stirring under low pressures of hydrogen after a reaction (instead of bubbling argon), some active catalyst remained, and 40% conversion was obtained after the first cycle for a 40 minute residence time. This observation implied that high pressures of hydrogen might be required to keep the catalyst stable once it was activated. Therefore we constructed a high-pressure batch reactor with the ability to add additional substrate without depressurizing the batch reaction mixture. This set up is shown in Figure 57, and its operation is covered in detail in the Experimental Section. Figure 58 shows the result of re-using the catalyst three times with this batch setup. Since additional substrate could be added with the reactor at 200 psi of hydrogen, with reactions being performed at 400 psi, the reaction mixture was in contact with high pressures of hydrogen at all points in time. This behavior could be due to beta-hydride elimination of the diamine ligand being more likely in the absence of hydrogen.^[172-174] As can be observed in Figure 58, substantial reuse of the catalyst was possible using this batch reactor. The accurate quantification of catalyst stability in this experiment was neither possible nor desired; the purpose of this experiment was only to verify that high pressures of hydrogen resulted in a re-useable catalyst. The process design implication of these experimental results

was that high pressures were necessary at all points in the catalyst recycle loop. Thus, even our surge tank would need to be kept near 400 psi hydrogen at all times.

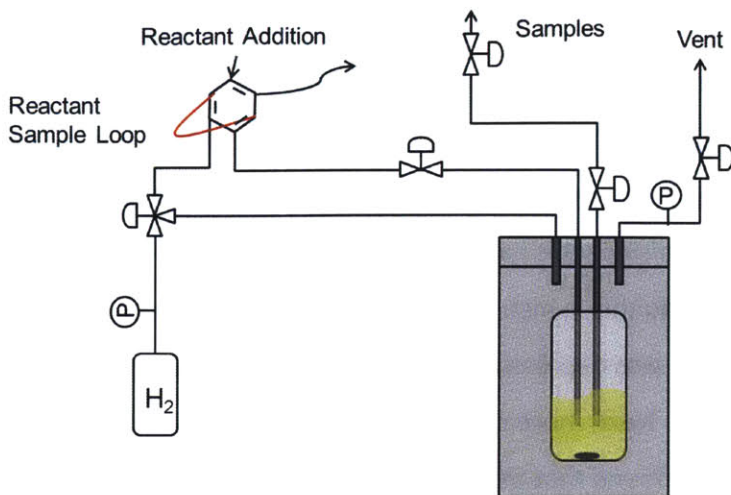


Figure 57. Batch system for re-using catalyst without reducing hydrogen pressure below 200 psi in between catalyst uses.

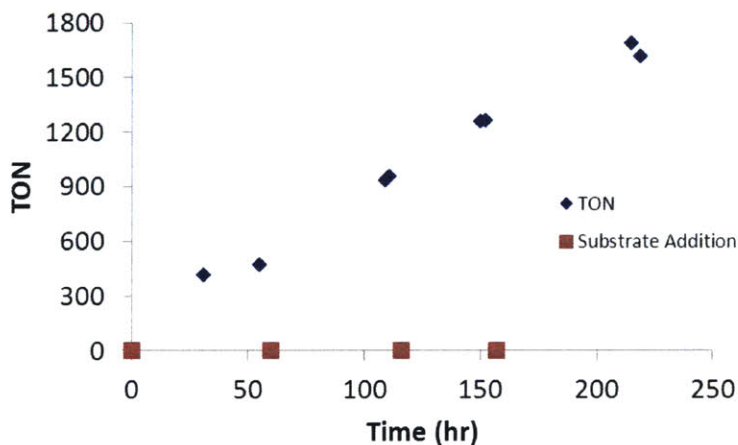


Figure 58. Batch catalyst re-use results the setup shown in Figure 57. Data represents three separate re-uses of the catalyst, showing that some catalyst activity is maintained between cycles. Time waited in between cycles not included. See Supporting Information for details.

4.4.2 Design Space Exploration in Flow

Once the batch reaction was optimized to 40 minutes, and the catalyst was shown to be recyclable, kinetic screening in flow was chosen as an efficient way to fine-tune the conditions of operation. Although flow systems generally take a few residence times to reach a steady-state, it has recently been shown that transient performance of a plug flow reactor can generate accurate kinetic data very efficiently.^[69] Residence time distribution experiments performed on our packed bed reactor confirmed that it was effectively a plug flow reactor in the liquid phase, ensuring that we could use this technique. The layout of our flow system to screen kinetic behavior is shown in , the details of which can be found in the Experimental Section. Multiple pumps were used to deliver separate feedstocks that were mixed with hydrogen before entering our packed bed reactor.

In order to screen the dependence of the reaction rate on potassium tert-butoxide concentration, the system was run with a linear ramping of potassium tert-butoxide flowrate with a nearly constant total flowrate (Figure 59). At low potassium tert-butoxide concentrations, the reaction rate is reduced. However, at increasingly high potassium tert-butoxide concentrations, the reaction rate plateaus. Figure 59 also shows the results of varying TPP concentration on the reaction rate while operating at partial conversion. TPP was found to have little effect on the reaction rate over this concentration range. Therefore, for our cathat can be maintained without affecting our reaction rate significantly. This is an important point because maintaining concentrations within a narrow range in our catalyst recycle system would have required additional control loops.

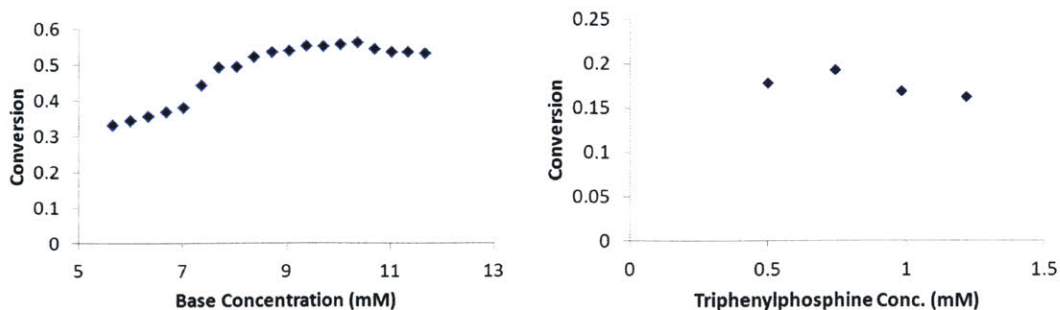


Figure 59. Base and TPP concentrations have little effect on kinetics near our operating point, giving us robust kinetic behavior near our operating conditions.

The substrate concentration was ramped using a setup similar to that in . When ramping the substrate concentration, we found that we generated the same amount of product regardless of the inlet concentration of substrate (see Figure 60). Thus, under our conditions, the reaction is approximately zero order in substrate. This had a number of implications on our process design.

For a catalyst recycle system involving a nanofiltration membrane, we expect the product rejections to increase with time and plateau during start-up. This, combined with the ‘snowball effect’^[175] associated with a closed loop recycle system, imply that we would build up a high concentration of product in our recycle loop. If we operate the reactor at higher substrate concentrations, this buildup would likely result in significant loss of permeation at steady-state due to concentration polarization and/or fouling at the membrane surface.^[40] If our reaction rate was first order in substrate, we would pay a penalty in reaction rate when trying to reduce substrate concentration. For zero order kinetics, however, there is no rate penalty for operating at lower substrate concentrations. Using this information, we were able to operate at lower concentrations of **1** (0.08 M) to reduce fouling of the nanofiltration membrane without decreasing the reaction rate in our reactor.

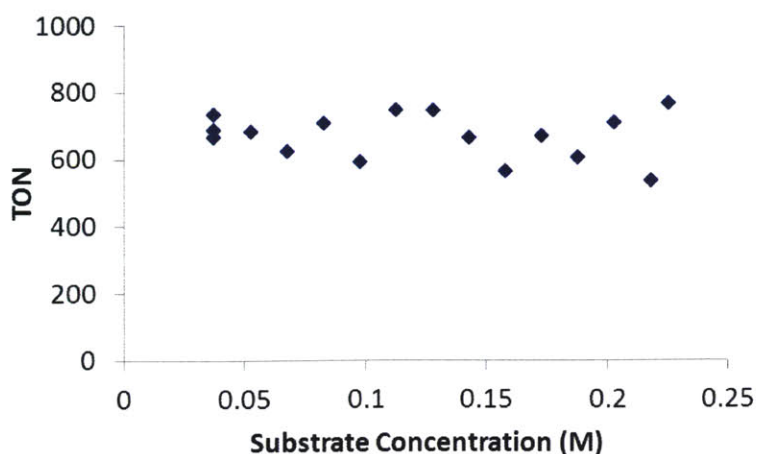


Figure 60. TON obtained as a function of inlet substrate concentration. Substrate concentration has no effect on reaction rate.

The residence time was screened by linearly ramping all of the pump flow rates simultaneously. This approach was similar to the approach of Moore and Jensen, however in their case nonlinear pump flow rate changes were employed.^[69] The residence time of a fluid exiting the reactor can be calculated using the equation:

$$V_{Reactor} = \int_{t_{enter}}^{t_{exit}} Q(t) dt \tag{2}$$

Here, the $V_{Reactor}$ is the dynamic hold up of the liquid in the reactor, t_{exit} is the time at which the fluid was collected, and $Q(t)$ is the flowrate as a function of experimental time. The equation can be solved for t_{enter} , the time at which the fluid packet of interest entered the transient packed bed reactor. Once t_{enter} is deduced, the difference between t_{exit} and t_{enter} gives us our residence time experienced by the fluid leaving the reactor at time t_{exit} . Using this technique, the conversion as a function of residence time is obtained efficiently. Figure 61 shows this yield as a function of residence time. The linearity is consistent with our zero-order rate dependence on substrate concentration. This data was obtained in a few hours with our system, which compares well with cumbersome steady-state flow experiments that would take

over 10 hours to produce 10 data points, assuming three reactor residence times are required to reach each steady state.

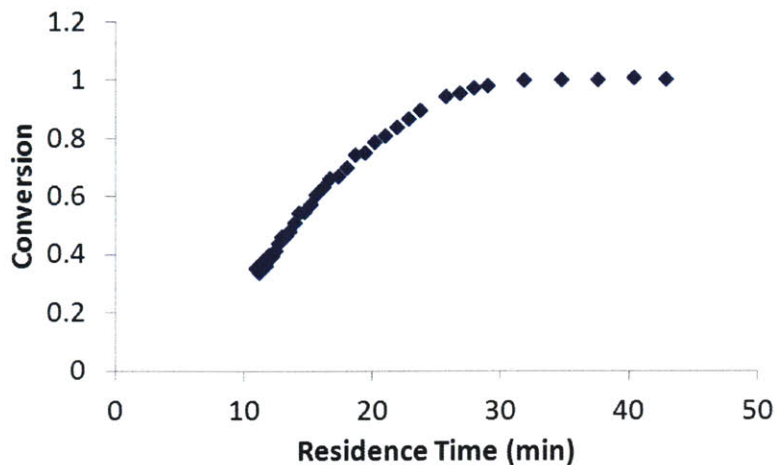


Figure 61. Yield as a function of residence time obtained during a kinetic ramping experiment.

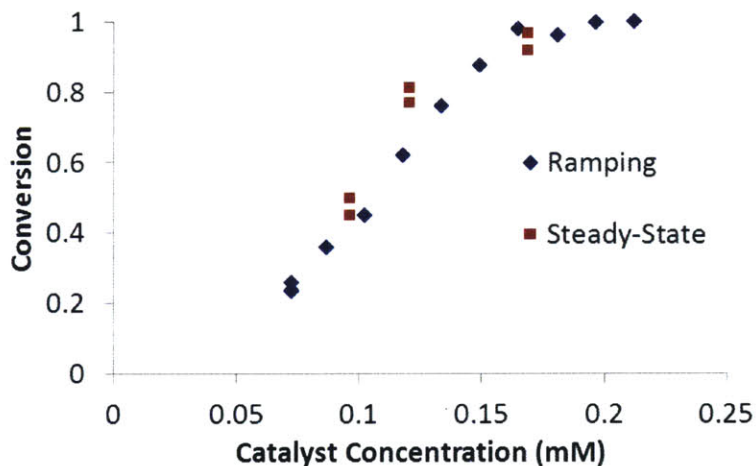


Figure 62. Conversion as a function of catalyst concentration obtained during a kinetic ramping experiment. Steady-state data were obtained afterwards to verify the accuracy of the more efficient ramping approach.

Finally, catalyst concentration was ramped under our optimized conditions at a five-minute residence time and 400 psi high of hydrogen. The result of this experiment is shown in Figure

62. Since our yield has a strong dependence on catalyst concentration even at this 5 minute residence time, we can conclude that we are not mass-transfer limited under our operating conditions. This implies a minimum mass transfer coefficient of 0.0045 sec^{-1} , which is consistent with literature values for small scale upflow packed bed reactors near our flow rates (also referred to as flooded bed reactors).^[176, 177] From Figure 62 it can be seen that catalyst concentrations near 0.225 mM would allow for both high conversions and robust kinetics. Figure 62 includes steady-state data points that verify that the approach of Moore and Jensen^{ref} is accurate for our high-pressure multiphase packed bed reactor. In our estimation, using this ramping approach reduced the amount of time necessary to produce these results to about a third of the time, even when including the more complicated data analysis.

4.4.3 Continuous Recycle Performance

After verifying the recyclability of the catalyst in batch and exploring the kinetics of this reaction in flow, a small-scale flow system was built to recycle catalyst **3**, and is shown schematically in Figure 56. There are a number of small-scale process blocks that are discussed in detail in the Experimental and Process Design Sections. Here, a general overview of the process flow diagram will be given and its performance discussed. It is a well-known phenomenon that, when scaling up an oxygen-sensitive chemistry, much better oxygen exclusion is observed on scale.^[5] In order to more accurately predict what can be achieved in larger scale systems, we needed to use the most rigorous oxygen exclusion techniques that were practical on a laboratory scale. For this reason, all the reagents were handled in a glovebox prior to being loaded into the continuous recycle system. This was not the case for our earlier batch reactions.

Starting with the left-hand side of Figure 56, an inlet substrate solution is mixed with an inlet potassium tert-butoxide/TPP solution and a recycle stream with the membrane retentate stream. Before combining with the two inlet feeds, this recycle stream is mixed with a hydrogen source at a fixed mass flow rate. This allows the flow direction and approximate flow rate to be

visually verified through the clear tubing of the recycle stream. The two inlet streams and recycle stream are mixed in a four-way cross, and enter the packed bed reactor at approximately 400 psi. After the reaction, the mixture proceeds to the nanofiltration module. In this module, gas/liquid separation occurs and hydrogen is vented through 400 psi of back pressure. The level of the liquid in the module is measured with a laser and used to automatically control the inlet flows via a LabVIEW script. A product stream permeates through the nanofiltration module, and a concentrated catalyst solution enters the in-line HPLC pump which re-pressurizes the recycle line back to the inlet conditions. In this way, our catalyst is continuously separated and recycled back to the reactor. It should be noted that at no point in this system does the pressure fall below 400 psi. This increases the stability of our catalyst. At three points in the system, automatic sampling valves with sample loops are used to probe the conditions in the system. At the experimental times defined by the LabVIEW script, these valves switch and their loops are flushed out into a fraction collector by a controlled syringe pump. Throughout all the runs, the control system responded to membrane flux decline due to fouling and concentration polarization by reducing inlet flowrates. During normal operation, significant hydrogen outgassing was observed from the permeate stream, implying that hydrogen has not been depleted in the retentate side. This outgassing rate was measured to be 2 SCCM at 400 psi when the permeate flow rate was 500 $\mu\text{L}/\text{min}$. This implies that our solvent in the retentate side of the membrane is near saturation with hydrogen. An in-house gas/liquid separator was used to continuously remove this hydrogen before the permeate sample valve. Our sample loop on the permeate stream was therefore always full of only liquid, allowing the direct quantification of absolute concentrations in our system via the use of isobutylbenzene as an external standard (GC).

In order to test the recyclability of the catalyst in our flow system, catalyst and base were first loaded into the entire system (see Experimental Section for details). Next, substrate, base, and TPP were loaded into the inlet pumps and the system was allowed to operate automatically for 19 hours. Since no catalyst was co-fed into the system during this time, the initial charge of

catalyst was allowed to deactivate over this time period. Figure 63 shows the fraction of product in the retentate stream throughout the run. This data was obtained via the retentate valve which was automatically actuated/flushed every hour during the run.

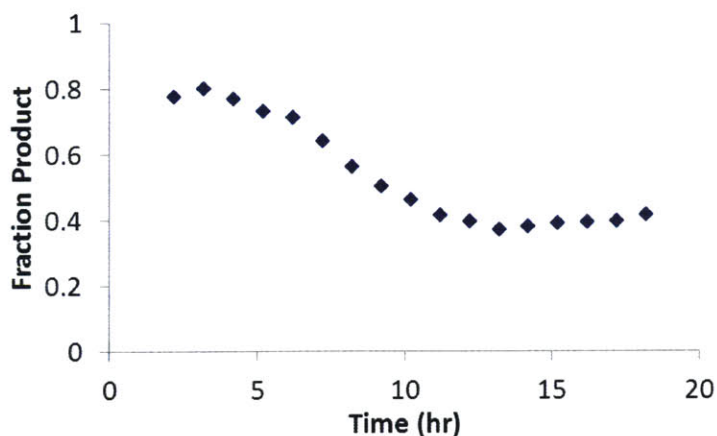


Figure 63. Fraction product in the retentate of our system as a function of experimental time. No catalyst is co-fed during this run.

It can be seen that the product fraction declined significantly during the 19 hour period due to catalyst deactivation. The catalyst solution did not become a darker orange (indicative of oxidation), so we do not believe oxidation to be the major mechanism of catalyst deactivation. Loss of the catalyst through the membrane during this run was insignificant, with an average catalyst rejection of 99.6%. Our ruthenium concentration in the product stream was maintained below 200 ppb. A catalyst turn over number (TON) of 10,800 was obtained for this run. The residence time in our reactor under these conditions was 5 minutes. Our system is able to deliver this result by operating at relatively high catalyst concentrations (to obtain short residence times) and continuously separating and recycling the catalyst while maintaining its activity under high pressures of hydrogen gas. In this sense, catalyst recycle loop is used as both a process intensification technique and a way to improve TONs. After gauging the catalyst recyclability in our system, we designed an experiment which would allow for high conversions to be obtained over 24 hours. The system was started up similarly to the previous example

except that in this case, catalyst was co-fed along with the substrate into the system. This co-feed ratio is much higher than the ratio of catalyst to substrate within the reactor, which reflects the reuse of the catalyst in the system. A substrate:catalyst cofeed ratio of 9400:1 was chosen for this continuous run. Figure 64 shows the conversion versus experimental time for this run. Conversions in the permeate, retentate, and reactor outlet are maintained high throughout the 24 hour experiment. Near the end of the experiment, the substrate feed was cut in half in order to compensate for a slight decline in conversion. This was necessary because the amount of catalyst co-fed into the system was too low. This action was taken before a significant decline in permeate conversion was observed. The overall TON obtained in this experiment reflects this reality: a TON of 4750 was obtained for this 24 hour run. The TON per pass in the reactor approached 250, demonstrating that the catalyst was reused over 15 times on average in this system. The flow system performed the equivalent of 60 reactions, separations, and recycles during this time period, with catalyst being partially purged (via sampling) and partially made-up every cycle. Furthermore, the ruthenium measured in the permeate (via AAS) was always below 200 ppb, with a rejection of 99.6%. During the run, however, the enantioselectivity declined from 97% to 93%. This is likely due to the partial degradation of the catalyst into a species that catalyze formation of the byproduct. It could be due to a racemization of the diamine ligand via a beta hydride elimination, a reaction which has been observed in the literature for similar catalysts.^[173]

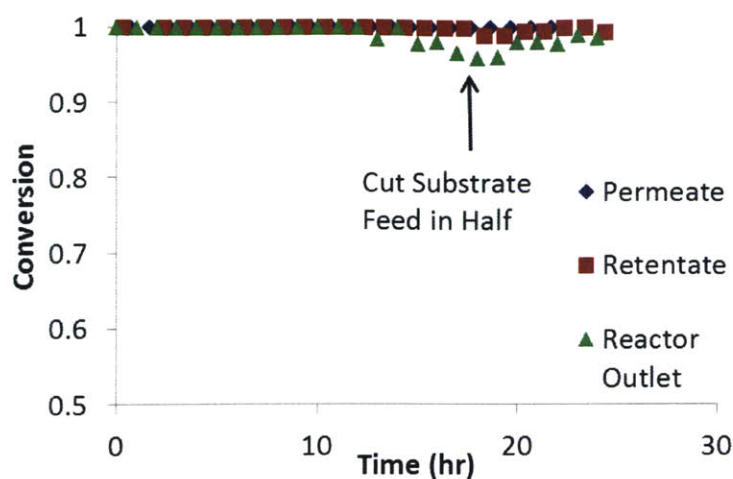


Figure 64. Conversion as a function of time during a system run which includes a catalyst co-feed.

Our product rejection versus time is shown in Figure 65, which shows an initial rise and plateau. This substantial increase in product rejection occurs despite the low concentrations of substrate which are employed in this system. Increases in rejection via membrane fouling and concentration polarization are disadvantages of nanofiltration applications and can be probed efficiently and automatically with our system. The product rejection increases from an initial value of -20% to 40% during the 24 hour run. The negative rejection is consistent with independent rejection tests for the product, and implies that, under dilute conditions with no fouling, our product is actually more permeable than our solvent mixture. This significant increase in rejection was minimized through the use of a high recirculation rate through the retentate side of the membrane using the high-flow pneumatic pump.

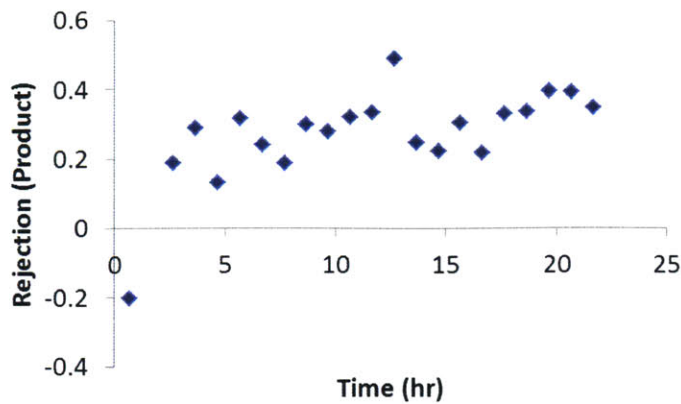


Figure 65. Rejection of product by the membrane as a function of experimental time for our run with a catalyst cofeed.

These rejections as a function of experimental time were fed into a dynamic Jacobian® model, along with the experimentally observed permeation rate. Residence time distributions of the individual process blocks were incorporated into this Jacobian® model. Using this semi-empirical model, the expected permeate, retentate, and reactor outlet product concentrations can be calculated assuming full conversions are obtained. Figure 66 shows the retentate and permeate experimental data plotted against the dynamic model calculations for our inlet conditions. The close match verifies our understanding of the dynamic mass balances in the system under actual operation, and ensures that the system is operating as intended. This model is a good starting point for discovering systems-level improvements in our pilot through simulation, and is discussed in more detail in Chapter 6.

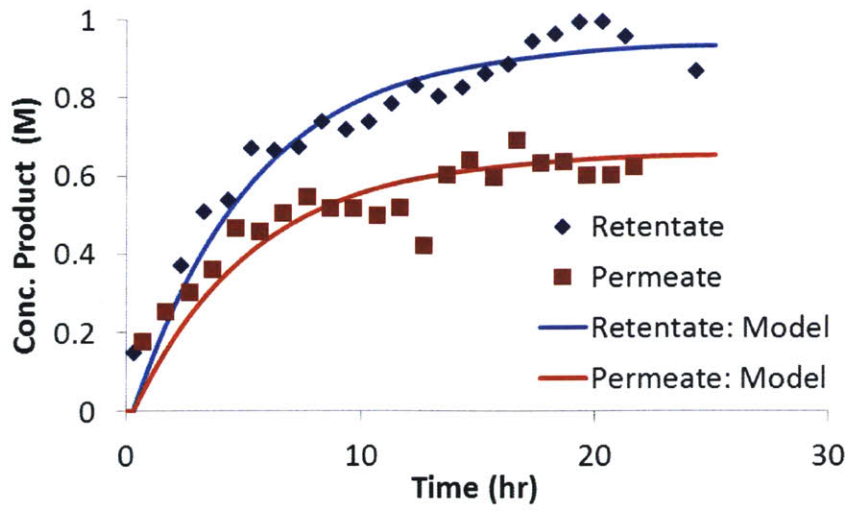


Figure 66. Dynamic Jacobian[®] model calculations match our experimental product concentrations at two points in our system.

4.5 Economic Analysis

The catalyst recycle pilot presented in this chapter was used as a basis for economic comparison with more commonly used production processes. Our characterization of the kinetics of this system provided the basis for considering a wide range of theoretical competitive processes. A number of important assumptions were necessary in obtaining an order-of-magnitude estimate of various scaled-up process configurations. These assumptions will be categorized below as general assumptions and process-specific assumptions.

Our general assumptions apply to all of the process configurations which were analyzed. As we were only interested in one specific chemical transformation, our estimates provide a present cost of each process instead of a net present value. For our present cost analysis, we assumed a 10 year plant lifespan, with a 7% discount rate. We consider, specifically, the asymmetric hydrogenation of α -tetralone, as discussed earlier in this chapter. We ignored the time-to-market costs associated with differences in development times for the various process configurations. Since we were only interested in an order of magnitude comparison of process costs, only major equipment was considered, with large Wroth factors (here we use 4 for all major process block capital costs) to attempt to take into account ancillary equipment and FDA compliance.^[178] We ignored the costs associated with safety measures, which might be radically different for some of the processes presented, particularly due to differences in required reactor volume under high-pressures of hydrogen. Process blocks and the various process configurations were specified so as to meet a given tablet production rate (2000 t/y or 200 t/y). 2000 t/y was the base-case tablet production rate, with 30 wt% API loading in the tablets.^[178] A lower production rate of 200 t/y was also considered, to investigate whether process scale is expected to have a large impact on relative present cost. Our catalyst cost was assumed to be between 5-40\$/g following the suggestion of Cornils et al.^[5] Catalysts cost of \$5, \$15, and \$40/g were considered to simultaneously probe on-scale catalyst cost as well as any potential savings from metal recovery. It should be noted that ruthenium should cost near \$2.1/g, so much of the

catalyst cost is associated with the enantioselective ligands.^[179, 180] Present cost for a ten-year investment was calculated according to:

$$PV = \sum Capital\ Costs + \sum_{i=1}^{10} \frac{Operating\ Costs}{(1 + 0.07)^i} \quad (21)$$

Our adsorption process used 3-aminopropyl silica gel, and the cost on scale was obtained from Silicycle as less than \$1/g, and so \$0.5/g was used as a conservative estimate. Large-scale membrane module applications were assumed to make use of Evonik's 40-40 spiral-wound membrane modules which are 4" in diameter and 40" in length. These modules contain 5m² of membrane surface area, and were costed at \$15,000 each. The membrane packaged in the module would cost approximately \$6000, and is expected to have a one year lifetime. The membrane used in our experiments is not on the market, so this cost refers to a popular Puramem 380S membrane with a 600 MWCO. Flow/batch reactors were costed as high-pressure horizontal vessels, while adsorbers were treated as low-pressure horizontal vessels.^[181] The concentration of the feed for all processes was 0.6M in substrate and 12mM in potassium tert-butoxide. The cost of this base is uncertain, since we found the reaction to work best with very pure (sublimed grade, 99.9% Sigma Aldrich) base. We used \$20/mol at the suggestion of Dumrath et al.^[180] This source likely overestimates the cost but for a much less pure material. The recycle of the potassium tert-butoxide, although not a focus of our studies, has a significant positive impact on process economics. We assumed a factor of 7 reduction in the use of this relatively expensive base (we applied a factor of 9 reduction experimentally in our recycle system). In all cases, the reactor was operated at 400 psi of hydrogen pressure, and it was assumed that, on scale, sufficient mass transfer could be obtained in a flow reactor (via static mixers, etc.) to allow at least 64% of the reactor volume to be liquid.

Four major process configurations were considered. First, a simple flow reactor with a downstream 3-aminopropyl silica gel to remove the ruthenium to 170 ppb was considered. This material has been used in the literature to perform ruthenium removal on a similar catalyst for a similar reaction mixture.^[182] The substrate to catalyst ratio in the reactor was 500. This

allowed for a direct comparison with our catalyst recycle system, which had a feed of 0.6 M, with a membrane to reduce ruthenium contamination to 200 ppb in the product. Substrate-to-catalyst ratio in our reactor was also 500, however our nanofiltration/recycle system could obtain TONs of 4750. Another difference is that in the recycle loop, the substrate concentration was 0.1 M due to the dilution from the recycle stream. Due to the zero-order dependence of the reaction on substrate, this dilution had no effect on process costs. For zero-order substrate kinetics, a fall in substrate concentration reduces throughput, yet reduces residence time enough to keep reactor size constant to meet a fixed production rate. For this reason, residence times are 6 times higher in systems without a recycle loop. This has no impact on reactor size or process economics for this chemistry. High residence time reactors were also specified for the nanofiltration and adsorption processes. The catalyst concentration can be reduced by a factor of 20 in both of these processes, with a consequent 20-fold increase in residence time in the reactors. These modifications to the processes create reactor volumes approaching 10,000 L (increased from ~500 L), but capital cost increases are far outweighed by catalyst cost savings. The increase in process safety concerns due to the larger scale high-pressure reactor is outside of the scope of this analysis. Our theoretical 100 minute residence time reactor with nanofiltration and catalyst recycle proved to be our best economic scenario. The 600 minute residence time reactor with adsorption had much higher costs than our recycle, and so a process with a 600 minute residence time reactor, with no adsorption step, was also considered. For this case, it was assumed that downstream processes would remove ruthenium via waste streams, and so contamination was not an issue. This process, surprisingly, was still inferior to a nanofiltration/recycle system. This is mainly due to catalyst cost savings for a \$15/g catalyst cost assumption.

A theoretical 100 hour residence-time batch reactor was also considered. The performance of this reactor was predicted using our kinetic experiments. Any residence time of this magnitude would allow for a catalyst concentration near 200 ppb (in ruthenium), making downstream catalyst removal irrelevant. However, the high residence time causes large reactor

volumes to be necessary, adding to capital and operation costs. Twice as many operators per reactor were assumed for batch reactors compared with flow reactors, following the textbook approach. It was assumed that the batch reactors operated with 77% efficiency, which would imply relatively efficient operation.^[178] Again, concentrations of 0.6M substrate for the feed were used. Post-reaction base quenching, if necessary, is not expected to be a significant cost and was not considered, although this would likely impact efficiency of reactor usage. Since this analysis ignores safety concerns, it is economically favorable to use one large reactor (at 75% liquid holdup) with reduced catalyst loading. This is unrealistic, since the size of the high-pressure reactor would be 100,000 L, combined with an extremely long (100 hour) residence time. The parallelization of multiple smaller batch reactors, which could potentially deal with the safety concern, would drastically increase to the number of operators necessary for this chemical process and significantly increase process operation costs, rendering the process uncompetitive with our nanofiltration/recycle system.

Table 8. Summary of order-of-magnitude economic evaluations of six different process configurations.

	NF_5min	AD_5min	NF_100min	AD_600min	Batch_100hr	React_600min
Reactor Volume (L)	1,152	1,152	9,717	9,717	106,450	9,717
Number of Reactors	1	1	1	1	1	1
Cap - Reactor	\$0.07M	\$0.07M	\$0.24M	\$0.24M	\$1.26M	\$0.24M
Cap - Absorber	\$0.00M	\$0.02M	\$0.00M	\$0.02M	\$0.00M	\$0.00M
Cap - Nanofiltration	\$0.31M	\$0.00M	\$0.31M	\$0.00M	\$0.00M	\$0.00M
Op - Solvent	\$4.36M	\$4.36M	\$4.36M	\$4.36M	\$4.36M	\$4.36M
Op - Reactor	\$0.16M	\$0.16M	\$0.16M	\$0.16M	\$0.32M	\$0.16M
Op - Absorber	\$0.00M	\$15.15M	\$0.00M	\$0.76M	\$0.00M	\$0.00M
Op - Nanofiltration	\$0.78M	\$0.00M	\$0.78M	\$0.00M	\$0.00M	\$0.00M
Op - Catalyst	\$7.88M	\$74.88M	\$0.39M	\$3.74M	\$0.37M	\$3.74M
Op- Base	\$0.20M	\$1.20M	\$0.20M	\$1.20M	\$1.20M	\$1.20M
Total Capital	\$0.38M	\$0.09M	\$0.55M	\$0.26M	\$1.26M	\$0.24M
Total Operating	\$13.38M	\$95.75M	\$5.89M	\$10.22M	\$6.25M	\$9.46M
Present Cost (10-yr)	\$94.35M	\$672.59M	\$41.93M	\$72.05M	\$45.18M	\$66.70M

The results of the economic analysis using a 2000 t/y production rate and \$15/g catalyst for six different cases involving four different theoretical processes are shown in Table 8. The first case is a direct scale-up of our experimental conditions for nanofiltration/recycle of the hydrogenation catalyst. The capital costs of such a process are expected to be relatively small compared with the operating costs. In fact, the capital costs of all processes considered in this economic analysis are substantially smaller than associated operating costs in a 10-year present cost analysis.

The solvent cost of 4.36M for this process is the same for the other processes, with the understanding that this solvent cost may, in a real chemical production plant, be shared with other upstream or downstream processes. Furthermore, we are ignoring opportunities for the recycle of the solvent in the overall process scheme. We also ignore any potential energy savings obtained through solvent incineration, which is a common practice. Our economic estimates do not consider energy costs, as simple calculations showed that their magnitudes were much smaller than material operating costs. Even larger than the solvent cost is the catalyst cost, which is predicted to be over \$7M/y. Replacement of the nanofiltration membrane once per year, using the price of a Puramem 360S (since PEEK 800 is not yet on the market), amounts to \$0.78M/y. Replacing the nanofiltration/recycle process block with an adsorber makes the operating costs substantially higher. Column 2 in Table 8 shows that this process incurs a cost of over \$70M/y in catalyst, with an additional 15.2M/y in adsorption bed material. Smaller savings in capital costs and module maintenance costs do not make up for the catalyst and adsorption bed cost increases. The third column of Table 8 presents the economic effects of increasing the residence time of the reactor in our nanofiltration/recycle process from 5 to 100 minutes. This allows for a lower catalyst loading, and a reduced catalyst cost for the process. The disadvantage is a significant increase in reactor size, which is a safety concern (an increase from 500 L to almost 10,000 L). Using this approach, the catalyst cost is reduced to \$0.39M/y, with other operating costs being unchanged. Column 4 shows the adsorption process in which the reactor residence time was also increased by a factor of 20, to 600 minutes. The catalyst cost for this case is reduced to \$3.74M/y, and adsorbent operating costs are reduced to \$0.76M/y, The base cost of \$1.2M/y is still very high compared with \$0.2M/y for our nanofiltration process. Column six presents a process in which no adsorption is used after the reactor, and it is assumed that other, unspecified downstream processes purify the mixture adequately. This simple process, consisting of only a high-pressure flow reactor, is still inferior to our nanofiltration recycle system due to the catalyst cost savings and and base cost savings. Finally, column five shows the economic aspects of a homeopathic batch reactor. The catalyst

loading here is low enough to make catalyst costs irrelevant, however a 100,000 L reactor is necessary, which presents significant safety concerns. The capital cost for such a reactor begins to become significant relative to the operating costs, and the base cost of \$1.2M/y makes the nanofiltration recycle system economically competitive. One large batch reactor is unlikely to be pursued industrially. The parallelization of smaller batch modules as possible, but such a case would explode operation costs, since two operators are typically required per reactor and each costs \$160,000 per year. Thus, even 4-5 additional operators for safety purposes, or due to the complexity of multiple batch reactors, is enough to make the batch process uncompetitive with the nanofiltration/recycle system. The 100 hour residence time presents further practical difficulties outside of the scope of this analysis. We found that changing the scale of production (200-2000 t/year) had little effect on these trends. Variation of catalyst costs within a reasonable cost range (5-40\$/g) also had little effect on the cost trends. This order-of-magnitude economic analysis demonstrates that our nanofiltration system is a potentially competitive and industrially relevant process.

4.6 Conclusion

A small-scale flow system was developed to continuously separate and recycle an asymmetric ketone hydrogenation catalyst. This catalyst was used to reduce α -tetralone on a batch scale, and batch recycle tests implied that the catalyst was most stable when kept under high pressures of hydrogen. This fact required us to re-design a commercial nanofiltration module to include a high-pressure holding tank with liquid level control. The kinetics of this transformation were explored efficiently in flow via the transient operation of a small-scale packed bed reactor. Our kinetic studies showed that the cocatalyst concentrations were not major drivers of reaction rate, and so control systems to maintain their concentrations in the recycle loop were not necessary. We also learned that, near our operating conditions, the reaction rate was zero order in substrate concentration. This allowed us to operate at lower concentrations of substrate to help reduce membrane fouling, without having an appreciable impact on our reaction rate. During a 24 hour run, we were able to maintain high yields in our system, with a turnover number near 5000 for the process. This represents significant catalyst re-use when considering that the approximate substrate-to-catalyst ratio in the reactor is only 250. The rigor with which we can investigate catalyst reusability can be conceptualized by considering the average residence time of the full recycle loop, which is about 24 minutes. After 24 hours of operation, we have recycled the (continuously changing) contents of the loop an average of 60 times. The PEEK nanofiltration membrane survived the harsh conditions of this reaction while providing 99.6% rejection throughout the run. For this reason, ruthenium leaching in the permeate stream remained less than 200 ppb. The enantioselectivity (ee) of our transformation was reduced from 97% to 93% during the run, implying that some of our deactivated catalyst is catalyzing the production of the wrong enantiomer. Finally, we constructed a dynamic process model to verify our understanding of this flow system. Our small-scale catalyst recycle process was used to efficiently perform a systems-level evaluation of nanofiltration as a catalyst recycling approach for this chemistry. Future work should focus

on making the process more robust and adding the necessary control systems to run this system for more than a week and obtained a true controlled state. The rate of catalyst purge from the system should be controlled by the enantioselectivity measured in the system, so as to obtain a steady-state ee value in the system. An economic analysis is also included, which demonstrates the expected cost of this process compared more common batch and flow systems. Our analysis shows that as long as catalyst cost is a substantial operating cost, our catalyst recycle system is expected to be a competitive process to those typically used in pharmaceutical production.

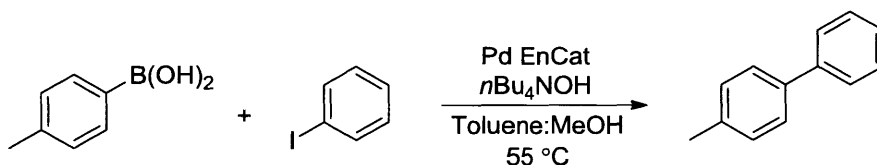
5 Separation and Recycle of a Buchwald-Hartwig Amination Catalyst in a Small Scale Flow System

5.1 Introduction

Palladium-catalyzed cross-coupling reactions have had a significant influence on modern drug synthesis.^[183] Buchwald-Hartwig Amination is a palladium-catalyzed C-N bond forming reaction which is most commonly used in the amination of aryl halides. Early catalyst systems used for this reaction required high catalyst loadings and active substrates.^[184-186] The 2nd generation precatalyst systems with a 2-aminobiphenyl group showed efficient room temperature oxidative addition of aryl chlorides to palladium.^[187] Furthermore, this precatalyst was stable in air. The 2-aminobiphenyl group undergoes reductive elimination readily in the presence of base to afford the air-sensitive, highly active, Pd(0) catalyst. Later, the 3rd generation precatalyst was created using a methylsulfonate anion coordinating the catalyst, which allowed for larger ligands such as tBuXPhos and BrettPhos to be incorporated into the catalyst.^[188] Such catalysts were also shown to be significantly more stable in solution, and so might perform well in a continuous catalyst recycle system.^[188] Furthermore, the presence of these larger ligands allow for the possibility of using nanofiltration to efficiently separate the 3rd generation catalyst from the product. Applications in flow systems were improved though the creation of an N-methylated 2-aminobiphenyl version of the catalyst, which guarantees the solubility of the precatalyst in toluene.^[189]

Palladium catalyst immobilization and recycling, as applied to coupling reactions, have been thoroughly reviewed.^[190] Palladium particles dispersed on heterogeneous substrates have been used in coupling reactions, including Buchwald-Hartwig Amination.^[191-194] Palladium catalysts have been recycled via immobilization of an organometallic complex to a polymer^[191, 195-197] and nanoparticles.^[198-200] Despite the anchoring of palladium to a solid support, there is much evidence to suggest that leached homogeneous palladium is often the active species,

which may or may not return to the support.^[201] One such example of palladium immobilization is the Pd EnCat system developed by Ley et al., which relies on a polyurea-encapsulated Pd(OAc)₂ precatalyst. Scheme 11 depicts the application of this catalyst to a Suzuki coupling reaction. Full conversions were obtained at a residence time of 4 minutes (TOF 3 h⁻¹).^[202] The relatively high catalyst loading resulted in a TON of around 5 for this system, with 1-13 ppm palladium found in the product. There was effectively 480 mol% palladium at steady state in the reactor corresponding to 19 mol% Pd relative to the total reagent throughput. Microwave-assisted reactions with this immobilized catalyst were able to give TON of 500.^[203] To put these results in perspective, one can consider the fact that adding about 1 ppm Pd(OAc) to a more difficult substrate can go to full conversion in 4 hours (TON: 5000, TOF 1250 h⁻¹).^[204] Furthermore, TONs in the millions have been reported for 90 second reactions under microwave conditions for similar substrates.^[205] Despite this, papers continue to be published claiming to employ recyclable catalysts for palladium-catalyzed coupling reactions, by employing aryl iodide substrates.^[206] This highlights the difficulty in maintaining activity when immobilizing a palladium coupling catalyst, and the need to consider more difficult substrates for which higher palladium loadings, and the presence of a ligated catalyst, is actually required. We take up the challenge of recycling a palladium catalyst with a more difficult substrate in this Chapter.



Scheme 11. Simple Suzuki coupling reaction over PdEnCat.^[202]

An alternative approach to the immobilization of coupling catalysts used functionalized GMA-*co*-EDMA [poly(glycidylmethacrylate-*co*-ethylene dimethacrylate)] was used to enact a simple Suzuki coupling reaction. This approach used the functionalized polymer is shown in Figure 67. A TON of slightly over 200 was obtained for the palladium, with a TOF of 1.8 h⁻¹ (and

a yield of 59%) over a 96 hour period where reportedly little change yield occurred.^[207] About 15-20% of the Pd had leached during this period.

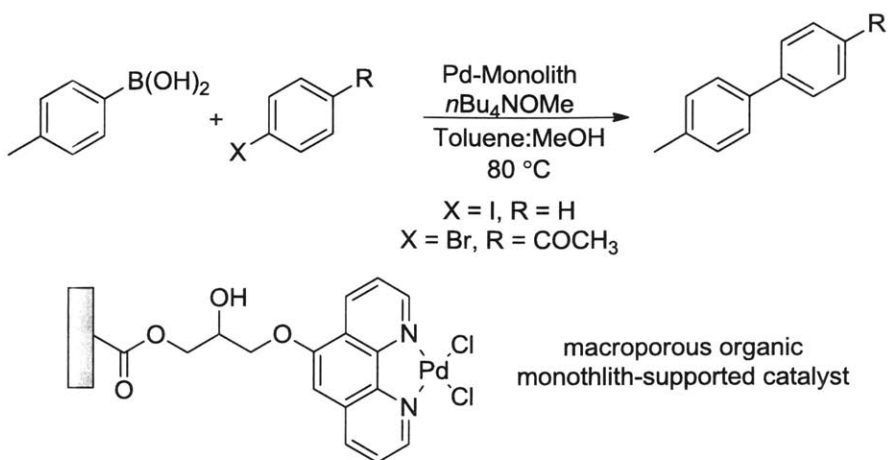
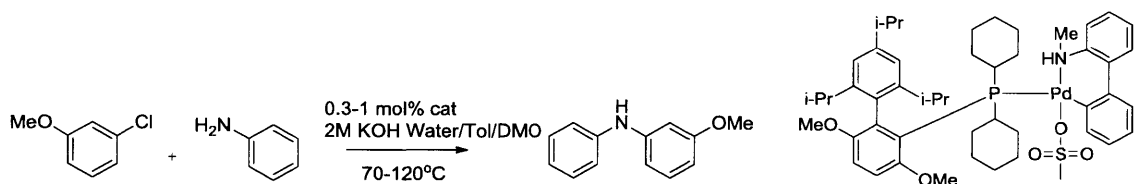


Figure 67. Suzuki Reaction scheme with polymer-anchored catalyst packed in a microchannel.^[207]

The recycling of homogeneous palladium coupling catalysts has also struggled. This is due in part to catalyst instability and handling difficulties, as well as a focus on substrates which are too reactive. Nanofiltration of post-reaction mixtures involving aryl iodides^[208, 209] and aryl bromides^[210] have been investigated, often with significant catalyst rejections >90%, however with relatively low TONs. For example, TONs below 2000 were reported for a heck reaction with iodobenzene as a substrate.^[208, 209] Ionic liquids with a modified palladium catalyst were used in conjunction with nanofiltration in a Suzuki-Miyaura reaction involving an aryl bromide.^[211] For batch process yields near 80%, TONs less than 500 were obtained. Liquid/liquid based approaches would likely require the palladium catalyst to be in the organic phase, since stoichiometric salt generation would otherwise accumulate in an aqueous recycle loop in flow. Such a scenario would require high recycle purge rates, and substantially reduced catalyst TONs in a continuous flow system. Employing the catalyst in an organic phase, however, carries the disadvantage of requiring a water-soluble product – such an approach was demonstrated by Li et al.^[212] In 2009, Schoeps et al. applied nanofiltration to a molecular weight enlarged Buchwald-Hartwig amination catalyst.^[213] Unfortunately, 24 hour residence

times were necessary for coupling aryl chlorides to morpholine. When a catalyst is designed with separation being the priority, low activities are often observed, and this study was no exception. In 2010, Dumrath et al. published an example of recycling a palladium catalysts for the hydroxylation of an aryl bromide.^[214] These researchers recovered the palladium catalysts as a solid at room temperature after the homogeneous reaction. Peeva et al. applied a PEEK membrane to a continuous-flow, closed loop recycle system for a Heck coupling reaction involving an aryl iodide.^[215] As some degraded palladium catalyst passes through the membrane during nanofiltration-recycle applications, a hybrid approach using a downstream absorbents after nanofiltration was developed.^[216] In such a system, palladium nanoparticles are rejected by the membrane, while smaller palladium degradation products are captured by the absorbent. This is a useful approach especially due to the difficulty of removing palladium nanoparticles with absorbents. In this chapter, we consider the reaction shown in Scheme 12, and design a continuous nanofiltration-recycle system using the more difficult aryl chloride substrate. This substrate is low enough in activity so that recycled palladium nanoparticles and other palladium species lacking the proper ligand-palladium structure shown in Scheme 12 are exceedingly unlikely to catalyze this transformation. This will allow us to better access the recyclability of the 3rd Generation BrettPhos palladium catalyst, independent of the presence other palladium species.



Scheme 12. Buchwald-Hartwig Amination of an m-chloroanisole using the N-Methylated 3rd Generation BrettPhos catalyst.

5.2 Process Design

5.2.1 Nanofiltration Cell

The nanofiltration module used in this section is identical to that described in Chapter 4. The one difference is that the sightglass use for liquid level control in Chapter 4 has been replaced with a gasket and plug to completely seal off the cavity. The same pneumatic pump and tubing was used to recirculate the retentate side of the membrane module.

5.2.2 Holding Tank Design

Our holding tank was designed to provide a liquid-liquid separation for our mixture while serving as a surge tank with level control for our recycle loop. A 20 ml glass vial with an open top screw cap and septa was used for the holding tank. The septum could be pierced by both needles and sharpened PEEK tubing to provide inlets and outlets. To provide mixing, the septum was pierced with a rotating 1/16" PEEK tubing outfitted with a 10–32 Upchurch scientific nut. Figure 68 shows this mixing scheme, with the tubing attached to a DC motor (McMaster-Carr, 6331K13). As shown in the figure, the mixer is positioned to provide good mixing in the organic phase while neglecting the water phase. This prevents water from entering the recycle pump, while still providing mixing in the organic phase. Visual tracer tests showed mixing times on the order of 5 seconds.

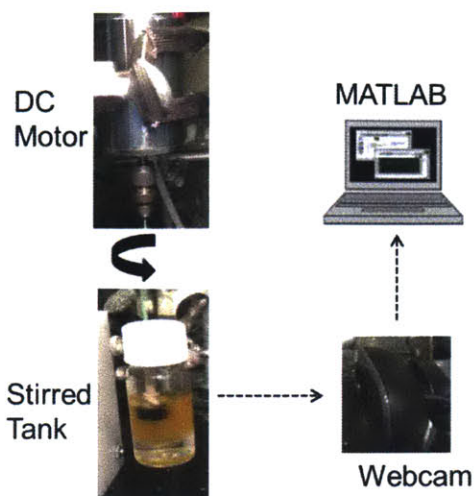


Figure 68. Custom holding tank with organic-phase mixing and liquid-liquid separation.

Figure 69 shows the entire control scheme. A webcam (Logitech, C270) is used to measure the height of the two phases present in the vial. LabVIEW calls a Matlab script to process the webcam output, and uses these results to control the organic feed pump and aqueous drain valve. The aqueous phase is drained out using an automatic two-way valve. We used a solenoid three-way valve (Gilson, 01540-13) with one outlet being plugged. The holding tank is kept under 5 psi of argon pressure during the entire run which serves to keep out oxygen and provide a driving force for draining the aqueous phase when the valve is opened.

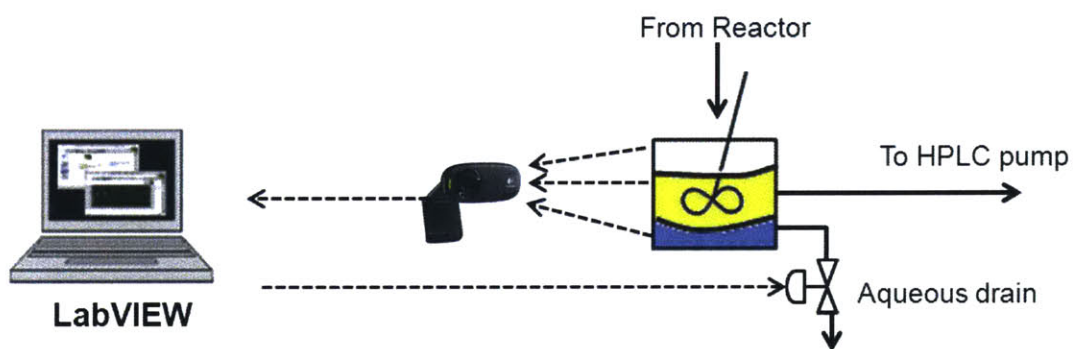


Figure 69. Scheme showing LabVIEW information flow to and from the holding tank.

The logic of the webcam image processing code in Matlab is as follows. First, using the Matlab interface, a region of interest (ROI) is manually drawn in the webcam's visual field. Next, the webcam processes the image in the ROI using a conversion to grayscale. The middle of the ROI is presumed to be organic. Using this assumption, the script looks only at the pixels below the middle of the ROI. The grayscale values of these pixels are averaged, creating the threshold which is subsequently used to distinguish between organic and non-organic phases. Next, all of the pixels in the ROI are assigned a value of zero in the case of being below this threshold (air, water) and one if above the threshold (organic). If a row of pixels has greater than 90% ones, it is presumed to be organic by the code. This method of distinguishing between organic and air/aqueous phases is robust to lighting changes, shadows, changes in organic or aqueous color (as long as the organic phase is always darker on a grayscale), and overhead mixing. These features distinguish our approach from the lab-scale liquid/liquid holding tank of Ley et. al.^[217] Their approach, using a green flotation ball, would not have worked due to the darkening of our organic phase during the run. In addition, adequate mixing would be difficult to obtain since disturbing the ball would result in control action. Finally, an additional flotation ball would have been necessary using the approach of Ley et. al, since the volumes of two phases need to be tracked.

5.2.3 Backpressure Regulator Parallelization

During early attempts to run the continuous recycle system, the robustness of Upchurch Scientific backpressure regulators was found to be limiting. To prevent this technology from limiting the length of a continuous recycle run, we chose to parallelize the backpressure regulators using an automatic 6-way valve. The mechanism of action is shown in Figure 70. The recycle pump pressure gauge, which measures the pressure in the membrane retentate, is monitored with a LabVIEW code. This script judges whether the pressure is outside of an acceptable range. When this is the case, the code causes the automatic 6-way valve to switch to

a fresh backpressure regulator. This allows for plenty of time to manually fix the isolated backpressure regulator and replace it as the new backup.

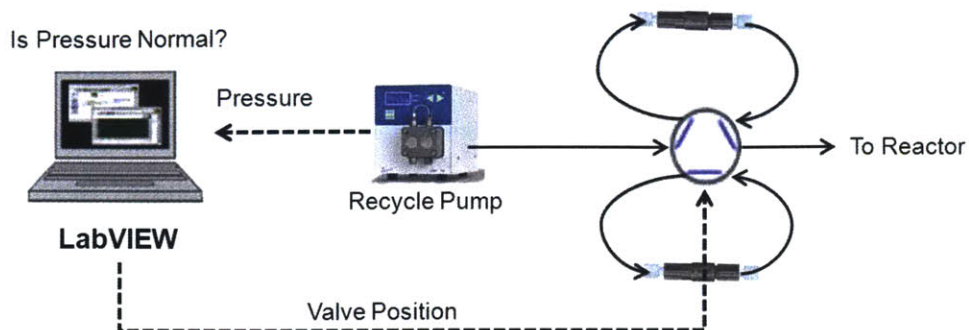


Figure 70. Parallelization of backpressure regulators to add to system robustness. This setup automatically uses a pressure measurement to decide when to switch between the parallelized backpressure regulators.

5.2.4 Pumping and Sampling System

In-house pump heads which used larger check valves than the original Knauer design, and doubled the number of check valves in the pump heads, were employed. Gasket seals were custom-made from Marco Rubber to approximate those from Knauer. These check valves added substantial robustness to the system and allowed it to operate for multiple days without pump failure.

A nearly identical sampling system to that described in Chapter 4 of this thesis was employed with this chemistry. The one exception is that no reactor sampling valve was employed; the valve was used for backpressure regulator parallelization without significant loss of information about system performance.

5.3 Experimental

5.3.1 Batch Reactions

Our dimethyloctanamide (DMO) was obtained from Frinton (FR-709), and vacuum distilled after reactions to recycle the expensive solvent. Other solvents (water, toluene, isopropanol) were obtained ACS grade from Sigma Aldrich. Aniline was vacuum distilled prior to use. All solid materials were weighed in open air and cycled 5 times under argon (Airgas, grade 5.0). Our catalyst was an N-Substituted 3rd-generation catalyst that is not currently sold, but the preparation procedure is published.^[189] Two stock solutions were made: base and organic stock solutions. The base stock solution was made by mixing 10 ml water with 1.12 g of KOH (Sigma Aldrich, ACS grade). The organic stock solution was made by mixing 0.73 ml aniline (Sigma Aldrich, ACS grade), 0.46 ml 3-chloroanisole (Sigma Aldrich, 98%), 100 mg biphenyl (internal standard), and 10 ml of a toluene/DMO mixture (i.e., 1:1 by volume, 2:1, etc.). The stock solutions were degassed by bubbling argon while stirring over a 15 minute period. Next, 3.14 mg of catalyst and 4.02 mg of BrettPhos were weighed accurately and cycled under argon (with a stir bar). In order to start on the reaction, 1 ml of each stock solution (organic and base) was added to the degassed vial of catalyst/ligand. The mixture was then submerged into a water bath at 70°C (with carefully aligned stirring. For a 1:1 Toluene:DMO mixture, a homogeneous phase should result). Samples were taken under a Schlenk line at different points in time during the reaction, always with purged needles.

5.3.2 Batch Recycle Tests

A mixture of pure substrates is made in a 1.2:1 molar ratio of aryl chloride:aniline. This solution is called the substrate stock. Upon completion of a batch reaction experiment, the reaction mixture is removed from the heating and mixing and allowed to stand for a recorded wait time (generally 10 minutes). Afterwards, an additional 1 ml of base stock solution (2 M KOH), is added. Next, 120 ul of substrate stock solution is added, and the reaction is repeated.

5.3.3 Packed Bed Reactions

A 0.5" outer diameter, 10 mm inner diameter, 10" long stainless steel tube (McMaster Carr) was used as a reactor. Stainless steel beads of 0.5 mm average diameter (Thomas Scientific, SSB05) were packed into the reactor by continuously loading while tapping on the side of the reactor. Once loaded, the beads were emptied, weighed, and loaded back into the reactor. This process was repeated to ensure consistency of packing density. As long as the beads were loaded slowly, while tapping continuously on the side of the reactor, the packing was found to be consistent with a void volume of 0.36 (105g of 316 stainless steel loaded into reactor). Valco fittings (Valco, ECEF8110.0) were used in conjunction with 40 μ m frits to hold the beads in the reactor. These Valco fittings provided female 10-32 inlet and outlet ports to the reactor. In all cases, flow into the reactor always entered the top of the reactor and exited the bottom of the reactor, with the reactor being clamped vertically. 8 ml stainless steel syringes from Harvard Apparatus were used to pump aqueous and organic solutions into the reactor using a Harvard PHD Ultra syringe pump. No backpressure was applied during these experiments. It should be noted that a 12.5" long reactor was used in our continuous recycle system (instead of a 11" long column). In this case, 128.5g of packing material was loaded into the reactor, corresponding to a void fraction of 0.36.

5.3.4 Nanofiltration Tests

Rejection of the precatalyst was tested by pressurizing our in-house membrane module with degassed toluene (Sigma Adrich, ACS grade), and allowing five system volumes to permeate. Next the HPLC pump feed was loaded with degassed precatalyst solution, and three system volumes were allowed to permeate. Finally, the permeate and retentate samples were measured by AAS to detect palladium rejection. Separate AAS tests were used to show palladium precatalyst and AAS palladium standards produced identical calibration curves. Activated catalyst from system runs, on the other hand, needed to be worked up with Aqua regia before being used on the AAS.

5.3.5 Continuous Recycle System Operation

During system start-up, rigorous degassing of all of the process blocks was undertaken. The recycle loop was broken and the holding tank was removed such that the simplified two-part system in Figure 71 resulted. The reactor section included the two inlet pumps (organic and aqueous), the mixing zone, and the reactor. This part of the system was degassed by loading degassed toluene onto the substrate pump and degassed 2M KOH onto the aqueous pump. The port for the recycle inlet to the reactor was also purged via a two way valve. Degassed solvent was wasted after passing through the system.

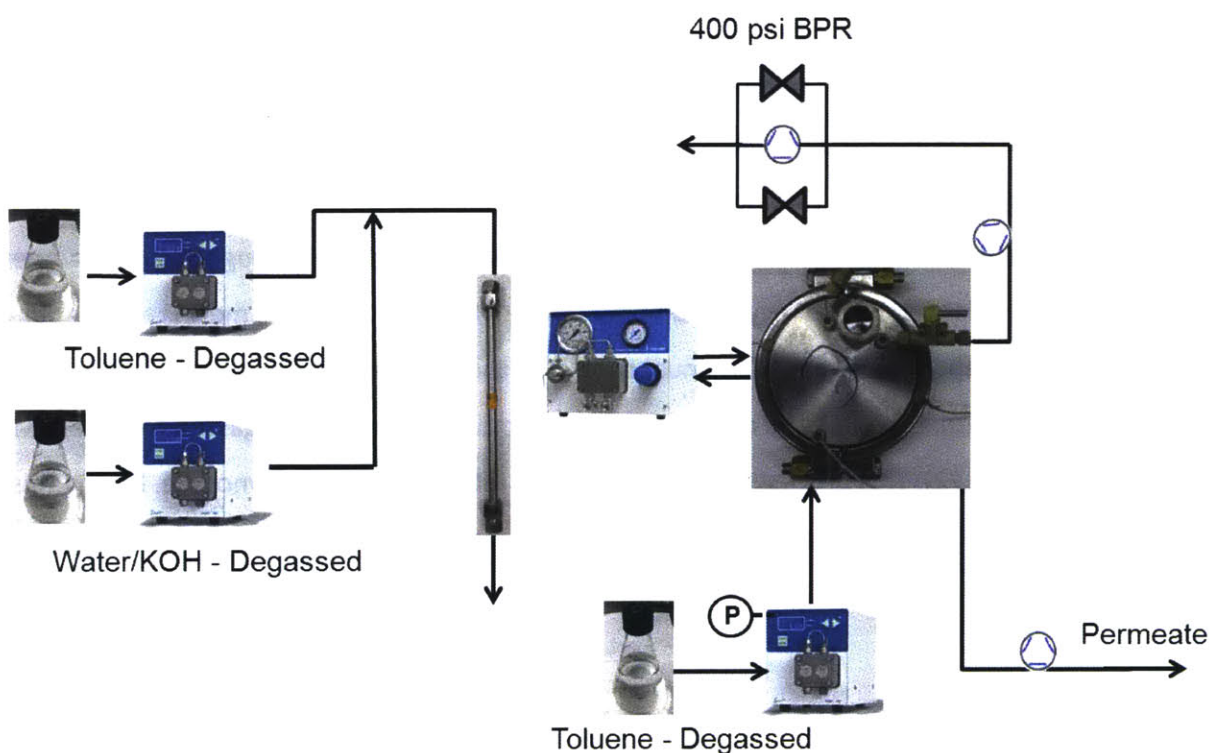


Figure 71. Degassing piecewise system without a holding tank before a start-up.

The second part of the system in Figure 71 involves the membrane module. The recycle HPLC pump was loaded with toluene and at least 10 volumes were flowed through the membrane module with active mixing. This process also pressurized the membrane module.

Once pressurized, the membrane module's pressure should never be allowed to decline due to the sensitivity of the 400 MWCO PEEK membrane (no other membrane used in this thesis behaved this way). For this reason, the pressure exerted by the pump was always recorded in LabVIEW. If the membrane module pressure were to fall to less than 20 bar at any point during the startup or operation, the run was discontinued. The automated valve which parallelized the back pressure regulators was switched during the start-up procedure to ensure both lines were degassed. Maximum pump flow rate was used during the valve switching. The degassed toluene feed into the membrane module was replaced with a 50/50 mixture of degassed toluene/DMO. 100 ml of this solution was put through the membrane module to ensure that the system had a significant DMO content during start-up.

Next, the recycle loop tubing was connected to the reactor inlet mixing block. The two-way valve was kept closed such that no fluid could flow in the degassed recycle loop. Due to the fact that the retentate had a dead end in this setup, the permeation rate through the membrane module was balanced by the recycle pump feed rate. The pressure in the membrane module was carefully kept near 30 bar via manual control of the recycle pump flow rate. At this point, the catalyst mixture was loaded onto the recycle pump to replace the degassed toluene/DMO mixture (Figure 72). This process loaded the catalyst into the membrane module. During this time, the outlet from the reactor was being collected into a holding tank which had been filled with argon.

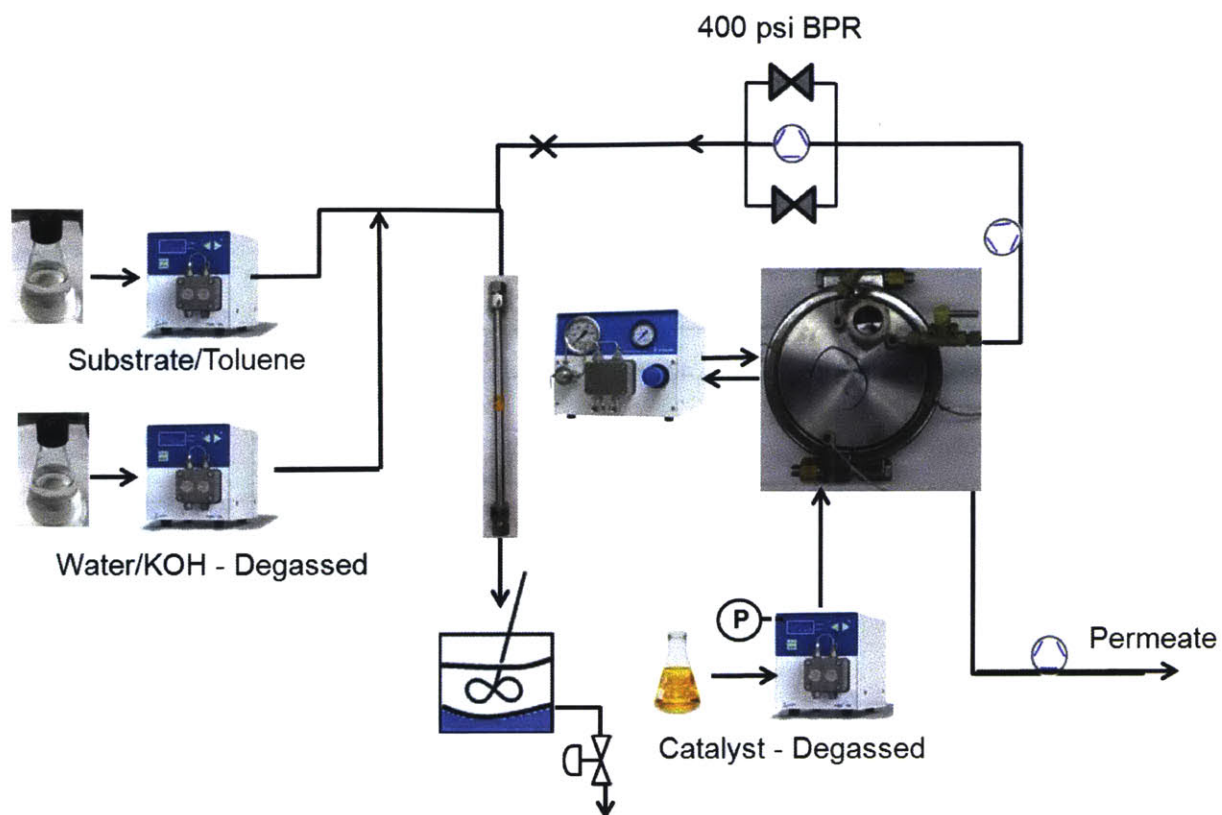


Figure 72. Catalyst loading into the system during start-up. Catalyst was kept separate from the reactor during this time.

Once 90% of the catalyst had been loaded into the membrane module, the liquid levels in the holding tank were at near-operating levels. During the start-up period, excess aqueous was manually drained using the 3-way valve. The substrate feed pump was switched from the degassed toluene to the substrate mixture. After five more minutes, the feed to the membrane module was connected to the organic phase in the holding tank. At this point, the recycle loop 2-way valve was opened and the recycle pump flow rate was increased to 400 $\mu\text{L}/\text{min}$. The substrate feed pump was manually controlled until the organic phase in the holding tank became colored. As soon as this occurred, the control system was started using the Matlab/LabVIEW scripts. Next, degassed toluene was loaded onto the 6-way valve flushing

pump. Once loaded, and once the 6-way valve lines had purged using this degassed mixture, the automated sampling system was started. The parallelized back-pressure regulator script was run as well to ensure the membrane was kept under pressure in case of a BPR failure. This final setup is shown in Figure 73.

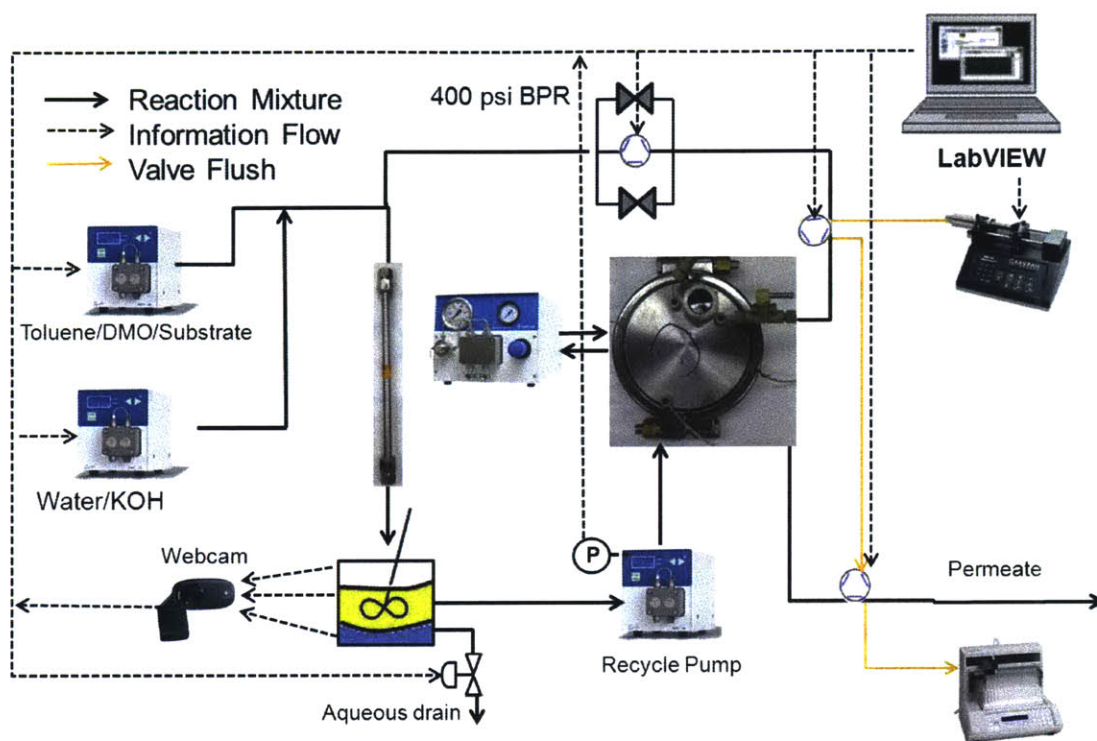


Figure 73. System after start-up was completed, and all control systems/automation was activated.

5.4 Results and Discussion

5.4.1 Batch Recycle Experiments

After performing a batch reaction using the procedure in the experimental section, a re-use of the catalyst could be performed conveniently through an approximate method. This involved the addition of substrate to a post-reaction mixture, without any separation of the catalyst

from the product. Separate tests showed that there was no significant product inhibition for our reaction. When performing such batch recycle tests, as detailed in the experimental section, the results shown in Table 9 were obtained. These results were obtained using aniline and p-chloroanisole as the substrate. It should be noted that, in order to analyze the results of subsequent reactions, leftover reactant/product from the first reaction needed to be systematically taken into account.

Table 9. Batch recycle experiments using p-chloroanisole as the substrate.

Excesss Reactant	Ligand (mol%)	Temp (°C)	Reaction #1	Reaction #2	Reaction # 3	Wait Time (min)
Aniline	-	100	12 m - 100%			
Aryl Chloride	-	100	12 m - 97.5%	12 m – 50% 28 m – 83%		35
Aniline	-	80	20 m – 100%	30 m – 50%		40
Aniline	1.5	90	20 m – 90%	20 min – 75% 30 min – 90%	20 min – 60%	40
Aryl Chloride	0.375	90	15 min – 92% 30 min – Full	15 min – 87% 30 min – 99.3%	15 min – 77% 30 min – 98%	50
Aryl Chloride	1.5	90	15 min – 87% 30 min – 99.3%	15 min – 77% 30 min – 98%		50

Table 9 records the first batch reaction as ‘Reaction #1’, with first catalyst re-use under the column header ‘Reaction #2’. An additional re-use of the catalyst is shown under the column header ‘Reaction #3’. The wait time in the final column corresponds to the amount of time the reaction mixtures were allowed to sit at room temperature, with no stirring, in between catalyst re-uses. Initial batch catalyst re-use experiments showed that excesses of either aryl

chloride or aniline could be used. Initial catalyst re-use tests also demonstrated that nearly half of the catalyst was degraded after one use. Upon the addition of extra ligand, significantly enhanced catalyst recyclability was observed. It should be noted that the addition of ligand, in addition to increasing the expense of the process, tended to slow the reaction down for this substrate. However, substantial recyclable was obtained (only ~17% activity loss over two re-uses, Table 9, row 5).

Further catalyst reuse experiments were performed using a more active substrate. These results are shown in Table 10. The first two rows show that the wait time at room temperature increases catalyst degradation. Most of the degradation of our catalyst in our system will occur within the reactor, but residence time outside of the reactor needs to be minimized in order to minimize catalyst degradation. An excess of aryl chloride were used in all cases in an attempt to minimize the formation of palladium nanoparticles (i.e., forcing the resting state of our catalyst away from Pd(0)). When additional ligand was added, a significantly enhanced catalyst recyclability was again observed. With this substrate, the additional ligand appeared to slightly enhance the rate of the reaction, rather than inhibit the reaction rate. For this reason, the m-chloroanisole substrate was selected for use in our system.

Table 10. Batch recycle experiments using m-chloroanisole as the substrate.

Excesss Reactant	Ligand (mol%)	Temp (°C)	Reaction #1	Reaction #2	Reaction # 3	Wait Time (min)
Aryl Chloride	-	70	12 min – 94% 20 min – Full	12 min – 66%		120
Aryl Chloride	-	70	10 min – 84% 20 min – Full	10 min – 74% 20 min – 95%		10
Aryl Chloride	1.5	50	---			
Aryl Chloride	0.75	70	10 min – 97.6% 20 min – Full	10 min – 77.5% 20 min – Full	10 min – 60% 20 min – 85%	10

Aryl Chloride	1.5	70	10 min – 95% 20 min – Full	10 min – 80% 20 min - Full	10 min – 74% 20 min – 97%	10
---------------	-----	----	-------------------------------	-------------------------------	------------------------------	----

The previously discussed work was performed using dimethyloctanamide (DMO) as the organic solvent. Due to the superior permeability of toluene through PEEK membranes (compared with DMO), and the high cost of DMO for development work, we began using toluene/DMO mixtures for our reactions. Batch reactions using 4:1, 2:1, and 1:1 toluene:DMO were tested and the results are shown in Table 11. Good catalyst activity and recyclability was observed using a 1:1 ratio. This was judged to be a good balance between throughput enhancement and slight reaction rate decline (due to mass transfer barriers).

Table 11. Batch recycle data using a 4:1, 2:1, and 1:1 mixtures of Toluene:DMO as the solvent to aid in system throughput. The substrates are aniline and m-chloroanisole.

Excess Reactant	Toluene: DMO	Ligand (mol%)	Temp (°C)	Reaction #1	Reaction #2	Reaction #3	Wait Time (min)
Aryl Chloride	4:1	1.5	70	5 min – 14% 15 min – 34%			
Aryl Chloride	2:1	1.5	70	5 min – 34% 20min – 95.2%	5 min – 45.4% 20 min – 88%	5 min – 26% 20 min – 69%	10
Aryl Chloride	1:1	1.5	70	5 min – 77% 20min – 96%	5 min – 59% 20 min – 98.7%	5 min – 64% 20 min – 98.6%	10

5.4.2 Packed Bed Reactor Tests

After exploring different conditions in batch, the optimal conditions were applied in flow. We chose a stainless steel packed bed reactor packed with 0.5mm stainless steel shots due to the chemical compatibility of the reactor, the high mass transfer rate of the design, and the low cost of the approach. When operating under trickle-bed conditions, we varied the flow rate to determine the conditions under which we needed to operate in our continuous recycle system.

Table 12 demonstrates the effectiveness of our reactor, with an organic flow rate near 150 $\mu\text{l}/\text{min}$ necessary for 97% conversion.

Table 12. Conversions as a function of flow rates for our packed bed.

Excess Reactant	Toluene: DMO	Organic Flow (ul/min)	Aqueous Flow (ul/min)	Temp ($^{\circ}\text{C}$)	Conversion
Aryl Chloride	1:1	700	700	70	47.5%
Aryl Chloride	1:1	350	350	70	77%
Aryl Chloride	1:1	225	225	70	94%
Aryl Chloride	1:1	150	150	70	97%

5.4.3 Continuous Recycle System

In order to obtain an estimate of our maximum possible TON for this catalyst in our system, we designed a continuous recycle run with no catalyst cofeed. During this experiment, only permeate samples were measured, and the decline in product was measured as the catalyst degraded. These results are shown in Figure 74. The system operated at partial conversion during the run, which tends to overestimate the TON which can be obtained in a true steady-state system. This is due to the rate of reaction being faster at partial conversions than higher conversions. We obtained a TON of 630 during for this experiment, with no significant byproducts measured by GC. Our rejection throughout the run was found to be 92.5% by AAS.

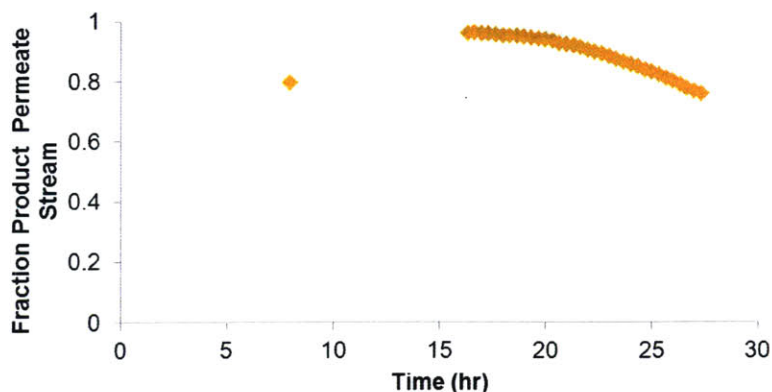


Figure 74. Fraction product in permeate stream for an initial charge of catalyst in our recycle system.

An additional system run with a reduced initial catalyst charge was performed to ensure that lower catalyst loadings could not be used, and the results are shown in Figure 75. For this shorter run, much lower conversions were obtained using 60% of the catalyst loading used in the continuous recycle run used to produce Figure 74.

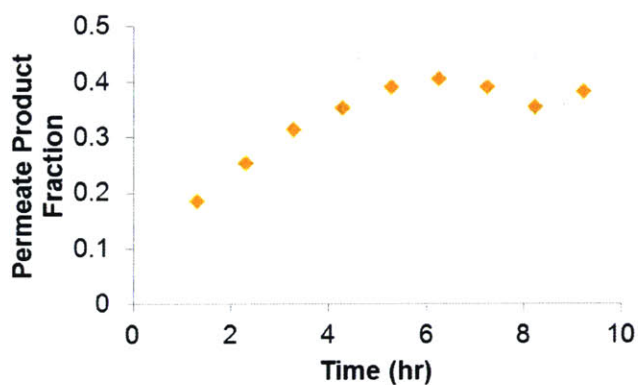


Figure 75. Reduced product fractions shown for reduced (60%) catalyst loading.

The results of the previous system runs with no catalyst cofeed were used to design a run with a catalyst cofeed. After a normal system start up, a substrate: catalyst ratio of 1000:1 was

used to continuously replenish any catalyst lost or deactivated in our system. The product fractions measured throughout a 60 hour run for such an experiment is shown in Figure 76.

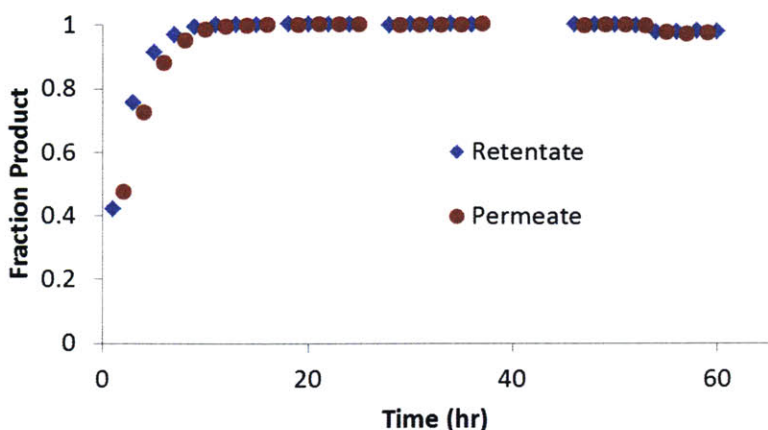


Figure 76. Permeate and retentate product fractions throughout our continuous-coupling catalyst recycle experiment.

Our product fraction increases during the first 10 hours and is maintained high throughout the rest of the 60 hour run. The reason for partial conversion during the first 10 hours is due to the start-up procedure. In order to optimize catalyst stability, substrate is flowed into the reactor before catalyst. This creates a surge in substrate during the initial start-up. Our TON for this run, including all of the product which exited the system and remained in it after the run, was 550. In order to better evaluate the value added by the recycle system, this overall TON of 550 can be compared to the substrate/catalyst ratio in the reactor during the run. Our average substrate/catalyst ratio can be conservatively estimated to be 50 for this recycle run. Thus, our catalyst is re-used in our recycle loop ~10 times on average. If we assume the control system to be accurate, we can infer that the permeation rate balances the substrate feed rate. This substrate feed rate is known directly from our control system operation throughout the run. Using this inference, the approximate permeation rate through the membrane as a function of

time throughout the run is shown in Figure 77. Indications are made where our parallelized backpressure regulators were used to prevent system failure.

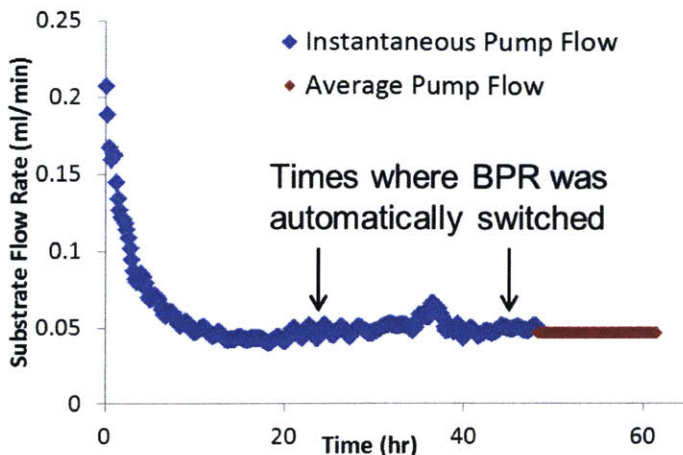


Figure 77. Organic pump flow rate into system as a function experimental time.

Also of interest was the DMO content in the system throughout the run. During the initial design phase, it was thought that an additional control loop would be necessary in order to keep the DMO concentration in the system within an acceptable range. As shown in Figure 78, consistent with solvent-only recycle tests, the DMO concentration in the system is close to the feed concentration (in this case, 45% volume). This self-regulating behavior is due to the membrane's DMO permeation rate increasing with increasing volume fractions of DMO. When DMO concentrations fall, there is a subsequent decline in DMO permeation rate. This stable behavior may exist with a significant offset from the feed DMO concentration, depending upon the relative permeation of DMO and toluene. This offset can also be affected by membrane fouling during an actual continuous run. Using pure solvents, we found that a 40% DMO feed gave near 45% DMO in the system at steady-state. During our actual run, we found that a 45% DMO feed corresponded, surprisingly, to a system content of 45% DMO. It should be noted that, during our system startup, 50% DMO was loaded into the system, which explains the decline in DMO from 50% to 45% throughout the run. Our system stayed within 40 to 55% DMO

throughout the 60 hour run, which has the effect of enhancing our mass transfer rate within the reactor compared to using pure toluene or lower DMO (5-10% of DMO). This is also verified by our high conversions throughout the run.

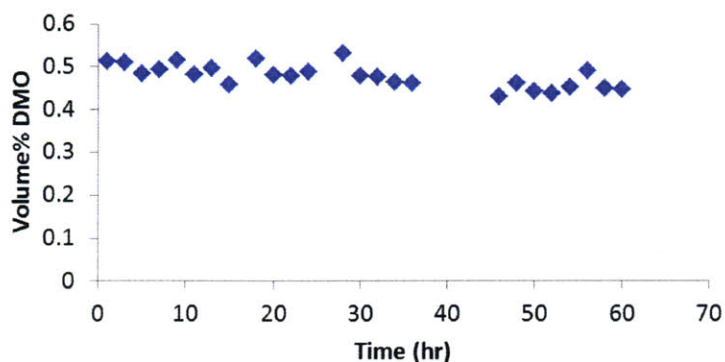


Figure 78. DMO content in recycle system (Volume%) as a function of experimental time.

During our continuous run, palladium rejections were substantially less than precatalyst rejections with the 400 MWCO PEEK membranes. We obtained rejections in the range of 84 to 90% throughout the run (see Figure 79), compared with a pre-catalyst rejection of 97%. This is likely due to catalyst degradation into smaller species which pass through the nanofiltration membrane. Studies have suggested^[216] that larger nanoparticles which form from Pd(0) aggregates are more likely to be rejected by nanofiltration membranes, and so our active catalyst combined with palladium nanoparticles may make up much of our retentate palladium. Our product rejections are between 20 and 40% which is quite low compared with other product rejections reported in this thesis. Figure 80 below shows the product rejection dynamic changes throughout the 60 hour run.

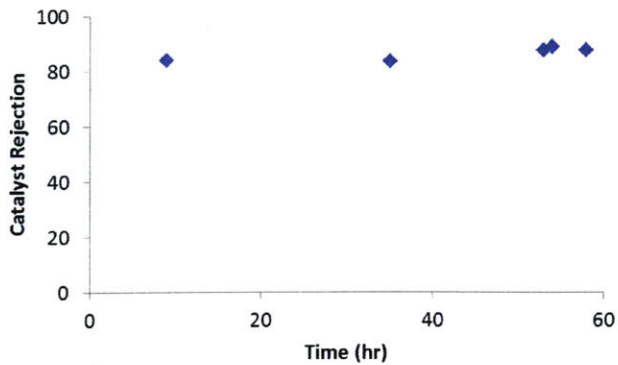


Figure 79. Rejection of palladium as a function of experimental time (AAS).

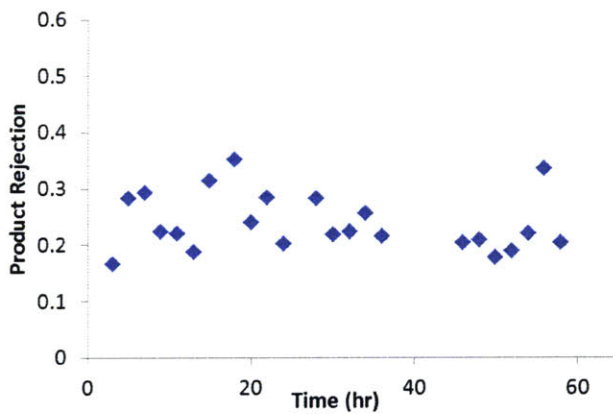


Figure 80. Rejection of product as a function of experimental time.

The fact that our product rejection does not continuously increase allows the system to reach a steady-state concentration of product. Absolute product and reactant concentrations are shown in Figure 81 as a function of operation time. In this plot, absolute concentrations of product in the retentate and permeate autosample valves are shown. Due to the presence of two phases at the reactor outlet, a reactor outlet sampling valve would not provide absolute concentrations. It can be seen that product permeate concentrations approach and eventually

reach 1 M over the 60 hour period. Since our feed is 1 M in our limiting reactant, aniline, this means that our system has reached a controlled state of operation. This also helps to validate the operation of the system. It should be noted that despite a 1 M aniline feed, the reactor concentration is much less than this due to the recycle loop (0.2 M). This tends to decrease the reaction rate and is a disadvantage of a close loop recycle system involving a nanofiltration membrane.

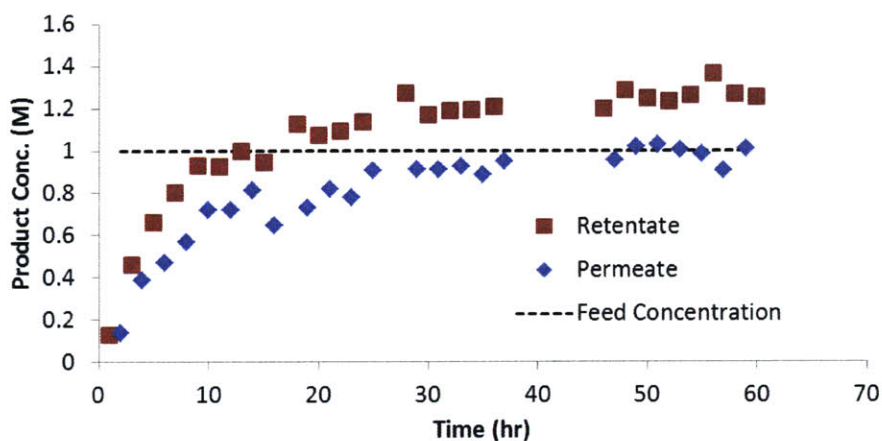


Figure 81. Concentrations of product in the retentate and permeate streams as a function of experimental time.

The system was designed to run for a few days, which adds to the difficulty of obtaining a good overall TON for our catalyst. This is an effect of the low throughput in our system. Due to a low permeation rate through the 400 MWCO PEEK membranes, it takes over 12 hours to permeate a complete system volume. Thus, it might take weeks for this system to permeate enough product such that the initial catalyst loading becomes small relative to the amount of catalyst co-fed into the system. Only at this point would be the ratio of substrate:catalyst in the cofeed be realized as the steady-state TON. For our results, the effects of the high-usage of catalyst from the start-up were still very relevant to our TONs.

At 50 hours into the experiment, the substrate feed pump experienced a check valve failure. In order to continue the run despite this partial pump failure, the control system flow rate range was increased. This allowed for the control system to set a nominal flowrate on the pump substantially higher than the actual flowrate from the pump. The difference in nominal pump flow rate (pump flow rate set point) and actual pump flow rate is due to intermittent backflow in the pump such that accurate flowrate from the pump is only intermittent as well. Our control system pushed the nominal pump flow rate high enough such that, despite intermittent flow interruption, the average flow rate from the pump balances the permeation rate in the system. This average flowrate, as measured by volume collection of permeate, is shown in Figure 77 between 50 and 60 hours. Figure 82 shows that during this time, the holding tank liquid level experienced more noise, but adequate control was still maintained throughout this ten-hour period.

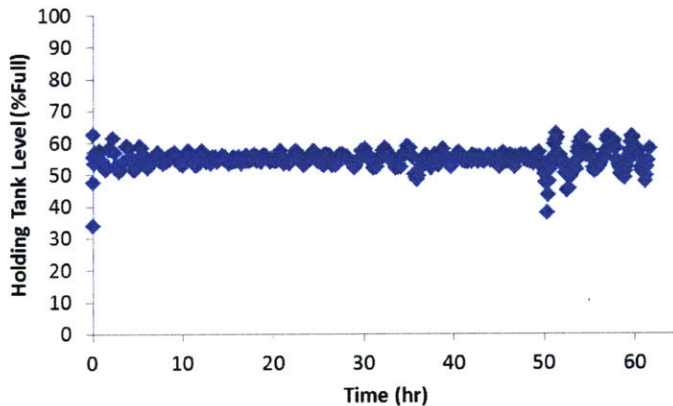


Figure 82. Holding tank liquid level as a function of time throughout the continuous recycle run.

Although we have obtained reasonable results with this system, there is the possibility of future work greatly improving upon these results. Although our recycle-loop residence time for this system is near 3.7 hours, the residence time necessary to permeate one system volume, once our permeation rate has fallen to 45 ul/min due to fouling, is approximately 16.4 hours. It

should be noted that both of these long residence times (3.7 hours for the recycle loop, 16.4 hours to permeate a full system volume) are due to the low membrane throughput per module volume. These numbers would be substantially worse (~45 hrs to permeate one system volume) if our membrane module volume had not been optimized (Chapter 4). In fact, for our system, this would have prevented steady-state from being able to be obtained during our 60 hour run. Considering our reaction residence time (~15 minutes), it is easy to see that this system suffers from a membrane throughput bottleneck. The active catalyst spends the vast majority of system residence time unproductively. Our batch recycle tests suggests that times of these magnitudes do indeed affect catalyst stability (Table 10, rows 1 and 2). This presents significant opportunity for future work.

5.5 Conclusions

Our coupling catalyst recycle system was able to recycle a 3rd generation BrettPhos palladium catalyst continuously for 60 hours and obtain high process yields. Importantly, we applied the system to a more difficult model substrate than other examples in the literature. Specifically, this work focused on 3-chloranisole, which cannot be coupled to aniline without significant amounts of both Pd(0) and the finely tuned dialkylbiaryl ligand (BrettPhos). The design of our continuous recycle system required a liquid-liquid separation prior to our nanofiltration block. To achieve the liquid-liquid separation while simultaneously providing a surge tank, we designed a webcam-based level measurement system for a two-phase holding tank with overhead stirring. We used a 400 MWCO PEEK membrane, custom-made from our collaborators in the Livingston Group at Imperial College, London. This membrane provided base compatibility along with a 97% rejection of our precatalyst, although only low fluxes were possible (4.8 L/m²h pure solvent mixture, 0.48 L/m²h under actual operating conditions). For this reason, a 1:1 ratio of toluene:DMO mixture was used to modestly improve throughput. This catalyst proved difficult to quantitatively remove from the product, with rejections in the range of 84% to 90% being obtained for a continuous run. A TON of 550 was obtained with a

substrate:catalyst ratio of 50 in the reactor. This substrate:catalyst ratio was shown to be near what is necessary to obtain full yield in our system, and so we have demonstrated significant catalyst reusability. Various system improvements were made in order to increase system robustness. New pumps with twice as many (larger) check valves were employed, along with parallelized backpressure regulators. We suggest that significantly improved results could be obtained with higher throughput membranes, as our throughput per volume of membrane module bottlenecked our process's productivity. Future work should focus on options to debottleneck this process.

6 Dynamic Process Modeling

6.1 Introduction

In Chapter 4, we designed and constructed a small-scale recycle system for a hydrogenation catalyst. A dynamic model for the process was constructed in order to aid in the design of future experiments as well as to demonstrate that the system performance was well-understood. The latter goal would be realized by performing the necessary residence time distribution (RTD) experiments to characterize the behavior of the various process blocks. The former goal would require the deactivation rate of the catalyst to be understood well enough to predict the amount of fresh catalyst to feed into the system at steady-state. Both of these goals require a functional differential-algebraic model of the process which can be solved as efficiently as possible.

Differential algebraic equations systems (DAEs) include, upon proper manipulation, both ordinary differential equations (ODEs) and algebraic equations. Jacobian[®] (RES Group Inc.) solves difficult DAE problems by first solving for a consistent set of initial conditions by employing a nonlinear equation (NLE) solver, the default of which is a Newton-Raphson method with a number of (often proprietary) enhancements. Generally, these enhancements are: an improved line search, enhanced stepsize selection strategies, variable boundary handling, and singularity avoidance. When this method does not converge, the program automatically tries using other NLE solvers. The algebraic equations are organized in upper triangular form and solved in smaller blocks to reduce computation time; this is made possible by the frequency of very sparse matrices in chemical process DAE systems. Once initialized, a modified Gear's method using backwards differencing is employed to integrate the system. The algorithm exploits the sparsity of the DAE matrices for efficient storage and computation. A smart event detection algorithm guarantees that state events will be identified correctly,^[218] which is useful in simulating the discontinuities during system start-up.

We use the Jacobian[®] software to simulate 24 hours of operation of our hydrogenation catalyst recycle system. This typically takes less than a minute using one CPU. Due to this efficiency, we can integrate Jacobian[®] with Matlab to fit data to our model and extract values of kinetic parameters using only one CPU (typically less than 10 minutes to converge). Our model equations and comparison of model predictions with experimental process performance are included in this Chapter.

6.2 Model Assumptions

Our model focused on the accurate simulation of our hydrogenation catalyst recycle system described in Chapter 4. After an attempt to construct a dynamic model of our catalyst recycle processes using Aspen Dynamics[®], a Jacobian[®] model (RES Group, Inc.) was constructed and found to operate much more efficiently. The efficiency is mainly due to the program's ability to automatically take advantage of the sparsity of the matrices involved in solving our differential algebraic equations (DAEs). Simulations of dynamic step-changes in feed flow rates and compositions were also handled reliably in Jacobian. Our Jacobian[®] model consists of dynamic mass balances relating the reactor, membrane, and sampling valve flowrates and concentrations. This is shown schematically in Figure 83. A number of assumptions were made in this simplified model, and are detailed below. The complete model is included in Appendix EE.

- 1) Only the liquid phase and liquid phase residence times are considered.
- 2) All reactive behavior is modeled using CSTR-in-series approaches to approximate experimental RTDs.
- 3) Concentration polarization near the membrane, insomuch as it contributes to the accumulation within the recycle loop, is ignored. This assumption is necessary due to our lack of ability to probe the concentrations within this boundary layer.

4) Sample valves within the system are approximated as continuous splitters. Splitters continuously withdraw small amounts of liquid from the system rather than periodically removing larger volumes from the system. The amount that is removed during these discrete samples is very small (<0.25% of system volume).

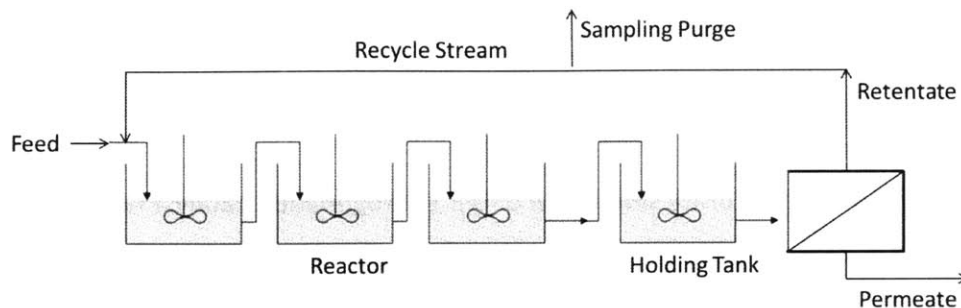


Figure 83. Abstraction of our catalyst recycle process which is simulated using our dynamic model.

6.3 Model Equations

6.3.1 Reactor

In addition to mass balances, kinetic terms are also included in these equations to model the reactions, including catalyst deactivation. However, it was found that Jacobian[®] was most useful for predicting mass balances dynamically, and not kinetic behavior. The plug flow reactor was modeled using a series of CSTRs in Jacobian. This prevents the effects of numerical diffusion associated with solving the dynamic dispersion equation:

$$\frac{\partial C_A}{\partial t} + \frac{\partial C_A}{\partial \tau} = D \frac{\partial^2 C_A}{\partial x^2} - k C_A^n \quad (22)$$

Where C_A is the concentration of our species of interest, D is the dispersion number, t is experimental time, τ is the residence time, x is our reactor dimension (1-dimensional model), k

is the reaction rate constant, and n is the order of the reaction in species A. With the tanks-in-series approach, the number of tanks and series is related to our measure dispersion number (obtained experimentally via RTDs, see Chapter 4) with the following relationship:

$$\frac{1}{N} = 2 \left(\frac{D}{uL} \right) \quad (23)$$

Where N is our number of tanks in series, and $\frac{D}{uL}$ is our nondimensional dispersion (dispersion coefficient divided by our linear velocity multiplied by our reactor length). Writing our tanks-in-series models for each species of interest:

$$\frac{V_{Reactor}}{N} \frac{dC_{R,j}}{dt} = F_{j-1}C_{R,j-1} - F_jC_{R,j} - k_rC_{C,j} \quad (24)$$

$$\frac{V_{Reactor}}{N} \frac{dC_{P,j}}{dt} = F_{j-1}C_{P,j-1} - F_jC_{P,j} + k_rC_{C,j} \quad (25)$$

$$\frac{V_{Reactor}}{N} \frac{dC_{C,j}}{dt} = F_{j-1}C_{C,j-1} - F_jC_{C,j} - k_dC_{C,j} \quad (26)$$

$$j = 1 \dots N \text{ tanks} \quad (27)$$

Where $V_{Reactor}$ is the volume of our reactor (i.e., dynamic liquid holdup), $C_{R,j}$ is our reactant concentration in tank j , F_j is our flow rate in tank j , P denotes our product, and C denotes our catalyst. In addition, k_r is our reaction rate constant and k_d is our catalyst deactivation rate constant. The order of the latter reaction is not known and is initially guessed as first order in catalyst concentration. For our pack bed reactor, N was equal to 92 tanks-in-series. A lack of mass transfer limitation was verified using catalyst ramping experiments for our shortest residence times (Chapter 4).

6.3.2 Nanofiltration Module

The retentate side of the membrane module during these experiments behaved as a CSTR (Chapter 4). The membrane process block is shown schematically in Figure 84.

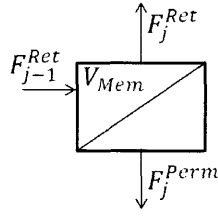


Figure 84. Nanofiltration module abstraction.

A reaction term in this process block was not included, because our system typically operated at full conversion. For the simulation of partial conversion runs, however, this nonideality would need to be approximated. A dynamic continuously stirred membrane module equation took the following form:

$$\frac{V_{Mem}}{N} \frac{dC_{ij}}{dt} = F_{j-1}^{Ret} C_{i,j-1} - F_j^{Ret} C_{ij} - F_j^{Perm} C_{ij}^{Perm} \quad (28)$$

$$F_j^{Ret} = F_{j-1}^{Ret} - F_j^{Perm} \quad (29)$$

$$F_j^{Perm} = \frac{F^{Perm}}{N} \quad (30)$$

Where V_{Mem} is the volume of the membrane module, C_{ij} is the concentration of species i in tank j , F_j^{Ret} is the retentate flow rate, and F_j^{Perm} is the permeate flow rate. In our case, $N=1$, which simplifies this equation set. A simple rejection equation was employed, with the exception of matching the permeate and retentate stream concentrations when a species was at zero concentration.

$$Rej_i = 1 - \frac{C_i^{Perm}}{C_i} \quad (31)$$

Under operating conditions, it was necessary to add two empirical parameters to complement our theoretical equations. These parameters depended upon stirring conditions in the membrane, concentrations of species in the retentate/permeate, and the usage history of the membrane:

$$F^{Perm} = F_{final}^{Perm} - (F_{final}^{Perm} - F_{initial}^{Perm})e^{-at} \quad (32)$$

$$Rej_i = Rej_{i,final} - (Rej_{i,final} - Rej_{i,initial})e^{-bt} \quad (33)$$

$$j = 1 \dots N \text{ tanks} \quad (34)$$

Where a is an empirical parameter characterizing our rate of permeation flow rate decline from the experimentally measured $F_{initial}^{Perm}$ until the experimentally measured F_{final}^{Perm} . Similarly, b is an empirical parameter characterizing our rate of rejection increase of species i from the experimentally measured $Rej_{i,initial}$ until the experimentally measured $Rej_{i,final}$. These parameters were extracted from rejection and flow rate data using Excel, and entered into our Jacobian® model.

6.3.3 Splitter

Our splitter, which served to simulate our loss of material through sampling, was modeled using the algebraic mass balance:

$$F_{in} - F_{purge} = F_{out} \quad (35)$$

$$C_{j,out} = C_{j,in} = C_{j,purge} \quad (36)$$

6.3.4 Mixer

The mixer at the entrance of our system was modeled using the mass balance for each species:

$$F_{in}C_{j,in} + F_{rec}C_{j,rec} = F_{out}C_{j,out} \quad (37)$$

6.3.5 Overall Balance

It was necessary to include an overall mass balance for our system, which allowed our model to calculate the flow rate into the system, F_{in} :

$$F_{in} = F_{perm} - F_{purge} \quad (38)$$

6.3.6 Start-Up

First, our model assigns initial conditions to rejections, permeation rates, and concentrations in the system. Next, catalyst at the (experimentally determined) loading concentration is allowed to flow into the system and recycle for an experimentally determined time frame. This has the effect of equilibrating the catalyst throughout the system (although there is some nonuniformity, which can be predicted by the model). Next, this loading solution is replaced by the substrate/catalyst cofeed solution, and these concentrations are treated as a step-change to the feed concentrations in the system.

6.4 Parameter Fitting

Data from an experimental run could be used to fit parameters (i.e., rate constants) using our dynamic model. Despite creating a functional set of code which performed this operation, our data proved insufficient to obtain accurate kinetic parameter estimates. This was due to our relatively short runs being dominated by variations in oxygen contamination between runs. This is a known issue in small scale oxygen-sensitive experiments, and for our complex small-scale flow system the issue is exacerbated. Our model was still useful to aid in system understanding/improvement, predicting dynamic mass balances, and solving for the concentrations of species at other places in the system. Our parameter-fitting approach is briefly described here, with scripts included in various Appendices, to aid in any future work.

In order to perform dynamic simulations with parameter fitting, the dynamic Jacobian[®] model (Appendix E) was interfaced with a Matlab optimization code (Appendix F). Note that this script calls another important Matlab code, given in Appendix G. This interfacing was achieved by a C++ script (Appendix H), which was provided by Spencer Schaber. The simulation is run using the Matlab interface. When the Matlab code runs, a C++ script is run which calls the Jacobian[®] dynamic model. The Jacobian[®] model is run with a set of parameters chosen by Matlab's `fmincon` function. After Jacobian[®] runs, a CVS file is outputted which is then read by Matlab. Matlab then uses the predicted model concentrations to compute the sum of squared differences between experimental data points and the predicted concentrations from the dynamic model. In this way, concentrations from the sampling valves in the experimental system can be directly fit. The semi-empirical parameters which govern the membrane rejection and flux decline are incorporated into the Jacobian[®] model before these kinetic parameters are fit, although these can be simultaneously fit as well.

6.5 Model Applications

6.5.1 Metathesis Catalyst Recycle

The Matlab/Jacobian[®] code was tested by fitting the metathesis 50 hour continuous recycle data (Figure 43). This test was mainly to aid in the debugging of our model, and to ensure that the results which were provided made sense. This process also verifies the integrity of our dynamic mass balances. The reaction rate constant and deactivation rate constant for the metathesis catalyst was fit. Our Jacobian[®] model simulates the residence time distribution from each process block in our metathesis system, and is given in Appendix I. The Matlab code used to initiate the fit is given in Appendix J. This script imports the data and initiates the parameter-fitting sequence. This script calls another Matlab script which calculates the goodness of fit and generates plots (Appendix K). This script calls the C++ code (Appendix H), which executes the Jacobian script (Appendix I). As can be seen from Figure 85, the Jacobian[®] model can produce the correct dynamic trends over the 50 hour period. This does not demonstrate the successful extraction of kinetic parameters, but does demonstrate that the Jacobian[®]/Matlab codes can be used for this purpose if there is sufficient data. Figure 85 also demonstrates that our model is unable to account for rising substrate concentrations in the system (despite their small values), which is likely due to product inhibition of the catalyst. This was not included in our model. Due to the presence of partial conversions, product inhibition, and the likelihood of the reaction occurring outside of the reactor, we judged our hydrogenation system to be a more appropriate target for applying this model.

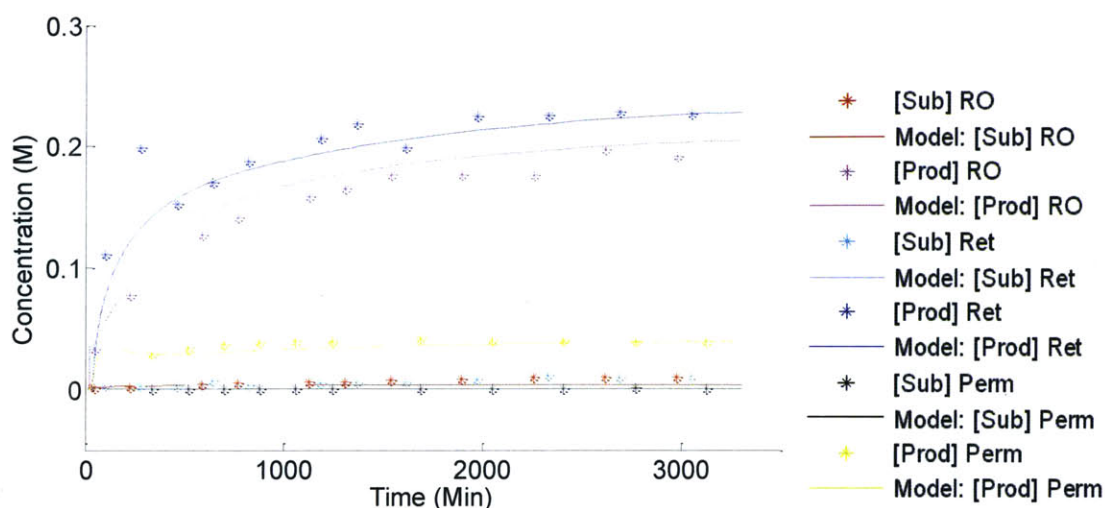


Figure 85. Fit of dynamic model of metathesis catalyst recycle system to continuous data. Abbreviations for legend: [Sub] = Substrate Concentration, [Prod] = Product Concentration, RO = Reactor Outlet, Ret = Retentate Stream, Perm = Permeate Stream.

6.5.2 Hydrogenation Catalyst Recycle

Our hydrogenation system provided a simple test of our Jacobian® dynamic model. The model was developed in order to predict more optimal experiments from continuous recycle data, thus reducing the number of experiments necessary to obtain a functional system with high yields. Product inhibition is not expected to be an issue with this chemistry, and mass transfer limitations were shown to be absent in the system. Using our kinetic screening platform, we found base/TPP concentration to have only a small effect on the kinetics. We were also able to understand the dependence of reaction rate on catalyst and substrate concentration. However, a catalyst deactivation rate constant using our continuous recycle run (with no catalyst co-feed) was insufficient to fit the parameter with any accuracy. Although more data would likely lead to a more accurate evaluation of our rate constant, it would defeat the purpose of the model, which was to reduce the number of experiments necessary to design a catalyst cofeed experiment using kinetic parameter extraction. Therefore, our dynamic model was employed to test the dynamic mass balances of our hydrogenation system. Once we were

able to experimentally determine the correct catalyst cofeed ratio, we obtained nearly full conversions and full selectivity, so that kinetic terms were not necessary in our model. Our completed Jacobian® model included the residence time distributions of the process blocks in our system, the system flow rates, feed concentrations, and empirical membrane rejections. This model accurately predicted the evolution of product concentration in our system (Figure 86). Our permeate and retentate data is plotted along with the dynamic model predictions.

The close agreement between the model and data show that we have developed a good understanding of the system using our residence time distribution experiments. The close agreement helps to verify the assumptions of our model, and the integrity of our automated sampling system. Furthermore, despite the failure to reach a perfectly controlled state, the dynamic model ensures that we are indeed very close to the theoretical steady state concentrations of the system.

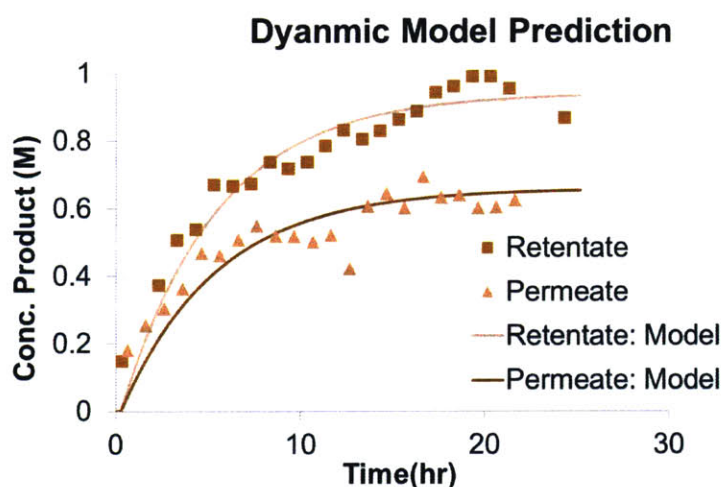


Figure 86. Dynamic model prediction of our continuous hydrogenation run. Full conversion is assumed in the model; only product concentrations are considered.

6.6 Conclusions

This chapter described the assumptions and model equations necessary to construct a dynamic process model of our hydrogenation catalyst recycle system. Jacobian® was chosen as the dynamic simulation software due to its state-of-the-art numerical methods which allow for extremely efficient computation. Our dynamic model made use of tanks-in-series models to represent the experimental RTD's of individual process blocks. In this way, a dynamic plug flow reactor can be solved efficiently without issues from numerical diffusion. Our model makes a number of simplifying assumptions, including ignoring the gas phase, ignoring the possibility of accumulated material in the concentration polarization layer above the membrane, and approximating discrete removal of samples in the real system by a continuous splitter.

Our experimental hydrogenation catalyst recycle system produced retentate and permeate product concentrations throughout a 24 hour run. Since nearly full yields were obtained, the kinetics could be ignored in our model, and our dynamic model was instead used to calculate dynamic mass balances. Some empirical data from the continuous system was necessary due to inadequate theoretical models. This included the permeation rate as a function of operation time, changes in species rejections as a function of time, the experimental RTD's of the individual process blocks, and feed concentrations/flow rates. Using this data, the model equations were used to predict the evolution of product concentrations throughout the system during the 24 hour period. Our results show a good match between our experimental data (in the permeate and retentate streams) and our dynamic model, validating our approach and model assumptions. Despite being able to predict dynamic concentration changes in our system, our model, combined with Matlab, was unable to make inferences regarding the values of kinetic parameters. Although our parameter fitting codes work correctly, our continuous recycle runs did not constitute sufficient data for accurate parameter estimation. Therefore, an experimental approach was used to design catalyst co-feed experiments throughout this thesis.

Small changes to this dynamic model were made in order to approximately represent our continuous metathesis recycle system as well, and similarly validated our understanding of our system dynamics and mass balances. In this case, an inadequate kinetic understanding of our system limited the accuracy with which the model could fit our data. Particularly, the kinetics of product inhibition in our system would need to be further elucidated.

Overall, this dynamic model is a useful starting point for process understanding, dynamic process optimization, control system applications, and parameter estimation from continuous catalyst recycle experiments. Careful consideration must be given when employing this model in experimental design. It is likely that the superior approach is experimental trial-and-error, combined with additional control systems to find and maintain a controlled state during system operation.

7 Conclusion

7.1 Summary of Thesis Contributions

This thesis undertook the challenge of designing, building, and operating a number of small scale flow systems for the continuous recycle of important organometallic homogeneous catalysts. Both thermomorphic and nanofiltration separation approaches are investigated, with nanofiltration emerging as the more general and practical approach to recycling homogeneous catalysts in flow. Our development of thermomorphic solvent systems in flow focused on a model allylic alcohol isomerization catalyst. Using nanofiltration membranes, small-scale continuous recycle systems for a ring-closing metathesis catalyst, an asymmetric ketone hydrogenation catalyst, and a Buchwald–Hartwig amination catalyst were studied.

In Chapter 2, an experimental flow system was used as a screening platform to discover a number of water-containing thermomorphic solvent systems. In particular, a thermomorphic water/ethanol/ethyl acetate system was identified as a good solvent system to recycle a water-soluble version of Wilkinson's catalyst. Our model chemistry was the isomerization of 1-octen-3-ol to 3-octanone. These solvents are relatively benign, cheap, and were found to dissolve the catalyst salts at room temperature and at the reaction temperature. The kinetic-limitation of reactions in this thermomorphic solvent system were then leveraged to create a faster reaction than a biphasic reaction system from the literature. This was done by increasing catalyst loading, although temperature could also be increased. This demonstrated that mass transfer limitations had been overcome using the thermomorphic solvent system, which also improves system scalability. Our solvent system produced a TOF of 450 h^{-1} compared to larger scale batch data from the literature at only 30 h^{-1} due to mass transfer limitations. However, the chemical and solubility constraints imposed by using such a narrow range of three-solvent mixtures was found to relegate thermomorphic solvent system to niche applications of homogeneous

catalysis. The remainder of this thesis focused on the more general nanofiltration as an approach to catalyst separation and recycle.

In Chapter 3, we designed a functional small scale metathesis catalyst recycle system with a total internal volume of less than 3 ml. A Teflon AF[®] membrane reactor was employed to efficiently remove ethylene gas, the reaction byproduct. A novel microfluidic holding tank with an integrated laser-based liquid level measurement was designed and employed in the system. In addition, a novel microfluidic nanofiltration module with a new high-pressure sealing technique was designed and implemented. Both of these process blocks may find use in other areas of microfluidics. The results of this recycle system were improved metathesis TONs (935) along with a significant reduction of ruthenium (less than one ppm) in the permeate stream – a 100 fold reduction in ruthenium compared with the membrane retentate stream. This work is the smallest-scale example of a continuous catalyst recycle system using nanofiltration in the literature to date. Despite some successes of this system, the high product rejections and product inhibition rendered the system industrially impractical. The unrealistic substrate employed as a model chemistry was also a weakness of this work. Choosing the easiest possible substrate for a catalyst recycle system, although practically appealing, makes it more difficult to judge the merits of a completed recycle system. The hydrogenation and amination substrates chosen for subsequent recycle processes did not repeat this mistake.

In Chapter 4, we chose to recycle a ruthenium catalyst used to asymmetrically hydrogenate α -tetralone. Unlike the metathesis work, this catalyst had not yet been recycled in the literature, and so significant batch development work was necessary in finding optimal catalyst recycle conditions. Ultimately, we found that high pressures of hydrogen were necessary to ensure catalyst stability. A base-compatible 800 MWCO PEEK membrane from the Livingston Group at Imperial College, London was used with this chemistry. Furthermore, we designed a kinetic screening platform to efficiently screen concentrations and residence times in flow in order to optimize our TOFs prior to building our recycle system (since the kinetics of this particular chemistry were much less explored in the literature). We found no dependence of

reaction rate on substrate concentration, which is ideal for a catalyst recycle system. From the metathesis work, we learned that a slightly larger scale of work would offer significant practical advantages. Not only would clogging be avoided, but larger scale commercial membrane modules could be employed as a starting point for membrane module enhancement (avoiding the cumbersome sealing technique required for our microfluidic module). Therefore, we designed and built a hydrogenation catalyst recycle system with a total internal volume of less than 50 ml. In this system, a pre-existing membrane module was redesigned in order to both minimize internal volume and provide a location for liquid level measurement with a laser. In this way, a high-pressure holding tank for gas-liquid separation and liquid level control was integrated into the membrane module. This allowed for our catalyst to be separated and recycled in a continuous system without decreasing the pressure at any point during the system. High yields could be maintained with a catalyst co-feed throughout a 24 hour run. In our continuous recycle system, we were able to obtain a TON of 4750 with substrate:catalyst ratios of 250 in the reactor, and ruthenium leaching of less than 200 ppb through the nanofiltration membrane. Some decline in enantioselectivity (from 97% to 93%) was observed for our longest (24 hour) run.

In Chapter 5, we took on the challenge of recycling a highly active 3rd generation BrettPhos Buchwald-Hartwig amination catalyst. We chose to couple aniline with 3-chloroanisole, which will be the first time that a (relatively inactive) aryl chloride substrate is employed in a continuous coupling catalyst recycle system. Such a substrate makes high yields very difficult to obtain without a fully intact Palladium–ligand catalyst system (as opposed to palladium nanoparticles and leached palladium without a ligand). Batch catalyst recycle experiments demonstrated that an excess of aryl chloride, an excess of BrettPhos ligand, and reduced residence time outside of the reactor helped to increase catalyst stability. This continuous recycle system required two separation blocks: a liquid/liquid separation to remove the aqueous base, and a nanofiltration step to separate the organic-soluble product from the organic-soluble catalyst. The former separation required designing a novel small-scale holding

tank with an overhead mixer. This holding tank used a WebCam to detect differences in grayness between the organic and aqueous phases in order to control the organic feed rate into the system and the aqueous drain rate, respectively. Our continuous recycle system for this chemistry was run for 60 hours, at which point a controlled state was observed. We obtained a TON of 550, a factor of 10 higher than our substrate:catalyst ratio of 50 within the reactor. However, for this chemistry, significant palladium leaching was observed, with rejections of only 84- 90% throughout our 60 hour run. This is consistent with literature applications applying OSN to palladium coupling catalysts.

In Chapter 6, we built a dynamic Jacobian[®] model which can be used to model the performance of the dynamic processes described in this thesis. The model can be interfaced with Matlab for parameter-fitting using continuous recycle data. The accuracy of the dynamic mass balances in the model, which make use of empirical RTDs and membrane rejections/permeation rates for a real recycle run, are demonstrated using our best understood system: the hydrogenation catalyst recycle system. We were able to show a close agreement between the evolution of concentrations of product in the real system and our dynamic model. However, the model was an impractical tool for the designing of catalyst cofeed experiments using limited catalyst recycle data. More experiments could solve this problem, but is less efficient than experimental trial-and-error for the purposes of this thesis. The model was also applied to our metathesis catalyst recycle system, with reasonable agreement between observed reactant/product concentration evolution and our continuous data. This model is a useful starting point for process optimization, predicting concentrations at other points in the system, and performing parameter fitting to extract kinetic parameters.

In sum, we have successfully designed three small scale flow systems to investigate the benefits and disadvantages of continuous catalyst recycle systems using nanofiltration as a catalyst separation strategy.

7.2 Future Work and Recommendations

Applications of catalyst recycle systems using thermomorphic solvent systems, although not a very general approach, may certainly find some important industrial applications in the future. Thermomorphic solvent systems may be best suited to optimize the production of a generic drug molecule. In this case, the time-to-market is less important, and the many issues and challenges which arise upon the specific application of a thermomorphic solvent system to a chemical transformation, and its effect on upstream and downstream processes, can be confronted. The major challenge here is to identify the relevant industrial chemical transformation, using a substrate identical to or very similar to an actual pharmaceutical drug. Changing from model substrates to drug molecules with a thermomorphic solvent system is unlikely to work, due to the differences in solubilities of the two molecules (combined with any byproducts or leftover material from upstream processes). Therefore, if thermomorphic solvent systems are able to have a positive effect on fine chemical production, the best approach may be to find a severely mass transfer limited, liquid/liquid reaction using an organometallic catalyst which resides in a phase different from the generic drug product. At this point, the value added to the process by switching to a thermomorphic solvent system may be investigated. In such cases, there is the potential for substantially reduced reaction times (and therefore, reduce catalyst deactivation between recycles). This is consistent with our conclusion in Chapter 2, which is that these solvent systems are likely to only have niche applications (at best) in drug production.

Our continuous metathesis catalyst recycle system, although introducing novel and useful microfluidic process blocks, is not in itself a practical application. Future work should focus on substantially larger substrate molecules, which are identical to or similar to known drug precursors. This will of course require membranes with higher MWCOs and molecular weight enhanced metathesis catalysts. This will help to improve membrane throughput per module volume, and in turn, TONs. Large ring-closing metathesis substrates are typically run much

more dilute, to prevent cross metathesis, and so the dilution which occurs in the reactor when running a catalyst recycle system is to the advantage of the chemistry. There is still the disadvantage of product inhibiting the catalysis, which is an intrinsic drawback to applying metathesis in a continuous catalyst recycle system. A series of membrane modules, with pure solvent feeds, could be used to extract more product before the catalyst is recycled, but this would introduce substantial process complexity. In sum, if further metathesis work is undertaken, the next logical step is to investigate whether better or worse results are obtained when using a realistic drug molecule; the outcome here is difficult to predict theoretically due to substantial differences between our model substrate and real drug precursors. If future work is pursued, larger scale systems (~50 ml total internal volume) are preferred from a practical standpoint.

Our asymmetric hydrogenation catalyst recycle system is perhaps the most promising application in this thesis. One of the main reasons for this is the zero-order dependence of the reaction rate on substrate concentration. This allows the dilution in the recycle loop to have no effect on our turnover frequencies, although throughput is still affected. We were able to increase TONs of this catalyst enough to warrant further investigation. Using our pumping technology and control systems, 24 hour runs were achieved with high-yields. However, a declining enantioselectivity indicated that the system was not at a true controlled state. Therefore, additional control loops would need to be implemented to maintain the enantioselectivity at a constant level in the system, likely by varying the rate at which to purge catalyst (and deactivated catalyst) from the recycle loop. This would reduce the TON, but allow a higher enantioselectivity at the controlled state. This, combined with new pumping infrastructure which can be operated for longer periods of time without failure, could allow the system to achieve a true control state. A run on the order of a week could be a very useful demonstration from this small-scale pilot. Such a run might also benefit from an additional control loop, which controls the catalyst cofeed rate based upon the measured yields at the reactor outlet. This would allow for a more optimal use of fresh catalyst, improving turnover

numbers. The accuracy of our dynamic model also creates the opportunity for significant process optimization, although this would require the extraction of kinetic parameters such as the deactivation kinetics. The dynamic model might also be a useful starting point for predicting the control parameters for two additional control loops.

Our coupling catalyst recycle system demonstrated significant recyclability of the catalyst, with palladium rejections in the 84-90% range. However, the dilution of the reaction mixture in the reactor (by the recycle flow rate) has a substantial negative impact upon catalyst performance. This can be dealt with in future work, while simultaneously using a more relevant example for a starting material and debottlenecking the process (currently due to the low throughput of the 400 MWCO PEEK membranes). A larger, drug-like molecule (near 350 or even 400 MW) could be chosen as the product for a coupling reaction. A larger molecular weight cut off membrane, possibly a Puramem 600, can be used for the membrane instead of the current 400 MWCO peek membrane. This would be the de-bottleneck the process, allowing very high throughput and more efficient catalyst reuse. A reduction in catalyst rejections might be observed for this higher molecular weight cut off membrane, but two membranes in series would still perform substantially better than the current configuration, with much higher throughput. If rejections are too low, molecular enhanced BrettPhos ligands can be developed. This system would inherit the problem of base incompatibility of the membrane. To solve this problem, weak acid may be able to quench the KOH, before the holding tank, to ensure that the membrane does not see any strong base. Even though this adds some complexity to the process, the residence time in the recycle loop, and the residence time to permeate a full system volume, could be improved substantially, which should improve TONs and time to reach steady-state. Furthermore, this configuration would allow for the possibility of reducing the dilution effect in the recycle system by slowing the recycle flowrate to a fraction of the permeation rate. This is made possible only by the substantially improve dynamics due to the above-mentioned changes in membrane material. Too slow of a retentate flow rate would of course lead to clogging, so this flow rate needs to be experimentally optimized. Although the

results of our system from Chapter 5 have significant disadvantages, the potential system described above solves almost all of these problems, and warrants pursuit.

The scale-up of a continuous catalyst recycle system should also be investigated in future work, as this last piece of information is critical to maximizing the amount of information which can be obtained from the small-scale recycle experiments. Understanding the scale-up of the membrane module is a good start, since there is a deficit of such analyses in the literature for nanofiltration membranes. Ultimately, the implementation of spiral-wound modules could improve throughput-per-volume, and lead to improved system performance. Their configuration may also lead to reduced fouling due to the higher degree of confinement above the membrane. If our small-scale modules are unable to predict the performance of larger-scale modules, then the challenge of creating proper downscale membrane modules will exist.

The overall picture painted by these specific suggestions for future work reflect a general optimism about the potential of continuous small-scale catalyst recycle systems to produce useful data for chemical process design. Future work should focus only on realistic substrates, aiming for longer runs with more control loops, and understanding system scale-up.

8 References

- [1] M. J. Muldoon, *Dalton Transactions* **2010**, 39, 337.
- [2] B. Cornils, W. A. Herrmann, *Journal of Catalysis* **2003**, 216, 23.
- [3] C. Jones, *Topics in Catalysis* **2010**, 53, 942.
- [4] D. J. Cole-Hamilton, *Vol. 299*, **2003**, pp. 1702.
- [5] B. Cornils, W. A. Herrmann, *Applied Homogeneous Catalysis with Organometallic Compounds*, Wiley-VCH, Weinheim, Germany, **2002**.
- [6] J. Hagen, *Industrial Catalysis*, Wiley-VCH, Weinheim, Germany, **2006**.
- [7] C. E. Garrett, K. Prasad, *Advanced Synthesis & Catalysis* **2004**, 346, 889.
- [8] *Guideline on the Specification Limits for Residues of Metal Catalysts*, European Medicines Agency, London, U.K., **2007**.
- [9] V. Hessel, *Chemical Engineering & Technology* **2009**, 32, 1655.
- [10] T. Noel, S. L. Buchwald, *Chemical Society Reviews* **2011**, 40, 5010.
- [11] T. Chinnusamy, S. Yudha S, M. Hager, P. Kreitmeier, O. Reiser, *ChemSusChem* **2012**, 5, 247.
- [12] C. W. Kohlpaintner, R. W. Fischer, B. Cornils, *Applied Catalysis A: General* **2001**, 221, 219.
- [13] W. Keim, *Green Chemistry* **2003**, 5, 105.
- [14] B. Richter, A. L. Spek, G. van Koten, B.-J. Deelman, *Journal of the American Chemical Society* **2000**, 122, 3945.
- [15] D. F. Foster, D. Gudmunsen, D. J. Adams, A. M. Stuart, E. G. Hope, D. J. Cole-Hamilton, G. P. Schwarz, P. Pogorzelec, *Tetrahedron* **2002**, 58, 3901.
- [16] R. Hart, P. Pollet, D. J. Hahne, E. John, V. Llopis-Mestre, V. Blasucci, H. Huttenhower, W. Leitner, C. A. Eckert, C. L. Liotta, *Tetrahedron* **2010**, 66, 1082.
- [17] T. Fukuyama, M. Shinmen, S. Nishitani, M. Sato, I. Ryu, *Organic Letters* **2002**, 4, 1691.
- [18] R. A. Brown, P. Pollet, E. McKoon, C. A. Eckert, C. L. Liotta, P. G. Jessop, *Journal of the American Chemical Society* **2001**, 123, 1254.
- [19] D. J. Heldebrant, P. G. Jessop, *Journal of the American Chemical Society* **2003**, 125, 5600.
- [20] A. Behr, G. Henze, L. Johnen, C. Awungacha, *Journal of Molecular Catalysis A: Chemical* **2008**, 285, 20.
- [21] A. Behr, R. Roll, *Journal of Molecular Catalysis A: Chemical* **2005**, 239, 180.
- [22] J. Tijani, B. El Ali, *Applied Catalysis A: General* **2006**, 303, 158.
- [23] L. Phan, D. Chiu, D. J. Heldebrant, H. Huttenhower, E. John, X. Li, P. Pollet, R. Wang, C. A. Eckert, C. L. Liotta, P. G. Jessop, *Industrial & Engineering Chemistry Research* **2007**, 47, 539.
- [24] J. Fang, H. Jin, T. Ruddy, K. Pennybaker, D. Fahey, B. Subramaniam, *Industrial & Engineering Chemistry Research* **2007**, 46, 8687.
- [25] P. Pollet, R. J. Hart, C. A. Eckert, C. L. Liotta, *Acc. Chem. Res.* **2010**, 43, 1237.
- [26] E. M. Hill, Ph.D. Thesis thesis, Georgia Institute of Technology **2007**.
- [27] V. M. Blasucci, Z. A. Husain, A. Z. Fadhel, M. E. Donaldson, E. Vyhmeister, P. Pollet, C. L. Liotta, C. A. Eckert, *The Journal of Physical Chemistry A* **2009**, 114, 3932.
- [28] Z. A. Husain, Master Thesis, Georgia Institute of Technology **2009**.
- [29] C. A. McNamara, M. J. Dixon, M. Bradley, *Chemical Reviews* **2002**, 102, 3275.
- [30] M. Benaglia, A. Puglisi, F. Cozzi, *Chemical Reviews* **2003**, 103, 3401.
- [31] D. Astruc, F. Lu, J. R. Aranzaes, *Angewandte Chemie International Edition* **2005**, 44, 7852.

- [32] D. E. Bergbreiter, Y.-S. Liu, P. L. Osburn, *Journal of the American Chemical Society* **1998**, *120*, 4250.
- [33] D. E. Bergbreiter, P. L. Osburn, J. D. Frels, *Journal of the American Chemical Society* **2001**, *123*, 11105.
- [34] S. L. Desset, D. J. Cole-Hamilton, *Angewandte Chemie International Edition* **2009**, *48*, 1472.
- [35] F. O. Seidel, J. A. Gladysz, *Advanced Synthesis & Catalysis* **2008**, *350*, 2443.
- [36] P. Vandezande, L. E. M. Gevers, I. F. J. Vankelecom, *Chem. Soc. Rev.* **2008**, *37*, 365.
- [37] in *Nanowerk News*, **2010**.
- [38] X. J. Yang, A. G. Livingston, L. Freitas dos Santos, *Journal of Membrane Science* **2001**, *190*, 45.
- [39] D. Bhanushali, S. Kloos, D. Bhattacharyya, *J. Mem. Sci.* **2002**, *208*, 343.
- [40] L. G. Peeva, E. Gibbins, S. S. Luthra, L. S. White, R. P. Stateva, A. G. Livingston, *Journal of Membrane Science* **2004**, *236*, 121.
- [41] P. Silva, S. Han, A. G. Livingston, *J. Mem. Sci.* **2005**, *262*, 49.
- [42] A. Iwama, Y. Kazuse, *J. Mem. Sci.* **1982**, *11*, 297.
- [43] E. S. Tarleton, J. P. Robinson, C. R. Millington, A. Nijmeijer, *J. Mem. Sci.* **2005**, *252*, 123.
- [44] J. P. Robinson, E. S. Tarleton, K. Ebert, C. R. Millington, A. Nijmeijer, *Ind. Eng. Chem. Res.* **2005**, *44*, 3238.
- [45] J. T. Scarpello, D. Nair, L. M. Freitas dos Santos, L. S. White, A. G. Livingston, *Journal of Membrane Science* **2002**, *203*, 71.
- [46] H. P. Dijkstra, G. P. M. van Klink, G. van Koten, *Accounts of Chemical Research* **2002**, *35*, 798.
- [47] M. Janssen, C. Muller, D. Vogt, *Green Chemistry* **2011**, *13*, 2247.
- [48] A. Keraani, T. Renouard, C. Fischmeister, C. Bruneau, M. Rabiller-Baudry, *ChemSusChem* **2008**, *1*, 927.
- [49] P. van der Gryp, A. Barnard, J.-P. Cronje, D. de Vlieger, S. Marx, H. C. M. Vosloo, *Journal of Membrane Science* **2010**, *353*, 70.
- [50] M. Priske, K.-D. Wiese, A. Drews, M. Kraume, G. Baumgarten, *Journal of Membrane Science* **2010**, *360*, 77.
- [51] A. Tsoukala, L. Peeva, A. G. Livingston, H.-R. Bjørsvik, *ChemSusChem* **2012**, *5*, 188.
- [52] S. Aerts, H. Weyten, A. Buekenhoudt, L. E. M. Gevers, I. F. J. Vankelecom, P. A. Jacobs, *Chemical Communications* **2004**, 710.
- [53] H.-T. Wong, Y. H. See-Toh, F. C. Ferreira, R. Crook, A. G. Livingston, *Chemical Communications* **2006**, 2063.
- [54] C. G. Frost, L. Mutton, *Green Chemistry* **2010**, *12*, 1687.
- [55] M. W. Losey, R. J. Jackman, S. L. Firebaugh, M. A. Schmidt, K. F. Jensen, *Microelectromechanical Systems, Journal of* **2002**, *11*, 709.
- [56] S. K. Ajmera, C. Delattre, M. A. Schmidt, K. F. Jensen, *Sensors and Actuators B: Chemical* **2002**, *82*, 297.
- [57] T. Inoue, M. A. Schmidt, K. F. Jensen, *Industrial & Engineering Chemistry Research* **2007**, *46*, 1153.
- [58] K. D. Nagy, K. F. Jensen, *Chemistry Today* **2011**, 29.
- [59] M. W. Losey, M. A. Schmidt, K. F. Jensen, *Industrial & Engineering Chemistry Research* **2001**, *40*, 2555.
- [60] M. H. Al-Dahhan, F. Larachi, M. P. Dudukovic, A. Laurent, *Industrial & Engineering Chemistry Research* **1997**, *36*, 3292.

- [61] U. Kunz, A. Kirschning, H. L. Wen, W. Solodenko, R. Cecilia, C. O. Kappe, T. Turek, *Catalysis Today* **2005**, *105*, 318.
- [62] G. W. Lamb, F. A. Al Badran, J. M. J. Williams, S. T. Kolaczkowski, *Chemical Engineering Research and Design* **2010**, *88*, 1533.
- [63] J. Lim, S. N. Riduan, S. S. Lee, J. Y. Ying, *Advanced Synthesis & Catalysis* **2008**, *350*, 1295.
- [64] J. Lim, S. Seong Lee, J. Y. Ying, *Chemical Communications* **2010**, *46*, 806.
- [65] C. Simons, U. Hanefeld, I. W. C. E. Arends, A. J. Minnaard, T. Maschmeyer, R. A. Sheldon, *Chemical Communications* **2004**, 2830.
- [66] J. Madarász, G. Farkas, S. Balogh, Á. Szöllősy, J. Kovács, F. Darvas, L. Ürge, J. Bakos, *Journal of Flow Chemistry* **2011**, *1*, 62.
- [67] M. van den Berg, A. J. Minnaard, E. P. Schudde, J. van Esch, A. H. M. de Vries, J. G. de Vries, B. L. Feringa, *Journal of the American Chemical Society* **2000**, *122*, 11539.
- [68] W. M. Deen, *Analysis of Transport Phenomena*, Oxford University Press, New York, **1998**.
- [69] J. S. Moore, K. F. Jensen, *Angewandte Chemie International Edition* **2014**, *53*, 470.
- [70] O. Levenspiel, *Chemical Reaction Engineering*, 3rd ed., Wiley, New York, **1999**.
- [71] K. Nagy, *PhD Thesis, MIT* **2011**.
- [72] K. D. Nagy, B. Shen, T. F. Jamison, K. F. Jensen, *Organic Process Research & Development* **2012**, *16*, 976.
- [73] R. L. Hartman, J. P. McMullen, K. F. Jensen, *Angewandte Chemie International Edition* **2011**, *50*, 7502.
- [74] N.-T. Nguyen, Z. Wu, *J. Micromech. Microeng.* **2005**, *15*, R1.
- [75] J. Yoshida, A. Nagaki, T. Iwasaki, S. Suga, *Chemical Engineering & Technology* **2005**, *28*, 259.
- [76] A. Soleymani, H. Yousefi, I. Turunen, *Chemical Engineering Science* **2008**, *63*, 5291.
- [77] T. M. Floyd, M. A. Schmidt, K. F. Jensen, *Industrial & Engineering Chemistry Research* **2004**, *44*, 2351.
- [78] N. Zaborenko, E. R. Murphy, J. G. Kralj, K. F. Jensen, *Industrial & Engineering Chemistry Research* **2010**, *49*, 4132.
- [79] A. Gunther, M. Jhunjunwala, M. Thalmann, M. A. Schmidt, K. F. Jensen, *Langmuir* **2005**, *21*, 1547.
- [80] W. Ehrfeld, K. Golbig, V. Hessel, H. Lowe, T. Richter, *Industrial & Engineering Chemistry Research* **1999**, *38*, 1075.
- [81] R. Dreyfus, P. Tabeling, H. Willaime, *Physical Review Letters* **2003**, *90*, 144505.
- [82] A. Gunther, K. F. Jensen, *Lab on a Chip* **2006**, *6*, 1487.
- [83] H. Song, M. R. Bringer, J. D. Tice, C. J. Gerdtts, R. F. Ismagilov, *Applied Physics Letters* **2003**, *83*, 4664.
- [84] A. Bogdan, D. T. McQuade, *Vol. 5*, **2009**, p. 17.
- [85] J. R. Naber, S. L. Buchwald, *Angewandte Chemie International Edition*, *49*, 9469.
- [86] M. T. Kreutzer, F. Kapteijn, J. A. Moulijn, J. J. Heiszwolf, *Chemical Engineering Science* **2005**, *60*, 5895.
- [87] J. M. van Baten, R. Krishna, *Chemical Engineering Science* **2004**, *59*, 2535.
- [88] J. M. van Baten, R. Krishna, *Chemical Engineering Science* **2005**, *60*, 1117.
- [89] G. Berghel, A. Pintar, *Chemical Engineering Science* **1997**, *52*, 3709.
- [90] N. de Mas, A. Günther, M. A. Schmidt, K. F. Jensen, *Industrial & Engineering Chemistry Research* **2008**, *48*, 1428.

- [91] E. R. Murphy, J. R. Martinelli, N. Zaborenko, S. L. Buchwald, K. F. Jensen, *Angewandte Chemie International Edition* **2007**, *46*, 1734.
- [92] Y. Wada, M. A. Schmidt, K. F. Jensen, *Industrial & Engineering Chemistry Research* **2006**, *45*, 8036.
- [93] J. P. McMullen, K. F. Jensen, *Annual Review of Analytical Chemistry* **2010**, *3*, 19.
- [94] C. M. Griffiths-Jones, M. D. Hopkin, D. J. Jönsson, S. V. Ley, D. J. Tapolczay, E. Vickerstaffe, M. Ladlow, *Journal of Combinatorial Chemistry* **2007**, *9*, 422.
- [95] A. Sugimoto, T. Fukuyama, M. T. Rahman, I. Ryu, *Tetrahedron Letters* **2009**, *50*, 6364.
- [96] K. F. Jensen, J. Moore, *Organic Process Research & Development* **2012**.
- [97] A. Behr, G. Henze, R. Schomäcker, *Adv. Synth. Catal.* **2006**, *348*, 1485.
- [98] A. W. Francis, *Critical Solution Temperatures*, American Chemical Society, **1961**.
- [99] K. Nagy, **2010**.
- [100] Z. Jin, X. Zheng, B. Fell, *Journal of Molecular Catalysis A: Chemical* **1997**, *116*, 55.
- [101] D. E. Bergbreiter, Y.-S. Liu, *Tetrahedron Letters* **1997**, *38*, 7843.
- [102] M. Wende, R. Meier, J. A. Gladysz, *Journal of the American Chemical Society* **2001**, *123*, 11490.
- [103] F. Wen, H. Bönemann, J. Jiang, D. Lu, Y. Wang, Z. Jin, *Applied Organometallic Chemistry* **2005**, *19*, 81.
- [104] A. Behr, G. Henze, D. Obst, B. Turkowski, *Green Chem.* **2005**, *7*, 645.
- [105] A. Behr, L. Johnen, R. Nils, *Adv. Synth. Catal.* **2010**, *352*, 2062.
- [106] A. Behr, N. Toslu, *Chemical Engineering Technology* **2000**, *23*, 122.
- [107] J. M. Crosthwaite, S. N. V. K. Aki, E. J. Maginn, J. F. Brennecke, *The Journal of Physical Chemistry B* **2004**, *108*, 5113.
- [108] C. T. Wu, K. N. Marsh, A. V. Deev, J. A. Boxall, *Journal of Chemical & Engineering Data* **2003**, *48*, 486.
- [109] I. T. Horváth, J. Rábai, *Science* **1994**, *266*, 72.
- [110] E. de Wolf, G. van Koten, B.-J. Deelman, *Chemical Society Reviews* **1999**, *28*, 37.
- [111] C. M. Hansen, *Hansen Solubility Parameters: A User's Handbook, Second Ed.*, CRC Press, Boca Raton, FL, **2007**.
- [112] A. F. M. Barton, *Handbook of Solubility Parameters and Other Cohesion Parameters* 2nd Edition ed., CRC Press LLC, **1991**, pg. 55.
- [113] K. F. Jensen, *AIChE Journal* **1999**, *45*, 2051.
- [114] C. W. Kohlpaintner, R. W. Fischer, B. Cornilis, *Appl. Catal. A* **2001**, *221*, 219.
- [115] C. de Bellefon, S. Caravieilhés, É. G. Kuntz, *Comptes Rendus de l'Académie des Sciences - Series IIC - Chemistry* **2000**, *3*, 607.
- [116] M. Lombardo, C. Trombini, *Current Opinion in Drug Discovery & Development* **2010**, 717.
- [117] C. de Bellefon, R. Abdallah, T. Ireland, *Chemie Ingenieur Technik* **2004**, *76*, 633.
- [118] D. Balasubramanian, P. Mitra, *The Journal of Physical Chemistry* **1979**, *83*, 2724.
- [119] R. C. van der Drift, E. Bouwman, E. Drent, *Journal of Organometallic Chemistry* **2002**, *650*, 1.
- [120] C. S. Chin, S. Y. Lee, J. Park, S. Kim, *Journal of the American Chemical Society* **1988**, *110*, 8244.
- [121] T. M. Trnka, R. H. Grubbs, *Accounts of Chemical Research* **2000**, *34*, 18.
- [122] M. Scholl, S. Ding, C. W. Lee, R. H. Grubbs, *Organic Letters* **1999**, *1*, 953.
- [123] J. S. Kingsbury, J. P. A. Harrity, P. J. Bonitatebus, A. H. Hoveyda, *Journal of the American Chemical Society* **1999**, *121*, 791.

- [124] S. H. Hong, A. G. Wenzel, T. T. Salguero, M. W. Day, R. H. Grubbs, *Journal of the American Chemical Society* **2007**, *129*, 7961.
- [125] K. Vehlow, S. Gessler, S. Blechert, *Angewandte Chemie International Edition* **2007**, *46*, 8082.
- [126] J. Lim, S. S. Lee, S. N. Riduan, J. Y. Ying, *Advanced Synthesis & Catalysis* **2007**, *349*, 1066.
- [127] M. O'Brien, I. R. Baxendale, S. V. Ley, *Organic Letters* **2010**, *12*, 1596.
- [128] A. Polyzos, M. O'Brien, T. P. Petersen, I. R. Baxendale, S. V. Ley, *Angew. Chem., Int. Ed.* **2010**, *50*, 1190.
- [129] K. Skowerski, S. J. Czarnocki, P. Knapkiewicz, *ChemSusChem* **2013**, in press.
- [130] Q. Yao, A. Rodriguez Motta, *Tetrahedron Letters* **2004**, *45*, 2447.
- [131] M. Matsugi, D. P. Curran, *Journal of Organic Chemistry* **2005**, *70*, 1636.
- [132] Q. Yao, Y. Zhang, *Journal of the American Chemical Society* **2003**, *126*, 74.
- [133] B. Van Berlo, K. Houthoofd, B. F. Sels, P. A. Jacobs, *Adv. Synth. & Catal.* **2008**, *350*, 1949.
- [134] A. Keraani, C. d. Fischmeister, T. Renouard, M. Le Floch, A. Baudry, C. Bruneau, M. Rabiller-Baudry, *Journal of Molecular Catalysis A: Chemical* **2012**, *357*, 73.
- [135] M. J. Byrnes, A. M. Hilton, C. P. Woodward, W. R. Jackson, A. J. Robinson, *Green Chemistry* **2012**, *14*, 81.
- [136] Q. Yao, M. Sheets, *J. Organomet. Chem.* **2005**, *690*, 3577.
- [137] M. Sübner, H. Plenio, *Angewandte Chemie International Edition* **2005**, *44*, 6885.
- [138] D. Schoeps, K. Buhr, M. Dijkstra, K. Ebert, H. Plenio, *Chemistry-A European Journal* **2009**, *15*, 2960.
- [139] A. Kajetanowicz, J. Czaban, G. R. Krishnan, M. Malinska, K. Wozniak, H. Siddique, L. G. Peeva, A. G. Livingston, K. Grela, *ChemSusChem* **2013**, *6*, 182.
- [140] Y. Kaufman, R. Kasher, R. G. H. Lammertink, V. Freger, *Journal of Membrane Science* **2012**, *396*, 67.
- [141] N. Wagner, M. Fuereder, A. Bosshart, S. Panke, M. Bechtold, *Organic Process Research & Development* **2012**, *16*, 323.
- [142] J. T. Rundel, B. K. Paul, V. T. Remcho, *Journal of Chromatography A* **2007**, *1162*, 167.
- [143] A. B. Theberge, G. Whyte, M. Frenzel, L. M. Fidalgo, R. C. R. Wootton, W. T. S. Huck, *Chemical Communications (Cambridge, United Kingdom)* **2009**, 6225.
- [144] S. Liu, T. Fukuyama, M. Sato, I. Ryu, *Organic Process Research & Development* **2004**, *8*, 477.
- [145] J. F. Hartwig, *Organotransition Metal Chemistry: from Bonding to Catalysis*, University Science Books, **2010**.
- [146] J. G. Kralj, H. R. Sahoo, K. F. Jensen, *Lab on a Chip* **2007**, *7*, 256.
- [147] H. Sahoo, Ph.D. thesis, MIT **2008**.
- [148] S. L. Bournea, P. Koosa, M. O'Briena, B. Martinb, B. Schenkelb, I. R. Baxendalea, S. V. Ley, *Synlett* **2011**, *18*, 2643.
- [149] S. M. Roman, US **1991**.
- [150] W. Liu, P. J. Nichols, N. Smith, *Tetrahedron Letters* **2009**, *50*, 6103.
- [151] D. Nair, H.-T. Wong, S. Han, I. F. J. Vankelecom, L. S. White, A. G. Livingston, A. T. Boam, *Organic Process Research & Development* **2009**, *13*, 863.
- [152] A. Keraani, C. Fischmeister, T. Renouard, M. Le Floch, A. Baudry, C. Bruneau, M. Rabiller-Baudry, *Journal of Molecular Catalysis A: Chemical* **2012**, *357*, 73.
- [153] H.-U. Blaser, B. Pugin, F. Spindler, *J. Mol. Catal. A: Chem.* **2005**, *231*, 1.
- [154] R. Noyori, *Angew. Chem., Int. Ed.* **2002**, *41*, 2008.

- [155] E. J. Corey, R. K. Bakshi, S. Shibata, *J. Am. Chem. Soc.* **1987**, *109*, 5551.
- [156] U. Kragl, C. Dreisbach, *Angew. Chem., Int. Ed. Engl.* **1996**, *35*, 642.
- [157] G. Giffels, J. Beliczey, M. Felder, U. Kragl, *Tetrahedron: Asymmetry* **1998**, *9*, 691.
- [158] J. Woltinger, A. S. Bommarius, K. Drauz, C. Wandrey, *Org. Process Res. Dev.* **2001**, *5*, 241.
- [159] S. Laue, L. Greiner, J. Wöltinger, A. Liese, *Adv. Synth. Catal.* **2001**, *343*, 711.
- [160] P. N. Liu, P. M. Gu, F. Wang, Y. Q. Tu, *Org. Lett.* **2003**, *6*, 169.
- [161] X. Li, X. Wu, W. Chen, F. E. Hancock, F. King, J. Xiao, *Org. Lett.* **2004**, *6*, 3321.
- [162] J. Liu, B. Ma, Y. Feng, Y. He, Q.-H. Fan, *Inorg. Chim. Acta* **2014**, *409*, Part A, 106.
- [163] A. Hu, S. Liu, W. Lin, *RSC Advances* **2012**, *2*, 2576.
- [164] R. Liu, T. Cheng, L. Kong, C. Chen, G. Liu, H. Li, *J. Catal.* **2013**, *307*, 55.
- [165] A. Hu, H. L. Ngo, W. Lin, *J. Am. Chem. Soc.* **2003**, *125*, 11490.
- [166] T. Ohkuma, H. Takeno, Y. Honda, R. Noyori, *Adv. Synth. Catal.* **2001**, *343*, 369.
- [167] Y. Li, Y. Zhou, Q. Shi, K. Ding, R. Noyori, C. A. Sandoval, *Adv. Synth. Catal.* **2011**, *353*, 495.
- [168] J. Blacker, J. Martin, in *Asymmetric Catalysis on Industrial Scale*, Wiley-VCH Verlag GmbH & Co. KGaA, **2004**, pp. 201.
- [169] D. Stegeman, F. E. van Rooijen, A. A. Kamperman, S. Weijer, K. R. Westerterp, *Industrial & Engineering Chemistry Research* **1996**, *35*, 378.
- [170] J. C.-T. Lin, A. G. Livingston, *Chem. Eng. Sci.* **2007**, *62*, 2728.
- [171] M. Sairam, X. X. Loh, Y. Bhole, I. Sereewatthanawut, K. Li, A. Bismarck, J. H. G. Steinke, A. G. Livingston, *J. Membr. Sci.* **2010**, *349*, 123.
- [172] P. A. Dub, N. J. Henson, R. L. Martin, J. C. Gordon, *J. Am. Chem. Soc.* **2014**, *136*, 3505.
- [173] R. J. Hamilton, S. H. Bergens, *J. Am. Chem. Soc.* **2006**, *128*, 13700.
- [174] C. A. Sandoval, T. Ohkuma, K. Muñiz, R. Noyori, *J. Am. Chem. Soc.* **2003**, *125*, 13490.
- [175] W. L. Luyben, *Ind. Eng. Chem. Res.* **1994**, *33*, 299.
- [176] B. F. Alexander, Y. T. Shah, *The Canadian Journal of Chemical Engineering* **1976**, *54*, 556.
- [177] A. Lara Marquez, F. Larachi, G. Wild, A. Laurent, *Chem. Eng. Sci.* **1992**, *47*, 3485.
- [178] S. D. Schaber, D. I. Gerogiorgis, R. Ramachandran, J. M. B. Evans, P. I. Barton, B. L. Trout, *Industrial & Engineering Chemistry Research* **2011**, *50*, 10083.
- [179] **2014**.
- [180] A. Dumrath, C. Lübbe, M. Beller, in *Palladium-Catalyzed Coupling Reactions*, Wiley-VCH Verlag GmbH & Co. KGaA, **2013**, pp. 445.
- [181] W. D. Seider, J. D. Seader, D. R. Lewin, S. Widagdo, *Product and Process Design Principles*, John Wiley & Sons, Inc., **2009**.
- [182] K. McEleney, D. P. Allen, A. E. Holliday, C. M. Crudden, *Organic Letters* **2006**, *8*, 2663.
- [183] C. Torborg, M. Beller, *Advanced Synthesis & Catalysis* **2009**, *351*, 3027.
- [184] J. P. Wolfe, S. Wagaw, S. L. Buchwald, *Journal of the American Chemical Society* **1996**, *118*, 7215.
- [185] A. S. Guram, S. L. Buchwald, *Journal of the American Chemical Society* **1994**, *116*, 7901.
- [186] J. F. Hartwig, *Synlett* **1997**, *4*, 329.
- [187] M. R. Biscoe, B. P. Fors, S. L. Buchwald, *Journal of the American Chemical Society* **2008**, *130*, 6686.
- [188] N. C. Bruno, M. T. Tudge, S. L. Buchwald, *Chemical Science* **2013**, *4*, 916.
- [189] N. C. Bruno, N. Niljianskul, S. L. Buchwald, *The Journal of Organic Chemistry* **2014**, *79*, 4161.
- [190] Ā. Molnar, *Chemical Reviews* **2011**, *111*, 2251.
- [191] Y.-C. Yang, T.-Y. Luh, *The Journal of Organic Chemistry* **2003**, *68*, 9870.

- [192] W. Kleist, J.-K. Lee, K. Köhler, *European Journal of Inorganic Chemistry* **2009**, 2009, 261.
- [193] Y. Monguchi, Y. Fujita, K. Endo, S. Takao, M. Yoshimura, Y. Takagi, T. Maegawa, H. Sajiki, *Chemistry – A European Journal* **2009**, 15, 834.
- [194] Yin, J. r. Liebscher, *Chemical Reviews* **2006**, 107, 133.
- [195] Y. Hirai, Y. Uozumi, *Chemical Communications* **2010**, 46, 1103.
- [196] M. Guino, K. K. Hii, *Chemical Society Reviews* **2007**, 36, 608.
- [197] C. A. Parrish, S. L. Buchwald, *The Journal of Organic Chemistry* **2001**, 66, 3820.
- [198] M.-J. Jin, D.-H. Lee, *Angewandte Chemie* **2009**, 122, 1137.
- [199] A. R. Siamaki, A. E. R. S. Khder, V. Abdelsayed, M. S. El-Shall, B. F. Gupton, *Journal of Catalysis* **2011**, 279, 1.
- [200] D. Astruc, *Inorganic Chemistry* **2007**, 46, 1884.
- [201] M. Weck, C. W. Jones, *Inorganic Chemistry* **2007**, 46, 1865.
- [202] C. K. Y. Lee, A. B. Holmes, S. V. Ley, I. F. McConvey, B. Al-Duri, G. A. Leeke, R. C. D. Santos, J. P. K. Seville, *Chemical Communications* **2005**, 2175.
- [203] I. R. Baxendale, C. M. Griffiths-Jones, S. V. Ley, G. K. Tranmer, *Chemistry – A European Journal* **2006**, 12, 4407.
- [204] A. Alimardanov, L. Schmieder-van de Vondervoort, A. H. M. de Vries, J. G. de Vries, *Advanced Synthesis & Catalysis* **2004**, 346, 1812.
- [205] N. E. Leadbeater, *Chemical Communications* **2005**, 2881.
- [206] S. Sa, M. B. Gawande, A. Velhinho, J. P. Veiga, N. Bundaleski, J. Trigueiro, A. Tolstogousov, O. M. N. D. Teodoro, R. Zboril, R. S. Varma, P. S. Branco, *Green Chemistry* **2014**, 16, 3494.
- [207] K. F. Bolton, A. J. Canty, J. A. Deverell, R. M. Guijt, E. F. Hilder, T. Rodemann, J. A. Smith, *Tetrahedron Letters* **2006**, 47, 9321.
- [208] D. Nair, J. T. Scarpello, L. S. White, L. M. Freitas dos Santos, I. F. J. Vankelecom, A. G. Livingston, *Tetrahedron Letters* **2001**, 42, 8219.
- [209] D. Nair, J. T. Scarpello, I. F. J. Vankelecom, L. M. Freitas Dos Santos, L. S. White, R. J. Kloetzing, T. Welton, A. G. Livingston, *Green Chemistry* **2002**, 4, 319.
- [210] A. Tsoukala, L. Peeva, A. G. Livingston, H.-R. Bjørsvik, *ChemSusChem* **2011**, 5, 188.
- [211] H.-t. Wong, C. J. Pink, F. C. Ferreira, A. G. Livingston, *Green Chemistry* **2006**, 8, 373.
- [212] P. Li, J. S. Moore, K. F. Jensen, *ChemCatChem* **2013**, 5, 1729.
- [213] D. Schoeps, V. Sashuk, K. Ebert, H. Plenio, *Organometallics* **2009**, 28, 3922.
- [214] A. Dumrath, X.-F. Wu, H. Neumann, A. Spannenberg, R. Jackstell, M. Beller, *Angewandte Chemie International Edition* **2010**, 49, 8988.
- [215] L. Peeva, J. Arbour, A. Livingston, *Organic Process Research & Development* **2013**, 17, 967.
- [216] C. J. Pink, H.-t. Wong, F. C. Ferreira, A. G. Livingston, *Organic Process Research & Development* **2008**, 12, 589.
- [217] S. V. Ley, R. J. Ingham, M. O'Brien, D. L. Browne, *Beilstein Journal of Organic Chemistry* **2013**, 1051.
- [218] P. Taeshin, I. B. Paul, *Vol. 6, ACM*, **1996**, pp. 137.
- [219] I. Smallwood, *Solvent Recovery Handbook*, Blackwell Science Ltd, **2002**.

8.1 Appendix A

The UCST and LCST values are functions of composition. The exact composition corresponding to a given entry can be found in the corresponding references.

Solvent #1	Solvent #2	UCST (°C)	LCST (°C)	Reference
Water	Butyl Cellosolve	128	55	Solvent Recovery
Water	THF	138	71	Solvent Recovery Handbook
Water	MEK	139	-6	Solvent Recovery Handbook
Water	2-butoxy ethanol	128	48	Solvent Recovery Handbook
Water	Isobutanol	-	37	Solvent Recovery Handbook
Water	N-butanol	-	33	Solvent Recovery Handbook
Water	Phenol	-	34	Solvent Recovery Handbook
Water	Nitrobenzene	-	32	Solvent Recovery Handbook
Water	Furfural	-	51	Solvent Recovery
Pentane	Methanol	14.8	-	Solvent Recovery Handbook
Hexane	Methanol	35	-	Solvent Recovery Handbook
Heptane	Methanol	51	-	Solvent Recovery Handbook
Decane	Ethanol	-15	-	Solvent Recovery Handbook
Decane	Acetone	-6	-	Solvent Recovery Handbook
Hexane	DMF	68	-	Solvent Recovery Handbook
Decane	Acetic Acid	41	-	Solvent Recovery Handbook
Pentane	Nitrobenzene	25	-	Solvent Recovery Handbook
Hexane	Pyridine	-25	-	Solvent Recovery Handbook
Hexane	Acetonitrile	77	-	Solvent Recovery Handbook
Hexane	Furfural	92	-	Solvent Recovery Handbook
Hexane	Phenol	51	-	Solvent Recovery Handbook
Octadecane	Acetone	37	-	Critical Solution Temperatures ^[98]
Diisobutene	Acetonyl Acetone	31	-	Critical Solution Temperatures
Methylcyclohexane	Acetonyl Acetone	39	-	Critical Solution Temperatures
Dodecane	Ethanol	12	-	Critical Solution Temperatures
Benzene	Acetamide	143	-	Critical Solution Temperatures
Benzene	Diethylene Glycol	88.5	-	Critical Solution Temperatures
Toluene	Diethylene Glycol	134	-	Critical Solution Temperatures
2-Methylpentane	Diethyl Ketone	27.4		Critical Solution Temperatures
Paraffinic Oil	1,4 Dioxane	45		Critical Solution Temperatures

Ethylene glycol	Ethyl Acetate	56.5		Critical Solution Temperatures
Heptane	Acrylonitrile	28	-	Critical Solution Temperatures
Decane	DMPU	85	-	Behr et al. ^[20]
Heptane	N,N-DMA	-	-	Behr et al.
Decane	NMP	69	-	Behr et al.
Heptane	N-methyl formamide	90	-	Tijani et al. ^[22]
Heptane	PC	90	-	Tijani et al.
Heptane	Formamide	90	-	Tijani et al.
Heptane	Nitromethane	90	-	Tijani et al.
Heptane	DMSO	90		Tijani et al.

8.2 Appendix B

During the execution of these experiments, the prepared catalysts were sometimes left under a Schlenk line for periods of time on the order of a day and still used afterwards. To make sure that the catalyst did not oxidize considerably under these conditions, air-free phosphorus NMR was performed (see Experimental in Chapter 2). The table below compares the ratio of unoxidized catalyst to oxidized catalyst and finds that the number does not change significantly over a few days.

NMR results for catalyst degradation as a function of time. No measurable oxidation is found over 42 hours.

Time (h)	3 Catalyst	Oxidized TPPTS and 1 catalyst	Ratio
	peak areas	peak areas (overlapping)	
0	2.9	5.2	0.57
2	3.0	5.2	0.58
3	2.9	4.9	0.59
20	3.0	5.4	0.57
42	3.0	5.5	0.54

8.3 Appendix C

Hansen Solubility Program:

HansenProgram.m

```
function [storenames] = HansenProgram(catdel, pdel)
%Author: Everett J. O'Neal, Sep 1, 2011
%Copyright 2011 Massachusetts Institute of Technology. All rights reserved

%catdel and pdel are vectors of hansen solubilty parameters for the 2 solvents
%this program calculates "good" mediator solvents based upon certain rough
%criteria.
%catdel is the solvent that prefers the catalyst
%pdel is the solvent that prefers the product
%catdel is the nonpolar phase, pdel is the polar phase.
%Hansen solubility program. Needs to read in a file.

fid = fopen('Hansendata.txt');
%Must add this symbol' at the end of the file and it cant be anywhere else
M = textread('Hansendata.txt', '%[^\n]', 'bufsize', 40000); %Puts a line in each row
ff = fclose(fid);

for ii = 1:length(M)
    [dels names] = finddel(M,ii);
    %sort dels
    ii
    Del(ii,1:4) = dels;
    %sort names
    Name(89) = names;
end

%now that we have extracted that data, we must solvent-search with the
%following set of heuristics:
%1.) overall del parameter of solvent must be within 4 of catalystsolvent
LB = 0; %lower bound
UB = 10; %upper bound
LBCM = 0; %lower bound on C-M del differences
UBCM = 1;
LBPM = 0; %lower bound on product solvent-mediator differences
UBPM = 1;
LBCP = 0;
UBCP = 100;
SUMMEDLOW = 0
SUMMEDHIGH = 37.3;

%2.) del parameters should be between pdel and catdel.
Ocat = sqrt(catdel(1)^2 + catdel(2)^2 + catdel(3)^2);
Op = sqrt(pdel(1)^2 + pdel(2)^2 + pdel(3)^2);
count = 0;
storenames = {0};
for jj = 1:length(M)
    trig = 0;
    %trig =
testdel(Del,jj,catdel,pdel,Ocat,Op,LB,UB,LBCM,UBCM,LBPM,UBPM,LBCP,UBCP,SUMMEDLOW,SUMMEDHIGH);
%used for real
    %program, find mediator.
    trig = testtarget(Del,jj,catdel, pdel,Ocat,Op, LB, UB); %used to find solvents with
*similar* del parameters
    %to an inputted catdel.
    if trig == 1;
```

```

        count = count + 1;
        Name{jj}
        storenames{count} = Name{jj};
        storedel(count) = sqrt(Del(jj,1)^2 + Del(jj,2)^2 + Del(jj,3)^2);
    end
end

return

function [dels names] = finddel(M,linenum)
%Dels contain: [dispersion, polar, H-bond, MolarVolume(?)] hansen parameters
b = M(linenum);
count = 0;
    trigchar = 0; %Trigger after we meet the first character. we know afterwards that
numbers will be dels
    delcount = 0; % count dels we see
    charcount = 0; %count chars.
    while isempty(cell2mat(b)) == 0;
        count = count + 1; %count # first lines taken.
        [a b] = strtok(b);
        if isempty((str2num(char(a)))) == 1
            %We now know its a string
            trigchar = 1;
            charcount = charcount + 1;
            names(charcount) = a;
        else
            %we now know its a number
            if trigchar == 1
                delcount = delcount + 1;
                dels(delcount) = str2num(char(a));
            end
        end
    end
end
    % if isempty(cell2mat(shouldbel)) == 0 && isempty(cell2mat(shouldbe8)) == 0

return

function trigger = testdel(Del,jj,catdel,pdel,Ocat,
Op, LB, UB, LBCM, UBCM, LBPM, UBPM, LBCP, UBCP, SUMMEDLOW, SUMMEDHIGH)
%UB and LB are upper and lower bounds on mediator del similarity to
%catalyst del
    trigger = 0;
    currdel = sqrt(Del(jj,1)^2 + Del(jj,2)^2 + Del(jj,3)^2);
    CMdiff = sqrt(4*(Del(jj,1)-catdel(1))^2 + (Del(jj,2)-catdel(2))^2 + (Del(jj,3)-
catdel(3))^2);
    PMdiff = sqrt(4*(Del(jj,1)-pdel(1))^2 + (Del(jj,2)-pdel(2))^2 + (Del(jj,3)-pdel(3))^2);
    CPdiff = sqrt(4*(catdel(1)-pdel(1))^2 + (catdel(2)-pdel(2))^2 + (catdel(3)-pdel(3))^2);
    SUMMED = PMdiff + CMdiff;
    %if currdel < max(Ocat,Op) & currdel > min(Ocat,Op)
    if CMdiff < UBCM & CMdiff > LBCM
        if PMdiff < UBPM & PMdiff > LBPM
            if SUMMED < SUMMEDHIGH & SUMMED > SUMMEDLOW
                if CPdiff < UBCP & CPdiff > LBCP
                    trigger = 1; %found a suitable solvent;
                end
            end
        end
    end
end
%end
return

function trigger = testtarget(Del,jj,catdel,pdel,Ocat,Op ,LB,UB)

```

```
%UB and LB are upper and lower bounds on mediator del similarity to
%catalyst del
trigger = 0;
currdel = sqrt(Del(jj,1)^2 + Del(jj,2)^2 + Del(jj,3)^2);
currdeldiff = sqrt(4*(Del(jj,1)-catdel(1))^2 + (Del(jj,2)-catdel(2))^2 + (Del(jj,3)-
catdel(3))^2);
if currdeldiff < UB & currdeldiff > LB
    trigger = 1; %found a suitable solvent;
end

return
```

8.4 Appendix D

Dimensions of the retentate half of the membrane chuck, with values given in inches. The ϕ symbol denotes diameter.

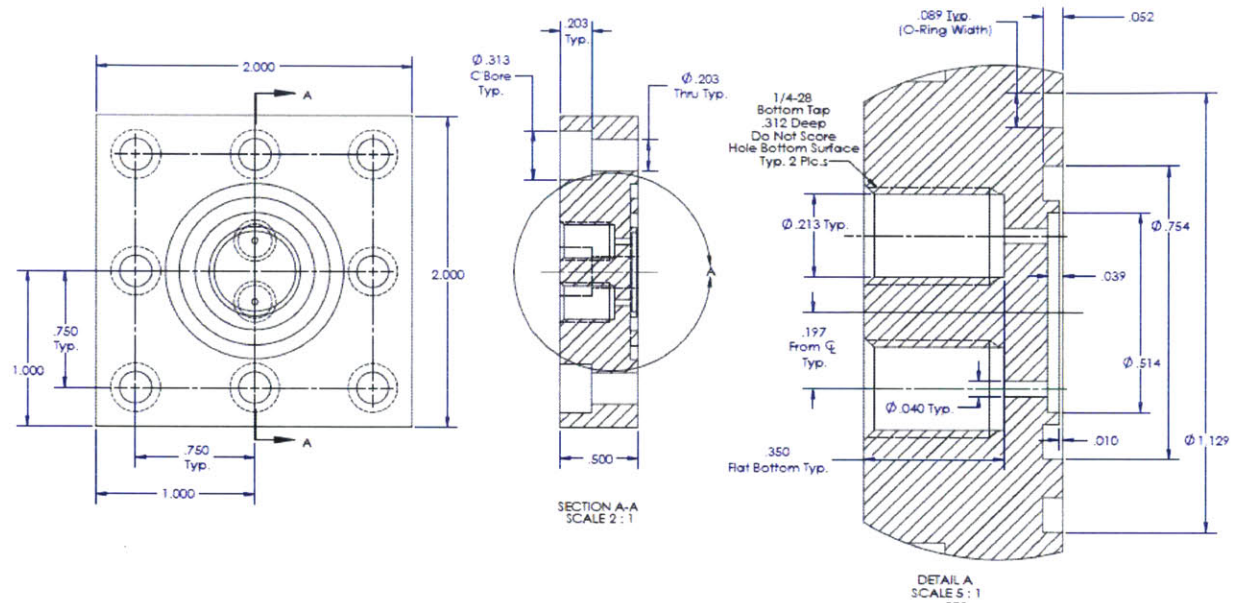


Figure 87. Engineering drawing of our microfluidic nanofiltration module.

8.5 Appendix EE

This appendix includes the Jacobian® code used to simulate our hydrogenation system.

HydrogPredictCofeedfrom5eo198.JAC

#Author: Everett J. O'Neal, Aug 10, 2013

#Copyright 2013 Massachusetts Institute of Technology. All rights reserved

```
DECLARE
  TYPE
    # identifier = default_value : lower_bound : upper_bound  UNIT = "string"
    C = .05 : 0 : 5 UNIT = "mmol/ml"
    F = 1 : 0 : 20000 unit = "ml/min"
    V = 1 : 0 : 1 #valve position
    R = .5 : 0 : 1 #rejection
    N = 1 : 0 : 1e10 #various numbers
  STREAM
    # identifier IS variable_type_list
    Streamvars is C, F
  ENUMERATION
    # identifier IS { identifier_list }
END # declares

MODEL CSTR # identifier
  PARAMETER
    # identifier AS parameter_type
    # identifier AS ARRAY(size_list) OF parameter_type
    kr as REAL
    kd as real
    V as REAL #volume of tank, units ml
  UNIT
    # identifier AS model_name
    # identifier AS ARRAY(size_list) OF model_name
  VARIABLE
    # identifier AS variable_type
    # identifier AS ARRAY(size_list) OF variable_type
    Cin, Cout as array(3) of C
    Fin as F
    Fout as F

  STREAM
    # identifier AS stream_type
    # identifier AS ARRAY(size_list) OF stream_type
    Inlet : Cin, Fin as Streamvars
    Outlet: Cout, Fout as Streamvars
  SELECTOR
    # identifier AS enumeration_type
    # identifier AS ARRAY(size_list) OF enumeration_type
    # identifier AS (identifier_list) DEFAULT default_value
  SET
    # parameter_name := parameter_expression ;
    #kr := 50; #Forward rate constant
    #kd := .19; #Catalyst Deactivation constant
    #V := 1;
  INTERMEDIATE
    # DIMENSION array_intermediate(size_list)
    # intermediate_name := expression ;
  EQUATION
    # equality_constraint
    Fin = Fout; # no accumulation in tanks
    #Fout = 1;
```

```

#Cin(1:3) = 1;

#We cant use zero-order kinetics if we run out of C(1) or it goes negative.
V*$Cout(1) = Fin*Cin(1) - Fout*Cout(1)-V*kr*Cout(3)*(1-exp(-100*Cout(1)));# - kr Cout(3);
V*$Cout(2) = Fin*Cin(2) - Fout*Cout(2)+V*kr*Cout(3)*(1-exp(-100*Cout(1)));# +kr*Cout(3);
V*$Cout(3) = Fin*Cin(3) - Fout*Cout(3)-V*kd*(1-exp(-100*Cout(3)));# -kd*Cout(3);

END # model

MODEL PBR
PARAMETER
# identifier AS parameter_type
# identifier AS ARR.Y(size_list) OF parameter_type
N as INTEGER
UNIT
# identifier AS model_name
# identifier AS ARR.Y(size_list) OF model_name
U as array(N) of CSTR
VARIABLE
# identifier AS variable_type
# identifier AS ARR.Y(size_list) OF variable_type
STREAM
# identifier AS stream_type
# identifier AS ARR.Y(size_list) OF stream_type
SELECTOR
# identifier AS enumeration_type
# identifier AS ARR.Y(size_list) OF enumeration_type
# identifier AS (identifier_list) DEFAULT default_value
SET

N := 126;
# parameter_name := parameter_expression ;
INTERMEDIATE
# DIMENSION array_i:intermediate(size_list)
# intermediate_name := expression ;
EQUATION
U(1:N-1).Outlet is U(2:N).Inlet;

# equality_constraint
END # model

MODEL ModelHoldTank# identifier
PARAMETER
# identifier AS parameter_type
# identifier AS ARR.Y(size_list) OF parameter_type
V as REAL #volume of tank, units ml
kr as real
kd as real

UNIT
# identifier AS model_name
# identifier AS ARR.Y(size_list) OF model_name
VARIABLE
# identifier AS variable_type
# identifier AS ARR.Y(size_list) OF variable_type
Cin, Cout as array(3) of C
Fin as F
Fout as F

STREAM
# identifier AS stream_type
# identifier AS ARR.Y(size_list) OF stream_type

```

```

Inlet : Cin, Fin as Streamvars
Outlet: Cout, Fout as Streamvars

SELECTOR
# identifier AS enumeration_type
# identifier AS ARRAY(size_list) OF enumeration_type
# identifier AS (identifier_list) DEFAULT default_value
SET
# parameter_name := parameter_expression ;
#kd := 2000;
INTERMEDIATE
# DIMENSION array_intermediate(size_list)
# intermediate_name := expression ;
EQUATION
Fin = Fout; # no accumulation in tanks
V*$Cout(1) = Fin*Cin(1) - Fout*Cout(1) -V*kr*Cout(3)*(1-exp(-100*Cout(1)));
V*$Cout(2) = Fin*Cin(2) - Fout*Cout(2) +V*kr*Cout(3)*(1-exp(-100*Cout(1)));
V*$Cout(3) = Fin*Cin(3) - Fout*Cout(3) -V*kd*(1-exp(-100*Cout(3)));

# equality_constraint
END # model

MODEL HPLC# identifier
PARAMETER
# identifier AS parameter_type
# identifier AS ARRAY(size_list) OF parameter_type
Nh as INTEGER

UNIT
# identifier AS model_name
# identifier AS ARRAY(size_list) OF model_name
UHPLC as array(Nh) of ModelHoldTank
VARIABLE
# identifier AS variable_type
# identifier AS ARRAY(size_list) OF variable_type
STREAM
# identifier AS stream_type
# identifier AS ARRAY(size_list) OF stream_type
SELECTOR
# identifier AS enumeration_type
# identifier AS ARRAY(size_list) OF enumeration_type
# identifier AS (identifier_list) DEFAULT default_value
SET
# parameter_name := parameter_expression ;
Nh := 2;
INTERMEDIATE
# DIMENSION array_intermediate(size_list)
# intermediate_name := expression ;
EQUATION
# equality_constraint
UHPLC(1:Nh-1).Outlet is UHPLC(2:Nh).Inlet;
END # model

MODEL Membrane# identifier
PARAMETER
# identifier AS parameter_type
# identifier AS ARRAY(size_list) OF parameter_type
kd as real
kr as real
V as Real
UNIT
# identifier AS model_name

```



```

# identifier AS ARRAY(size_list) OF model_name
VARIABLE
# identifier AS variable_type
# identifier AS ARRAY(size_list) OF variable_type
Cin, Cr, Cp as array(3) of C
Fin, Fr, Fp as F
Rej as array(3) of R

STREAM
# identifier AS stream_type
# identifier AS ARRAY(size_list) OF stream_type
Inlet : Cin, Fin as Streamvars
Ret: Cr, Fr as Streamvars
Perm: Cp, Fp as Streamvars
SELECTOR
# identifier AS enumeration_type
# identifier AS ARRAY(size_list) OF enumeration_type
# identifier AS (identifier_list) DEFAULT default_value
SET
# parameter_name := parameter_expression ;
#Rej(1) := .7;
#Rej(2) := .8;
INTERMEDIATE
# DIMENSION array_intermediate(size_list)
# intermediate_name := expression ;
EQUATION
Fin = Fr + Fp; # no accumulation in mem (flow)

#If zero concentration over membrane, Just treat Cp = Cr = 0;
For i :=1 to 2 do
if (Cr(i) < 1e-6) THEN ##RUN FAILS IF 0 is used!!
    Cp(i) = Cr(i); #Treat as splitter
    ELSE
        Rej(i) = 1 - Cp(i)/Cr(i);
    End
end
if (Cr(3) < 1e-9) THEN ##RUN FAILS IF 0 is used!!
    Cp(3) = Cr(3); #Treat as splitter
    ELSE
        Rej(3) = 1 - Cp(3)/Cr(3);
    End
V*$Cr(1) = Fin*Cin(1) - Fr*Cr(1) - Fp*Cp(1) -V*kr*Cr(3)*(1-exp(-100*Cr(1)));
V*$Cr(2) = Fin*Cin(2) - Fr*Cr(2) - Fp*Cp(2) +V*kr*Cr(3)*(1-exp(-100*Cr(1)));
V*$Cr(3) = Fin*Cin(3) - Fr*Cr(3) - Fp*Cp(3) -V*kd*(1-exp(-100*Cr(3)));

# equality_constraint
END # model

MODEL MemSeries# identifier
PARAMETER
# identifier AS parameter_type
# identifier AS ARRAY(size_list) OF parameter_type
Nm as real

UNIT
# identifier AS model_name
# identifier AS ARRAY(size_list) OF model_name
Umem as array(Nm) of Membrane
VARIABLE
# identifier AS variable_type
# identifier AS ARRAY(size_list) OF variable_type
#Cmix as array(3) of C
#Fmix as F

```

```

STREAM
# identifier AS stream_type
# identifier AS ARRAY(size_list) OF stream_type
#Mixed : Cin, Fin as Streamvars

SELECTOR
# identifier AS enumeration_type
# identifier AS ARRAY(size_list) OF enumeration_type
# identifier AS (identifier_list) DEFAULT default_value
SET
# parameter_name := parameter_expression ;
Nm := 2;

INTERMEDIATE
# DIMENSION array_intermediate(size_list)
# intermediate_name := expression ;
EQUATION
# equality_constraint
#Umem(1:Nm).Ep = .05/Nm; Can't do this. Need it to balance inlet flow rate.
Umem(1:Nm-1).Ret is Umem(2:Nm).Inlet;

#for n :=1 to Nm do
# Cmix(1:3) = Cmix(1:3) + Umem(1:Nm).C(1
#Fmix =
END # model

MODEL Tmix #inlet Tmix to system
PARAMETER
# identifier AS parameter_type
# identifier AS ARRAY(size_list) OF parameter_type
UNIT
# identifier AS model_name
# identifier AS ARRAY(size_list) OF model_name
VARIABLE
# identifier AS variable_type
# identifier AS ARRAY(size_list) OF variable_type
Ci1, Ci2, Cout as array(3) of C
Fi1, Fi2, Fout as F
STREAM
# identifier AS stream_type
# identifier AS ARRAY(size_list) OF stream_type
Inlet1 : Ci1, Fi1 as Streamvars
Inlet2: Ci2, Fi2 as Streamvars
Outlet: Cout, Fout as Streamvars
SELECTOR
# identifier AS enumeration_type
# identifier AS ARRAY(size_list) OF enumeration_type
# identifier AS (identifier_list) DEFAULT default_value
SET
# parameter_name := parameter_expression ;
INTERMEDIATE
# DIMENSION array_intermediate(size_list)
# intermediate_name := expression ;
EQUATION
# equality_constraint
#Fi1 + Fi2 = Fout; I REMOVED MASS BALANCE HERE DUE TO CLOSED RECYCLE LOOP
# BECOMES REDUNDANT WITH ALL OTHER MASS BALANCES + OVERALL MB
Fi1*Ci1(1:3) + Fi2*Ci2(1:3) = Fout*Cout(1:3);
END # model

MODEL Splitter# identifier
PARAMETER
# identifier AS parameter_type

```

```

# identifier AS ARRAY(size_list) OF parameter_type
Fp as real
UNIT
# identifier AS model_name
# identifier AS ARRAY(size_list) OF model_name
VARIABLE
# identifier AS variable_type
# identifier AS ARRAY(size_list) OF variable_type
Ci, Cp, Cout as array(3) of C
Fi, Fout as F
STREAM
# identifier AS stream_type
# identifier AS ARRAY(size_list) OF stream_type
Inlet : Ci, Fi as Streamvars
Purge: Cp, Fp as Streamvars
Outlet: Cout, Fout as Streamvars
SELECTOR
# identifier AS enumeration_type
# identifier AS ARRAY(size_list) OF enumeration_type
# identifier AS (identifier_list) DEFAULT default_value
SET
# parameter_name := parameter_expression ;
INTERMEDIATE
# DIMENSION array_intermediate(size_list)
# intermediate_name := expression ;
EQUATION
# equality_constraint
Fout = Fi - Fp;
Cp = Ci;
Cout = Ci;
END # model

```

```

SIMULATION Process# identifier
OPTIONS
# option_name := option_value
CSVOUTPUT := TRUE; # output reported time trajectories to [filename].csv, where
[filename] is the name of the current *.JAC file.

```

```

PARAMETER
# identifier AS parameter_type
# identifier AS ARRAY(size_list) OF parameter_type
Ntanks as real
#Nhplc as real
#Nmem as real
tr as real #run time
tr2 as real #run time #2
ts as real #start-up time
catloaded as real #frac of cat not lost to oxygen 0-1
kdd as real #deactivation time constant
krr as real #known from kinetic experiments

```

```

UNIT
# identifier AS model_name
# identifier AS ARRAY(size_list) OF model_name
CSTRrun as PBR
#HoldTankrun as ModelHoldTank
#HPLCrun as HPLC
Memrun as Membrane
Mixlrun as Tmix
SampRO as Splitter
SampRet as Splitter
#SampPerm as Splitter

```

```

VARIABLE
# identifier AS variable_type
# identifier AS ARRAY(size_list) OF variable_type
Recycle as V
FracprodRO as V #0-1
TONperpass as N

REPORT
# variable_list
# CSTRrun.U(3).Cout(1:3)

Memrun.Cr(1:2)
CSTRrun.U(Ntanks).Cout(1:3)
#Memrun.Cp(1:2)

#
# HldTankrun.Cout(1:3)
# HPLCrun.UHPLC(Nhplc).Cout(1:3)
# Memrun.Umem(Nmem).Cr(1:3)
#Memrun.Fp
#Memrun.Fr
#Memrun.Fin
#Memrun.Cr(3)
#Memrun.Cin(3)
#CSTRrun.U(Ntanks).Cout(3)
#Memrun.Cp(3)
#Mixlrun.Fout
#Mixlrun.Fil
#Mixlrun.Fi2
# Memrun.Umem(1).Fp
# Memrun.Umem(1).Fr
# Memrun.Umem(1).Fin
# HPLCrun.UHPLC(Nhplc).Fout
# HldTankrun.Fout
#Mixlrun.Ci2(3)
#Mixlrun.Cil(3)
#Mixlrun.Cout(1:3)

#For script
#HPLCrun.UHPLC(2).Cout(2)
#Memrun.Umem(1:Nmem).Fp
#Memrun.Umem(1:Nmem).Cp(1:3)
#Mixlrun.Cil(1:3)

#Fracprodro
# TONperpass
# SampRO.Fout
# SampRet.Fout
# SampRet.Ci(1)

SENSITIVITY
# parameter_name := parameter_expression ;

ASK
catloaded "0";
kdd "1";

SET
# parameter_name := parameter_expression ;
Ntanks := CSTRrun.N;
#Nhplc := HPLCrun.Nh;
#Nmem := Memrun.Nm ;
CSTRrun.U.V := 8/Ntanks; #Vol of individual tanks ml
#HldTankrun.V := .8; #holding tank active vol ml
#HPLCrun.UHPLC.V := .55/Nhplc; #HPLC volume ml

```

```

Memrun.V := 30;
krr := 334;

#deact

#Deactivation sets
#HoldTankrun.kd := kdd;
CSTRrun.U.kd := kdd;
Memrun.kd := kdd;
#HPLCrun.UHPLC.kd := kdd;

#rate const
#HoldTankrun.kr := krr;
CSTRrun.U.kr := krr;
#HPLCrun.UHPLC.kr := krr;
Memrun.kr := krr;

ts := 90; # Time to start-up system. Subtracted from TIME to compute trends
tr := 5*60;
tr2 := 600;
#AUTOSAMPLER PARAMETERS
SampRO.Fp := .05/60; #ml/min purge
SampRet.Fp := .1/60; #ml/min purge

INTERMEDIATE
# DIMENSION array_intermediate(size_list)
# intermediate_name := expression ;
EQUATION
# equality_constraint
SampRO.Inlet = CSTRrun.U(Ntanks).Outlet;
#HoldTankrun.Inlet = SampRO.Outlet;
#HPLCrun.UHPLC(1).Inlet = HoldTankrun.Outlet;
#Memrun.Umem(1).Inlet = HPLCrun.UHPLC(Nhplc).Outlet;
Memrun.Inlet = SampRO.Outlet;

if (Recycle = 1) then

    Mixlrun.Fi2 = 1.05; #ml/min

    #Also sample retentate.
    SampRet.Inlet = Memrun.Ret;
    #Now pass on to Mixer
    Mixlrun.Inlet2 = SampRet.Outlet;

    ##Fit in excel: Mixlrun.Fil = (8.5 + 32*EXP(-.3*(TIME/60-ts/60)))/1000; #quite
uncertain here !
    #Mixlrun.Fil = 1.90E-12*TIME^4 - 5.77E-09*TIME^3 + 6.11E-06*TIME^2 - 2.485-03*TIME
+ 5.61E-01; #quite uncertain here !
    Mixlrun.Fil = .296;
    Memrun.Rej(1) = .6;
    Memrun.Rej(2) = .4;
    Memrun.Rej(3) = .993;

else

    #below line just bookkeeping. initialization fails if some variable sets are
ignored obviously
    SampRet.Inlet = Memrun.Ret;
    #Should have:
    #let them both be equal for now. SampretOutlet exits system.
    Mixlrun.Fi2 = 1.05;

    Mixlrun.Ci2(1:3) = Mixlrun.Ci1(1:3); #makes reinitialization easier for equal
flows everywhere

```

```

model
    #We want to fill the catalyst quickly because otherwise deactivation occurs in our
    #if (TIME < .5*ts) then
    #Mixlrun.Fout = 1700 ;#ml/min
    #ELSE
    #Mixlrun.Fout = 1.05 ; #ml/min to get catalyst conc. right in retentate
    #end

    #Force blind flow-balance with open loop
    Mixlrun.Fi2 = Mixlrun.Fout-Mixlrun.Fil;

    Mixlrun.Fil = .296;
    Memrun.Rej(1) = .6;
    Memrun.Rej(2) = .4;
    Memrun.Rej(3) = .993;
end

    CSTRrun.U(1).Inlet = Mixlrun.Outlet;

    #Force Fin = Fout overall for process
    Memrun.Fp = Mixlrun.Fil;

    if (CSTRrun.U(Ntanks).Cout(2)+CSTRrun.U(Ntanks).Cout(1) < 1e-6) then
        FracProdRO = 0;
    else
        FracProdRO =
    CSTRrun.U(Ntanks).Cout(2)/(CSTRrun.U(Ntanks).Cout(2)+CSTRrun.U(Ntanks).Cout(1));
    end

    #if (TIME < 100) then
        TONperpass = 0;
    # else
        #tONperpass = 0;
    #
        TONperpass = (CSTRrun.U(1).Cin(1))/(CSTRrun.U(1).Cin(3) );
    #
    END

    INPUT
    # variable_name := time_expression ;
    Mixlrun.Cil(1:2) := 0; #Eqn for feed mmol/ml
    Mixlrun.Cil(3) := .00024*catloaded; #Eqn for feed mmol/ml cat loaded is frac not lost to
oxygen

    #Eqn for feed ml/min
    #Set loop flow rate (independent of inlet flow rate) we remove one mass
    #balance from loop in order to spec this.

    Recycle := 0;
    PRESET
    # variable_name := default_value : lower_bound : upper_bound ;
    SELECTOR
    # selector_name := selector_value ;
    INITIAL
    # equality_constraint ;

    CSTRrun.U(1:Ntanks).Cout(1:3) = 0;
    #PLCrn.UHPLC(1:Nhplc).Cout(1:3) = 0;
    #FoldTankrun.Cout(1:3) = 0;
    Memrun.Cr(1:3) = 0;
    SCHEDULE
    # schedule_task
    sequence
    Continue for ts

```

```

RESET
    Mixlrun.Ci1(1) := 7.52*.042/(.042+ Mixlrun.Fi1);
    Mixlrun.Ci1(2) := 0; #Eqn for feed mmol/ml
    Mixlrun.Ci1(3) := 0; #Eqn for feed mmol/ml
    Recycle :=1;
end
continue for tr

    RESET
    Mixlrun.Ci1(1) := 7.52*.021/(.021+Mixlrun.Fi1);
    Mixlrun.Ci1(2) := 0; #Eqn for feed mmol/ml
    Mixlrun.Ci1(3) := 0; #Eqn for feed mmol/ml
    Recycle :=1;
end
continue for tr2
end
END # simulation

```

```

ESTIMATION RateandDeact# identifier
OPTIONS
    # option_name := option_value
    #Dynamic_Scaling := TRUE;
    #estimation_tolerance := 1e-16;
    #Estimation_Print_level :=2;
    CSVOUTPUT := TRUE; # output reported time trajectories to [filename].csv, where
    [filename] is the name of the current *.JAC file.

```

```

PARAMETER
    # identifier AS parameter_type
    # identifier AS ARRAY(size_list) OF parameter_type
    Ntanks as real
    Nhplc as real
    Nmem as real
    tr as real #run time
    ts as real #start-up time
    kdest as real #deactivation time constant
    krest as real #rate constant
    dummyparam as real

```

```

UNIT
    # identifier AS model_name
    # identifier AS ARRAY(size_list) OF model_name
    CSTRrun as PBR
    #HoldTankrun as ModelHoldTank
    #HPLCrun as HPLC
    Memrun as Membrane
    Mixlrun as Tmix
    SampRO as Splitter
    SampRet as Splitter
    #SampPerm as Splitter

```

```

VARIABLE
    # identifier AS variable_type
    # identifier AS ARRAY(size_list) OF variable_type
    Recycle as V
    FracprodRO as V #0-1
    TONperpass as N

```

```

UNCERTAIN
    # parameter_name := default_value : lower_bound : upper_bound ;
    #kdest := 500 : 1e-1 : 1e5;
    #krest := 1000 : 1e-5 : 1e5;
    dummyparam := 1 : 1e-5: 1e5;

```

```

ASK
kdest "0";
krest "0";

SET
# parameter_name := parameter_expression ;
Ntanks := CSTRrun.N;
#Nhplc := HPLCrun.Nh;
#Nmem := Memrun.Nm ;
CSTRrun.U.V := 8/Ntanks; #Vol of individual tanks ml
#HoldTankrun.V := .8; #holding tank active vol ml
#HPLCrun.UHPLC.V := .55/Nhplc; #HPLC volume ml
Memrun.V := 30;

#deact

#Leactivation sets
#HoldTankrun.kd := kdd;
CSTRrun.U.kd := kdest;
Memrun.kd := kdest;
#HPLCrun.UHPLC.kd := kdd;

#rate const
#HoldTankrun.kr := krr;
CSTRrun.U.kr := krest;
#HPLCrun.UHPLC.kr := krr;
Memrun.kr := krest;

ts := 10; # Time to start-up system. Subtracted from TIME to compute trends
tr := 1500;
#AUTOSAMPLER PARAMETERS
SampRO.Fp := .05/60; #ul/min purge
SampRet.Fp := .1/60; #ul/min purge

INTERMEDIATE
# DIMENSION array_intermediate(size_list)
# intermediate_name := expression ;

EQUATION
# equality_constaint
SampRO.Inlet = CSTRrun.U(Ntanks).Outlet;
#HoldTankrun.Inlet = SampRO.Outlet;
#HPLCrun.UHPLC(1).Inlet = HoldTankrun.Outlet;
#Memrun.Umem(1).Inlet = HPLCrun.UHPLC(Nhplc).Outlet;
Memrun.Inlet = SampRO.Outlet;

if (Recycle = 1) then

    Mixlrun.Fout = 1.050 ;#ml/min

    #Also sample retentate.
    SampRet.Inlet = Memrun.Ret;
    #Now pass on to Mixer
    Mixlrun.Inlet2 = SampRet.Outlet;

    ##Fit in excel: Mixlrun.Fil = (8.5 + 32*EXP(-.3*(TIME/6)-ts/60))/1000;    #quite
uncertain here !
    Mixlrun.Fil = 1.90E-12*TIME^4 - 5.77E-09*TIME^3 + 6.11E-06*TIME^2 - 2.48E-03*TIME
+ 5.61E-01;
    #quite uncertain here !
    #Memrun.Umem(1:Nmem).Rej(1) = (.92-(.92-.52)*EXP(-.5*(TIME/60-ts/60)));
    #Memrun.Umem(1:Nmem).Rej(2) = (.826-(.825-.33)*EXP(-.5*(TIME/60-ts/60)));
    Memrun.Rej(1) = (.4-(.4-.2)*EXP(-(TIME/60-ts/60)));
    Memrun.Rej(2) = (.4-(.4-0)*EXP(-(TIME/60-ts/60)));
    Memrun.Rej(3) = .99;

```



```

else
    #below line just bookkeeping. initialization fails if some variable sets are
    ignored obviously
    SampRet.Inlet = Memrun.Ret;

    Mixlrun.Ci2(1:3) = Mixlrun.Ci1(1:3); #makes reinitialization easier for equal
    flows everywhere

    #We want to fill the catalyst quickly because otherwise deactivation occurs in our
    model
    if (TIME < .02*ts) then
        Mixlrun.Fout = 1700 ;#ml/min
    ELSE
        Mixlrun.Fout = 1.05 ; #ml/min to get catalyst conc. right in retentate
    end

    #Force blind flow-balance with open loop
    Mixlrun.Fi2 = Mixlrun.Fout-Mixlrun.Fil;

    Mixlrun.Fil = 1.90E-12*TIME^4 - 5.77E-09*TIME^3 + 6.11E-06*TIME^2 - 2.48E-03*TIME
+ 5.61E-01;
    Memrun.Rej(1) = .2;
    Memrun.Rej(2) = 0;
    Memrun.Rej(3) = .99;
end

CSTRrun.U(1).Inlet = Mixlrun.Outlet;

#Force Fin = Fout overall for process
Memrun.Fp = Mixlrun.Fil;

if (CSTRrun.U(Ntanks).Cout(2)+CSTRrun.U(Ntanks).Cout(1) < 1e-6) then
    FracProdRO = 0;
else
    FracProdRO =
CSTRrun.U(Ntanks).Cout(2)/(CSTRrun.U(Ntanks).Cout(2)+CSTRrun.U(Ntanks).Cout(1));
end

if (TIME < 2101) then

    TONperpass = 0;
else
    #tONperpass = 0;
    TONperpass = (CSTRrun.U(Ntanks).Cout(2) -
Mixlrun.Cout(2))/(CSTRrun.U(1).Cout(3)+CSTRrun.U(Ntanks).Cout(3))/2;
END

OBJECTIVE # objective_function_keyword
Weighted_Least_Squares
EXPERIMENT ContinuousRecycle# identifier
DATA
# variable_name[measurement_time] := measured_value : weight ;
CSTRrun.U(Ntanks).Cout(1) := IMPORT_DATA("C:\Documents and Settings\Everett\My
Documents\Thesis2012\Jacobian Model\RRO.txt",11);
CSTRrun.U(Ntanks).Cout(2) := IMPORT_DATA("C:\Documents and Settings\Everett\My
Documents\Thesis2012\Jacobian Model\PRO.txt",11);
Memrun.Cr(1) := IMPORT_DATA("C:\Documents and Settings\Everett\My
Documents\Thesis2012\Jacobian Model\HCsRet.txt",16);

```

```
Memrun.Cr(2) := IMPORT_DATA("C:\Documents and Settings\Everett\My
Documents\Thesis2012\Jacobian Model\HCpRet.txt",16);
```

```

INPUT
# variable_name := time_expression ;
Mixlrun.Cil(1:2) := 0; #Eqn for feed mmol/ml
#
Mixlrun.Cil(3) := .000182; #Eqn for feed mmol/ml
#Eqn for feed ml/min
#Set loop flow rate (independent of inlet flow rate) we remove one mass
#balance from loop in order to spec this.

Recycle := 0;
PRESET
# variable_name := default_value : lower_bound : upper_bound ;
SELECTOR
# selector_name := selector_value ;

INITIAL
# equality_constraint ;

CSTRrun.U(1:Ntanks).Cout(1:3) = 0;
Memrun.Cr(1:3) = 0;
SCHEDULE
# schedule_task
sequence
Continue for ts

RESET
Mixlrun.Cil(1) := .05; #Eqn for feed mmol/ml
Mixlrun.Cil(2) := 0; #Eqn for feed mmol/ml
Mixlrun.Cil(3) := 3.77e-5; #Eqn for feed mmol/ml
Recycle :=1;

end
continue for tr
end
END # estimation

```

```

SCRIPT TONcalc# identifier
PARAMETER
# identifier AS parameter_type
# identifier AS ARRAY(size_list) OF parameter_type
cTON as REAL
ccat as REAL
cprod as REAL
Vperm as real
testimport as real

ASK
# parameter-name quoted-string-prompt ;
SET
# parameter_name := parameter_expression ;
RUN

#LOAD "MetathesisDeactControl"
EXECUTE "Process"
Vperm := getintegral(STATUS, "Process", Memrun.Umem(1).Fp, TIME = ts:ts+tr)
+getintegral(STATUS, "Process", Memrun.Umem(2).Fp, TIME = ts:ts+tr);
cprod := 2.9*GETmaxVALUE(STATUS, "Process", HPLCrun.UHPLC(2).Cout(2))+
getintegral(STATUS, "Process", Memrun.Umem(1).Cp(2))/tr*getintegral(STATUS, "Process",
Memrun.Umem(1).Fp, TIME = ts:ts+tr)
+getintegral(STATUS, "Process", Memrun.Umem(2).Cp(2))/tr*getintegral(STATUS, "Process",
Memrun.Umem(2).Fp, TIME = ts:ts+tr);

```

```
#Not counting autosampler yet

ccat := 2.9*getmaxvalue(STATUS, "Process", Mix1run.Cil(3)) + Vperm*3.77e-5;
cTON := cprod/ccat;

Write "cumulative TON is ", cTON, STATUS END

# list of script commands
END # script
```

8.6 Appendix F

This script is used to initiate the interfacing of Matlab with Jacobian for the hydrogenation experimental data fitting.

RunJacFromMatlabHydrog.m

```
%Author: Everett J. O'Neal, Aug 10, 2013
%Copyright 2013 Massachusetts Institute of Technology. All rights reserved

%Read in csv Data files.
%There is Reag and Prod data at 3 points in this system:
%Reactor Outlet (RO,1), Retentate (Ret,2), Permeate (Perm,3)
%Store reagent and product as subsequent coluns in data matrix:
%columns: RO_R RO_P Ret_R Ret_P Perm_R Perm_P (6 columns)
%data_time matrix columns RO Ret Perm
%Each data set, however, has a different time vector
clear

%This data is created with "GasLiquidSampleLoops" script
[num,txt,row] = xlsread('H5eol98RO.xlsx'); % only 2 cols
[num2,txt,row] = xlsread('H5eol98Ret.xlsx'); % 3 calcs
[num3,txt,row] = xlsread('H5eol98Perm.xlsx'); %

M1 = length(num);
M2 = length(num2);
M3 = length(num3);
maxdataL = max([M1 M2 M3]);
data_time = zeros(maxdataL,3);
data = zeros(maxdataL,6);
model = data; %Same size matrix this way.

%RO data
data_time(1:M1,1) = num(:,1); %time column
data(1:M1,1) = num(:,2); %Reactor Cp/Cs conc.
%data(1:M1,2) = num(:,3); %Reactor Cp conc.

%Retentate data
data_time(1:M2,2) = num2(:,1); %time column
data(1:M2,2) = num2(:,2); %Ret R conc.
data(1:M2,3) = num2(:,3); %Ret P conc.

%Perm data
data_time(1:M3,3) = num3(:,1); %time column
data(1:M3,4) = num3(:,2); %perm Cp/Cs Conc.
%data(1:M3,6) = num3(:,3); %perm Cp Conc.

M = [M1 M2 M3];
%%%For what I'm doing
data_time = data_time*60; %convert to minutes
%data col 1: RO, col 2 & 3: Ret, col 4: Perm
hold on
%params: kr, kd, a, b (a,b are exponential fit for flow rate in= out)
options = optimset('Display', 'iter', 'TolFun', 1e-9, 'TolCon', 1e-7, 'DiffMinChange', .05);
%('MaxIter', 100, 'ToIX', 10, 'TolCon', 10, 'DiffMinChange', 10, 'TypicalX', [500 1000]);
```

```
X = [.466 2.6e-5 .476];
[X fval] = fmincon(@Hydrogynamics, X, [], [], [], [], [0; 0; .05], [.95; 50; 1], [],
options, M, data, data_time)
%best: 5.1856
%X =

% 7.4500 1.3000 50.0826 0.8600
```

8.7 Appendix G

This Matlab code is called by RunJacFromMatlabHydrog.m.

Hydrodynamics.m

%Author: Everett J. O'Neal, Aug 10, 2013

%Copyright 2013 Massachusetts Institute of Technology. All rights reserved

```
function ssq = hydrodynamics(p0, M, data, data_time)

M1 = M(1);
M2 = M(2);
M3 = M(3);
p0(2) = p0(2)/10000; %used with mindiffchange

%Run Jacobian using RunJacobian.c
runJacobian('Hydrog5e0198', 'Process', [p0(1); p0(2); p0(3)]);
% Read csv file output
[num4,txt,row] = xlsread('output/Process.csv');
mod_time = num4(:,1);
mod_output(:,1:4) = num4(:,2:5); %Store output in same order as data

%Need to round values or I run into uniqueness issues
%mod_time = round(mod_time*10e6)/10e6;
%mod_output = round(mod_output*10e6)/10e6;

%Need to remove redundant zeros from model output
%firstnonzero = find(mod_time,1);
%mod_time = mod_time((firstnonzero-1):end, :);
%mod_PRO = mod_PRO((firstnonzero-1):end, :);

%Shift model times to ignore 90 min start-up
mod_time = mod_time -90; %startup times appear negative.
%Remove all redudancies

mod_time = sort(mod_time, 1, 'ascend');
%ind = find(~diff(mod_time));
[mod_time I] = unique(mod_time);
mod_output = mod_output(I,:);

%Clean NaN from model output (NaN = 0)
ind = find(isnan(mod_output));
mod_output(ind) = 0;

%model has same organization as mod_output but no time column (time
%corresponds to various rows of data_time)
%We have 0's at the end of each column where no useful data is stored.

for ii = 1:4
    if ii == 1
        model(1:M1,ii) = interp1(mod_time, mod_output(:,ii), data_time(1:M1,1), 'linear');
    elseif ii > 1 & ii < 4
        model(1:M2,ii) = interp1(mod_time, mod_output(:,ii), data_time(1:M2,2), 'linear');
    else
        model(1:M3,ii) = interp1(mod_time, mod_output(:,ii), data_time(1:M3,3), 'linear');
    end
end
```

```

end

%Calculation sum of square differences manually over many variables

%ssq = sum(sum((model-data).^2, 1),2) %weighting every data point equally
%The zero's in model and data should b
% be irrelevant 0 - 0 if lined right

%Try special weighting:
[n m] = size(model);
ssq = 0;
for ii = 1:n %rows data
    for jj = 1:m %WANT WO WEIGHT 2-3 HEAVILY
        if jj == 2 | jj == 3
            w =15;
        else
            w = 1;
        end

        if data(ii,jj) < 1e-3
            ssq = ssq + (model(ii,jj)-data(ii,jj)).^2*w;
        else
            ssq = ssq + (model(ii,jj)-data(ii,jj)).^2/data(ii,jj).^2*w;
        end
    end
end

end
ssq
jj = rand();
if jj < 1 %ignore plotting most of time
hold on
%plot(data_time,data,'o');
%plot(mod_time, mod_output(:,1),'r')
%plot(mod_time, mod_output(:,2),'b')
for ii = 1:m
    if ii == 1
        figure(1)
        plot(data_time(1:M1,1), data(1:M1,ii), 'r*')
        plot(mod_time, mod_output(:,ii),'r')
        % plot(mod_time, mod_output(:,2),'b')
    elseif ii < 4
        figure(2)
        plot(data_time(1:M2,2), data(1:M2,ii), 'b*')
        plot(mod_time, mod_output(:,ii),'b')
    else
        figure(3)
        plot(data_time(1:M3,3), data(1:M3,ii), 'k*')
        plot(mod_time, mod_output(:,ii),'k')
    end
end
end

%legend('data - Prod', 'data - substrate', 'substrate','product')
pause(5)
end

return

```

8.9 Appendix H

This C++ script is included in the Matlab directory, and is called by other functions with interface Malab optimization algorithms with Jacobian.

RunJacobian.m

```
// Program to call Jacobian file from Matlab
// by Spencer Schaber, 22 March 2013
//

// Dependencies:
// * This was designed to run on Windows only for now (sorry).
// * This was tested using Matlab 2013a, 32-bit.
// * The code was compiled using the Microsoft SDK v. 7.1

// note: calling Matlab code must load Jacobian output data from *.csv file.
// This mex function does not return anything in plhs.
//
// Matlab syntax:
// >> mex -v -L. -lJACOBIAN runJacobian.c
// >> runJacobian(<InputFile>, <EstOrSimName>, <Params>)
// for example: >> runJacobian('GasOilCrack', 'RUN_GASOILSIM', [5.0; 10.0])
// where:
//   InputFile: string for filename of *.jac file
//   EstOrSimName: string for name of estimation or simulation in *.jac file
//   Params: column vector of parameter values
// For output data, read from the .csv file in the output directory
// with the same filename as the .jac file.
//
// Jacobian *.jac file must include the following:
// SIMULATION [simulationName]
// OPTIONS
//   #...
//   CSVOUTPUT := TRUE; # output reported time trajectories to [filename].csv,
//                       # where [filename] is the name of the current *.JAC file.
//   #...
// REPORT
//   #[comma-separated list of the full paths to the variables you want reported,
//   #e.g., "unit.liqConcs, unit.vapConcs" will print all elements of liqConcs
//   #and vapConcs from the unit named "unit" ]. The values will be reported
//   #in this order in the .csv file.
//
// #example:
// exptDes.ur.kinlluret.Conc(1:3, exptDes.ur.kinlluret.N_Z_PointsK+1)
//
// SENSITIVITY
//   #list of variables for which sensitivity data are needed
//
// #example:
// exptDes.ur.kinlluret.P
// ASK
// # list of *scalar* variables you want to take as inputs,
// # appearing in the order you will pass them to this mex function,
// # with a "0", "1", "2", etc next to them.
// #example:
// exptDes.ur.kinlluret.P(1) "0";
```



```

//      exptDes.ur.kinlllure.P(2) "1";
//      exptDes.ur.kinlllure.P(3) "2";
//      exptDes.ur.kinlllure.P(4) "3";
//      exptDes.ur.kinlllure.P(5) "4";
//      exptDes.ur.kinlllure.P(6) "5";
//      ...
//      END # end of simulation block

#include <string>
#include <string.h>
#include <fstream>
#include <iostream>
#include <sstream>
#include <stdio.h>
#include <stdlib.h>
#include <math.h>
#include <matrix.h>
#include <mex.h>
#include <vector>
#include "include/jacobian_c_interface.h"
#include "include/iohandling.h"

#ifdef WIN32
#include <tchar.h>
#endif

#define STRINGSIZE 256

#define MAX_PARAMS_TO_JACOBIAN 256

using namespace std ;
using namespace jacobian ;

/** parameters to pass to Jacobian */
double params[MAX_PARAMS_TO_JACOBIAN];
int nParamsToJacobian = 2;

/** specify paths to necessary Jacobian directories */
const char indir[STRINGSIZE] = ".\\input\\"; //!< path to Jacobian input directory relative
to Windows executable
const char outdir[STRINGSIZE] = ".\\output\\"; //!< path to Jacobian output directory
relative to Windows executable
const char codedir[STRINGSIZE] = ".\\input\\code\\"; //!< path to Jacobian code directory
relative to Windows executable
char InputFile[STRINGSIZE] = "GasOilCrack" ;
char SimOrEstName[STRINGSIZE] = "RUN_GASOILSIM" ;

char input_buffer[500]; //!< C-string used to store values passed in to Jacobian via
::myinput_handler

/** Reads data from CSV file output by Jacobian and store in variable jacobian_outputs.
// * @param[in] csvFileName path to CSV file to be read
// * @return 0 if successful, -2 if error reading file.
// */
//int read_CSV_file(std::string csvFileName);

```

```

/** the Jacobian handler that takes care of ask statements
 * @param[in] i
 * @param[in] prompt C-string for name or tag for variable requested
 * @return C-string form of the value for the requested variable.
 */
char *STDCALL myinput_handler(int i,const char *prompt)
{
    //std::ostringstream export_me;
    int i_param;

    // clear the input buffer:
    input_buffer[0] = '\0';

    i_param = atoi( prompt ); // convert C-string to integer (atoi(...))
    if ( (i_param < nParamsToJacobian) && (i_param >= 0) )
    {
        // We found the index for the desired decisions variable. Store it as a string to
make Jacobian happy:
        //export_me << params[i_param];
        char export_me[STRINGSIZE];
        sprintf(export_me, "%f", params[i_param]);
        //printf("setting params[%i] = %s", i_param, export_me);
        strcat(input_buffer, export_me ); // copy export_me to input_buffer
        //std::cout << "input_buffer = " << input_buffer << std::endl;
    }
    else
    {
        printf("Prompt '%s' not recognized.", prompt);

        //std::cout << "Prompt not recognized." << std::endl;
        //std::cout << prompt << " ";
        //std::cin >> input_buffer ;
    }
    return input_buffer;
}

/** The Jacobian handler that takes care of display.
 * @param[in] icode code for the message to display
 * @param[in] message C-string for message to display
 * @return 0 if successful
 */
int STDCALL myoutput_handler(int icode,const char *message)
{
    // if (printlevel>2) cout << "got " << message << endl ;
    //std::cout << "message: " << message << endl;
    printf("message: %s\n", message);
    //std::cout << "icode: " << icode << endl;
    return 0 ;
}

void mexFunction(int nlhs, mxArray *plhs[], int nrhs, const mxArray *prhs[])
{
    int irtn;
    char strFile[STRINGSIZE];
    mxArray *pData;
    double *pValues;
    int i;
    int rowLen;
    mxArray *InputFileData;
    int InputFileLength;

```

```

char *InputFileString;
mxArray *SimOrEstNameData;
int SimOrEstNameLength;
char *SimOrEstNameString;

// get strings for path to Jacobian .jac file and EstOrSimName from prhs:
//Copy input pointer InputFile
//const mxArray *
InputFileData = prhs[0];

//Make "InputFileString" point to the string
InputFileLength = mxGetN(InputFileData)+1;
InputFileString = (char*) mxMalloc(InputFileLength, sizeof(char)); //mxMalloc is similar
to malloc in C
mxGetString(InputFileData, InputFileString, InputFileLength);

InputFile[0] = '\0'; // clear InputFile
strcat(InputFile, InputFileString);

//Copy input pointer EstOrSimName
//const mxArray *
SimOrEstNameData = prhs[1];

//Make "InputFileString" point to the string
SimOrEstNameLength = mxGetN(SimOrEstNameData)+1;
SimOrEstNameString = (char*) mxMalloc(SimOrEstNameLength, sizeof(char)); //mxMalloc is
similar to malloc in C
mxGetString(SimOrEstNameData, SimOrEstNameString, SimOrEstNameLength);

SimOrEstName[0] = '\0'; // clear InputFile
strcat(SimOrEstName, SimOrEstNameString);

// get values for input to Jacobian file:
//Copy input pointer Params
//const mxArray *
pData = prhs[2];

//Get matrix Params
pValues = mxGetPr(pData);
rowLen = mxGetN(pData);
nParamsToJacobian = mxGetM(pData);
for (i = 0; i<nParamsToJacobian; ++i) params[i] = pValues[i];
if (rowLen != 1){
    printf("Error: you did not provide a vector of parameters.\n");
    abort();
}
}

// load and run Jacobian .jac file:
// Initialize the Jacobian API
irtn = jacobianInitialize(myinput_handler, myoutput_handler) ;
if(irtn!=JACOBIAN_SUCCESS) {
    printf(" %s:%s: jacobianInitialize failed and returned %i.\n",
        __FILE__, __LINE__, irtn);
    return;
}

// Set the Jacobian input directory
irtn=jacobianInputDirectory(indir) ;
if(irtn!=JACOBIAN_SUCCESS) {
    printf(" %s:%s: setting input directory %s failed and returned %i.\n",
        __FILE__, __LINE__, indir, irtn);
    return;
}
}

```

```

// Set the Jacobian code directory
irtn=jacobianCodeDirectory(codedir) ;
if(irtn!=JACOBIAN_SUCCESS) {
    printf("%s:%s: setting code directory %s failed and returned %i.\n",
        __FILE__, __LINE__, codedir, irtn);
    return;
}
// Set the Jacobian output directory
irtn=jacobianOutputDirectory(outdir) ;
if(irtn!=JACOBIAN_SUCCESS) {
    printf("%s:%s: setting output directory %s failed and returned %i.\n",
        __FILE__, __LINE__, outdir, irtn);
    return;
}

// Load input file
//string strFile=indir+InputFile+".JAC" ;

strFile[0] = '\0'; // clear strFile
strcat(strFile, indir);
strcat(strFile, InputFile);
strcat(strFile, ".JAC");
//printf("loading file \"%s\"...\n", strFile);
irtn=jacobianLoad(strFile) ;
if(irtn!=JACOBIAN_SUCCESS) {
    printf("%s:%s: failed while loading \"%s\" and returned %i.\n",
        __FILE__, __LINE__, strFile, irtn);
    return;
}

// Instantiate problem
//printf("instantiating problem \"%s\"...\n", SimOrEstName);
irtn=jacobianInstantiate(SimOrEstName) ;
if(irtn!=JACOBIAN_SUCCESS) {
    printf("%s:%s: failed while loading \"%s\" and returned %i.\n",
        __FILE__, __LINE__, SimOrEstName, irtn);
    return;
}

// Solve problem
//printf("solving problem \"%s\"...\n", SimOrEstName);
irtn=jacobianSolve(SimOrEstName) ;
if(irtn!=JACOBIAN_SUCCESS) {
    printf("%s:%s: failed while solving \"%s\" and returned %i.\n",
        __FILE__, __LINE__, SimOrEstName, irtn);
    return;
}

// Unload input file
//printf("unloading file \"%s\"...\n", InputFile);
irtn=jacobianUnload(InputFile) ;
if(irtn!=JACOBIAN_SUCCESS) {
    printf("%s:%s: failed while unloading \"%s\" and returned %i.\n",
        __FILE__, __LINE__, InputFile, irtn);
    return;
}

// // read CSV file output by JACOBIAN to get objective:
// string strCSV = outdir+SimOrEstName+".csv";
// std::cout << "Reading CSV file: \"" << strCSV << "\"..." << std::endl;
// irtn = read_CSV_file(strCSV.c_str());
// if (irtn!=0)
// {

```

```

//      cerr << __FILE__ <<" " << __LINE__                                     ;
//      cerr << " failed while reading CSV file." << endl ;
//      return -8;
//  }

    return;
} // end function mexFunction

// stuff for reading CSV files is highly C++ dependent, and Matlab only
// ships with a C compiler.  For ease of use, I adapted this file to pure C
// so the user need not install a C++ compiler

// #define MAX_OUTPUTS_FROM_JACOBIAN
// #define NOUTPUTS_FROM_JACOBIAN 2 //!< number of outputs to get from Jacobian.
// ** outputs received from Jacobian */
// double jacobian_outputs[MAX_OUTPUTS_FROM_JACOBIAN];

// ** sensitivities obtained from Jacobian */
// double jacobian_sensis[NMAX_OUTPUTS_FROM_JACOBIAN][NPARAMS_TO_JACOBIAN];
// int read_CSV_file(std::string csvFileName)
// {
//     string line_str;
//     std::stringstream line_ss;
//     string number_str;
//     string firstLine;
//     std::vector<double> csv_one_line;
//     std::ifstream infile(csvFileName.c_str());
//     //
//     int current_line = 0;
//     //
//     std::cout << infile << std::endl;
//     // // first line of file has labels. Print and get rid of the first line:
//     // std::getline(infile, firstLine);
//     // //std::cout << "labels: \"" << firstLine << "\"" << std::endl;
//     //
//     // // read every line of the CSV file; keep the entries from the very last one (final time):
//     // if ( infile ) // as long as the stream is still ok, try reading it.
//     // {
//     //     while ( std::getline(infile, line_str) ) // pull characters out of infile until
NEWLINE
//         {
//             csv_one_line.clear(); // make sure csv_one_line is empty
//             line_ss << line_str; //store one line to stringstream
//             while ( std::getline(line_ss, number_str, ',') ) // pull characters out of infile
until the next 'comma'
//                 {
//                     csv_one_line.push_back( atof( number_str.c_str() ) ); // convert string to
double (atof(...)) and store to csv_one_line
//                 }
//             line_ss.clear(); // clear stringstream of current line so we can re-fill it the
next time around.
// #ifndef NDEBUG
//     if ( current_line > 10000 ){ std::cout << "Reached 10,000th line. Stopping." <<
std::endl; return -1; }
//     ++current_line;
// #endif
//     }
// }
// else

```

```

// {
//     std::cerr << "Error reading CSV file output by Jacobian." << std::endl
//     << "Perhaps you have entered an incorrect path to the CSV file "
//     << "or the file does not exist." << std::endl;
//     return -2;
// }
//
// for (int iCSV = 0; iCSV < 1 + (NOUTPUTS_FROM_JACOBIAN) +
(NOUTPUTS_FROM_JACOBIAN)*(NPARAMS_TO_JACOBIAN); ++iCSV)
//     std::cout << "Entry " << iCSV << " from final line of CSV file = " <<
csv_one_line[iCSV] << ", " << std::endl;
//
//     std::cout << "for parameters passed to Jacobian:" << std::endl;
//     for (int ix = 0; ix < NPARAMS_TO_JACOBIAN; ++ix) std::cout << "params[" << ix << "] = "
<< params[ix] << std::endl;
//
//     for (int iFun = 0; iFun < (NOUTPUTS_FROM_JACOBIAN); ++iFun)
//     {
//         //the following assumes:
//         // * objective and constraint functions are final row in CSV file output by Jacobian
(final time values)
//         // * sensitivity analysis is enabled in Jacobian
//         jacobian_outputs[iFun] = csv_one_line[1+iFun];
//         std::cout << "jacobian_outputs[" << iFun << "] = " << jacobian_outputs[iFun] <<
std::endl;;
//     }
//
//     std::cout << "and sensitivities from Jacobian are: " << std::endl;
//     for (int iPar = 0; iPar < NPARAMS_TO_JACOBIAN; ++iPar)
//     {
//         for (int iFun = 0; iFun < (NOUTPUTS_FROM_JACOBIAN); ++iFun)
//         {
//             // order in CSV file is time, x1, x2, x3, ..., dx1/dp1, dx2/dp1, ..., dx1/dp2,
dx2/dp2, ...
//             jacobian_sensis[iFun][iPar]
//             = csv_one_line[1 + (NOUTPUTS_FROM_JACOBIAN) + iFun +
(NOUTPUTS_FROM_JACOBIAN)*iPar];
//             std::cout << "d(jacobian_output[" << iFun << "])/d(param[" << iPar << "]) = "
//             << jacobian_sensis[iFun][iPar] << std::endl;
//         } // for iFun
//     } // for iDecis
//     return 0;
// }

```

8.10 Appendix I

This appendix includes the Jacobian® code used in the production of our metathesis data fits.

MetCofeedwMatlabAug.JAC

#Author: Everett J. O'Neal, Aug 10, 2013

#Copyright 2013 Massachusetts Institute of Technology. All rights reserved

DECLARE

```
TYPE
# identifier = default_value : lower_bound : upper_bound  UNIT = "string"
C = .05 : 0 : 5 UNIT = "mmol/ml"
F = 1 : 0 : 20000 unit = "ml/min"
V = 1 : 0 : 1 #valve position
R = .5 : 0 : 1 #rejection
N = 1 : 0 : 1e10 #various numbers
STREAM
# identifier IS variable_type_list
Streamvars is C, F
ENUMERATION
# identifier IS { identifier_list }
END # declares
```

MODEL CSTR # identifier

PARAMETER

```
# identifier AS parameter_type
# identifier AS ARRAY(size_list) OF parameter_type
kr as REAL
kd as real
V as REAL #volume of tank, units ml
```

UNIT

```
# identifier AS model_name
# identifier AS ARRAY(size_list) OF model_name
```

VARIABLE

```
# identifier AS variable_type
# identifier AS ARRAY(size_list) OF variable_type
Cin, Cout as array(3) of C
Fin as F
Fout as F
```

STREAM

```
# identifier AS stream_type
# identifier AS ARRAY(size_list) OF stream_type
Inlet : Cin, Fin as Streamvars
Outlet: Cout, Fout as Streamvars
```

SELECTOR

```
# identifier AS enumeration_type
# identifier AS ARRAY(size_list) OF enumeration_type
# identifier AS (identifier_list) DEFAULT default_value
```

SET

```
# parameter_name := parameter_expression ;
#kr := 50; #Forward rate constant
#kd := .19; #Catalyst Deactivation constant
#V := 1;
```

INTERMEDIATE

```
# DIMENSION array_intermediate(size_list)
# intermediate_name := expression ;
```

EQUATION

```
# equality_constraint
```

```

Fin = Fout; # no accumulation in tanks
#Fout = 1;
#Cin(1:3) = 1;
V*$Cout(1) = Fin*Cin(1) - Fout*Cout(1) - kr*Cout(3)*Cout(1);
V*$Cout(2) = Fin*Cin(2) - Fout*Cout(2) +kr*Cout(3)*Cout(1);
V*$Cout(3) = Fin*Cin(3) - Fout*Cout(3) -kd*Cout(3)*Cout(3);
END # model

```

MODEL PBR

```

PARAMETER
# identifier AS parameter_type
# identifier AS ARRAY(size_list) OF parameter_type
N as INTEGER
UNIT
# identifier AS model_name
# identifier AS ARRAY(size_list) OF model_name
U as array(N) of CSTR
VARIABLE
# identifier AS variable_type
# identifier AS ARRAY(size_list) OF variable_type
STREAM
# identifier AS stream_type
# identifier AS ARRAY(size_list) OF stream_type
SELECTOR
# identifier AS enumeration_type
# identifier AS ARRAY(size_list) OF enumeration_type
# identifier AS (identifier_list) DEFAULT default_value
SET

N := 170;
# parameter_name := parameter_expression ;
INTERMEDIATE
# DIMENSION array_intermediate(size_list)
# intermediate_name := expression ;
EQUATION
U(1:N-1).Outlet is U(2:N).Inlet;

# equality_constraint
END # model

```

MODEL ModelHoldTank# identifier

```

PARAMETER
# identifier AS parameter_type
# identifier AS ARRAY(size_list) OF parameter_type
V as REAL #volume of tank, units ml
kr as real
kd as real

UNIT
# identifier AS model_name
# identifier AS ARRAY(size_list) OF model_name
VARIABLE
# identifier AS variable_type
# identifier AS ARRAY(size_list) OF variable_type
Cin, Cout as array(3) of C
Fin as F
Fout as F

STREAM
# identifier AS stream_type
# identifier AS ARRAY(size_list) OF stream_type
Inlet : Cin, Fin as Streamvars
Outlet: Cout, Fout as Streamvars

```



```

SELECTOR
# identifier AS enumeration_type
# identifier AS ARRAY(size_list) OF enumeration_type
# identifier AS (identifier_list) DEFAULT default_value
SET
# parameter_name := parameter_expression ;
#kd := 2000;
INTERMEDIATE
# DIMENSION array_intermediate(size_list)
# intermediate_name := expression ;
EQUATION
Fin = Fout; # no accumulation in tanks
V*$Cout(1) = Fin*Cin(1) - Fout*Cout(1) -kr*Cout(3)*Cout(1);
V*$Cout(2) = Fin*Cin(2) - Fout*Cout(2) +kr*Cout(3)*Cout(1);
V*$Cout(3) = Fin*Cin(3) - Fout*Cout(3) - kd*Cout(3)*Cout(3);

# equality_constraint
END # model

```

```

MODEL HPLC# identifier
PARAMETER
# identifier AS parameter_type
# identifier AS ARRAY(size_list) OF parameter_type
Nh as INTEGER

UNIT
# identifier AS model_name
# identifier AS ARRAY(size_list) OF model_name
UHPLC as array(Nh) of ModelHoldTank
VARIABLE
# identifier AS variable_type
# identifier AS ARRAY(size_list) OF variable_type
STREAM
# identifier AS stream_type
# identifier AS ARRAY(size_list) OF stream_type
SELECTOR
# identifier AS enumeration_type
# identifier AS ARRAY(size_list) OF enumeration_type
# identifier AS (identifier_list) DEFAULT default_value
SET
# parameter_name := parameter_expression ;
Nh := 2;
INTERMEDIATE
# DIMENSION array_intermediate(size_list)
# intermediate_name := expression ;
EQUATION
# equality_constraint
UHPLC(1:Nh-1).Outlet is UHPLC(2:Nh).Inlet;
END # model

```

```

MODEL Membrane# identifier
PARAMETER
# identifier AS parameter_type
# identifier AS ARRAY(size_list) OF parameter_type
kd as real
kr as real
V as Real
UNIT
# identifier AS model_name
# identifier AS ARRAY(size_list) OF model_name
VARIABLE
# identifier AS variable_type

```

```

# identifier AS ARRAY(size_list) OF variable_type
Cin, Cr, Cp as array(3) of C
Fin, Fr, Fp as F
Rej as array(3) of R

STREAM
# identifier AS stream_type
# identifier AS ARRAY(size_list) OF stream_type
Inlet : Cin, Fin as Streamvars
Ret: Cr, Fr as Streamvars
Perm: Cp, Fp as Streamvars
SELECTOR
# identifier AS enumeration_type
# identifier AS ARRAY(size_list) OF enumeration_type
# identifier AS (identifier_list) DEFAULT default_value
SET
# parameter_name := parameter_expression ;
#Rej(1) := .7;
#Rej(2) := .8;
INTERMEDIATE
# DIMENSION array_intermediate(size_list)
# intermediate_name := expression ;
EQUATION
Fin = Fr + Fp; # no accumulation in mem (flow)

#If zero concentration over membrane, Just treat Cp = Cr = 0;
For i :=1 to 3 do
if (Cr(i) < 1e-6) THEN ##RUN FAILS IF 0 is used!!
    Cp(i) = Cr(i);
ELSE
    Rej(i) = 1 - Cp(i)/Cr(i);
End
end

V*$Cr(1) = Fin*Cin(1) - Fr*Cr(1) - Fp*Cp(1) -kr*Cr(3)*Cr(1);
V*$Cr(2) = Fin*Cin(2) - Fr*Cr(2) - Fp*Cp(2) +kr*Cr(3)*Cr(1);
V*$Cr(3) = Fin*Cin(3) - Fr*Cr(3) - Fp*Cp(3) -kd*Cr(3)*Cr(3);

# equality_constraint
END # model

MODEL MemSeries# identifier
PARAMETER
# identifier AS parameter_type
# identifier AS ARRAY(size_list) OF parameter_type
Nm as real

UNIT
# identifier AS model_name
# identifier AS ARRAY(size_list) OF model_name
Umem as array(Nm) of Membrane
VARIABLE
# identifier AS variable_type
# identifier AS ARRAY(size_list) OF variable_type
#Cmix as array(3) of C
#Imix as F

STREAM
# identifier AS stream_type
# identifier AS ARRAY(size_list) OF stream_type
#Mixed : Cin, Fin as Streamvars

```

```

SELECTOR
# identifier AS enumeration_type
# identifier AS ARRAY(size_list) OF enumeration_type
# identifier AS (identifier_list) DEFAULT default_value
SET
# parameter_name := parameter_expression ;
Nm := 2;

INTERMEDIATE
# DIMENSION array_intermediate(size_list)
# intermediate_name := expression ;
EQUATION
# equality_constraint
#Umem(1:Nm).Fp = .0!/Nm; Can't do this. Need it to balance inlet flow rate.
Umem(1:Nm-1).Ret is Umem(2:Nm).Inlet;

#For n :=1 to Nm do
# Cmix(1:3) = Cmix(1:3) + Umem(1:Nm).C(1
#Fmix =
END # model

MODEL Tmix #inlet Tmix to system
PARAMETER
# identifier AS parameter_type
# identifier AS ARRAY(size_list) OF parameter_type
UNIT
# identifier AS model_name
# identifier AS ARRAY(size_list) OF model_name
VARIABLE
# identifier AS variable_type
# identifier AS ARRAY(size_list) OF variable_type
Ci1, Ci2, Cout as array(3) of C
Fi1, Fi2, Fout as F
STREAM
# identifier AS stream_type
# identifier AS ARRAY(size_list) OF stream_type
Inlet1 : Ci1, Fi1 as Streamvars
Inlet2: Ci2, Fi2 as Streamvars
Outlet: Cout, Fout as Streamvars
SELECTOR
# identifier AS enumeration_type
# identifier AS ARRAY(size_list) OF enumeration_type
# identifier AS (identifier_list) DEFAULT default_value
SET
# parameter_name := parameter_expression ;
INTERMEDIATE
# DIMENSION array_intermediate(size_list)
# intermediate_name := expression ;
EQUATION
# equality_constraint
#Fi1 + Fi2 = Fout; - REMOVED MASS BALANCE HERE DUE TO CLOSED RECYCLE LOOP
# BECOMES REDUNDANT WITH ALL OTHER MASS BALANCES + OVERALL MB
Fi1*Ci1(1:3) + Fi2*Ci2(1:3) = Fout*Cout(1:3);
END # model

MODEL Splitter# identifier
PARAMETER
# identifier AS parameter_type
# identifier AS ARRAY(size_list) OF parameter_type
Fp as real
UNIT
# identifier AS model_name
# identifier AS ARRAY(size_list) OF model_name
VARIABLE
# identifier AS variable_type

```

```

# identifier AS ARRAY(size_list) OF variable_type
Ci, Cp, Cout as array(3) of C
Fi, Fout as F
STREAM
# identifier AS stream_type
# identifier AS ARRAY(size_list) OF stream_type
Inlet : Ci, Fi as Streamvars
Purge: Cp, Fp as Streamvars
Outlet: Cout, Fout as Streamvars
SELECTOR
# identifier AS enumeration_type
# identifier AS ARRAY(size_list) OF enumeration_type
# identifier AS (identifier_list) DEFAULT default_value
SET
# parameter_name := parameter_expression ;
INTERMEDIATE
# DIMENSION array_intermediate(size_list)
# intermediate_name := expression ;
EQUATION
# equality_constraint
Fout = Fi - Fp;
Cp = Ci;
Cout = Ci;
END # model

```

SIMULATION Process# identifier

OPTIONS

```

# option_name := option_value
CSVOUTPUT := TRUE; # output reported time trajectories to [filename].csv, where
[filename] is the name of the current *.JAC file.

```

PARAMETER

```

# identifier AS parameter_type
# identifier AS ARRAY(size_list) OF parameter_type
Ntanks as real
Nhplc as real
Nmem as real
tr as real #run time
ts as real #start-up time
kdd as real #deactivation time constant
krr as real
a as real
b as real
f as real

```

UNIT

```

# identifier AS model_name
# identifier AS ARRAY(size_list) OF model_name
CSTRrun as PBR
HoldTankrun as ModelHoldTank
HPLCrun as HPLC
Memrun as MemSeries
Mixlrun as Tmix
SampRO as Splitter
SampRet as Splitter
#SampPerm as Splitter

```

VARIABLE

```

# identifier AS variable_type
# identifier AS ARRAY(size_list) OF variable_type
Recycle as V
FracprodRO as V #0-1
TONperpass as N

```

```

REPORT
# variable list
# CSTRrun.U(3).Cout(1:3)
CSTRrun.U(Ntanks).Cout(1:2)
Memrun.Umem(Nmem).Cr(1:2)
Memrun.Umem(Nmem).Cp(1:2)
#
# HoldTankrun.Cout(1:3)
# HPLCrun.UHPLC(Nhplc).Cout(1:3)
# Memrun.Umem(Nmem).Cr(1:3)
Memrun.Umem(Nmem).Fp
Memrun.Umem(Nmem).Fr
Memrun.Umem(Nmem).Fin
CSTRrun.U(Ntanks).Cout(3)
# Memrun.Umem(1).Fp
# Memrun.Umem(1).Fr
# Memrun.Umem(1).Fin
# HPLCrun.UHPLC(Nhplc).Fout
# HoldTankrun.Fout

#For script
#HPLCrun.UHPLC(2).Cout(2)
#Memrun.Umem(1:Nmem).Fp
#Memrun.Umem(1:Nmem).Cp(1:3)
#Mixrun.Cil(1:3)

Fracprodro
TONperpass
SampRO.Fout
SampRet.Fout

SENSITIVITY
# parameter_name := parameter_expression ;

ASK
krr "0";
kdd "1";
a "2";
b "3";
f "4";

SET
# parameter_name := parameter_expression ;
Ntanks := CSTRrun.N;
Nhplc := HPLCrun.Nh;
Nmem := Memrun.Nm ;
CSTRrun.U.V := .72/Ntanks; #Vol of individual tanks ml
HoldTankrun.V := .8; #holding tank active vol ml
HPLCrun.UHPLC.V := .55/Nhplc; #HPLC volume ml
Memrun.Umem.V := .55/Nmem;

#deact

#Deactivation sets
HoldTankrun.kd := kdd;
CSTRrun.U.kd := kdd;
Memrun.Umem.kd := kdd;
HPLCrun.UHPLC.kd := kdd;

#rate const
HoldTankrun.kr := krr;
CSTRrun.U.kr := krr;
HPLCrun.UHPLC.kr := krr;
Memrun.Umem.kr := krr;

```

```

ts := 10; # Time to start-up system. Subtracted from TIME to compute trends
tr := 3300;
#AUTOSAMPLER PARAMETERS
SampRO.Fp := .24/1000; #ul/min purge
SampRet.Fp := .12/1000; #ul/min purge

INTERMEDIATE
# DIMENSION array_intermediate(size_list)
# intermediate_name := expression ;
EQUATION
# equality_constraint
SampRO.Inlet = CSTRrun.U(Ntanks).Outlet;
HoldTankrun.Inlet = SampRO.Outlet;
HPLCrun.UHPLC(1).Inlet = HoldTankrun.Outlet;
Memrun.Umem(1).Inlet = HPLCrun.UHPLC(Nhplc).Outlet;

if (Recycle = 1) then

    Mixlrun.Fout = .07 ;#ml/min

    #Also sample retentate.
    SampRet.Inlet = Memrun.Umem(Nmem).Ret;
    #Now pass on to Mixer
    Mixlrun.Inlet2 = SampRet.Outlet;

    ##Fit in excel: Mixlrun.Fil = (8.5 + 32*EXP(-.3*(TIME/6)-ts/60))/1000;    #quite
uncertain here !
    Mixlrun.Fil = (8.5 + a*EXP(-b*(TIME/60-ts/60)))/1000;    #quite uncertain here
!

    #Memrun.Umem(1:Nmem).Rej(1) = (.92-(.92-.52)*EXP(-.5*(TIME/60-ts/60)));
    #Memrun.Umem(1:Nmem).Rej(2) = (.826-(.825-.33)*EXP(-.5*(TIME/60-ts/60)));
    Memrun.Umem(1:Nmem).Rej(1) = (.92-(.92-.52)*EXP(-f*(TIME/60-ts/60)));
    Memrun.Umem(1:Nmem).Rej(2) = (.826-(.825-.33)*EXP(-f*(TIME/60-ts/60)));
    Memrun.Umem(1:Nmem).Rej(3) = .99;

else

    #below line just bookkeeping. initialization fails if some variable sets are
ignored obviously
    SampRet.Inlet = Memrun.Umem(Nmem).Ret;

    Mixlrun.Ci2(1:3) = Mixlrun.Ci1(1:3); #makes reinitialization easier for equal
flows everywhere

    #We want to fill the catalyst quickly because otherwise deactivation occurs in our
model

    if (TIME < .02*ts) then
    Mixlrun.Fout = 1700 ;#ml/min
    ELSE
    Mixlrun.Fout = .07 ; #ml/min to get catalyst conc. right in retentate
    end

    #Force blind flow-balance with open loop
    Mixlrun.Fi2 = Mixlrun.Fout-Mixlrun.Fil;

    Mixlrun.Fil = (8.5 + a*EXP(-b*(0)))/1000;
    Memrun.Umem(1:Nmem).Rej(1) = .52;
    Memrun.Umem(1:Nmem).Rej(2) = .33;
    Memrun.Umem(1:Nmem).Rej(3) = .99;

end

CSTRrun.U(1).Inlet = Mixlrun.Outlet;

```

```

#Force Fin = Fout overall for process - Why not Memrun.Umem.Fp = Mixlrun.Fil - SampRO.Fp
- SampRet.Fp??
Memrun.Umem(1:Nmem).Fp = (Mixlrun.Fil-SampRO.Fp-SampRet.Fp)/Nmem;

if (CSTRrun.U(Ntanks).Cout(2)+CSTRrun.U(Ntanks).Cout(1) < 1e-6) then
    FracProdRO = 0;
else
    FracProdRO =
CSTRrun.U(Ntanks).Cout(2)/(CSTRrun.U(Ntanks).Cout(2)+CSTRrun.U(Ntanks).Cout(1));
end

if (TIME < 2101) then
    TONperpass = 0;
else
    #tONperpass = 0;
    TONperpass = (CSTRrun.U(Ntanks).Cout(2) -
Mixlrun.Cout(2))/(CSTRrun.U(1).Cout(3)+CSTRrun.U(Ntanks).Cout(3))/2;
END

INPUT
# variable_name := time_expression ;
Mixlrun.Cil(1:2) := 0; #Eqn for feed mmol/ml
Mixlrun.Cil(3) := .000182; #Eqn for feed mmol/ml

#Eqn for feed ml/m.n
#Set loop flow rate (independent of inlet flow rate) we remove one mass
#balance from loop in order to spec this.

Recycle := 0;
PRESET
# variable_name := default_value : lower_bound : upper_bound ;
SELECTOR
# selector_name := selector_value ;
INITIAL
# equality_constraint ;

CSTRrun.U(1:Ntanks).Cout(1:3) = 0;
HPLCrn.UHPLC(1:Nhplc).Cout(1:3) = 0;
HoldTankrun.Cout(1:3) = 0;
Memrun.Umem(1:Nmem).Cr(1:3) = 0;
SCHEDULE
# schedule_task
sequence
Continue for ts

RESET
    Mixlrun.Cil(1) := .05; #Eqn for feed mmol/ml
    Mixlrun.Cil(2) := 0; #Eqn for feed mmol/ml
    Mixlrun.Cil(3) := 3.77e-5; #Eqn for feed mmol/ml
    Recycle :=1;
end
continue for tr
end
END # simulation

ESTIMATION RateandDeact# identifier
OPTIONS
# option_name := option_value
#Dynamic_Scaling := TRUE;

```

```

#estimation_tolerance := 1e-16;
#Estimation_Print_level :=2;
CSVOUTPUT := TRUE; # output reported time trajectories to [filename].csv, where
[filename] is the name of the current *.JAC file.

```

PARAMETER

```

# identifier AS parameter_type
# identifier AS ARRAY(size_list) OF parameter_type
Ntanks as real
Nhplc as real
Nmem as real
tr as real #run time
ts as real #start-up time
kdest as real #deactivation time constant
krest as real #rate constant
dummyparam as real

```

UNIT

```

# identifier AS model_name
# identifier AS ARRAY(size_list) OF model_name
CSTRrun as PBR
HoldTankrun as ModelHoldTank
HPLCrun as HPLC
Memrun as MemSeries
Mixlrun as Tmix
SampRO as Splitter
SampRet as Splitter
#SampPerm as Splitter

```

VARIABLE

```

# identifier AS variable_type
# identifier AS ARRAY(size_list) OF variable_type
Recycle as V
FracprodRO as V #0-1
TONperpass as N

```

UNCERTAIN

```

# parameter_name := default_value : lower_bound : upper_bound ;
#kdest := 500 : 1e-5 : 1e5;
#krest := 1000 : 1e-5 : 1e5;
dummyparam := 1 : 1e-5: 1e5;

```

ASK

```

kdest "0";
krest "0";

```

SET

```

# parameter_name := parameter_expression ;
Ntanks := CSTRrun.N;
Nhplc := HPLCrun.Nh;
Nmem := Memrun.Nm ;
CSTRrun.U.V := .72/Ntanks; #Vol of individual tanks ml
HoldTankrun.V := .8; #holding tank active vol ml
HPLCrun.UHPLC.V := .55/Nhplc; #HPLC volume ml
Memrun.Umem.V := .55/Nmem;

```

#deact

```

#kdd := 200;
#Deactivation sets
HoldTankrun.kd := kdest;
CSTRrun.U.kd := kdest;
Memrun.Umem.kd := kdest;
HPLCrun.UHPLC.kd := kdest;

```

#rate const


```

#krr = 5;

CSTRrun.U.kr := krest;

ts := 30; # Time to start-up system. Subtracted from TIME to compute trends
tr := 3000;
#AUTOSAMPLER PARAMETERS
SampRO.Fp := .3/1000; #ul/min purge
SampRet.Fp := .3/1000; #ul/min purge

INTERMEDIATE
# DIMENSION array_intermediate(size_list)
# intermediate_name := expression ;

EQUATION
# equality_constraint

SampRO.Inlet = CSTRrun.U(Ntanks).Outlet;
HoldTankrun.Inlet = SampRO.Outlet;
HPLCrun.UHPLC(1).Inlet = HoldTankrun.Outlet;
Memrun.Umem(1).Inlet = HPLCrun.UHPLC(Nhplc).Outlet;

if (Recycle = 1) then
  Mixlrun.Fout = .07 ;#ml/min
  #Also sample retentate.
  SampRet.Inlet = Memrun.Umem(Nmem).Ret;
  #Now pass on to Mixer
  Mixlrun.Inlet2 = SampRet.Outlet;
  Mixlrun.Fil = (8.5 + 32*EXP(-.3*(TIME/60-ts/60)))/1000;
  Memrun.Umem(1:Nmem).Rej(1) = (.92-(.92-.52)*EXP(-.5*(TIME/60-ts/60)));
  Memrun.Umem(1:Nmem).Rej(2) = (.826-(.825-.33)*EXP(-.5*(TIME/60-ts/60)));
  Memrun.Umem(1:Nmem).Rej(3) = .99;

else
  #below line just bookkeeping. initialization fails if some variable sets are
  ignored obviously
  SampRet.Inlet = Memrun.Umem(Nmem).Ret;

  Mixlrun.Ci2(1:3) = Mixlrun.Ci1(1:3); #makes reinitialization easier for equal
  flows everywhere

  #We want to fill the catalyst quickly because otherwise deactivation occurs in our
  model
  Mixlrun.Fout = 1700 ;#ml/min
  #Force blind flow-balance with open loop
  Mixlrun.Fi2 = Mixlrun.Fout-Mixlrun.Fil;

  Mixlrun.Fil = (8.5 + 32*EXP(-.3*(0)))/1000;
  Memrun.Umem(1:Nmem).Rej(1) = .52;
  Memrun.Umem(1:Nmem).Rej(2) = .33;
  Memrun.Umem(1:Nmem).Rej(3) = .99;

end

CSTRrun.U(1).Inlet = Mixlrun.Outlet;

#Force Fin = Fout overall for process: What about SAMPLING? SampRet, SampRO
Memrun.Umem(1:Nmem).Fp = Mixlrun.Fil/Nmem;

```

```

if (CSTRrun.U(Ntanks).Cout(2)+CSTRrun.U(Ntanks).Cout(1) < 1e-6) then
    FracProdRO = 0;
else
    FracProdRO =
CSTRrun.U(Ntanks).Cout(2)/(CSTRrun.U(Ntanks).Cout(2)+CSTRrun.U(Ntanks).Cout(1));
end

if (TIME < 2101) then

    TONperpass = 0;
else
    #TONperpass = 0;
    TONperpass = (CSTRrun.U(Ntanks).Cout(2)-
Mixlrun.Cout(2))/(CSTRrun.U(1).Cout(3)+CSTRrun.U(Ntanks).Cout(3))/2;
END

OBJECTIVE # objective_function_keyword
Weighted_Least_Squares
EXPERIMENT ContinuousRecycle# identifier
DATA
# variable_name[measurement_time] := measured_value : weight ;
CSTRrun.U(Ntanks).Cout(1) := IMPORT_DATA("C:\Documents and Settings\Everett\My
Documents\Thesis2012\Jacobian Model\RRO.txt",11);
CSTRrun.U(Ntanks).Cout(2) := IMPORT_DATA("C:\Documents and Settings\Everett\My
Documents\Thesis2012\Jacobian Model\PRO.txt",11);
Memrun.Umem(Nmem).Cr(1) := IMPORT_DATA("C:\Documents and Settings\Everett\My
Documents\Thesis2012\Jacobian Model\RR.txt",11);
Memrun.Umem(Nmem).Cr(2) := IMPORT_DATA("C:\Documents and Settings\Everett\My
Documents\Thesis2012\Jacobian Model\RP.txt",11);

INPUT
# variable_name := time_expression ;
Mixlrun.Cil(1:2) := 0; #Eqn for feed mmol/ml
#
Mixlrun.Cil(3) := .000182; #Eqn for feed mmol/ml
#Eqn for feed ml/min
#Set loop flow rate (independent of inlet flow rate) we remove one mass
#balance from loop in order to spec this.

Recycle := 0;
PRESET
# variable_name := default_value : lower_bound : upper_bound ;
SELECTOR
# selector_name := selector_value ;

INITIAL
# equality_constraint ;

CSTRrun.U(1:Ntanks).Cout(1:3) = 0;
HPLCrn.UHPLC(1:Nhplc).Cout(1:3) = 0;
HoldTankrun.Cout(1:3) = 0;
Memrun.Umem(1:Nmem).Cr(1:3) = 0;
SCHEDULE
# schedule_task
sequence
Continue for ts

RESET
Mixlrun.Cil(1) := .05; #Eqn for feed mmol/ml
Mixlrun.Cil(2) := 0; #Eqn for feed mmol/ml
Mixlrun.Cil(3) := 3.77e-5; #Eqn for feed mmol/ml
Recycle :=1;

end
continue for tr
end
END # estimation

```

```

SCRIPT TONcalc# identifier
PARAMETER
# identifier AS parameter_type
# identifier AS ARRAY(size_list) OF parameter_type
cTON as REAL
ccat as REAL
cprod as REAL
Vperm as real
testimport as real

ASK
# parameter-name quoted-string-prompt ;
SET
# parameter_name := parameter_expression ;
RUN

#LOAD "MetathesisDeactControl"
EXECUTE "Process"
Vperm := getintegral(STATUS, "Process", Memrun.Umem(1).Fp, TIME = ts:ts+tr)
+getintegral(STATUS, "Process", Memrun.Umem(2).Fp, TIME = ts:ts+tr);
cprod := 2.9*GETmaxVALUE(STATUS, "Process", HPLCrun.UHPLC(2).Cout(2))+
getintegral(STATUS, "Process", Memrun.Umem(1).Cp(2))/tr*getintegral(STATUS, "Process",
Memrun.Umem(1).Fp, TIME = ts:ts+tr)
+getintegral(STATUS, "Process", Memrun.Umem(2).Cp(2))/tr*getintegral(STATUS, "Process",
Memrun.Umem(2).Fp, TIME = ts:ts+tr);
#Not counting autosampler yet

ccat := 2.9*getmaxvalue(STATUS, "Process", Mix1run.Cil(3)) + Vperm*3.77e-5;
cTON := cprod/ccat;

Write "cumulative TON is ", cTON, STATUS END

# list of script commands
END # script

```

8.11 Appendix J

This Matlab code initiates the fitting procedure for our metathesis data.

RunJacFromMatlabMetathesis.m

```
%Author: Everett J. O'Neal, Aug 10, 2013
%Copyright 2013 Massachusetts Institute of Technology. All rights reserved

%Read in csv Data files.
%There is Reag and Prod data at 3 points in this system:
%Reactor Outlet (RO,1), Retentate (Ret,2), Permeate (Perm,3)
%Store reagent and product as subsequent columns in data matrix:
%columns: RO_R RO_P Ret_R Ret_P Perm_R Perm_P (6 columns)
%data_time matrix columns RO Ret Perm
%Each data set, however, has a different time vector
clear

[num,txt,row] = xlsread('ROdata.xlsx');
[num2,txt,row] = xlsread('Retdata.xlsx');
[num3,txt,row] = xlsread('Permdata.xlsx');
M1 = length(num);
M2 = length(num2);
M3 = length(num3);
maxdataL = max([M1 M2 M3]);
data_time = zeros(maxdataL,3);
data = zeros(maxdataL,6);
model = data; %Same size matrix this way.

data_time(1:M1,1) = num(:,1); %time column
data(1:M1,1) = num(:,2); %Reactor P conc.
data(1:M1,2) = num(:,3); %Reactor R conc.
%Retentate data

data_time(1:M2,2) = num2(:,1); %time column
data(1:M2,3) = num2(:,2); %Ret P conc.
data(1:M2,4) = num2(:,3); %Ret R conc.
%Perm data
data_time(1:M3,3) = num3(:,1); %time column
data(1:M3,5) = num3(:,2); %perm P conc.
data(1:M3,6) = num3(:,3); %perm R conc.

M = [M1 M2 M3];

%params: kr, kd, a, b (a,b are exponential fit for flow rate in= out)
options = optimset('Display', 'iter', 'TolFun', 1e-2, 'DiffMinChange', .10, 'DiffMaxChange',
10000);
%('MaxIter', 100, 'TolX', 10, 'TolCon', 10, 'DiffMinChange', 10, 'TypicalX', [500 1000]) ;
X = [ 8.4194 0.8574 49.2730 0.5033];
ff = metathesisdynamics(X, M, data, data_time)

%[X fval] = fmincon(@metathesisdynamics, X, [], [], [], [], [0; 0; 20; .1], [1e4; 1e4; 55;
10], [], options, M, data, data_time)
%best: 5.1856
%X =

% 7.4500 1.3000 50.0826 0.8600
```

8.12 Appendix K

Metathesisdynamics.m

```
%Author: Everett J. O'Neal, Aug 10, 2013
%Copyright 2013 Massachusetts Institute of Technology. All rights reserved

function ssq = metathesisdynamics(p0, M, data, data_time)

M1 = M(1);
M2 = M(2);
M3 = M(3);

%Need to deduce 2nd exponential parameter via mass balance from experiment.
%When we vary rate of flux decline, we force integrated flux = 38.4ml
t = [0:.1:50]*60;
a = p0(3); %cant have perm > 70 ul/min total..
c = 38.4*1000 - trapz(t,8.5+(0*t));
tm = max(t);
options = optimset('TolFun', 1e-8);
b = fsolve(@(x) -a./x.*60.*(exp(-tm/60*x)-1)-c, .2, options);
ymin = 8.5 + a*exp(-b*t/60);
VolumePerm = trapz(t,ymin)/1000;
%Run Jacobian using RunJacobian.c
runJacobian('MetCofeedwMatlab', 'Process', [p0(1); p0(2); p0(3); b; p0(4)]);
% Read csv file output
[num4,txt,raw] = xlsread('output/Process.csv');
mod_time = num4(:,1);
mod_output(:,1:6) = num4(:,2:7); %Store output in same order as data

%Need to round values or I run into uniqueness issues
mod_time = round(mod_time*10e6)/10e6;
mod_output = round(mod_output*10e6)/10e6;

%Need to remove redundant zeros from model output
%firstnonzero = find(mod_time,1);
%mod_time = mod_time((firstnonzero-1):end, :);
%mod_PRO = mod_PRO((firstnonzero-1):end, :);
%Remove all redundancies:
mod_time = sort(mod_time, 1, 'ascend');
%ind = find(~diff(mod_time));
[mod_time I] = unique(mod_time);
mod_output = mod_output(I,:);

%Clean NaN from model output (NaN = 0)
ind = find(isnan(mod_output));
mod_output(ind) = 0;

%model has same organization as mod_output but no time column (time
%corresponds to various rows of data_time)
%We have 0's at the end of each column where no useful data is stored.

for ii = 1:6
    if ii < 3
        model(1:M1,ii) = interp1(mod_time, mod_output(:,ii), data_time(1:M1,1), 'linear');
    elseif ii < 5
        model(1:M2,ii) = interp1(mod_time, mod_output(:,ii), data_time(1:M2,2), 'linear');
    else
        model(1:M3,ii) = interp1(mod_time, mod_output(:,ii), data_time(1:M3,3), 'linear');
```

```

    end
end

%Calculation sum of square differences manually over many variables

%ssq = sum(sum((model-data).^2, 1),2) %weighting every data point equally
%The zero's in model and data should b
% be irrelevant 0 - 0 if lined right

%Try special weighting:
[n m] = size(data);
ssq = 0;
for ii = 1:n %rows data
    for jj = 1:m
        if data(ii,jj) < 1e-3
            ssq = ssq + (model(ii,jj)-data(ii,jj)).^2;
        else
            ssq = ssq + (model(ii,jj)-data(ii,jj)).^2/data(ii,jj).^2;
        end
    end
end
end
ssq
jj = rand();
if jj < 1 %ignore plotting most of time
hold on
for ii = 1:6
    if ii == 1
        plot(data_time(1:M1,1), data(1:M1,ii), 'r*')
        plot(mod_time, mod_output(:,1),'r')
    elseif ii == 2
        plot(data_time(1:M1,1), data(1:M1,ii), 'm*')
        plot(mod_time, mod_output(:,2),'m')
    elseif ii == 3
        plot(data_time(1:M2,2), data(1:M2,ii), 'c*')
        plot(mod_time, mod_output(:,3),'c')
    elseif ii == 4
        plot(data_time(1:M2,2), data(1:M2,ii), 'b*')
        plot(mod_time, mod_output(:, 4),'b')
    elseif ii == 5
        plot(data_time(1:M3,3), data(1:M3,ii), 'k*')
        plot(mod_time, mod_output(:,5),'k')
    elseif ii == 6
        plot(data_time(1:M3,3), data(1:M3,ii), 'y*')
        plot(mod_time, mod_output(:,6),'y')
    end
end
end

legend(['Sub] RO', 'Model: [Sub] RO', '[Prod] RO', 'Model: [Prod] RO', '[Sub] Ret', 'Model:
[Sub] Ret', ...
'[Prod] Ret', 'Model: [Prod] Ret', '[Sub] Perm', 'Model: [Sub] Perm', '[Prod] Perm', 'Model:
[Prod] Perm')

return

```